

Western Australian School of Mines

**Corrosion Monitoring Based on Recurrence Quantification Analysis
of Electrochemical Noise and Machine Learning Methods**

Yang Hou

**This thesis is presented for the Degree of
Doctor of Philosophy
of
Curtin University**

April 2018

Declaration

To the best of my knowledge and belief this thesis contains no material previously published by any other person except where due acknowledgment has been made. This thesis contains no material which has been accepted for the award of any other degree or diploma in any university.

Signature:Yang Hong.....

Date:17/04/2018.....

Abstract

Electrochemical noise (EN) refers to random fluctuations of current and potential generated by electrochemical processes. The EN measurement has been widely used for corrosion mechanism studies and corrosion monitoring practices. One of its advantages is that EN could provide valuable information regarding the occurrence and propagation of localised corrosion events. However, the optimal approach for the analysis of EN data remains uncertain.

In this project, two frameworks based on recurrence quantification analysis (RQA) of EN data have been developed. One of the frameworks is a principal component analysis (PCA)-based corrosion monitoring scheme and the other is a random forest (RF)-based corrosion type diagnostic model. Different case studies were carried out to demonstrate the feasibility and capability of both frameworks.

In case study I, the corrosion of carbon steel in aqueous media resulting in uniform corrosion, pitting corrosion and passivation was investigated on a laboratory scale. Recurrence quantification analysis was applied to short segments of electrochemical current noise measurements and four variables were extracted from each segment. The PCA-based corrosion monitoring scheme was demonstrated to be able to detect non-uniform corrosion automatically and continuously.

In case study II, electrochemical noise data were generated with carbon steel samples immersed in chloride containing solutions with sand deposit on the working surfaces. Feature variables extracted with recurrence quantification analysis of EN data were demonstrated to be useful indicators for monitoring localised corrosion under deposit.

In case study III, three corrosion systems, i.e. uniform corrosion, pitting corrosion and passivation were generated by the same way presented in case study I. Twelve features were extracted from the electrochemical noise segments by recurrence quantification analysis. Machine learning methods, i.e. linear discriminant analysis (LDA) and random forest (RF), were used to identify the different corrosion types from those features. Both models gave satisfactory performance, but the RF model showed better prediction accuracy of 93% than the LDA model (88%). Furthermore,

an estimation of the importance of the variables by use of the RF model suggested the RQA variables laminarity (*LAM*) and determinism (*DET*) played the most significant role with regard to identification of corrosion types.

In case study IV, the corrosion of carbon steel immersed in CO₂ saturated aqueous solutions, in the presence and absence of sand deposits, were investigated by electrochemical noise measurement and recurrence quantification analysis. Uniform corrosion occurred at samples not covered by sand while localised corrosion took place at samples covered with sand. These two different corrosion types can be accurately predicted by random forest and principal component models based on recurrence quantification analysis. The study demonstrated that the PCA-based framework can be used as an automated online corrosion monitoring scheme to ensure the integrity of pipelines.

In case study V, the effect of cargo materials – iron ore and coal – on the corrosion of cargo hulls in carriers was investigated. Tests were also conducted with the steel samples in contact with moist silica sand and immersed in NaCl solution, which generated localised corrosion and general corrosion, respectively. The electrochemical noise was measured and recurrence quantification analysis was carried out to extract feature variables. A random forest model developed using these feature variables as predictors was able to discriminate between the two types of corrosion. The effect of iron ore and coal cargoes on the corrosion types of the steel samples was identified by the model. Visual and microscopic observations of the retrieved steel samples confirmed the prediction results. This work provides a novel analytical approach for future on-line monitoring of carrier structures in contact with cargoes.

Overall, this research innovatively combined the use of recurrence quantification analysis of electrochemical noise data and machine learning methods to develop models for corrosion monitoring and corrosion type identification. Case studies demonstrate that the proposed methodologies are potentially feasible for automated online corrosion monitoring practices.

Acknowledgements

I would like to thank my supervisors Prof. Chris Aldrich, Dr Katerina Lepkova and Dr Laura Machuca Suarez for their countless hours of guidance, inspiration and support throughout my Ph.D. study. Special thanks to Prof. Brian Kinsella for giving me such great support in conducting experiments in Curtin Corrosion Centre and his active participation in this research project. I found a great wealth of knowledge from you all.

I am grateful to my student colleagues Erika Suarez-Rodriguez, Silvia Salgar Md Mayeedul Islam and Yousuf Abdulwahhab, and the staff in Corrosion Centre, particularly Yu Long, Hoda Ehsani and Kod Pojtanabuntoeng. They not only helped me in the laboratory but also provided great ideas for my research.

I would also like to express my gratitude to Curtin University for offering me scholarship to complete this research project.

I dedicate this thesis to my parents Suqin Shi and Runer Hou, my brother Chao Hou, and my husband Chong Feng. Thank you all for supporting me to pursue my dream in a foreign country. I would never have had the confidence and endurance to finish this project without your unconditional love.

Peer Reviewed Publications

Journal Publications

1. Y. Hou, C. Aldrich, K. Lepkova, L.L. Machuca, B. Kinsella, Monitoring of carbon steel corrosion by use of electrochemical noise and recurrence quantification analysis, *Corrosion Science*, 112, 63-72 (2016). Impact Factor: 4.862. Citations: 13.

2. Y. Hou, C. Aldrich, K. Lepkova, L.L. Machuca, B. Kinsella, Analysis of electrochemical noise data by use of recurrence quantification analysis and machine learning methods, *Electrochimica Acta*, 256, 337-347 (2017). Impact Factor: 5.116. Citation: 1.

3. Y. Hou, C. Aldrich, K. Lepkova, B. Kinsella, Detection of under deposit corrosion in a CO₂ environment by using electrochemical noise and recurrence quantification analysis, *Electrochimica Acta*, 274, 160-169 (2018). Impact Factor: 5.116.

4. Y. Hou, C. Aldrich, K. Lepkova, B. Kinsella, Identifying corrosion of carbon steel buried in iron ore and coal cargoes based on recurrence quantification analysis of electrochemical noise and random forest method, *Electrochemical Acta*, 283, 212-220 (2018). Impact Factor: 5.116.

International Conference

Y. Hou, C. Aldrich, K. Lepkova, L.L. Machuca, B. Kinsella, Application of electrochemical noise technique to monitor carbon steel corrosion under sand deposit, paper no. 9103, NACE International Corrosion Conference Series, 2017.

I warrant that I have obtained, where necessary, permission from the copyright owners to use any third-party copyright material reproduced in the thesis, or to use any of my own published work in which the copyright is held by another party.

Statement of Contribution by Others

I, Yang Hou, as the first author of the publications comprising this thesis was primarily involved in planning and conducting the experiments, data analysis and interpretation and manuscript preparation. Contributions by the co-authors is mentioned below and the written statements from the co-authors are included in Appendix 3.

Chris Aldrich significantly contributed to the conception of data interpretation and the preparation and appraisal of the manuscripts. Kateřina Lepková greatly helped with the design and execution of all experiments as well as the preparation and critical revision of the manuscripts. Laura Machuca Suarez participated in the experiment design, particularly with respect to microbiologically influenced corrosion, and helped with the preparation and revision of the manuscripts. Brian Kinsella provided valuable ideas regarding the experiment design and actively participated in data analysis, preparation and modification of the manuscripts.

All the experiments were conducted at the Corrosion Centre of Curtin University. Financial support for this research was provided by Curtin Strategic International Research Scholarship (CSIRS).

Table of Contents

LIST OF SYMBOLS AND ABBREVIATIONS	XI
CHAPTER 1 INTRODUCTION.....	1
1.1 Background	1
1.2 Objectives	3
1.3 Thesis structure	4
CHAPTER 2 LITERATURE REVIEW	6
2.1 Development of Electrochemical noise	6
2.2 Data acquisition and analysis	7
2.2.1 Data acquisition	7
2.2.2 Data interpretation.....	8
2.3 Industrial application of electrochemical noise technique.....	23
2.4 Summary	24
CHAPTER 3 METHODOLOGY	27
3.1 Recurrence plot and quantifications	27
3.2 Machine learning methods.....	30
3.2.1 Principal component analysis	30
3.2.2 Linear discriminant analysis	31
3.2.3 Random forest.....	34
3.3 Corrosion monitoring and diagnostic frameworks	36
3.3.1 PCA model for scenario 1	37
3.3.2 RF model for scenario 2	39
REFERENCES	40
CHAPTER 4 CASE STUDY I.....	61
Monitoring of Carbon Steel Corrosion by Use of Electrochemical Noise and Recurrence Quantification Analysis.....	62
4.1 Introduction.....	63
4.2 Experimental work	66
4.3 Results and discussion	68
4.3.1 Electrochemical noise measurements	68
4.3.2 Application of corrosion monitoring scheme	77
4.4 Summary	79
References.....	80

CHAPTER 5 CASE STUDY II.....	83
Application of Electrochemical Noise Technique to Monitor Carbon Steel Corrosion under Sand Deposit	84
5.1 Introduction	85
5.2 Experimental procedure	86
5.2.1 Test materials and procedures	86
5.2.2 Electrochemical measurements.....	87
5.2.3 Surface analysis	88
5.3 Results and discussion	88
5.3.1 Open circuit potential	88
5.3.2 Electrochemical impedance measurements	89
5.3.3 Resistance comparisons.....	90
5.3.4 Electrochemical noise	92
5.3.5 Recurrence quantification analysis (RQA).....	93
5.4 Summary	96
References.....	98
CHAPTER 6 CASE STUDY III	101
Analysis of Electrochemical Noise Data by Use of Recurrence Quantification Analysis and Machine Learning Methods	102
6.1 Introduction	103
6.2 Experimental work	105
6.2.1 Materials	105
6.2.2 Electrochemical tests.....	105
6.2.3 Surface analysis	107
6.3 Results and discussion	107
6.3.1 Surface morphologies of specimens.....	107
6.3.2 Corrosion type identification	109
6.3.3 Electrochemical impedance spectroscopy (EIS).....	118
6.4 Summary	121
References.....	123
CHAPTER 7 CASE STUDY IV	126
Detection of Under Deposit Corrosion in a CO ₂ Environment by using Electrochemical Noise and Recurrence Quantification Analysis	127
7.1 Introduction	128

7.2 Experimental work	130
7.2.1 Materials	130
7.2.2 Electrochemical noise measurement	130
7.2.3 Post-test surface analysis	132
7.3 Results and discussion	132
7.3.1 Surface morphology	132
7.3.2 Electrochemical noise	134
7.3.3 Recurrence quantification analysis (RQA) of EN signals	136
7.3.4 Application of corrosion monitoring map	144
7.4 Summary	145
References	147
CHAPTER 8 CASE STUDY V	151
Identifying Corrosion of Carbon Steel Buried in Iron Ore and Coal Cargoes Based on Recurrence Quantification Analysis of Electrochemical Noise	152
8.1 Introduction	153
8.2 Experimental work	155
8.2.1 Materials	155
8.2.2 Electrochemical noise measurement	156
8.2.3 Surface profile analysis	157
8.3 Results and discussion	158
8.3.1 Corrosion of carbon steel in NaCl solution and in moist silica sand	158
8.3.2 Corrosion of carbon steel exposed to coal and iron ore	162
8.3.3 Discrimination of corrosion types using localisation index and shot noise parameter	166
8.4 Summary	168
References	170
CHAPTER 9 CONCLUSIONS AND FUTURE WORK	174
9.1 Development and application of a PCA model for corrosion process monitoring	175
9.1.1 Development of the framework	175
9.1.2 Case studies	176
9.2 Development and application of a RF model for corrosion type diagnosis	177
9.2.1 Development of the framework	177
9.2.2 Case studies	177

9.2.3 Estimation of variable importance	179
9.3 Recommendations for future work.....	179
CHAPTER 10 APPENDICES.....	181
Appendix 1. Validation of EN measurements	181
Appendix 2. Application of Electrochemical Noise Technique to Study Corrosion Induced by Sulphate Reducing Bacteria.....	186
Experimental.....	187
Materials.....	187
Bacteria cultures	189
Analytical methods.....	191
Bacteria cell density and activity.....	191
Test media chemistry	191
Electrochemical noise measurement.....	191
Post-test analysis.....	192
Results and discussion.....	193
Visual observations.....	193
Monitoring of bacteria activities and solution chemistry	194
Microscopic analysis.....	195
Electrochemical noise	198
Recurrence quantification analysis of EN.....	203
Summary.....	205
References.....	207
Appendix 3. Written Statements from Co-authors of the Publications	208
Appendix 4. Copyright Statements	214

LIST OF SYMBOLS AND ABBREVIATIONS

A	working surface area of an electrode
A_2	working electrode with a surface area of 2 cm ²
A_6	working electrode with a surface area of 6 cm ²
A_{10}	working electrode with a surface area of 10 cm ²
B	Stern-Geary coefficient
\mathbf{D}_j	distance matrix of segment j
DET	determinism
$ENTR1$	entropy of diagonal line length
$ENTR2$	entropy of recurrence period density
H	Heaviside function
Imp_j	importance of predictor variable j
L_{mean}	average length of diagonal lines in a recurrence plot
L_{max}	maximum length of diagonal lines in a recurrence plot
LAM	laminarity
\mathbf{P}_k	loading matrix of the first k principal components
$\tilde{\mathbf{P}}_k$	loading matrix of the $m-k$ remaining principal components, where m is the total number of principal components
\mathbf{Q}	the matrix containing all recurrence quantification variables
\mathbf{Q}^T	transpose of matrix \mathbf{Q}
\mathbf{q}_{new}	recurrence quantification variable vector extracted from newly measured EN data
$\mathbb{R}^{n \times m}$	the set of real numbers with dimensions of n by m
$\mathbf{R}_{i,j}$	$(i, j)^{\text{th}}$ point of the recurrence matrix
\mathbf{R}_j	recurrence matrix
R_n	noise resistance

RR	recurrence rate
$RT1$	recurrence time of 1 st type
$RT2$	recurrence time of 2 nd type
\mathbf{S}	covariance matrix of \mathbf{Q}
\mathbf{S}_B	between-class scatter
\mathbf{S}_w	within-class scatter
\mathbf{t}_{new}	principal component scores of \mathbf{q}_{new}
\mathbf{T}_k	score matrix of the first k principal components
$TRANS$	transitivity
TT	trapping time
V_{max}	maximum length of vertical lines in a recurrence plot
\mathbf{W}	projection matrix
ε	threshold used to generate recurrence plots
σ	standard deviation
$\mathbf{\Lambda}_k$	a diagonal matrix containing the k eigenvalues
$\tilde{\mathbf{\Lambda}}_k$	diagonal matrix containing the $m-k$ remaining eigenvalues, where m is the total number principal components
\mathcal{L}_T	calculated control limit
DC	direct current
ECN	electrochemical current noise
EN	electrochemical noise
EPN	electrochemical potential noise
GMM	Gaussian mixture model
LDA	linear discriminant analysis
LOI	line of identity
NOC	normal operation condition

OOB	out-of-bag
PCA	principal component analysis
PC	principal component
RF	random forest
RP	recurrence plot
RQA	recurrence quantification analysis
UDC	under deposit corrosion
ZRA	zero resistance ammeter

CHAPTER 1 INTRODUCTION

1.1 Background

Corrosion is a risk many structures, including production facilities, pipelines, bridges and ships. Failure of these structures may lead to significant economic losses, waste of valuable resources and disasters like severe injuries or even loss of lives [1, 2]. Therefore, it is crucial to closely monitor the corrosion process and design proper corrosion mitigation programmes.

Corrosion monitoring is particularly beneficial to capital intensive industries such as oil and gas [3]. It enables the diagnosis of corrosion problems in operating equipment and facilitates the scheduling of process shutdowns and the evaluation and control of the effectiveness of the corrosion mitigation strategies [3].

A number of corrosion monitoring techniques have been applied in the field [4], including electrical resistance, linear polarisation resistance and electrochemical impedance spectroscopy. Most of these techniques can give an indication of the average degradation rate of the monitored structures, but few can detect the occurrence of localised corrosion events, which may lead to failures without being noticed [5, 6]. Visual observation of weight-loss coupons used widely in industry can give a hint about the incidence of localised corrosion, however, this method is subjective and slow, which cannot reflect the real-time condition of the monitored structure.

Electrochemical noise (EN) is one of the few online techniques that is capable of monitoring localised corrosion *in-situ* [7, 8]. It has been applied for corrosion mechanism studies [9, 10] and accepted in field corrosion monitoring practices [11, 12]. EN refers to random fluctuations of current and potential in electrochemical processes, which can be measured potentiostatically, galvanostatically and using zero resistance ammeter (ZRA). Although EN measured under potentiostatic and galvanostatic conditions are useful for mechanistic investigations, they are not particularly suitable for online corrosion monitoring since both approaches require additional potential or current to be applied. By contrast, with the help of a ZRA and a potentiometer, both potential and current can be measured simultaneously at the freely corroding conditions of the monitored system. This also facilitates the

calculation of the so-called noise resistance, which can be used as the polarisation resistance to estimate average corrosion rates [13, 14].

To correctly apply the EN technique for localised corrosion monitoring, skilled and experienced personnel are required to interpret a large amount of data properly and make decisions quickly. A variety of analytical approaches have been proposed since the emergence of this technique, including:

- (i) Statistical parameters, such as current and potential standard deviations [15, 16], skewness and kurtosis [17] as well as localisation index or pitting factor [18];
- (ii) Power spectral density (PSD) with roll-off slope [19, 20];
- (iii) Shot noise analysis with characteristic charge and frequency [21];
- (iv) Wavelet analysis with energy distribution plot (EDP) [22], standard deviation of partial signal (SDPS) [23] and entropy [24];
- (v) Hilbert spectral transient analysis [25];
- (vi) Chaos methods with correlation dimension and Lyapunov exponent [26, 27];
- (vii) Fractal analysis with fractal dimension and Hurst exponent [28-30];
- (viii) Recurrence quantification analysis [31, 32].

However, over the years, contradictory results have been observed with these approaches and there is still no consensus as to what analytical method is optimal, leaving the door to exploring suitable indicators for localised corrosion still wide open.

Recurrence plot (RP) with its quantification analysis (RQA), developed in the late 20th century, is a non-linear methodology that allows a 2-D representation of multi-dimensional non-linear dynamic systems, making it possible to detect graphical patterns and structural changes in the time series data. Moreover, it can also reveal similarities between data series by direct observation of the plots and comparison of quantification variables [31]. RP-based methods have been successfully applied to a number of areas such as the detection of dynamical transitions [33, 34], ecological regimes [35, 36], economical dynamics [37, 38], medical signal analysis [39, 40], chemical reactions [41, 42] and damage detection [43], to name but a few. Cazares-Ibanez et al. [44] were among the first to apply RQA for the interpretation of EN data

generated from corrosion process. A number of investigations [32, 44-49] have demonstrated that feature variables extracted from EN data by use of RQA are able to characterise the corresponding corrosion processes.

With the rapid development of machine learning methods, multiple parameters could be used collectively as predictors and direct output regarding corrosion types could be produced. For example, Li et al. [50] employed the artificial neural network to discriminate between pitting, uniform corrosion and passivation. They used noise resistance, characteristic charge and frequency and relative energies of wavelet crystals D1 – D7 as predictors and various corrosion types as direct outputs. The trained neural network showed excellent prediction accuracy regarding the corrosion types.

So far, no reports have been found to treat EN data by combining the multiple feature variables from recurrence quantification analysis and machine learning methods. It is promising that automated and effective EN monitoring frameworks can be developed from this combination.

1.2 Objectives

Based on the analysis of literature, the gaps and opportunities lying in the interpretation of electrochemical noise data for corrosion monitoring and corrosion type identification have been recognised. On this basis, the objectives of this study are set as follows:

1. Design corrosion monitoring and diagnostic frameworks based on the use of RQA variables extracted from EN data and machine learning methods.
The frameworks will be able to:
 - a. Discriminate different corrosion types, especially to distinguish localised corrosion from uniform corrosion and passivation.
 - b. Monitor corrosion processes continuously and flag unexpected corrosion processes automatically.

2. Examine the feasibility of the designed frameworks using preliminary EN data generated from uniform corrosion, pitting and passivation of carbon steel samples exposed to NaCl, $\text{NaHCO}_3 + \text{NaCl}$ and NaHCO_3 solutions.
3. Carry out different case studies to evaluate the feasibility of the developed methodologies for corrosion monitoring and localised corrosion detection.

1.3 Thesis structure

This thesis is structured as follows:

Chapter 2 gives a detailed literature review on the study of electrochemical noise, with the emphasis on data interpretation approaches for corrosion monitoring and corrosion type identification, especially the detection of localised corrosion.

Chapter 3 introduces the main methodologies used in this study for the development of corrosion monitoring and diagnostic frameworks. Recurrence plot and recurrence quantification analysis are presented explicitly, while the descriptions of machine learning methods tend to be in a conceptual way in order to assist the understanding of the complex mathematical background. At the end of Chapter 3, two formal frameworks for corrosion monitoring and diagnosis are proposed based on a principal component analysis (PCA) model and a random forest (RF) model.

Chapter 4 to Chapter 8 show the applications of the proposed methodologies to different corrosion case studies. Specifically, in Chapter 4, electrochemical noise data are collected from the corrosion of carbon steel in aqueous media resulting in uniform corrosion, pitting corrosion and passivation. The automated corrosion monitoring scheme based on four RQA variables and PCA model is demonstrated to be able to differentiate between uniform and non-uniform corrosion, but the discrimination between pitting and passivation is less satisfactory.

Chapter 5 presents an application of RQA variables derived from electrochemical noise data to monitor carbon steel corrosion under sand deposit in an aqueous media with the presence of oxygen.

Chapter 6 investigated the effect of electrode sizes on the EN data with the corrosion systems same as in Chapter 4 and with extended length of test for passivation.

Twelve RQA variables are extracted and used as predictors for the RF model. Better discrimination between pitting and passivation is obtained compared to that in Chapter 4.

Chapter 7 is associated with the CO₂ corrosion of carbon steel immersed in standard brine solution with and without sand deposit. The PCA-based corrosion monitoring scheme with twelve RQA variables is mainly applied for the detection of under deposit corrosion (UDC).

Chapter 8 deals with the application of the RF model to study the corrosivity of cargo materials – iron ore and coal cargoes. EN data were first collected from two model systems which represented general corrosion and localised corrosion. A RF model was established to distinguish between the two types of corrosion. Afterwards, the corrosion types associated with iron ore and coal were identified by the model and the results were confirmed by visual and microscopic observations of the retrieved steel samples after tests.

Chapter 9 summaries the achievements and limitations of this study along with some recommendations for the future work.

Additional information and application are presented in the Appendix 1 and 2.

Appendix 1 shows the evaluation of the instrument used for data acquisition and validation of the measured EN data.

Appendix 2 shows an application of electrochemical noise and recurrence quantification analysis to study microbiologically influenced corrosion.

Appendix 3 presents the written statements from co-authors of the publications.

Appendix 4 presents the copyright statements related to all the publications included in this thesis.

CHAPTER 2 LITERATURE REVIEW

2.1 Development of Electrochemical noise

When it comes to “noise”, one would most likely associate it with some unwanted background signals that may superimpose with the targeted signals, compromising the extraction of useful information from the target signals. Indeed, studies of “noise” by electrical engineers have long been carried out in order to avoid or eliminate the “noise”. However, the study of electrochemical noise (EN) generated during corrosion processes has completely opposite goals.

Electrochemical noise is defined as the spontaneous fluctuations of potential and current. The sources of the electrochemical noise depend on particular corrosion situations, such as general corrosion, pitting, crevice corrosion, hydrogen evolution, erosion and microbiologically induced corrosion.

Iverson [51] pioneered the use of EN to study corrosion phenomena in the late 1960s'. At about the same time, Fleischmann and Oldfield [52], Tyagai [53] and Baker [54, 55] examined the EN arising from electrochemical reactions from theoretic perspectives. Initial work in corrosion studies focused on the analysis of potential or current fluctuations independently under galvanostatic or potentiostatic conditions [56-59]. The simultaneous acquisition and interpretation of both potential and current noise data was subsequently made possible by Eden and Hladky [60] using a zero resistance ammeter (ZRA).

The value of potentiostatic current noise measurement is well appreciated mainly in the studies of passivity and pitting corrosion of various materials as well as corrosion mechanisms [10, 61-66]. In comparison, fewer applications of galvanostatic potential noise measurement are documented [67-69]. Although both techniques are valid research methods, the imposition of perturbations to the corrosion system may not be able to provide true representations of the actual corrosion situations, making them unsuitable for practical corrosion monitoring applications [70, 71]. By contrast, the ZRA-based EN measurement allows simultaneous recording of potential and current noise originating from natural corroding processes of the electrode [71]. Nowadays, EN with ZRA has attracted extensive attentions owing to its ease of setting

up, non-destructiveness, non-intrusiveness and especially the ability to indicate the occurrence of localised corrosion [13, 21, 24, 72-75].

2.2 Data acquisition and analysis

2.2.1 Data acquisition

According to a standard guide produced by American Society for Materials and Testing [76], the ZRA-based EN measurement typically involves two nominally identical working electrodes (WEs) made from the test materials and one reference electrode (RE) (either standard reference electrode such as a saturated calomel electrode or a third identical WE). The two WEs are short-circuited through a ZRA which registers the current fluctuations between them, meanwhile the potential of the paired WE is measured with respect to the RE via a high sensitivity voltmeter. The generated electrochemical noise signals are then sampled in the time domain using analogue-to-digital conversion techniques and stored in a PC.

The concept of the EN measurement may seem simple, but the results are likely to be contaminated by a number of factors such as unwanted noise, errors and artefacts from the voltage and current measurement devices as well as analogue-to-digital converter [70]. Therefore, it is important to evaluate the measuring instrument and validate the obtained EN data.

The ASTM standard gives a suggestion for the evaluation and qualification of instrumentation, but the descriptions are not explicit or definitive in terms of the capabilities and limitations of the modern EN measuring systems. More recently, a detailed guideline for performing and assessing the EN measurement equipment by dummy cells has been developed by the European Cooperative Group on Corrosion Monitoring of Nuclear Materials (ECG-COMON) as an outcome of the round-robin EN testing carried out by sixteen member laboratories [77, 78]. The dummy cell was consisted of three resistors with equal resistance value connected in a star-arrangement. The dummy cells with resistance values of 100 Ω , 10 k Ω , 1 M Ω or 100 M Ω could be used, resembling different corrosion resistance systems. EN measurements were conducted on each of the dummy cell with three different sampling rates, e.g. 1 Hz, 10 Hz and 1000 Hz. It was suggested that the evaluation of the instrument and the

validation of EN data should be carried out in both time domain and frequency domain. In time domain analysis, the EN data were plotted and checked for quantisation which appeared as a set of clear steps in the time record. Quantisation is a reflection of the resolution of the data acquisition system [70]. In frequency domain, the power spectral densities (PSD) of the obtained EN data were calculated. By analysing PSDs and comparing them with the thermal noise PSDs of the resistors, whether the baseline noise of the measuring system was acceptable or too high can be determined. In addition, the good overlap of PSDs of the EN data recorded at different sampling rates indicated the presence and proper use of anti-aliasing filter. All the EN tests shown in the case studies of this thesis were validated according to this guideline [77].

While the conventional identical two WE configuration is used, a number of modifications of this design are also proposed by different researchers to suit specific investigating purposes [5, 8, 79-86]. However, it is beyond the scope of the present thesis to cover them all. More detailed discussion regarding the experimental setup and other design aspects such as electrode size and sampling rate can be found in [87, 88].

2.2.2 Data interpretation

The interpretation of EN data can be principally divided into two directions – estimation of corrosion rate and identification of the type of corrosion.

Estimation of corrosion rate

One of the most common methods for the analysis of electrochemical noise data is to calculate the so-called noise resistance (R_n). R_n is generally calculated from the equation $R_n = \frac{\sigma_E}{\sigma_I}$, where σ_E is the standard deviation of potential noise and σ_I is the standard deviation of current noise [60]. Values of R_n are frequently found to be comparable to the polarisation resistance R_p normally obtained with linear polarisation technique [13, 14, 87]. Similarly, a frequency dependent parameter named noise impedance (Z_n) can be derived from the power spectral densities (PSD) of both potential and current noise based on $Z_n = \frac{\sqrt{\Psi_v(f)}}{\sqrt{\Psi_i(f)}}$, where $\Psi_v(f)$ is the PSD of potential

noise at a specified frequency f and $\Psi_i(f)$ is the PSD of current noise at the same frequency [13].

A number of theoretical and experimental efforts have been made to investigate the relationships among R_n , Z_n and R_p [13, 89-92]. The major conclusions drawn from these studies can be summarised as follows:

- The equation $R_n = R_p$ is generally accepted, provided that the response of the metal-solution interface can be described by R_p (i.e. the impedance of electrodes is R_p in the bandwidth of frequency under study) and the collected noise data are not affected by considerable instrumental noise or other unwanted noise sources.
- The noise impedance Z_n is equal to the impedance modulus of the electrode on condition that a true reference electrode rather than a third identical WE is used for potential noise measurement.
- If the observations (1) and (2) are true, then R_n and Z_n could be used the same way as R_p to estimate the changes in corrosion rate of the investigated metal material.

Detection/identification of corrosion types

While the noise resistance methods are widely accepted and well established for corrosion rate estimation, more attention has been paid to the possibility of deriving valuable information from the EN measurement to identify corrosion types, since other corrosion monitoring techniques (e.g. linear polarisation, electrical resistance) could not provide such information [92].

Table 2-1 presents a list of analytical approaches proposed over the past five decades and associated parameters for corrosion type identification.

Table 2-1: Parameters used for corrosion type identification extracted by analysis of electrochemical noise data.

Method	Feature	Remark	Reference
Basic statistical analysis	Mean \bar{E} and standard deviation σ_E of potential noise	High values of \bar{E} and σ_E indicate the occurrence of localised corrosion.	[15, 16]
	Localisation index (LI)	Uniform: $0.001 < LI < 0.01$; Pitting: $0.1 < LI < 1$; Mixed: $0.01 < LI < 0.1$.	[18, 93, 94]
	Skewness and Kurtosis	Skewness describes the asymmetry of the probability distribution of the EN data and Kurtosis is a measure of the EN shape. High value of kurtosis indicated localised corrosion.	[17]
Shot noise	Characteristic charge q and characteristic frequency f_n	Localised corrosion: high q and low f_n ;	[95-100]
Power spectra	Roll-off slope of potential noise	Corrosion product film formation: -14 to -32 dB/decade; Pitting or crack initiation: -36 to -50 dB/decade; Repassivation: -26 dB/decade	[19]

Table 2-1: Continued.

Method	Feature	Remark	Reference
Power spectral density PSD	Roll-off slope of potential noise PSD	Pitting: -20 dB/decade; Uniform: -40 dB/decade.	[101-103]
	Roll-off slope of current noise PSD	Pitting: -40 dB/decade.	[104]
	Roll-off slope of potential noise PSD	Passivation: -15 to -25 dB/decade; Pitting: -20 to -25 dB/decade; Uniform: 0 to -7 dB/decade.	[20]
	Roll-off slope of current noise PSD	Passivation: 1 to -1 dB/decade; Pitting: -7 to -14 dB/decade; Uniform: 0 to -7 dB/decade.	
	Roll-off slope of current noise PSD	Pitting: -20 dB/decade; decreased pit initiation rate is indicated by decreased absolute value of roll-off slope; Passivation: -40 dB/decade.	[105, 106]
	Roll-off slope of current noise PSD	Uniform: -9 to -10 dB/decade; Passive state: -3 dB/decade.	[107]

Table 2-1: Continued.

Method	Feature	Remark	Reference
Wavelet analysis	Energy distribution plot (EDP) of current	1. The time evolution of the peak position in an EDP plot indicates the changes in the corroding system;	[22, 75, 108-113]
	EDP of potential	2. The maximum energy tends to accumulate in high frequency crystals in an EDP for localised corrosion process.	[114-119]
	Standard deviation of partial signal (SDPS) of current	The SDPS plot can provide a discriminating power to categorize EN signals by the intensity of various frequencies they represent.	[110, 111, 120-122]
	Entropy	The entropy of the high-frequency crystals in pitting is lower than that of the passive situation	[24]
Hilbert spectral transient analysis	Instantaneous frequency contribution.	The instantaneous frequency contribution of individual localized corrosion phenomena in time can be located by the Hilbert spectrum.	[25, 123-127]

Table 2-1: Continued.

Method	Feature	Remark	Reference
Chaos methods	Correlation dimension (D_c);	The correlation dimension increases from passivation, localised, mixed corrosion to uniform corrosion.	[26]
		The correlation dimension of potential signal increases from passivation, uniform to localised corrosion.	[27, 128-130]
	Largest Lyapunov exponent (LLE)	The presence of positive LLE is an indication of chaotic process; The value of LLE reflects the chaotic degree.	[18, 27, 73, 131-133]
Fractal analysis	Hurst exponent (H_u); Fractal dimension D_f	Pitting corrosion: $H < 0.5$ and by $D > 1$. General corrosion/passive state: $H > 0.5$ and $D < 1$.	[117, 134, 135]
		The fractal dimension of the electrochemical noise signal has a direct relationship with that of the corroded surface.	[28, 29]
Recurrence plot	Recurrence rate (RR)	RR quantifies the periodicity of the signal dynamics.	[31]

Table 2-1: Continued.

Method	Feature	Remark	Reference
Recurrence plot	Determinism (<i>DET</i>)	<i>DET</i> contains information about the duration of a stable interaction; or the predictability of the system dynamics.	[32, 44-49]
	Entropy (<i>ENTR</i>)	<i>ENTR</i> reflects the complexity of the dynamics contained in the signal.	
	Maximum Line (<i>MaxLine</i>)	<i>MaxLine</i> can be considered as the inverse of <i>LLE</i> .	
Cross Recurrence Plot	Correlation of recurrence probability (C_{index}); Similarity of recurrence probability (S_{index})	<ol style="list-style-type: none"> 1. C_{index} detects the phase synchronisation between potential and current; 2. S_{index} measures both the phase and amplitude related synchronisations between potential and current. 	[136, 137]

DC drift removal

Since the current and potential signals generated from the natural corrosion processes are usually nonlinear and nonstationary, direct current (DC) drift components are present in the EN signals, which may significantly affect the outcome of any data analysis [123]. To minimise this effect, pre-processing of the current or potential noise data to remove the DC drift becomes necessary. Moving average [138, 139], polynomial [140, 141], linear [97, 140, 142] and wavelet analysis based trend removal methods as well as empirical mode decomposition have been employed to deal with this issue. Among them, the moving average and polynomial drift removal procedures are considered inadequate since they suffer from the risk of eliminating

useful information [88, 123]. Homborg et al. [123] compared different trend removal methods and demonstrated that the wavelet method and empirical mode decomposition were able to define a reliable DC drift component which could be subtracted from the raw data with high confidence. However, as Robert. A. Cottis, one of the pioneering workers who promoted the application of EN measurement, pointed out, “it is probably best to limit drift removal to the subtraction of a straight line unless there is sound evidence for the existence of an alternative drift function” [92]. In fact, most of the analytical methods presented in Table 2-1 were applied on the linearly detrended EN data, except for the wavelet methods and Hilbert spectral analysis, which intrinsically defined the possible DC drift components.

Statistical parameters

Equations (2-1) through (2-3) show the definitions of the commonly used statistical parameters skew, kurtosis and localisation index. Here N is the number of data contained in the current or potential noise signal, x_i represents the individual current or potential value and \bar{x} is the mean value of the current or potential signal. The localised index is defined as the current standard deviation divided by the root mean square (r.m.s) of current.

$$Skewness = \frac{1}{N-1} \sum_{i=1}^N \left(\frac{x_i - \bar{x}}{\sqrt{x_i^2}} \right)^3 \quad (2-1)$$

$$Kurtosis = \frac{1}{N-1} \sum_{i=1}^N \left(\frac{x_i - \bar{x}}{\sqrt{x_i^2}} \right)^4 - 3 \quad (2-2)$$

$$LI = \frac{\sigma_I}{I_{r.m.s}}, I_{r.m.s} = \sqrt{\frac{1}{N} \left(\sum_{i=1}^N I_i^2 \right)} \quad (2-3)$$

Cottis and his co-workers [97-99] systematically examined the reliability of these statistical parameters as indicators for corrosion types and implied that none of them was reliable diagnostic parameter for corrosion type identification. Similar conclusions were also obtained by [93, 143].

Power spectra

Apart from the time domain statistics, the EN data can also be transformed to frequency domain via fast Fourier transformation (FFT) or maximum entropy method (MEM) [19, 101-103]. As a result, the power spectrum is obtained, in which the potential or current power spectral density (PSD) (i.e. the power of potential or current per unit of frequency) is plotted against frequency. Commonly, the PSD of current or potential is denoted as Ψ_E (V^2/Hz) or Ψ_I (A^2/Hz). Figure 2-1 shows a typical power spectrum displayed on a log-log scale. The roll-off slope as indicated by the arrow is an important parameter which has been used for corrosion type identification. As implied in Table 2-1, -20 dB/decade (roll-off slope of potential power spectrum) might be a criterion for the presence of pitting. Nevertheless, contradictory results have been observed. Therefore, power spectra with the roll-off slope cannot be regarded as a reliable tool for corrosion type identification.

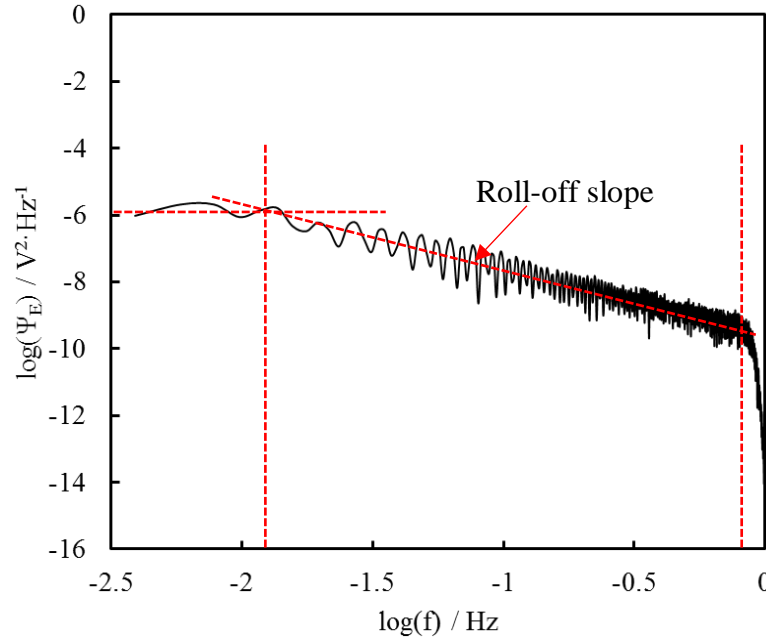


Figure 2-1: An example potential power spectrum plotted on a log-log scale.

Shot noise parameters

The parameters “characteristic charge (q)” and “characteristic frequency (f_n)” derived based on shot noise theory seem to be more robust measures for the detection of localised corrosion [98]. The q and f_n can be calculated according to equations (2-4)

and (2-5), where q is the charge in transient, f_n is the frequency of the transient, Ψ_E and Ψ_I are the low frequency limits of potential and current PSD respectively and B is the Stern-Geary coefficient.

$$q = \frac{\sqrt{\Psi_E \Psi_I}}{B} \quad (2-4)$$

$$f_n = \frac{B^2}{\Psi_E} \quad (2-5)$$

Transients featured with large value of q and low frequency f_n are expected to indicate localised corrosion. f_n has been used together with the noise resistance R_n to discriminate between corrosion types and severity with some success [144]. However, it would be an issue for the calculation of f_n when there is no low frequency plateau in the power spectrum, thereby no accurate potential PSD. In this case, Cottis [14] recommended the power spectral density at 10^{-3} Hz or 10^{-2} Hz may be feasible in practice.

Wavelet analysis

Generally, the precondition of calculating the PSD is that the signal should be stationary. However, this is rarely the case for natural corrosion processes [14, 22, 109, 127]. Wavelet analysis can be considered as a superior technique to the classic FFT methods because it can be used confidently without the presumption of signal stationarity [22]. Unlike the Fourier transform which uses the combinations of sine and cosine waves for the construction or decomposition of original EN signals, wavelet analysis employs a series of wavelet functions that allow for the simultaneous conservation of frequency information on different scales and the time domain aspects such as the transient amplitude and duration [14, 22]. By scaling and translation of these wavelets, the EN signal can be analysed at different timescales, also known as crystals [127, 145]. The fraction of total energy in each crystal can be calculated and plotted against the crystal index. The resultant plot is called an energy distribution plot (EDP). The corresponding literatures shown in Table 2-1 have demonstrated that comparing the relative energy contained in different crystals could reveal underlying corrosion mechanisms and differentiate between corrosion types. Specifically, it is generally accepted that:

- The crystals D1 – D3 corresponding to short time scale processes that are under activation control and related to metastable pitting.
- Crystals D7 and D8 represent long time scale processes such as uniform corrosion that are under diffusion control.
- Crystals D4 – D6 are associated with medium time scale processes that are under activation-diffusion mixed control. Localised corrosion is indicated if the peak of EDP is located in these crystals.

Recently, Cottis et al. [146] carried out a comprehensive comparison of the spectral and wavelet techniques in the analysis of electrochemical noise data. They concluded that the energy was similar to the PSD and the peak of EDP in medium time scales (i.e. crystals D4 – D6) as an indication of localised corrosion was equivalent to the criterion based on a roll-off slope more negative than -1 in a power spectrum, although the EDP provided a more positive indication. Similar to the EDP, Shahidi et al. [120] proposed a standard deviation of partial signal (SDPS) plot and claimed that the SDPS plot could provide better understanding of the corrosion behaviour than the EDP. A partial signal is the signal reconstructed via multiplying each contributing wavelet by its corresponding coefficients. In other words, each partial signal is related to a certain wavelet crystal. Plotting the standard deviation of the partial signal against its corresponding crystal index produces the SDPS plot. Comparing the slope values of the SDPS plots in the region after the peak seemed to be able to reveal the information about corrosion severity in terms of the pit density. However, this method remains to be seen whether it has the general applicability. Another parameter derived from wavelet analysis is called wavelet entropy [24], which was shown to be able to distinguish between passivation and pitting corrosion. Unfortunately, this was just one case study and no further applications were found in the literatures.

Hilbert spectra

The Hilbert spectra was innovatively introduced for the analysis of electrochemical noise by Homborg et al. [124]. To some extent, the idea of Hilbert spectral analysis is similar to that of the wavelet methods, i.e. to characterise the EN data in both time and frequency domain at the same time. However, Homborg et al. [124] argued that the empirical mode decomposition of EN followed by Hilbert-Huang transformation outweighed the wavelet methods since the former allowed the use of

intrinsic properties of the EN signal rather than user-defined scales and wavelet functions, making it more flexible and adaptive. Basically, the Hilbert spectrum is presented in a triaxial coordinate system, i.e. time (s), instantaneous frequency (Hz) and a colour bar indicating the relative contributions of the instantaneous frequencies. For an easier interpretation of information visible in a Hilbert spectrum, the relative amplitudes of the original EN signal is also displayed at the left hand side of the Hilbert spectrum. Alternatively, the Hilbert spectrum can be represented in a 2-dimensional plot, which shows the relative contribution of the cumulated instantaneous frequency over the entire analysed time span. Overall, the Hilbert spectra can improve the discrimination of the frequency characteristics of different corrosion mechanisms [147]. However, the interpretation of the Hilbert spectra is somehow complicated and counter-intuitive at times. It can be considered as a powerful tool for corrosion mechanistic studies, but may not be feasible for corrosion monitoring in practice.

Chaotic analysis

The electrochemical noise data have also been analysed from the perspective of chaos theory. In corrosion studies, the EN time record after DC trend removal is usually embedded in a so-called phase space and represented by an m -dimensional attractor with certain geometrical structures. The features of the trajectories obtained from different corrosion systems can yield crucial information on the nature and behaviour of the dynamic systems [148]. The most widely used parameters to characterise the topology of an attractor are probably correlation dimension and Lyapunov exponent, respectively representing the static and dynamic features of an attractor [26]. Correlation dimension measures the degree of freedom of the evolutionary dynamical system, while the Lyapunov exponent characterises the unpredictability of the investigated process. More specifically, if there exists at least one positive Lyapunov exponent, then the system is said to exhibit deterministic chaos. Otherwise, if there is no positive Lyapunov exponents, then long-term evolution of the system is predictable. Early work done by Legat and Dolecek [26] suggested that the potential noise signals obtained from uniform corrosion processes had a higher correlation dimension than that from localised corrosion process. However, Xia et al. [27, 128] arrived at the opposite conclusion. In spite of this, they all agreed that passivating system generated potential noise with the lowest correlation dimension.

On the contrary, according to Men et al. [133], passivity showed the highest correlation dimension, while uniform corrosion had the lowest correlation dimension. Unlike the correlation dimension, the presence of positive LLE was found in most of the EN signals regardless of their origins, indicating that the electrochemical corrosion processes are intrinsically chaotic. Nonetheless, the degree of the chaotic behaviour for different corrosion systems may vary. Men et al. [133] reported a passivating system with the lowest LLE , whereas Bahena et al. [149] and Rodriguez et al. [150] found the lowest LLE value during localised corrosion and the highest in passivation. The inconsistency of observations could be attributed to a number of factors, such as the actual corrosion systems chosen to study, data acquisition methods (e.g. instrumentation, data sampling rate, length of data analysed), choices of embedding parameters (i.e. time delay and embedding dimension) and the approaches used for DC trend removal, etc.

Fractal analysis

EN time series can also be analysed from fractal point of view. In corrosion studies, the fractal features of EN signals are usually depicted with three parameters – spectral power exponent (β), fractal dimension (D_f) and Hurst exponent (H_u). The relationship between these parameters [151] can be expressed as equation (2-6):

$$D_f = 2 - H_u = (5 - \beta)/2 \quad (2-6)$$

Where β is the exponent of the frequency dependent part of the potential or current PSD. The Hurst exponent H_u is usually calculated based on rescaled range analysis [30] according to equation (2-7):

$$R/S = (T/2)^{H_u} \quad (2-7)$$

Where R represents the difference between the maximum and minimum values of the variable, S the standard deviation of the time series, T is the period of time measured. H_u varies between 0 and 1. $H_u = 0.5$ indicates a complete random behaviour, i.e. there is no correlation between the present and the future element; when $0.5 < H_u < 1$, it means that the phenomenon is persistent or autocorrelated; $H_u < 0.5$ implies anti-persistence or negative autocorrelation [29]. Naturally, the fractal dimension should be in the range of 1 – 2. The application of fractal analysis to interpret EN data has

focused on the assessment of corrosion inhibition [30, 151-153] or the effectiveness of coatings [154, 155]. Basically, if an inhibitor was effective or a coating was less susceptible to corrosion, then the derived H_u was normally less than 0.5. Another interesting finding was that the fractal dimension of the EN signal had a linear relationship with the fractal dimension of the actual corrosion morphology [29].

Recurrence plot based analysis

The term “recurrence plot” was established in 1987 by Eckmann et al. [156], and it was designed for visualisation of the possible recurrent behaviours in the dynamics of a dynamical system. It was 18 years later that the RP was first introduced in EN analysis by Cazares-Ibanez et al. [44] in a study on the pitting corrosion of copper in different saline solutions at various potentials. Cazares-Ibanez et al. found that, by qualitative and quantitative analysis of the recurrence plots generated from the electrochemical current signals, it was able to characterise the electrochemical dynamics like the passive layer formation and the presence of pitting corrosion of copper. They also concluded that pitting corrosion was associated with a high value (approximately 0.9) of the quantification parameter “determinism”, thereby should be deemed as a quasi-periodic process. The low level of chaoticity of pitting corrosion process was also confirmed by the relatively high values of a second quantification parameter named “maximum line”, which was considered as the inverse of the largest Lyapunov exponent (the parameter obtained from chaotic analysis and mentioned before). After this pioneering work, a few more applications were found using the recurrence plots to study the corrosion dynamics from the corresponding electrochemical potential or current oscillations. The corrosion systems investigated include pitting [48], corrosion fatigue crack initiation [46] and intergranular corrosion [31] of stainless steels, hydrostatic pressure influenced corrosion [157] and crevice corrosion [32] of Ni-Cr-Mo-V high strength steels, corrosion protection by nanostructured films on stainless steel [47], the corrosion behaviours of AZ80 magnesium alloy influenced by ultrasonic vibration solidification treatment [158], reinforce steel corrosion [49], copper corrosion under non-uniform magnetic field [159] and the corrosion behaviour of carbon steel in the presence of a specific inhibitor [160]. Recurrence plot and its quantification have been proved to be a powerful tool for

understanding and tracking changes of the corrosion dynamics by extracting useful information from EN data.

Lately, Liu et al. [136, 137] proposed the use of cross recurrence plot (CRP) for EN analysis. Unlike RP that uses only potential or current signal, CRP calculates the distances between the simultaneously obtained current and potential data. The parameters “determinism” and synchronisation indices extracted from the CRPs were used for detecting localised corrosion on nickel alloy 718. The proposed method may be instructive for corrosion mechanism investigations and field monitoring practices.

Combinative use of EN parameters

Another branch of mathematical approaches associated with the EN measurement has set its target specifically at corrosion type discrimination and identification with the help of modern machine learning (or pattern recognition) techniques. This has involved training unsupervised or supervised models with combinative use of the aforementioned feature parameters, e.g. standard deviation, skew, kurtosis, characteristic frequency and the relative energy in different wavelet crystals, etc.

For example, Reid et al. [161] trained a supervised neural network model to distinguish various types of corrosion. Statistical parameters skew and kurtosis calculated from a set of current and potential data segments were used as inputs of the model. Each set of inputs was assigned with a corresponding corrosion form as output, e.g. general corrosion, pit initiation, pit propagation, transgranular stress corrosion cracking and intergranular corrosion cracking. During training, the network was required to learn and establish a sort of relationship between the given inputs and outputs according to certain learning rules. After training, the neural network would be able to categorise new inputs (data not used for training and associated corrosion form not known) as certain corrosion forms. Similarly, Li et al. [50] also employed the artificial neural network to determine corrosion types, but the input arguments were noise resistance, characteristic charge and frequency and relative energies of wavelet crystals D1 – D7. In both studies, the neural network models showed excellent (100%) discriminating power with respect to corrosion types.

Additionally, Huang et al. [162, 163] implemented non-supervised cluster analysis (CA) and supervised discriminant analysis (DA) on EN statistical parameters to separate and identify the pitting stages of carbon steel samples in a typical pitting environment (0.5 M NaHCO₃ solution with the presence of Cl⁻). Three clusters were identified corresponding to metastable pitting, intermediate state and stable pitting. The beginning of stable pitting state was confirmed by the occurrence of macroscopic pit on the steel surface. Similarly, Hu et al. [8] used cluster analysis to identify crevice corrosion stages. More recently, Meng et al. [164] also employed the combination of CA and DA to classify failure states of a coating under marine alternating hydrostatic pressure.

From these investigations, it can be expected that automated diagnostic scheme for on-line corrosion monitoring will be developed by using feature parameters collectively and machine learning techniques.

2.3 Industrial application of electrochemical noise technique

In addition to various laboratory studies, EN technique has been gradually accepted by many fields of industry as part of the corrosion monitoring programmes [11].

Amoco's Corporate Research facility (located in Naperville, Illinois, USA) employed EN measurement to detect localised corrosion on a heat transfer surface in a cooling water environment [12]. The obtained current and potential data were analysed by visual check of time records for transients, in combination with the monitoring of maximum, minimum, mean and standard deviation values as well as localisation index. It was proved that EN was sensitive to the onset of localised corrosion and it facilitated the optimisation of biocide and inhibitor treatment.

Chevron installed EN probes at Canada's Simonette sour oil processing facility in 1997 for corrosion monitoring [17]. The aim was to gain a better understanding of corrosion activities in the stabiliser system and to improve the inhibition program. The parameters being monitored were mainly raw current and potential time records and noise resistance based corrosion rate. This application was considered successful because corrosion engineers were able to determine the effect of temperature on

corrosion rate and evaluate the efficiency of the chemical treatment in real time through the analysis of EN data.

Pitting and stress corrosion cracking were identified as the most likely modes of corrosion failure for the underground nuclear waste storage tanks at Hanford site in the US [11]. Conventional corrosion monitoring techniques like coupon exposure, linear polarisation resistance and electrical resistance showed limited capability to provide early warnings of such localised corrosion attack. Instead, electrochemical noise monitoring system was introduced inspired by the encouraging results obtained from laboratory studies. Three parameters were mainly monitored as indicators for further operations, i.e. noise resistance, localised index and a so-called pitting function which was associated with the characteristics of current transients.

More recently, electrochemical noise measurement was adopted by a Kuwaiti refinery to monitor corrosion rate of their cooling water systems [165]. The corrosion rate was calculated from the noise resistance according to equation: $CR = G/R_n$, where G was a calibrated factor with respect to the weight loss corrosion rate instead of the Stern-Geary constant B .

Moreover, there are a number of patents revolve around the electrochemical noise measurement and analysis that have been archived over the past few decades [166-170]. Apart from introducing more reliable data acquisition apparatus to distinctive service environment, these patents also endeavoured to develop more robust and intuitive indicators to monitor the average corrosion rate, identify localised corrosion events in real time and assist timely remediation of the dangerous corrosion events.

2.4 Summary

The literature review discussed the development of electrochemical noise as a tool for corrosion studies, factors influencing the measurement of reliable EN data, various analytical methods proposed for data interpretation and industrial applications of EN for corrosion monitoring. The gaps and opportunities in EN analysis are summarised as follows:

- It is well appreciated that EN is capable of offering an indication of the nature of the corrosion process, especially the occurrence and propagation of localised corrosion events. However, the optimal approach for the analysis of EN data remains uncertain.
- Currently, the established method for identifying the specific patterns such as transients (typical for metastable pitting and pit propagation) in current or potential signals, relies on ‘manual’ examination or interpretation by professional and experienced users. For long-term corrosion monitoring practices in a plant or in the field, training of skilled personnel is needed, which can be costly and time consuming.
- An efficient corrosion monitoring program requires quick screening of a large amount of raw data and transforming the raw data into a few pertinent indicators to convey the maximum amount of information [161]. Hence, it is necessary to develop sensitive and intuitive indicators for automated EN monitoring.
- The machine learning methods seem attractive since they could produce direct output regarding corrosion types using multiple predictor variables simultaneously as inputs, which could potentially deskill the corrosion monitoring task. Among them, artificial neural network and cluster and discriminant analysis are mainly reported in literature. The most frequently used input variables include statistical parameters, characteristic frequency and the relative energy in different wavelet crystals.
- Recurrence plot and its quantification appear to be suitable for the analysis of EN data since a number of parameters could be extracted from the image representations of the EN signals, without having to make any presumptions. So far, no studies using variables obtained from recurrence quantification analysis (RQA) of EN data in combination with the advanced machine learning methods are available. An automated EN monitoring framework can be developed with this combination.

Based on the above observations, the objectives of this study are:

1. Design corrosion monitoring and diagnostic frameworks based on the use of RQA variables extracted from EN data and machine learning methods.
The frameworks will be able to:
 - a. Discriminate different corrosion types, especially to distinguish localised corrosion from uniform corrosion and passivation.
 - b. Monitor corrosion processes continuously and flag unexpected corrosion processes automatically.
2. Examine the feasibility of the designed frameworks using preliminary EN data generated from uniform corrosion, pitting and passivation of carbon steel samples exposed to NaCl, NaHCO₃+NaCl and NaHCO₃ solutions.
3. Carry out different case studies to evaluate the feasibility of the developed methodologies for corrosion monitoring and localised corrosion detection.

CHAPTER 3 METHODOLOGY

3.1 Recurrence plot and quantifications

Recurrence plot (RP) is a graphical tool first introduced by Eckmann et al. [156] to visualise the recurrence behaviours in dynamic systems based on phase space reconstruction. It can be mathematically expressed as a matrix according to equation (3-1)

$$\mathbf{R}_{i,j} = H(\varepsilon - \|\mathbf{x}_i - \mathbf{x}_j\|), i, j = 1, 2, \dots, N \quad (3-1)$$

where \mathbf{x}_i and \mathbf{x}_j represent the states of the reconstructed phase space trajectory at time i and j , respectively; N is the total number of states in the trajectory; $\|\cdot\|$ calculates the distance between \mathbf{x}_i and \mathbf{x}_j ; ε is a user defined threshold and H is the Heaviside function which gives 0 and 1 depending on the sign of the content within the bracket. Therefore, $\mathbf{R}_{i,j}$ refers to the $(i,j)^{th}$ point in the recurrence matrix. For more information about the phase space trajectory, please refer to [171]. In this thesis, the recurrence plots are constructed without converting the original time recordings into phase space trajectories. Instead, for a given signal, the Euclidean distance between each pair of the current or potential values is computed and compared with a pre-defined threshold value. If the distance is equal to or less than the threshold, then $\mathbf{R}_{i,j} = 1$ (a white dot in the RP), otherwise $\mathbf{R}_{i,j} = 0$ (a black dot in the RP). As a result, the RP is represented by a black-and-white image, in which, the white dots could form different patterns, as illustrated in Figure 3-1.

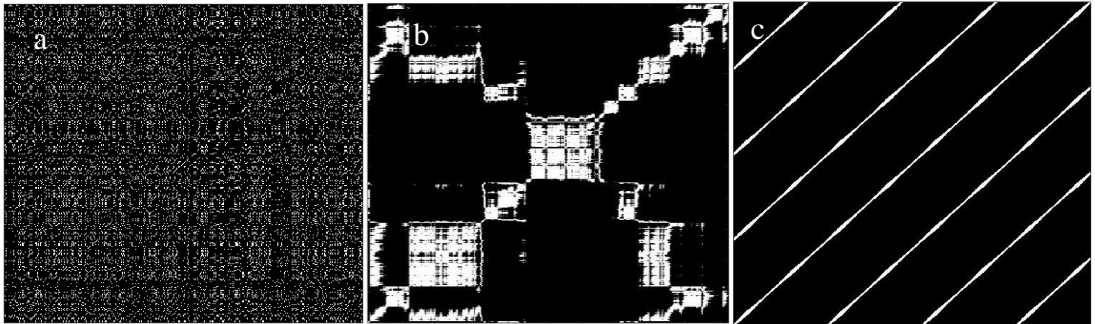


Figure 3-1: Illustration of the patterns present in a RP.

Apparently, the RPs always have a white main diagonal line, i.e. the line of identity (LOI). Other basic features include single white dot, i.e. the recurrence point (Figure 3-1(a)), diagonal lines which are the white lines parallel to the LOI (Figure 3-1(b)) and horizontal/vertical lines which are those parallel to the main axes (Figure 3-1(c)). Note that both the x and y axes of the RP are time indices.

Thanks to the pioneering work done by Zbilut and Webber [172, 173], the RPs can be quantified by several variables on the basis of the abovementioned features. They defined measures of complexity using recurrence rate, determinism, divergence (the inverse of the maximum length of the diagonal line structures), entropy and trend. Marwan [174] further extended their work and defined new variables named laminarity, maximum length of vertical line structures and trapping time. He also developed a comprehensive Matlab toolbox named “Cross Recurrence Plot (CRP)” toolbox, which allowed for the generation of RPs and various quantification variables. This software is currently available online and free to download and use. In fact, in the present study, all the calculations regarding RPs and their quantifications are carried out using this toolbox. The quantification variables employed in this work are summarised in Table 3-1.

Recurrence rate (RR) simply counts the fraction of white dots in the RP. Determinism (DET) measures the ratio of recurrence points that form diagonal line structures to the total number of recurrence points. The length of a diagonal or vertical line means the number of consecutive recurrence points that form the line. The minimum line length can be specified by user and the default is 2. The entropy of the diagonal lines ($ENTR1$) refers to the Shannon entropy of the frequency distribution of the diagonal line lengths. Analogous to the definition of determinism, laminarity (LAM) is the ratio of the recurrence points forming vertical lines to the entire recurrence points in the RP. Trapping time (TT) simply calculates the average length of the vertical lines. The two types of recurrence time were introduced by Gao [175]. The 1st type of recurrence times refer to the time difference between any two recurrence points aligning in the vertical direction and the 2nd type of recurrence times excludes the recurrence points forming the vertical line structures except the first points. Average recurrence times ($RT1$ and $RT2$) are reported in this study. Further, the entropy of the

recurrence time density (*ENTR2*) can be obtained. Lastly, the RQA variable transitivity (*TRANS*) is generated based on complex network theory [176, 177].

Table 3-1: Recurrence quantification variables used in present work.

Number	RQA variable	Equation
1	Recurrence rate	$RR = \frac{1}{N^2} \sum_{i,j=1}^N R_{i,j}(\varepsilon)$
2	Determinism	$DET = \frac{\sum_{l=l_{min}}^N l P(l)}{\sum_{i,j}^N R_{i,j}(\varepsilon)}, \quad l_{min} = 2$ <p>$P(l)$ – Histogram of the diagonal lines of length l.</p>
3	Averaged length of diagonal lines	$L_{mean} = \frac{\sum_{l=l_{min}}^N l P(l)}{\sum_{l=l_{min}}^N P(l)}$
4	Maximal length of diagonal line	$L_{max} = \max(\{l_i; i = 1, 2, \dots, N_l\})$ <p>N_l – Total number of diagonal lines.</p>
5	Entropy of diagonal line length	$ENTR1 = - \sum_{l=l_{min}}^N p(l) \ln p(l)$ <p>$p(l)$ – Probability distribution of diagonal lines.</p>
6	Laminarity	$LAM = \frac{\sum_{v=v_{min}}^N v P(v)}{\sum_{v=1}^N v P(v)}, \quad v_{min} = 2$ <p>$P(v)$ – Histogram of vertical lines of length v.</p>
7	Trapping time	$TT = \frac{\sum_{v=v_{min}}^N v P(v)}{\sum_{v=v_{min}}^N P(v)}$
8	Maximal length of vertical line	$V_{max} = \max(\{v_i; i = 1, 2, \dots, N_v\})$ <p>N_v – Total number of vertical lines.</p>
9	Recurrence times of 1 st type	$RT1, \{RT1(i) = t_i - t_{i-1} i = 1, 2, \dots\}$
10	Recurrence times of 2 nd type	$RT2, \{RT2(i) = t'_i - t'_{i-1} i = 1, 2, \dots\}$

Table 3-1: Continued.

Number	RQA variable	Equation
11	Entropy of recurrence period density	$ENTR2 = -\frac{1}{\ln(t_{max})} \cdot \sum_{t=1}^{t_{max}} P(t) \cdot \ln(P(t))$ <p> $P(t) = R(t) / \sum_{k=1}^{t_{max}} R(k)$ – Recurrence time probability density. $R(t)$ – The histogram of recurrence times. t_{max} – The maximum recurrence time. </p>
12	Transitivity	$TRANS = \frac{\sum_{i,j,k=1}^N R_{i,j} \cdot R_{j,k} \cdot R_{k,i}}{\sum_{i,j,k=1}^N R_{i,j} \cdot R_{k,i}}$

The threshold (ε) has a significant influence on the RQA variables. If ε is too small, there may not be enough recurrence points or recurrence structures. On the other hand, if ε is too large, almost every point would be recurrence point, which may lead to many artefacts [171]. Several options for the selection of ε have been advocated in literature. For example, ε can be chosen according to the phase space diameter [178, 179], recurrence rate [180], standard deviation of the observational noise [181], and standard deviation of the measured time series [176]. Nevertheless, the selection of optimal criterion is strongly dependent on the system under study [171].

In this work, the threshold value is determined according to the standard deviation of the collected current or potential signals.

3.2 Machine learning methods

3.2.1 Principal component analysis

Principal component analysis (PCA) is a statistical procedure that transforms the original multivariate data to a new set of variables containing the linear combinations of original variables [182]. The main purpose is to reduce the dimensionality meanwhile retaining the majority of the variance of the original dataset [183]. The new variables are called the principal components (PCs) and the individual

values in the PCs are called the PC scores. The number of PCs to keep can be determined by the cumulative percentage of variance explained by the PCs, typically between 70% – 95% [184].

For example, given a dataset containing three variables and 50 measurements for each variable, it can be visualised in a 3D scatter plot shown in Figure 3-2 (red circles). The maximum variation of the original variables lies along the direction of t_1 and the second largest lies along the direction of t_2 , which is orthogonal to t_1 . Principal component analysis of this dataset results in three principal components. The first PC accounts for 69% of the variance, which is corresponding to the variation in t_1 , while the second PC accounts for 30% of the variance, corresponding to the variation in t_2 . That is to say, the cumulative variance explained by the first two PCs is 99%. Therefore, the three dimensional dataset can be represented by two principal components. The advantage of this procedure will become more obvious if the original dataset contains more variables, e.g. twelve. In fact, PCA has been widely used for process monitoring in many fields [185-188].

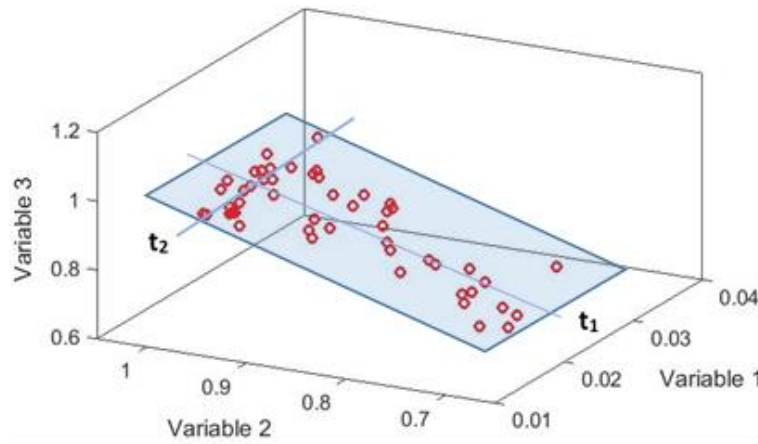


Figure 3-2: Three-dimensional scatter plot of a dataset, showing the maximum variations lying along the directions of t_1 and t_2 .

3.2.2 Linear discriminant analysis

Linear discriminant analysis (LDA) is similar to PCA regarding the linear transformation of original dataset to a new set of features. The major difference is that PCA captures the maximum variance of original multivariate data without considering

its class information, while LDA attempts to project the data onto the directions that optimise the class separability [189, 190].

Figure 3-3 shows a simple two-variable, two-class dataset that illustrates the idea of LDA. The solid blue squares represent data of class 1 and solid red circles represent data of class 2. There are many directions that the data can be projected onto. Clearly, if the data are projected onto direction d_1 , the two classes (represented by empty red circles and blue squares) cannot be well separated. By contrast, in the case of direction d_2 , the two classes are well separated after projection. LDA produces the optimal projection direction like d_2 such that the between class scatter of the data is maximised and the within class scatter is minimised.

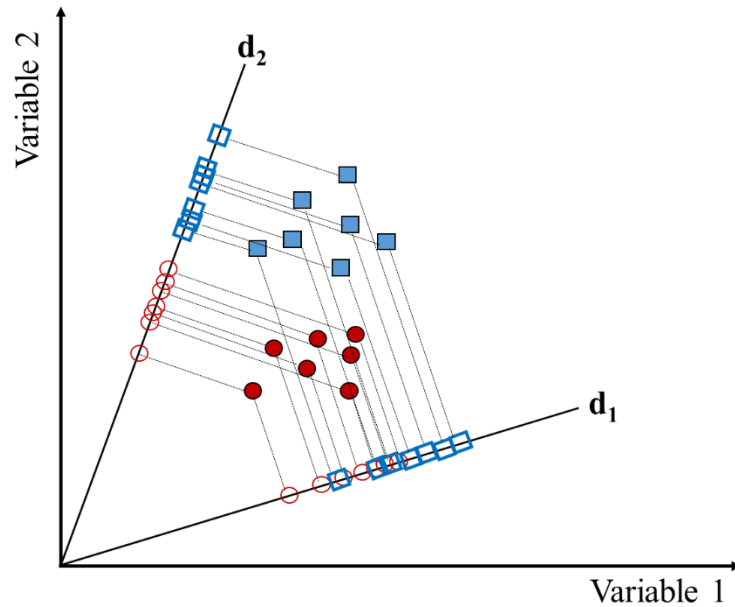


Figure 3-3: Two-variable, two-class dataset projection on direction (d_1) random and (d_2) used by LDA.

LDA is also suitable for multi-class problems. For c classes, LDA generates $(c - 1)$ projections that best discriminate the classes. Usually, the results are presented with a scatter plot showing the projected data on the two most discriminative directions [190].

In the present work, LDA is carried out on the labelled recurrence variables. Firstly, the recurrence variables are stacked into a matrix $\mathbf{X} \in R^{n \times m}$, where n represents the total number of data points for all the c classes (i.e. forms of corrosion),

and m represents the total number of RQA variables which is equal to twelve (Table 3-1) in this study.

The core of LDA is to find a projection matrix \mathbf{W} so that the various classes can be best separated. Mathematically, this is realised by maximizing the ratio of $J(\mathbf{W}) = \frac{|\mathbf{W}^T \mathbf{S}_B \mathbf{W}|}{|\mathbf{W}^T \mathbf{S}_W \mathbf{W}|}$, where \mathbf{S}_B is the between-class scatter calculated according to equation (3-2) and \mathbf{S}_W is the within-class scatter computed from equation (3-3). N_k is the total number of data points pertaining to class k , \mathbf{m}_k is the mean vector of data points belonging to class k , m is the total mean of all the samples, and x_n represents the data points of the variable matrix \mathbf{X} .

$$\mathbf{S}_B = \sum_{k=1}^C N_k (x_n - \mathbf{m}_k)(\mathbf{m}_k - m)^T \quad (3-2)$$

$$\mathbf{S}_W = \sum_{k=1}^C \sum_{n \in C_k} (x_n - \mathbf{m}_k)(x_n - \mathbf{m}_k)^T \quad (3-3)$$

After the best solution of \mathbf{W} is obtained, \mathbf{X} can be projected onto the vectors of \mathbf{W} by equation (3-4), where \mathbf{y}_1 and \mathbf{y}_2 can be expressed as LDA feature 1 and LDA feature 2, respectively.

$$\mathbf{Y} = [\mathbf{y}_1, \mathbf{y}_2] = \mathbf{XW} \quad (3-4)$$

3.2.3 Random forest

Random forest (RF) is an ensemble learning method, consisting of multiple decision trees designed to solve classification or regression problems [191]. For a classification task, such as to identify different corrosion types in current study, the tree model produces discrete outputs corresponding to different classes. Figure 3-4 shows a simple classification task performed by a tree model.

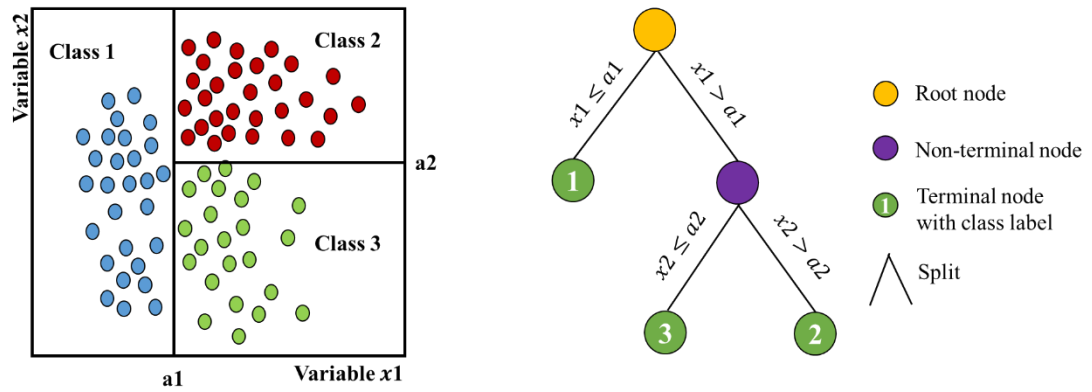


Figure 3-4: Three-class classification problem with discrimination boundaries and associated classification tree.

As can be seen, a number of nodes and splits constitute the decision tree model. Popular learning algorithm for a decision tree model recursively search for a binary partition on each node to generate output variables with the purest class labels. In the case of multivariate input data space, the splitting creates a collection of non-overlapping hyper-rectangular subspaces with the splits perpendicular to one of the coordinate axes of the input data space [182, 192].

The decision tree algorithm is potentially capable of fitting almost all data distributions, but it is susceptible to overfitting. Random forest, suggested by Breiman [193], improves the generalisation of the model by constructing an ensemble of decision trees using (a) randomly selected subsets of the original data to train individual trees and (b) randomly selected subsets of predictor variables for splitting at each node. For each tree in the forest, there exists a set of data that is excluded during training, which is called out-of-bag (OOB) sample. The classification error of the RF model can be estimated by predicting the OOB data using the tree grown from the bagged data and aggregating the predictions of OOB data from all the trees in the forest

[193]. The generated prediction error is known as OOB error. It has been shown that this error of the RF model converges to a limit when the number of trees grown in the forest is sufficiently large [191].

The RF algorithms also facilitate the quantification of the importance of each variable in the tree ensemble with respect to the final prediction accuracy. This is realised by permuting the OOB objects of each predictor variable, one at a time, and determine the decrease in model accuracy [182].

Given that R is a random forest containing T trees and p is the number of predictor variables in the training data. In this study, the predictor variables refer to the twelve RQA variables extracted from the EN signals of different corrosion systems. The importance of each RQA variable Imp_j can be obtained following the procedures presented below:

1. For tree t , where $t = 1, 2, \dots, T$:
 - Identify the OOB objects and the indices of the predictor variables that were used to grow tree t ;
 - Estimate the OOB error ε_t ;
 - For each predictor variable x_j , $j \in \{1, 2, \dots, p\}$, firstly permute the values of x_j randomly, followed by estimating the model error, ε_{tj} , using the OOB objects containing the permuted values of x_j . Afterwards, take the difference $d_t = \varepsilon_{tj} - \varepsilon_t$. Note that predictor variables not used when growing tree t are attributed with a difference of 0.
2. For each predictor variable in the training data, compute the mean, \bar{d}_j , and standard deviation, σ_j , of all the differences.
3. Compute the importance estimation of the OOB predictor variable x_j with $Imp_j = \bar{d}_j / \sigma_j$.

If the RQA variable is significant for the model, then permuting its values should result in greater model error. Otherwise, it should have little or even no influence on the model. Therefore, larger Imp_j values correspond to more influential RQA variables.

3.3 Corrosion monitoring and diagnostic frameworks

In this study, two scenarios are considered:

1. Unsupervised corrosion monitoring: EN data collected under normal operation conditions (NOC) are considered as a reference and any unexpected changes from NOC need to be captured by the monitoring program. However, the reason for the change is unknown and related personnel need to check for it.
2. Supervised corrosion monitoring: EN data collected from several known corrosion forms are used as the database and associated treatment plan regarding each case scenario has been scheduled. During the corrosion process monitoring, newly measured EN data are automatically classified as one of the known corrosion conditions and corresponding treatment can be carried out promptly.

In this study, two frameworks for corrosion monitoring and diagnosis are proposed targeting at these two scenarios. Both frameworks require segmentation of the EN recordings followed by recurrence quantification analysis to extract the predictor variables. The pre-treatment of the EN data is illustrated in Figure 3-5.

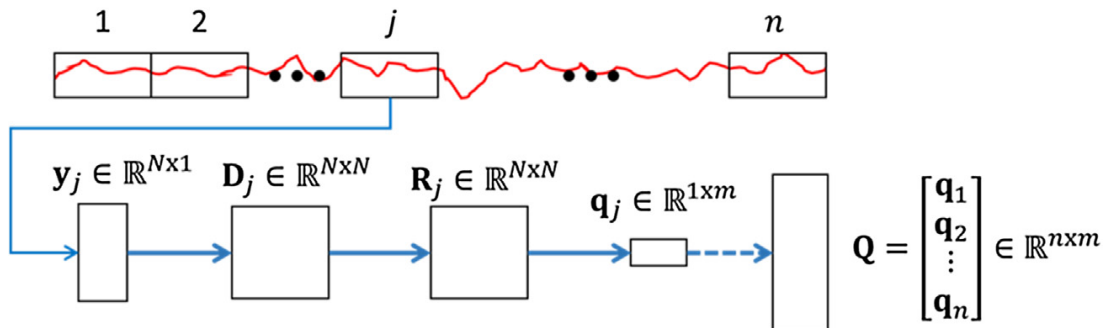


Figure 3-5: Pre-treatment of EN recordings by consecutive segmentation and recurrence quantification analysis

The collected electrochemical noise signal over a period of time is segmented into n non-overlapping time series each containing N measurements. The distance matrix \mathbf{D}_j contains the Euclidean distances between each pair of points in the time series segment \mathbf{y}_j and \mathbf{R}_j the recurrence matrix, is simply the thresholded version of \mathbf{D}_j . Vector \mathbf{q}_j is derived from \mathbf{D}_j and contains m recurrence variables. The matrix \mathbf{Q} contains the n recurrence variable vectors extracted from all the n segments of the electrochemical noise signal.

3.3.1 PCA model for scenario 1

Regarding scenario 1, a PCA model consisting of an off-line calibration stage and an on-line application stage is proposed, as shown in Figure 3-6.

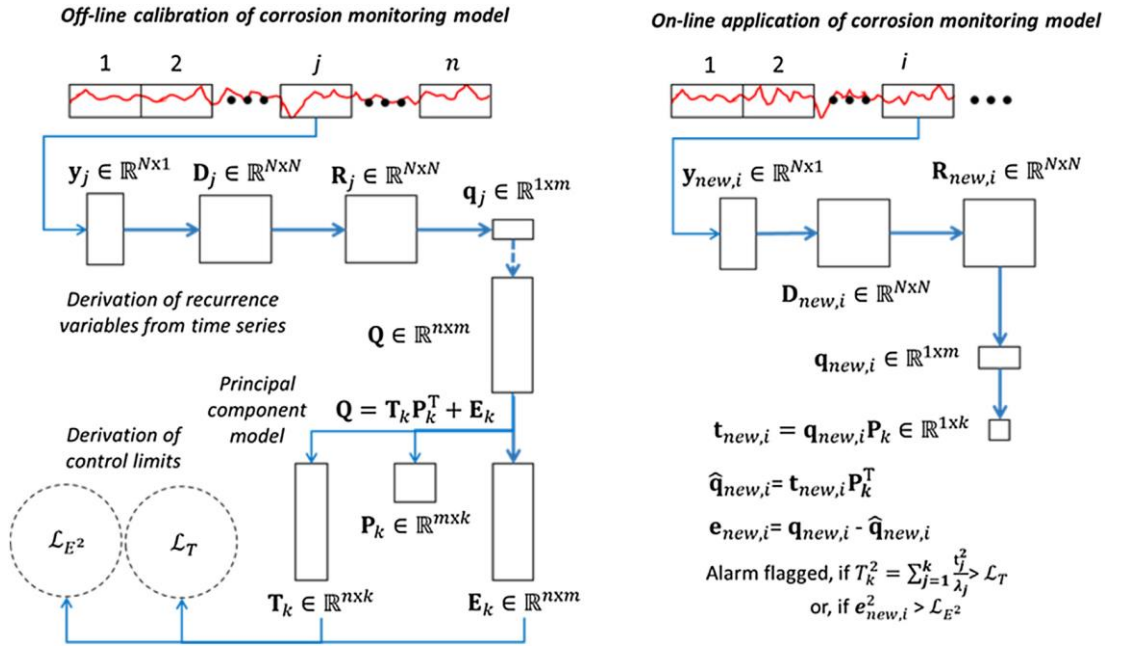


Figure 3-6: Off-line calibration (left) and on-line monitoring of corrosion from electrochemical noise (right).

In the off-line stage, $\mathbf{Q} \in \mathbb{R}^{n \times m}$ and represents the reference data containing the variables from RQA. The principal components of \mathbf{Q} can be obtained according to equations (3-5) and (3-6).

$$\mathbf{S} = \frac{\mathbf{Q}^T \mathbf{Q}}{n-1} = \mathbf{P}_k \mathbf{\Lambda}_k \mathbf{P}_k^T + \tilde{\mathbf{P}}_k \tilde{\mathbf{\Lambda}}_k \tilde{\mathbf{P}}_k^T \quad (3-5)$$

$$\mathbf{T}_k = \mathbf{Q} \mathbf{P}_k \quad (3-6)$$

Where \mathbf{S} is the covariance matrix of \mathbf{Q} , typically scaled to zero mean and unit variance in the columns, \mathbf{P}_k is the loading matrix of the first $k < m$ principal components, $\mathbf{\Lambda}_k$ is a diagonal matrix containing the k eigenvalues of the decomposition, $\tilde{\mathbf{P}}_k$ is the loading matrix of the $m-k$ remaining principal components and $\tilde{\mathbf{\Lambda}}_k$ is a diagonal matrix containing the $m-k$ remaining eigenvalues of the decomposition, and $\mathbf{T}_k \in \mathbb{R}^{n \times k}$ is the score matrix of the principal component model consisting of the first k principal components. The value of k is determined on condition that the cumulative percentage of variance explained by the first k PCs reaches at least 80%.

To calibrate the PCA model, a decision boundary \mathcal{L}_T is calculated for the principal component scores \mathbf{T}_k of the reference data. In this study, a Gaussian mixture model is proposed to generate the decision boundary, which can be done using a free Matlab toolbox developed by Tax [194].

A Gaussian Mixture Model (GMM) is a parametric probabilistic model, which can be represented by equation (3-7), where \mathbf{X} is the multivariate data with dimension D , G is the total number of Gaussian components, ω_k is the prior probability of the k th component satisfying $\sum_{k=1}^G \omega_k = 1$, $\theta_k = \{\mu_k, \Sigma_k\}$ denotes the probability parameters of the k th Gaussian component, $p(\mathbf{X}|\theta_k)$ represents the probability density function of the k th Gaussian component, which can be expressed as equation (3-8), $\theta = \{\{\omega_1, \theta_1\}, \{\omega_2, \theta_2\}, \dots, \{\omega_G, \theta_G\}\}$ denotes the parameters for all the G components and $p(\mathbf{X}|\theta)$ is the weighted sum of the individual probability functions, i.e. the probability density of the overall mixture model [195].

$$p(\mathbf{x}|\theta) = \sum_{k=1}^G \omega_k p(\mathbf{X}|\theta_k) \quad (3-7)$$

$$p(\mathbf{X}|\theta_k) = \frac{1}{(2\pi)^{D/2} |\Sigma_k|^{1/2}} \exp \left\{ -\frac{1}{2} (\mathbf{X} - \mu_k)^T \Sigma_k^{-1} (\mathbf{X} - \mu_k) \right\} \quad (3-8)$$

Training of the GMM is to estimate the above set of parameters θ normally by using the modified expectation-maximisation (EM) approach [196]. In this study, the GMM used to fit the reference scores \mathbf{T}_k contains five Gaussian components and the rejection rate of the decision boundary that encloses \mathbf{T}_k is set as 5%, i.e. the decision boundary is a 95% control limit.

In the on-line monitoring stage (Figure 3-6), newly measured EN data will be subjected to RQA to generate a new set of variables \mathbf{q}_{new} . Then \mathbf{q}_{new} is projected onto the PCA model to generate new principal component scores $\mathbf{t}_{new} = \mathbf{q}_{new} \mathbf{P}_k$. If it falls out of the control limit \mathcal{L}_T , then the alarm flag will be activated, implying that unexpected changes of the corrosion process have occurred and the system needs to be checked for fault conditions.

3.3.2 RF model for scenario 2

In the case that EN data originating from several corrosion types can be collected, a supervised RF model can be established to identify these corrosion types.

Pre-processing of the EN data is also based on recurrence quantification analysis to generate the variable matrix $\mathbf{Q} \in \mathbb{R}^{n \times m}$, as illustrated by Figure 3-5. Since the EN data are collected from different corrosion types, the variables are labelled, such as ‘1’ for uniform corrosion, ‘2’ for pitting corrosion and ‘3’ for passivation.

The RF diagnostic framework also involves an off-line training stage and an on-line application stage. Training of the RF model is conducted on the labelled variable matrix \mathbf{Q} , of which 70% are used as training dataset and 30% are used as test dataset in order to check the generalisation of the trained model.

Once the model is established, it can be used for on-line corrosion monitoring. Newly measured EN data is processed to obtain the RQA variables, which are subsequently fed to the RF model for prediction. As a result, the corrosion type of the monitored system can be identified without having to retrieve the sensors from the system.

In the following chapters, case studies will be presented to demonstrate the capability and feasibility of the frameworks for corrosion monitoring and diagnosis.

REFERENCES

- [1] M. Finsgar, J. Jackson, Application of corrosion inhibitors for steels in acidic media for the oil and gas industry: A review, *Corros Sci*, 86 (2014) 17-41.
- [2] K.M. Usher, A.H. Kaksonen, I. Cole, D. Marney, Critical review: Microbially influenced corrosion of buried carbon steel pipes, *Int Biodeter Biodegr*, 93 (2014) 84-106.
- [3] C.F. Britton, 4.36 - Corrosion Monitoring and Inspection A2 - Cottis, Bob, in: M. Graham, R. Lindsay, S. Lyon, T. Richardson, D. Scantlebury, H. Stott (Eds.) *Shreir's Corrosion*, Elsevier, Oxford, 2010, pp. 3117-3166.
- [4] A.K. Agrawal, Corrosion Monitoring A2 - Buschow, K.H. Jürgen, in: R.W. Cahn, M.C. Flemings, B. Ilchner, E.J. Kramer, S. Mahajan, P. Veyssi re (Eds.) *Encyclopedia of Materials: Science and Technology (Second Edition)*, Elsevier, Oxford, 2001, pp. 1698-1701.
- [5] Y. Tan, Sensing localised corrosion by means of electrochemical noise detection and analysis, *Sensors and Actuators B: Chemical*, 139 (2009) 688-698.
- [6] Y.X. Qiao, Y.G. Zheng, W. Ke, P.C. Okafor, Electrochemical behaviour of high nitrogen stainless steel in acidic solutions, *Corros Sci*, 51 (2009) 979-986.
- [7] M. Shahidi, H. Tajabadipour, H.G. Hakemi, M.R. Gholamhosseinzadeh, Comparison of Electrochemical Noise Method with the Conventional Electrochemical Techniques for Investigation of the Pitting Corrosion on Al Alloys AA6061 and AA5052, *Int J Electrochem Sc*, 8 (2013) 11734-11751.
- [8] Q. Hu, Y.B. Qiu, X.P. Guo, J.Y. Huang, Crevice corrosion of Q235 carbon steels in a solution of NaHCO₃ and NaCl, *Corros Sci*, 52 (2010) 1205-1212.
- [9] S.M. Hoseinie, A.M. Homborg, T. Shahrabi, J.M.C. Mol, B. Ramezanzadeh, A Novel Approach for the Evaluation of Under Deposit Corrosion in Marine Environments Using Combined Analysis by Electrochemical Impedance Spectroscopy and Electrochemical Noise, *Electrochim Acta*, 217 (2016) 226-241.

- [10] J. Xu, T. Sun, L. Zhang, J. Li, Y. Jiang, Potentiostatic Electrochemical Noise Analysis of 2101 Lean Duplex Stainless Steel in 1 mol/L NaCl, *Journal of Materials Science & Technology*, 28 (2012) 474-480.
- [11] G.L. Edgemon, E. Barr, *Applications of Electrochemical Noise: Real Time Plant and Field Challenges*, NACE International, 2001.
- [12] M.A. Winters, P.S. Stokes, H.F. Nichols, Simultaneous corrosion and fouling monitoring under heat transfer in cooling water systems, *Electrochemical Noise Measurement for Corrosion Applications*, ASTM International 1996.
- [13] A. Aballe, A. Bautista, U. Bertocci, F. Huet, Measurement of the noise resistance for corrosion applications, *Corrosion*, 57 (2001) 35-42.
- [14] R. Cottis, Interpretation of electrochemical noise data, *Corrosion*, 57 (2001) 265-285.
- [15] C.A. Loto, Electrochemical noise evaluation and data statistical analysis of stressed aluminium alloy in NaCl solution, *Alexandria Engineering Journal*, (2017).
- [16] C.A. Loto, Electrochemical noise measurement and statistical parameters evaluation of stressed α -brass in Mattsson's solution, *Alexandria Engineering Journal*, (2017).
- [17] E. Barr, R.B. Goodfellow, L.M. Rosenthal, Noise Monitoring in Canada's Simonette Sour Oil Processing Facility, *CORROSION 2000*, NACE International, 2000.
- [18] D.-H. Xia, S.-Z. Song, Y. Behnamian, Detection of corrosion degradation using electrochemical noise (EN): review of signal processing methods for identifying corrosion forms, *Corrosion Engineering, Science and Technology*, 51 (2016) 527-544.
- [19] C.A. Loto, R.A. Cottis, Electrochemical Noise Generation during Stress Corrosion Cracking of Alpha-Brass, *Corrosion*, 43 (1987) 499-504.

- [20] A. Legat, V. Doleček, Corrosion Monitoring System Based on Measurement and Analysis of Electrochemical Noise, *Corrosion*, 51 (1995) 295-300.
- [21] H.A. Al-Mazeedi, R.A. Cottis, Parameter maps for the assessment of corrosion type from electrochemical noise data, *Corrosion/2004*; New Orleans, LA; USA; 28 Mar.-1 Apr. 2004, NACE International, P.O. Box 218340, Houston, TX, 77218, USA, 2004.
- [22] A. Aballe, M. Bethencourt, F.J. Botana, M. Marcos, Using wavelets transform in the analysis of electrochemical noise data, *Electrochim Acta*, 44 (1999) 4805-4816.
- [23] M. Bahrami, M. Shahidi, S. Hosseini, Comparison of electrochemical current noise signals arising from symmetrical and asymmetrical electrodes made of Al alloys at different pH values using statistical and wavelet analysis. Part I: neutral and acidic solutions, *Electrochim Acta*, 148 (2014) 127-144.
- [24] R. Moshrefi, M.G. Mahjani, M. Jafarian, Application of wavelet entropy in analysis of electrochemical noise for corrosion type identification, *Electrochem Commun*, 48 (2014) 49-51.
- [25] A.M. Homborg, T. Tinga, X. Zhang, E.P.M. van Westing, P.J. Oonincx, G.M. Ferrari, J.H.W. de Wit, J.M.C. Mol, Transient analysis through Hilbert spectra of electrochemical noise signals for the identification of localized corrosion of stainless steel, *Electrochim Acta*, 104 (2013) 84-93.
- [26] A. Legat, V. Dolecek, Chaotic Analysis of Electrochemical Noise Measured on Stainless-Steel, *J Electrochem Soc*, 142 (1995) 1851-1858.
- [27] D. Xia, S. Song, J. Wang, J. Shi, H. Bi, Z. Gao, Determination of corrosion types from electrochemical noise by phase space reconstruction theory, *Electrochem Commun*, 15 (2012) 88-92.
- [28] E. García-Ochoa, J. Genesca, Understanding the inhibiting properties of 3-amino-1,2,4-triazole from fractal analysis, *Surface and Coatings Technology*, 184 (2004) 322-330.

- [29] E. García-Ochoa, F. Corvo, Copper patina corrosion evaluation by means of fractal geometry using electrochemical noise (EN) and image analysis, *Electrochem Commun*, 12 (2010) 826-830.
- [30] E. Sarmiento, J.G. González-Rodríguez, J. Uruchurtu, Fractal analysis of the corrosion inhibition of carbon steel in a bromide solution by molybdates, *ECS Transactions*, 2008, pp. 221-232.
- [31] E. García-Ochoa, J. González-Sánchez, N. Acuña, J. Euan, Analysis of the dynamics of Intergranular corrosion process of sensitised 304 stainless steel using recurrence plots, *J Appl Electrochem*, 39 (2009) 637-645.
- [32] T. Zhang, Y.A. Cong, Y.W. Shao, G.Z. Meng, F.H. Wang, Electrochemical noise analysis on the crevice corrosion behavior of Ni-Cr-Mo-V high strength steel using recurrence plots, *J Appl Electrochem*, 41 (2011) 289-298.
- [33] L.L. Trulla, A. Giuliani, J.P. Zbilut, C.L. Webber, Recurrence quantification analysis of the logistic equation with transients, *Physics Letters A*, 223 (1996) 255-260.
- [34] E. Ngamga, A. Nandi, R. Ramaswamy, M.C. Romano, M. Thiel, J. Kurths, Recurrence analysis of strange nonchaotic dynamics, *Physical Review E*, 75 (2007) 036222.
- [35] A. Facchini, C. Mocenni, N. Marwan, A. Vicino, E. Tiezzi, Nonlinear time series analysis of dissolved oxygen in the Orbetello Lagoon (Italy), *Ecological Modelling*, 203 (2007) 339-348.
- [36] R. Proulx, P. Côté, L. Parrott, Multivariate recurrence plots for visualizing and quantifying the dynamics of spatially extended ecosystems, *Ecological Complexity*, 6 (2009) 37-47.
- [37] C.-Z. Yao, Q.-W. Lin, Recurrence plots analysis of the CNY exchange markets based on phase space reconstruction, *The North American Journal of Economics and Finance*, 42 (2017) 584-596.

- [38] P.M. Addo, M. Billio, D. Guégan, Nonlinear dynamics and recurrence plots for detecting financial crisis, *The North American Journal of Economics and Finance*, 26 (2013) 416-435.
- [39] D. Cui, J. Wang, L. Wang, S. Yin, Z. Bian, G. Gu, Symbol Recurrence Plots based resting-state eyes-closed EEG deterministic analysis on amnesic mild cognitive impairment in type 2 diabetes mellitus, *Neurocomputing*, 203 (2016) 102-110.
- [40] J. Schlenker, V. Socha, L. Riedlbauchová, T. Nedělka, A. Schlenker, V. Potočková, Š. Malá, P. Kutílek, Recurrence plot of heart rate variability signal in patients with vasovagal syncope, *Biomed Signal Proces*, 25 (2016) 1-11.
- [41] B. Babaei, R. Zarghami, H. Sedighikamal, R. Sotudeh-Gharebagh, N. Mostoufi, Investigating the hydrodynamics of gas–solid bubbling fluidization using recurrence plot, *Advanced Powder Technology*, 23 (2012) 380-386.
- [42] H. Castellini, L. Romanelli, Applications of recurrence quantified analysis to study the dynamics of chaotic chemical reaction, *Physica A: Statistical Mechanics and its Applications*, 342 (2004) 301-307.
- [43] J.M. Nichols, S.T. Trickey, M. Seaver, Damage detection using multivariate recurrence quantification analysis, *Mechanical Systems and Signal Processing*, 20 (2006) 421-437.
- [44] E. Cazares-Ibanez, G.A. Vazquez-Coutino, E. Garcia-Ochoa, Application of recurrence plots as a new tool in the analysis of electrochemical oscillations of copper, *J Electroanal Chem*, 583 (2005) 17-33.
- [45] D. Mayorga-Cruz, O. Sarmiento-Martinez, C.M. Campos, J. Uruchurtu, Analysis of Michelson optical interferometry using recurrence plots during corrosion of aluminium in NaCl solution, *ECS Transactions*, 20 (2009) 433-446.
- [46] N. Acuna-Gonzalez, E. Garcia-Ochoa, J. Gonzalez-Sanchez, Assessment of the dynamics of corrosion fatigue crack initiation applying recurrence plots to the analysis of electrochemical noise data, *Int J Fatigue*, 30 (2008) 1211-1219.

- [47] C. Lopez-Melendez, E.M. Garcia-Ochoa, M.I. Flores-Zamora, R.G. Bautista-Margulis, C. Carreno-Gallardo, C.P.C. Morquecho, J.G. Chacon-Nava, A. Martinez-Villafane, Dynamic Study of Current Fluctuations of Nanostructured Films, *Int J Electrochem Sc*, 7 (2012) 1160-1169.
- [48] L.S. Montalban, P. Henttu, R. Piche, Recurrence quantification analysis of electrochemical noise data during pit development, *Int J Bifurcat Chaos*, 17 (2007) 3725-3728.
- [49] E. Garcia-Ochoa, F. Corvo, Using recurrence plot to study the dynamics of reinforcement steel corrosion, *Prot Met Phys Chem+*, 51 (2015) 716-724.
- [50] J. Li, W.K. Kong, J.B. Shi, K. Wang, W.K. Wang, W.P. Zhao, Z.M. Zeng, Determination of Corrosion Types from Electrochemical Noise by Artificial Neural Networks, *Int J Electrochem Sc*, 8 (2013) 2365-2377.
- [51] W.P. Iverson, Transient Voltage Changes Produced in Corroding Metals and Alloys, *J Electrochem Soc*, 115 (1968) 617-618.
- [52] M. Fleischmann, J.W. Oldfield, Generation-recombination noise in weak electrolytes, *Journal of Electroanalytical Chemistry and Interfacial Electrochemistry*, 27 (1970) 207-218.
- [53] V. Tyagai, Faradaic noise of complex electrochemical reactions, *Electrochimica Acta*, 16 (1971) 1647-1654.
- [54] G.C. Barker, Faradaic Reaction Noise, *J Electroanal Chem*, 82 (1977) 145-155.
- [55] G.C. Barker, Noise connected with electrode processes, *Journal of Electroanalytical Chemistry and Interfacial Electrochemistry*, 21 (1969) 127-136.
- [56] K. Hladky, J.L. Dawson, The measurement of localized corrosion using electrochemical noise, *Corros Sci*, 21 (1981) 317-322.
- [57] J. Dawson, K. Hladky, D. Eden, Electrochemical noise--some new developments in corrosion monitoring, *UK Corrosion'83-Proceedings of the Conference*, 1983, pp. 99-108.

- [58] J. Dawson, M. Ferreira, Electrochemical studies of the pitting of austenitic stainless steel, *Corros Sci*, 26 (1986) 1009-1026.
- [59] C. Gabrielli, F. Huet, M. Keddam, H. Takenouti, Application of electrochemical noise measurements to the study of localized and uniform corrosion, 8 th European Congress of Corrosion., 1985.
- [60] D.A. Eden, K. Hladky, Electrochemical Noise - Simultaneous Monitoring of Potential and Current Noise Signals from Corroding Electrodes, (1987).
- [61] Y. Miyata, T. Handa, H. Takazawa, An analysis of current fluctuations during passive film breakdown and repassivation in stainless alloys, *Corros Sci*, 31 (1990) 465-470.
- [62] W.J. Tobler, S. Virtanen, Effect of Mo species on metastable pitting of Fe18Cr alloys—A current transient analysis, *Corros Sci*, 48 (2006) 1585-1607.
- [63] A.R. Trueman, Determining the probability of stable pit initiation on aluminium alloys using potentiostatic electrochemical measurements, *Corros Sci*, 47 (2005) 2240-2256.
- [64] Z. Jiang, T. Norby, H. Middleton, Evaluation of metastable pitting on titanium by charge integration of current transients, *Corros Sci*, 52 (2010) 3158-3161.
- [65] M.G. Figueroa, M.F.L. de Mele, R.C. Salvarezza, A.J. Arvia, Electrochemical behaviour of copper in potassium thiocyanate solution—II. Analysis of potentiostatic current transients, *Electrochimica Acta*, 32 (1987) 231-238.
- [66] M. Pagitsas, M. Pavlidou, S. Papadopoulou, D. Sazou, Chlorates induce pitting corrosion of iron in sulfuric acid solutions: An analysis based on current oscillations and a point defect model, *Chemical Physics Letters*, 434 (2007) 63-67.
- [67] F. Safizadeh, E. Ghali, Monitoring passivation of Cu–Sb and Cu–Pb anodes during electrorefining employing electrochemical noise analyses, *Electrochimica Acta*, 56 (2010) 93-101.

- [68] N. Ebrahimi, J.J. Noël, M.A. Rodríguez, D.W. Shoesmith, The self-sustaining propagation of crevice corrosion on the hybrid BC1 Ni–Cr–Mo alloy in hot saline solutions, *Corros Sci*, 105 (2016) 58-67.
- [69] C. Gabrielli, M. Keddam, Review of applications of impedance and noise analysis to uniform and localized corrosion, *Corrosion*, 48 (1992) 794-811.
- [70] R.A. Cottis, 4 - Electrochemical noise for corrosion monitoring A2 - Yang, Lietai, *Techniques for Corrosion Monitoring*, Woodhead Publishing 2008, pp. 86-110.
- [71] J. Dawson, *Electrochemical Noise Measurement: The Definitive In-Situ Technique for Corrosion Applications?*, *Electrochemical Noise Measurement: The Definitive In-Situ Technique for Corrosion Applications?* 1996.
- [72] F. Hass, A.C.T.G. Abrantes, A.N. Diogenes, H.A. Ponte, Evaluation of naphthenic acidity number and temperature on the corrosion behavior of stainless steels by using Electrochemical Noise technique, *Electrochim Acta*, 124 (2014) 206-210.
- [73] A.N. Chen, F.H. Cao, X.N. Liao, W.J. Liu, L.Y. Zheng, J.Q. Zhang, C.A. Cao, Study of pitting corrosion on mild steel during wet-dry cycles by electrochemical noise analysis based on chaos theory, *Corros Sci*, 66 (2013) 183-195.
- [74] R.A. Cottis, M.A. Al-Ansari, G. Bagley, A. Pettiti, Electrochemical noise measurements for corrosion studies, *Mater Sci Forum*, 289-2 (1998) 741-754.
- [75] E.C. Rios, A.M. Zimer, P.C.D. Mendes, M.B.J. Freitas, E.V.R. de Castro, L.H. Mascaro, E.C. Pereira, Corrosion of AISI 1020 steel in crude oil studied by the electrochemical noise measurements, *Fuel*, 150 (2015) 325-333.
- [76] G. ASTM, 199-09 “Standard Guide for Electrochemical Noise Measurement”, American society for testing materials, 2009.
- [77] S. Ritter, F. Huet, R.A. Cottis, Guideline for an assessment of electrochemical noise measurement devices, *Mater Corros*, 63 (2012) 297-302.
- [78] R.W. Bosch, R.A. Cottis, K. Csecs, T. Dorsch, L. Dunbar, A. Heyn, F. Huet, O. Hyokyvirta, Z. Kerner, A. Kobzova, J. Macak, R. Novotny, J. Oijerholm, J.

- Piippo, R. Richner, S. Ritter, J.M. Sanchez-Amaya, A. Somogyi, S. Vaisanen, W.Z. Zhang, Reliability of electrochemical noise measurements: Results of round-robin testing on electrochemical noise, *Electrochimica Acta*, 120 (2014) 379-389.
- [79] M. Benish, J. Sikora, E. Sikora, B.A. Shaw, M.R. Yaffe, A. Krebs, G.A. Martinchek, A New Electrochemical Noise Technique for Monitoring the Localized Corrosion of 304 Stainless Steel in Chloride - Containing Solutions, *Corrosion 1998*, NACE International, 1998.
- [80] R.B. Miller II, A. Sadek, A. Rodriguez, M. Iannuzzi, C. Giai, J.M. Senko, C.N. Monty, Use of an electrochemical split cell technique to evaluate the influence of *Shewanella oneidensis* activities on corrosion of carbon steel, *PloS one*, 11 (2016) e0147899.
- [81] M. Curioni, A.C. Balaskas, G.E. Thompson, An alternative to the use of a zero resistance ammeter for electrochemical noise measurement: Theoretical analysis, experimental validation and evaluation of electrode asymmetry, *Corros Sci*, 77 (2013) 281-291.
- [82] S. Mabbutt, D. Mills, Technical note Novel configurations for electrochemical noise measurements, *Brit Corros J*, 33 (1998) 158-160.
- [83] S.S. Jamali, D.J. Mills, A critical review of electrochemical noise measurement as a tool for evaluation of organic coatings, *Prog Org Coat*, 95 (2016) 26-37.
- [84] S. Caines, F. Khan, Y. Zhang, J. Shirokoff, Simplified electrochemical potential noise method to predict corrosion and corrosion rate, *Journal of Loss Prevention in the Process Industries*, 47 (2017) 72-84.
- [85] U. Bertocci, F. Huet, R.P. Nogueira, Use of Multiple Reference Electrodes in Electrochemical Noise Measurements, *Corrosion*, 59 (2003) 629-634.
- [86] A. Legat, Monitoring of steel corrosion in concrete by electrode arrays and electrical resistance probes, *Electrochim Acta*, 52 (2007) 7590-7598.

- [87] P. Pistorius, Design aspects of electrochemical noise measurements for uncoated metals: electrode size and sampling rate, *Corrosion*, 53 (1997) 273-283.
- [88] D.-H. Xia, Y. Behnamian, Electrochemical noise: a review of experimental setup, instrumentation and DC removal, *Russ J Electrochem+*, 51 (2015) 593-601.
- [89] R. Cottis, S. Turgoose, Electrochemical noise measurements-a theoretical basis, *Materials Science Forum*, Trans Tech Publ, 1995, pp. 663-672.
- [90] U. Bertocci, C. Gabrielli, F. Huet, M. Keddam, Noise resistance applied to corrosion measurements I. theoretical analysis, *J Electrochem Soc*, 144 (1997) 31-37.
- [91] U. Bertocci, C. Gabrielli, F. Huet, M. Keddam, P. Rousseau, Noise resistance applied to corrosion measurements ii. experimental tests, *J Electrochem Soc*, 144 (1997) 37-43.
- [92] R.A. Cottis, An evaluation of electrochemical noise for the estimation of corrosion rate and type, *CORROSION 2006*, NACE International, 2006.
- [93] A. Najiub, F. Mansfeld, Evaluation of corrosion inhibition of brass in chloride media using EIS and ENA, *Corros Sci*, 43 (2001) 2147-2171.
- [94] D. Eden, D. John, J. Dawson, International patent WO 87/07022, World Intellectual Property Organization, 19 (1987).
- [95] H. Al-Mazeedi, R. Cottis, A practical evaluation of electrochemical noise parameters as indicators of corrosion type, *Electrochimica Acta*, 49 (2004) 2787-2793.
- [96] F. Hass, A.C.T.G. Abrantes, A.N. Diógenes, H.A. Ponte, Evaluation of naphthenic acidity number and temperature on the corrosion behavior of stainless steels by using Electrochemical Noise technique, *Electrochimica Acta*, 124 (2014) 206-210.
- [97] J.M. Sanchez-Amaya, R.A. Cottis, F.J. Botana, Shot noise and statistical parameters for the estimation of corrosion mechanisms, *Corros Sci*, 47 (2005) 3280-3299.

- [98] R.A. Cottis, M.A.A. Al-Awadhi, H. Al-Mazeedi, S. Turgoose, Measures for the detection of localized corrosion with electrochemical noise, *Electrochimica Acta*, 46 (2001) 3665-3674.
- [99] S. Turgoose, R. Cottis, Corrosion testing made easy: Electrochemical noise and impedance, NACE International, (2000).
- [100] M.G. Pujar, N. Parvathavarthini, R.K. Dayal, S. Thirunavukkarasu, Assessment of intergranular corrosion (IGC) in 316(N) stainless steel using electrochemical noise (EN) technique, *Corros Sci*, 51 (2009) 1707-1713.
- [101] P. Searson, J. Dawson, Analysis of Electrochemical Noise Generated by Corroding Electrodes under Open-Circuit Conditions, *J Electrochem Soc*, 135 (1988) 1908-1915.
- [102] F. Mansfeld, H. Xiao, Electrochemical noise analysis of iron exposed to NaCl solutions of different corrosivity, *J Electrochem Soc*, 140 (1993) 2205-2209.
- [103] J.C. Uruchurtu, J.L. Dawson, Noise Analysis of Pure Aluminum under Different Pitting Conditions, *Corrosion*, 43 (1987) 19-26.
- [104] R.J.K. Wood, J.A. Wharton, A.J. Speyer, K.S. Tan, Investigation of erosion–corrosion processes using electrochemical noise measurements, *Tribol Int*, 35 (2002) 631-641.
- [105] Y.F. Cheng, J.L. Luo, M. Wilmott, Spectral analysis of electrochemical noise with different transient shapes, *Electrochimica Acta*, 45 (2000) 1763-1771.
- [106] Y.F. Cheng, B.R. Rairdan, J.L. Luo, Features of electrochemical noise generated during pitting of inhibited A516-70 carbon steel in chloride solutions, *J Appl Electrochem*, 28 (1998) 1371-1375.
- [107] S. Girija, U.K. Mudali, V.R. Raju, R.K. Dayal, H.S. Khatak, B. Raj, Determination of corrosion types for AISI type 304L stainless steel using electrochemical noise method, *Materials Science and Engineering: A*, 407 (2005) 188-195.

- [108] A. Aballe, M. Bethencourt, F.J. Botana, M. Marcos, Wavelet transform-based analysis for electrochemical noise, *Electrochemistry Communications*, 1 (1999) 266-270.
- [109] M.T. Smith, D.D. Macdonald, Wavelet analysis of electrochemical noise data, *Corrosion*, 65 (2009) 438-448.
- [110] M. Shahidi, M.R. Gholamhosseinzadeh, Electrochemical evaluation of AA6061 aluminum alloy corrosion in citric acid solution without and with chloride ions, *J Electroanal Chem*, 757 (2015) 8-17.
- [111] M. Shahidi, R. Farrehi Moghaddam, M.R. Gholamhosseinzadeh, S.M.A. Hosseini, Investigation of the cathodic process influence on the electrochemical noise signals arising from pitting corrosion of Al alloys using wavelet analysis, *J Electroanal Chem*, 693 (2013) 114-121.
- [112] Y. Li, R. Hu, J. Wang, Y. Huang, C.-J. Lin, Corrosion initiation of stainless steel in HCl solution studied using electrochemical noise and in-situ atomic force microscope, *Electrochimica Acta*, 54 (2009) 7134-7140.
- [113] A. Aballe, M. Bethencourt, F.J. Botana, M. Marcos, R.M. Osuna, Electrochemical noise applied to the study of the inhibition effect of CeCl₃ on the corrosion behaviour of Al–Mg alloy AA5083 in seawater, *Electrochimica Acta*, 47 (2002) 1415-1422.
- [114] F.H. Cao, Z. Zhang, J.X. Su, Y.Y. Shi, J.Q. Zhang, Electrochemical noise analysis of LY12-T3 in EXCO solution by discrete wavelet transform technique, *Electrochimica Acta*, 51 (2006) 1359-1364.
- [115] A.-M. Lafront, F. Safizadeh, E. Ghali, G. Houlachi, Study of the copper anode passivation by electrochemical noise analysis using spectral and wavelet transforms, *Electrochimica Acta*, 55 (2010) 2505-2512.
- [116] X.F. Liu, J. Zhan, Q.J. Liu, The influence of tensile stress on electrochemical noise from aluminum alloy in chloride media, *Corros Sci*, 51 (2009) 1460-1466.

- [117] L.-j. Zhang, X.-b. Zhu, Z. Zhang, J.-q. Zhang, Electrochemical noise characteristics in corrosion process of AZ91D magnesium alloy in neutral chloride solution, *Transactions of Nonferrous Metals Society of China*, 19 (2009) 496-503.
- [118] C. Cai, Z. Zhang, F. Cao, Z. Gao, J. Zhang, C. Cao, Analysis of pitting corrosion behavior of pure Al in sodium chloride solution with the wavelet technique, *J Electroanal Chem*, 578 (2005) 143-150.
- [119] Y. Shi, Z. Zhang, J. Su, F. Cao, J. Zhang, Electrochemical noise study on 2024-T3 Aluminum alloy corrosion in simulated acid rain under cyclic wet–dry condition, *Electrochimica Acta*, 51 (2006) 4977-4986.
- [120] M. Shahidi, S.M.A. Hosseini, A.H. Jafari, Comparison between ED and SDPS plots as the results of wavelet transform for analyzing electrochemical noise data, *Electrochimica Acta*, 56 (2011) 9986-9997.
- [121] M.J. Bahrami, M. Shahidi, S.M.A. Hosseini, Comparison of electrochemical current noise signals arising from symmetrical and asymmetrical electrodes made of Al alloys at different pH values using statistical and wavelet analysis. Part I: Neutral and acidic solutions, *Electrochimica Acta*, 148 (2014) 127-144.
- [122] M.J. Bahrami, S.M.A. Hosseini, M. Shahidi, Comparison of electrochemical current noise signals arising from symmetrical and asymmetrical electrodes made of Al alloys at different pH values using statistical and wavelet analysis. Part II: Alkaline solutions, *Electrochimica Acta*, 148 (2014) 249-260.
- [123] A.M. Homborg, T. Tinga, X. Zhang, E.P.M. van Westing, P.J. Oonincx, J.H.W. de Wit, J.M.C. Mol, Time–frequency methods for trend removal in electrochemical noise data, *Electrochim Acta*, 70 (2012) 199-209.
- [124] A.M. Homborg, E.P.M. van Westing, T. Tinga, X. Zhang, P.J. Oonincx, G.M. Ferrari, J.H.W. de Wit, J.M.C. Mol, Novel time–frequency characterization of electrochemical noise data in corrosion studies using Hilbert spectra, *Corros Sci*, 66 (2013) 97-110.

- [125] A.M. Homborg, E.P.M. van Westing, T. Tinga, G.M. Ferrari, X. Zhang, J.H.W. de Wit, J.M.C. Mol, Application of transient analysis using Hilbert spectra of electrochemical noise to the identification of corrosion inhibition, *Electrochim Acta*, 116 (2014) 355-365.
- [126] A.M. Homborg, C.F. Leon Morales, T. Tinga, J.H.W. de Wit, J.M.C. Mol, Detection of microbiologically influenced corrosion by electrochemical noise transients, *Electrochimica Acta*, 136 (2014) 223-232.
- [127] A.M. Homborg, R.A. Cottis, J.M.C. Mol, An integrated approach in the time, frequency and time-frequency domain for the identification of corrosion using electrochemical noise, *Electrochim Acta*, 222 (2016) 627-640.
- [128] D. Xia, J. Shi, W. Gong, R. Zhou, Z. Gao, J. Wang, The significance of correlation dimension obtained from electrochemical noise, *Electrochemistry*, 80 (2012) 907-912.
- [129] R. Zhao, D.H. Xia, S.Z. Song, W. Hu, Detection of SCC on 304 stainless steel in neutral thiosulfate solutions using electrochemical noise based on chaos theory, *Anti-Corros Method M*, 64 (2017) 241-251.
- [130] X. Wang, J. Wang, X. Yue, Characterization of corrosion process of Q235 carbon steel in simulated concrete pore solution by EIS and EN techniques, *Int J Electrochem Sc*, 9 (2014) 6558-6571.
- [131] J. Stringer, A.J. Markworth, Applications of deterministic chaos theory to corrosion, *Corros Sci*, 35 (1993) 751-760.
- [132] W. Li, K. Nobe, A.J. Pearlstein, Potential/current oscillations and anodic film characteristics of iron in concentrated chloride solutions, *Corros Sci*, 31 (1990) 615-620.
- [133] H. Men, B. Sun, X. Zhao, X. Li, J. Liu, Z. Xu, Dynamics of stainless steel corrosion based on the theory of phase space reconstruction and chaos, *Anti-Corros Method M*, 63 (2016) 214-225.

- [134] H. Greisiger, T. Schauer, On the interpretation of the electrochemical noise data for coatings, *Prog Org Coat*, 39 (2000) 31-36.
- [135] E. Sarmiento, J. González-Rodríguez, J. Uruchurtu, O. Sarmiento, M. Menchaca, Fractal analysis of the corrosion inhibition of carbon steel in a bromide solution by lithium chromate, *Int. J. Electrochem. Sci*, 4 (2009) 144-155.
- [136] W. Liu, D. Wang, X. Chen, C. Wang, H. Liu, Electrochemical noise monitoring of sulphur corrosion for nickel alloy 718, *Corrosion Engineering, Science and Technology*, 51 (2016) 545-549.
- [137] W. Liu, D. Wang, X. Chen, C. Wang, H. Liu, Recurrence plot-based dynamic analysis on electrochemical noise of the evolutive corrosion process, *Corros Sci*, (2017).
- [138] Y. Tan, S. Bailey, B. Kinsella, Factors affecting the determination of electrochemical noise resistance, *Corrosion*, 55 (1999) 469-475.
- [139] Y.J. Tan, S. Bailey, B. Kinsella, The monitoring of the formation and destruction of corrosion inhibitor films using electrochemical noise analysis (ENA), *Corros Sci*, 38 (1996) 1681-1695.
- [140] U. Bertocci, F. Huet, R. Nogueira, P. Rousseau, Drift removal procedures in the analysis of electrochemical noise, *Corrosion*, 58 (2002) 337-347.
- [141] A.M. Nagiub, Comparative electrochemical noise study of the corrosion of different alloys exposed to chloride media, *Engineering*, 6 (2014) 1007.
- [142] F. Mansfeld, Z. Sun, C.H. Hsu, A. Nagiub, Concerning trend removal in electrochemical noise measurements, *Corros Sci*, 43 (2001) 341-352.
- [143] F. Mansfeld, Z. Sun, Technical Note: Localization Index Obtained from Electrochemical Noise Analysis, *Corrosion*, 55 (1999) 915-918.
- [144] K. Wang, J. Wang, W. Hu, Evaluation of temperature effect on the corrosion process of 304 stainless steel in high temperature water with electrochemical noise, *Materials & Design*, 82 (2015) 155-163.

- [145] A. Aballe, M. Bethencourt, F.J. Botana, M. Marcos, J.M. Sanchez-Amaya, Use of wavelets to study electrochemical noise transients, *Electrochim Acta*, 46 (2001) 2353-2361.
- [146] R.A. Cottis, A.M. Homborg, J.M.C. Mol, The relationship between spectral and wavelet techniques for noise analysis, *Electrochimica Acta*, 202 (2016) 277-287.
- [147] A.M. Homborg, T. Tinga, E.P.M. Van Westing, X. Zhang, G.M. Ferrari, J.H.W. De Wit, J.M.C. Mol, A critical appraisal of the interpretation of electrochemical noise for corrosion studies, *Corrosion*, 70 (2014) 971-987.
- [148] C. Aldrich, B.C. Qi, P.J. Botha, Analysis of electrochemical noise data with phase space methods, *Miner Eng*, 19 (2006) 1402-1409.
- [149] D. Bahena, I. Rosales, O. Sarmiento, Guardi, #225, R. n, C. Menchaca, J. Uruchurtu, Electrochemical Noise Chaotic Analysis of NiCoAg Alloy in Hank Solution, *International Journal of Corrosion*, 2011 (2011).
- [150] F.J. Rodriguez, E.M. Garcia, F.J. Boerio, J.G. Llongueras, Oscillation and Chaos in Pitting Corrosion of Steel, NACE International, 1999.
- [151] J.G. Sarmiento, J.G. González-Rodríguez, J. Uruchurtu, A study of the corrosion inhibition of carbon steel in a bromide solution using fractal analysis, *Surface and Coatings Technology*, 203 (2008) 46-51.
- [152] E. García-Ochoa, J. Genesca, Understanding the inhibiting properties of 3-amino-1,2,4-triazole from fractal analysis, *Surface and Coatings Technology*, 184 (2004) 322-330.
- [153] I.A. Hermoso-Díaz, J.G. Gonzalez-Rodriguez, J. Uruchurtu-Chavarín, Use of EIS and electrochemical noise fractal analysis to study *Salvia hispanica* as green corrosion inhibitor for carbon steel, *Int J Electrochem Sc*, 11 (2016) 4253-4266.
- [154] M.A. González-Núñez, J. Uruchurtu-Chavarín, R/S fractal analysis of electrochemical noise signals of three organic coating samples under corrosion conditions, *Journal of Corrosion Science and Engineering*, 6 (2003).

- [155] M. Moon, B. Skerry, Interpretation of corrosion resistance properties of organic paint films from fractal analysis of electrochemical noise data, *Journal of Coatings Technology*, 67 (1995) 35-44.
- [156] J.-P. Eckmann, S.O. Kamphorst, D. Ruelle, Recurrence plots of dynamical systems, *EPL (Europhysics Letters)*, 4 (1987) 973.
- [157] Y.E. Yang, T. Zhang, Y.W. Shao, G.Z. Meng, F.H. Wang, Effect of hydrostatic pressure on the corrosion behaviour of Ni-Cr-Mo-V high strength steel, *Corros Sci*, 52 (2010) 2697-2706.
- [158] T. Sun, Z. Wang, J. Li, T. Zhang, Effect of ultrasonic vibration solidification treatment on the corrosion behavior of AZ80 magnesium alloy, *Int. J. Electrochem. Sci*, 8 (2013) 7298-7319.
- [159] E. Garcia-Ochoa, F. Corvo, J. Genesca, V. Sosa, P. Estupiñán, Copper Corrosion Under Non-uniform Magnetic Field in 0.5 M Hydrochloric Acid, *Journal of Materials Engineering and Performance*, 26 (2017) 2129-2135.
- [160] J. Cruz-Borbolla, E. Garcia-Ochoa, J. Narayanan, P. Maldonado-Rivas, T. Pandiyan, J.M. Vásquez-Pérez, Electrochemical and theoretical studies of the interactions of a pyridyl-based corrosion inhibitor with iron clusters (Fe15, Fe30, Fe45, and Fe60), *Journal of Molecular Modeling*, 23 (2017) 342.
- [161] S. Reid, G.E.D. Bell, G.L. Edgemon, The use of skewness, kurtosis and neural networks for determining corrosion mechanism from electrochemical noise data, *Corrosion 98*; San Diego, CA; USA; 22-27 Mar. 1998, National Association of Corrosion Engineers, P.O. Box 218340, Houston, TX 77084, USA, 1998, pp. 176/171.
- [162] J.Y. Huang, Y.B. Qiu, X.P. Guo, Cluster and discriminant analysis of electrochemical noise statistical parameters, *Electrochim Acta*, 54 (2009) 2218-2223.
- [163] J.Y. Huang, X.P. Guo, Y.B. Qiu, Z.Y. Chen, Cluster and discriminant analysis of electrochemical noise data, *Electrochim Acta*, 53 (2007) 680-687.

- [164] F. Meng, L. Liu, Y. Li, F. Wang, Studies on electrochemical noise analysis of an epoxy coating/metal system under marine alternating hydrostatic pressure by pattern recognition method, *Progress in Organic Coatings*, 105 (2017) 81-91.
- [165] H. Al-Mazeedi, M. Miyazawa, Y. Ishikawa, L. Abraham, Application of modified electrochemical noise technique in Kuwaiti open cooling water system: Part II. On-site real time monitoring, *European Corrosion Congress, EUROCORR 2015*, 2015, pp. 1226-1237.
- [166] X. Guo, J. Huang, y. Qiu, Z. Dong, Analysis method for localized corroding based on electrochemistry noise, *Google Patents*, 2007.
- [167] R. Martin, Process for real-time detection and inhibition of localized corrosion, *Google Patents*, 2002.
- [168] K. Hladky, R. Wessels, Electrochemical noise as a localized corrosion indicator, *Google Patents*, 2010.
- [169] L. Han, X. Liu, Y. zhang, S. Xu, Dew point corrosion monitoring method based on electrochemical noise, *Google Patents*, 2014.
- [170] D.A. Eden, D.G. John, J.L. Dawson, Corrosion monitoring, *Google Patents*, 1992.
- [171] N. Marwan, M. Carmen Romano, M. Thiel, J. Kurths, Recurrence plots for the analysis of complex systems, *Physics Reports*, 438 (2007) 237-329.
- [172] C.L. Webber Jr, J.P. Zbilut, Dynamical assessment of physiological systems and states using recurrence plot strategies, *Journal of applied physiology*, 76 (1994) 965-973.
- [173] J.P. Zbilut, C.L. Webber, Embeddings and delays as derived from quantification of recurrence plots, *Physics letters A*, 171 (1992) 199-203.
- [174] N. Marwan, Encounters with neighbours: current developments of concepts based on recurrence plots and their applications, *Norbert Marwan*2003.

- [175] J.B. Gao, Recurrence time statistics for chaotic systems and their applications, *Phys Rev Lett*, 83 (1999) 3178-3181.
- [176] N. Marwan, J.F. Donges, Y. Zou, R.V. Donner, J. Kurths, Complex network approach for recurrence analysis of time series, *Physics Letters, Section A: General, Atomic and Solid State Physics*, 373 (2009) 4246-4254.
- [177] S. Boccaletti, V. Latora, Y. Moreno, M. Chavez, D.U. Hwang, Complex networks: Structure and dynamics, *Physics Reports*, 424 (2006) 175-308.
- [178] R. Gilmore, Topological analysis of chaotic time series, *Applications of Soft Computing* San Diego, CA, 1997, pp. 243-257.
- [179] J.P. Zbilut, C.L. Webber Jr, Embeddings and delays as derived from quantification of recurrence plots, *Physics Letters A*, 171 (1992) 199-203.
- [180] J.P. Zbilut, J.M. Zaldivar-Comenges, F. Strozzi, Recurrence quantification based Liapunov exponents for monitoring divergence in experimental data, *Physics Letters, Section A: General, Atomic and Solid State Physics*, 297 (2002) 173-181.
- [181] M. Thiel, M.C. Romano, J. Kurths, R. Meucci, E. Allaria, F.T. Arecchi, Influence of observational noise on the recurrence quantification analysis, *Physica D: Nonlinear Phenomena*, 171 (2002) 138-152.
- [182] C. Aldrich, L. Auret, Unsupervised process monitoring and fault diagnosis with machine learning methods, Springer 2013.
- [183] V. Venkatasubramanian, R. Rengaswamy, S.N. Kavuri, K. Yin, A review of process fault detection and diagnosis: Part III: Process history based methods, *Comput Chem Eng*, 27 (2003) 327-346.
- [184] W.L. Martinez, A.R. Martinez, A. Martinez, J. Solka, Exploratory data analysis with MATLAB, CRC Press 2010.
- [185] M.R. Malik, B.J. Isaac, A. Coussement, P.J. Smith, A. Parente, Principal component analysis coupled with nonlinear regression for chemistry reduction, *Combustion and Flame*, 187 (2018) 30-41.

- [186] T.A. Catelani, J.R. Santos, R.N.M.J. Páscoa, L. Pezza, H.R. Pezza, J.A. Lopes, Real-time monitoring of a coffee roasting process with near infrared spectroscopy using multivariate statistical analysis: A feasibility study, *Talanta*, 179 (2018) 292-299.
- [187] Z. Li, U. Kruger, X. Wang, L. Xie, An error-in-variable projection to latent structure framework for monitoring technical systems with orthogonal signal components, *Chemometrics and Intelligent Laboratory Systems*, 133 (2014) 70-83.
- [188] W. Ku, R.H. Storer, C. Georgakis, Disturbance detection and isolation by dynamic principal component analysis, *Chemometrics and Intelligent Laboratory Systems*, 30 (1995) 179-196.
- [189] P.B. Garcia-Allende, O.M. Conde, J. Mirapeix, A. Cobo, J.M. Lopez-Higuera, Quality control of industrial processes by combining a hyperspectral sensor and Fisher's linear discriminant analysis, *Sensors and Actuators B: Chemical*, 129 (2008) 977-984.
- [190] G. Dougherty, *Pattern recognition and classification: an introduction*, Springer Science & Business Media 2012.
- [191] L. Auret, C. Aldrich, Change point detection in time series data with random forests, *Control Engineering Practice*, 18 (2010) 990-1002.
- [192] L. Auret, C. Aldrich, Empirical comparison of tree ensemble variable importance measures, *Chemometrics and Intelligent Laboratory Systems*, 105 (2011) 157-170.
- [193] L. Breiman, Random Forests, *Mach. Learn.*, 45 (2001) 5-32.
- [194] D. Tax, *Ddtools: The Data Description Toolbox for MATLAB*, Version 2.1. 2, Delft University of Technology, Delft, Netherlands, (2015).
- [195] J. Yu, A nonlinear kernel Gaussian mixture model based inferential monitoring approach for fault detection and diagnosis of chemical processes, *Chem Eng Sci*, 68 (2012) 506-519.

[196] M.A.T. Figueiredo, A.K. Jain, Unsupervised learning of finite mixture models, IEEE Transactions on Pattern Analysis and Machine Intelligence, 24 (2002) 381-396.

Every reasonable effort has been made to acknowledge the owners of copyright material. I would be pleased to hear from any copyright owner who has been omitted or incorrectly acknowledged.

CHAPTER 4 CASE STUDY I

Y. Hou, C. Aldrich, K. Lepkova, L.L. Machuca, B. Kinsella, Monitoring of carbon steel corrosion by use of electrochemical noise and recurrence quantification analysis, *Corrosion Science*, 112, 63-72 (2016).

This chapter presents the published paper with modified formats and contents that match the overall style of the thesis.

Monitoring of Carbon Steel Corrosion by Use of Electrochemical Noise and Recurrence Quantification Analysis

Abstract

The corrosion of carbon steel in aqueous media resulting in uniform corrosion, pitting corrosion and passivation was investigated on a laboratory scale. Recurrence quantification analysis was applied to short segments of electrochemical current noise measurements. These segments were converted to recurrence variables, which could be used as reliable predictors in a multilayer perceptron neural network model to identify the type of corrosion. In addition, an automated corrosion monitoring scheme is proposed, based on the principal component scores of the recurrence variables. This approach used the uniform corrosion measurements as reference data and could differentiate between uniform and non-uniform corrosion.

Keywords: Carbon steel; Electrochemical noise; Pitting corrosion; Recurrence quantification analysis; Process monitoring; Neural networks

4.1 Introduction

It is well-established that corrosion is a major global problem causing damage in the order of hundreds of billions of dollars in the USA alone [1, 2] and damage on a similar scale in other developed economies. The most dangerous form of corrosion is localized, where unexpected, rapid damage to local metal structures can lead to catastrophic failure [3]. These failures are difficult to prevent, since localized corrosion is difficult to measure reliably, despite extensive investigation over many years. For example, although visual observation of weight-loss coupons used widely in industry can give an indication of the incidence of localized corrosion, these methods are very slow and cumbersome. Likewise, electrical resistance methods are also not particularly useful, as localized corrosion is often associated with negligible change on the electrical resistance of the metal. In contrast, methods based on electrochemical noise (EN) measurement have shown more promise as reliable indicators of localized corrosion [3-6].

Electrochemical noise can be ascribed to the formation of microcells on the surfaces of metals subject to corrosion. These microcells give rise to oscillating current and potentials that contain important information on the dynamics of the corrosion process [7, 8]. As a consequence, the detection of localized corrosion based on electrochemical noise measurements has been studied based on a number of different analytical approaches. These include statistical analysis of the data [9-11], Fast Fourier transforms, maximum entropy methods [12, 13] with power spectral density analysis, wavelet transforms [14] with transient analysis and energy distribution, phase space methods with correlation dimension [7, 15] and recurrence quantification analysis [8, 16-22].

Recurrence quantification analysis (RQA) in particular, is an emerging approach to the analysis of time series data. The RQA approach allows characterization of data by a similarity matrix, typically containing the Euclidean distances between subsequent measurements in the time series. A number of variables, such as recurrence ratio (RR), determinism (DET), entropy ($ENTR1$) and average diagonal line length (L_{mean}), can be derived from a binary or thresholded version of the similarity matrix. In previous studies [16-22], authors implied that recurrence ratio and determinism were related to the initiation rate and interaction time of microcells

on the metal respectively. The dynamics of uniform corrosion tends to be associated with higher recurrence ratio and low determinism value, while localized corrosion is characterised with low recurrence ratio and higher determinism. In spite of all the efforts of applying RQA to study corrosion dynamics based on EN data, recurrence variables have not been used for corrosion type identification and process monitoring.

Table 4-1 gives an overview of corrosion systems studied via RQA of electrochemical noise measurements. On the one hand, a large proportion of scholarly work has focused on the study of the corrosion of stainless steel using RQA. This is the first time a study applies RQA to corrosion processes at carbon steel. On the other hand, the authors mostly used the physical meanings of RQA variables *DET* and/or *RR* to indicate the dynamics of different corrosion stages or regimes.

Table 4-1: Recurrence quantification analysis of electrochemical noise in corrosion systems.

Variables	Corrosion System	References
<i>DET</i>	Analysis of electrochemical oscillations generated from pitting corrosion of copper in different saline solutions at various potentials	[8]
<i>DET</i>	Changes in the dynamics of corrosion fatigue in UNS S31603 stainless steel immersed in natural seawater	[16]
<i>DET, RR</i>	Protective effect of nanostructured films on austenitic stainless steel 304	[17]
<i>DET, ENTR1, RR</i>	Initiation, steady state progress and decay of pitting in austenitic stainless steel 316 in 300 mg/L of NaCl in deionized water	[18]
<i>DET, ENTR1, RR</i>	Intergranular corrosion of sensitized stainless steel UNS S30400 immersed in 0.5 M H ₂ SO ₄ & 0.01 M KSCN solution	[19]
<i>DET, RR</i>	Effect of hydrostatic pressure on corrosion of Ni-Cr-Mo-V stainless steel in a 3.5% NaCl solution	[20]
<i>DET, RR</i>	Effect of ultrasonic vibrational solidification treatment on corrosion of AZ80 Mg alloy	[21]
<i>D, R</i>	Carbon reinforcement steel in concrete exposed to a 3% NaCl solution	[22]

In this study, four RQA variables, i.e. *DET, ENTR1, RR, L_{mean}* are used simultaneously from the statistical point of view, rather than exploring the relationship of specific parameter(s) with corrosion processes. The automated corrosion monitoring scheme based on RQA variables and PCA model is established, aiming at detecting different corrosion mechanisms online. In addition, these variables are used as predictors in a neural network model to predict different corrosion behaviour in the steel.

4.2 Experimental work

The chemical composition of the carbon steel (1030) used in the experiments is as follows (wt.%): C (0.37), Mn (0.80), Si (0.282), P (0.012), S (0.001), Cr (0.089), Ni (0.012), Mo (0.004), Sn (0.004), Al (0.01), and Fe (balance). Two rectangular samples with surface area of $1.4\text{ cm} \times 1.5\text{ cm}$ were made from the same material and soldered with a conducting wire to each for electrical connection. Subsequently, the samples were electro-coated (Powercron 6000CX) and embedded in epoxy resin (Epofix), leaving 2.1 cm^2 of the steel surface exposed. The final shape of the sample is illustrated in Figure 4-1. Before tests, the exposed surfaces of the steel samples were abraded on silicon carbide paper up to 1200 grit, rinsed with ultra-pure water and ethanol and dried with nitrogen. This procedure was conducted prior to each run of the tests. The same set of steel samples with identical grinding procedures prior to each run were used in all the tests. After tests, the surfaces of the samples were examined for localized corrosion and the maximum pit depth was measured using optical 3D microscopy (Infinite focus microscope, Alicona Instruments, Austria).

Three test solutions were used, viz. 0.1 M sodium chloride (NaCl; Merck, 99.7%), 0.5 M sodium hydrogen carbonate (NaHCO_3 ; Merck, 99.7%), and a solution containing 0.45 M sodium hydrogen carbonate and 0.1 M sodium chloride ($0.45\text{ M NaHCO}_3 + 0.1\text{ M NaCl}$). These solutions were used to set up uniform corrosion, passivation and pitting systems, respectively. All the solutions were prepared with ultra-pure water (Milli-Q system, resistivity $18.2\text{ M}\Omega\text{ cm}$) and analytical reagents.

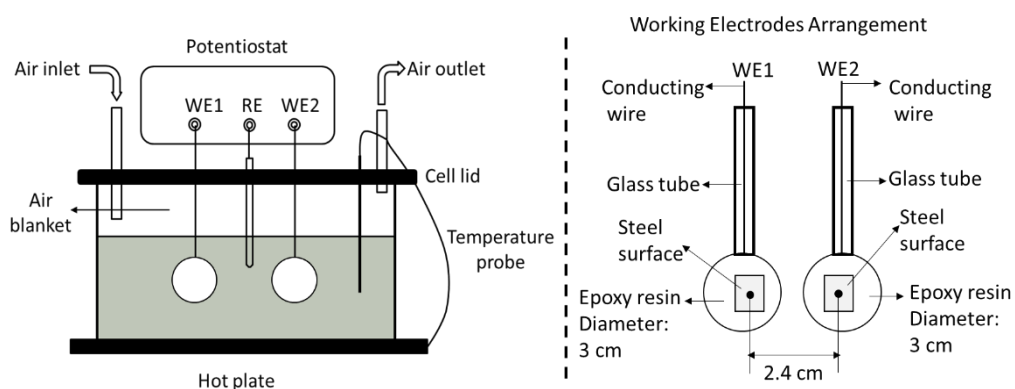


Figure 4-1: Experimental setup.

Electrochemical noise (EN) measurement were carried out in a configuration which is schematically shown in Figure 4-1. Two nominally identical aforementioned carbon steel samples were placed parallel to each other as working electrodes (WE 1 and WE 2). The inter-electrode spacing was fixed at 2.4 cm (centre-to-centre). In addition, a commercial Ag/AgCl electrode was used as reference electrode (single junction electrode placed in a capillary with a porous ceramic tip and filled with 3 M KCl solution designed to give a potential of 0.210 V against S.H.E). The current flowing through the two working electrodes was measured using a zero resistance ammeter mode (ZRA) of Gamry Reference 600 and the potential of the short-circuited WEs was measured with regard to the commercial reference electrode. ESA410 data acquisition software was employed to collect the EN data. The sampling rate was 2 Hz.

All the test solutions were air-saturated in a separate cell before pumping into the test cell equipped with the electrodes. During the tests, the temperature of the solution was controlled at 30 ± 1 °C by a hot plate with a temperature probe. The oxygen level in the solution was kept constant by continuously pumping air through the cell, creating an air blanket on top of the solution.

For uniform and passivation tests, the EN measurement started immediately after immersion of the test samples. After exposure to the test solutions, the samples were taken out of the test cell and rinsed immediately with ultra-pure water and ethanol, followed by drying with nitrogen gas. Afterwards, the surfaces of the two working electrodes were directly observed under optical microscope.

For pitting corrosion tests, the specimens were pre-passivated in 0.5 M NaHCO₃ solution for four hours (without EN recording), before NaCl was added to yield a solution of 0.45 M NaHCO₃ + 0.1 M NaCl. The EN signals were recorded immediately after the NaCl solution was added. The experimental conditions are summarized in Table 4-2. All the tests were done in duplicate. Potential and current noise were recorded simultaneously and the electrochemical current noise (ECN) was subjected to the analytical process described above. The electrochemical potential noise (EPN) signals were used as an indicator of the repeatability of the tests.

Table 4-2: Experimental conditions.

Corrosion Type	Solution	pH	Test Duration
Uniform	0.1 M NaCl	6.6	18 h
Pitting	0.45 M NaHCO ₃ +0.1 M NaCl	8.6	19 h
Passivation	0.5 M NaHCO ₃	8.4	2.5 h

4.3 Results and discussion

4.3.1 Electrochemical noise measurements

The electrochemical noise (EN) data (after linear detrending) associated with the three types of corrosion in Table 4-2 are shown in Figure 4-2 (a)-(c). The microscopic appearance of the same sample surface associated with three different types of corrosion is shown in Figure 4-2 (d)-(f). Amplified images of current and potential noise signals corresponding to the time intervals starting from vertical dashed lines in Figure 4-2 are displayed in Figure 4-3.

It can be seen from Figure 4-2 and Figure 4-3 that the electrochemical current and potential signals show different behaviours for different corrosion systems. During the test period for uniform corrosion, high frequency fluctuations were observed for both potential and current noise. The maximum amplitude for potential was 12 mV while that for current was around 15 μ A. The enlarged portion of EN signals presented in Figure 4-3 (a) shows no distinctive peaks. In the case of pitting corrosion, current noise fluctuated rapidly around zero with very small amplitude (approx. 0.02 μ A) for about seven hours. Afterwards, the current signal showed typical peaks for metastable pitting, i.e., sudden rise followed by exponential decline, as indicated in Figure 4-3 (b). The amplitude was increased to approximately 0.03 μ A at this stage. After 10 h of EN recording, the amplitude grew larger with a maximum value of 0.63 μ A. Potential noise showed similar patterns. It also should be noted that after pitting test, only one of the working electrodes was pitted. The maximum pit depth measured was 55 μ m. But the other working electrode had a passive-like appearance. In contrast, for

passivation system, the EN signals fluctuated with a relatively lower frequency with amplitudes no more than $0.02 \mu\text{A}$ and 2 mV , respectively.

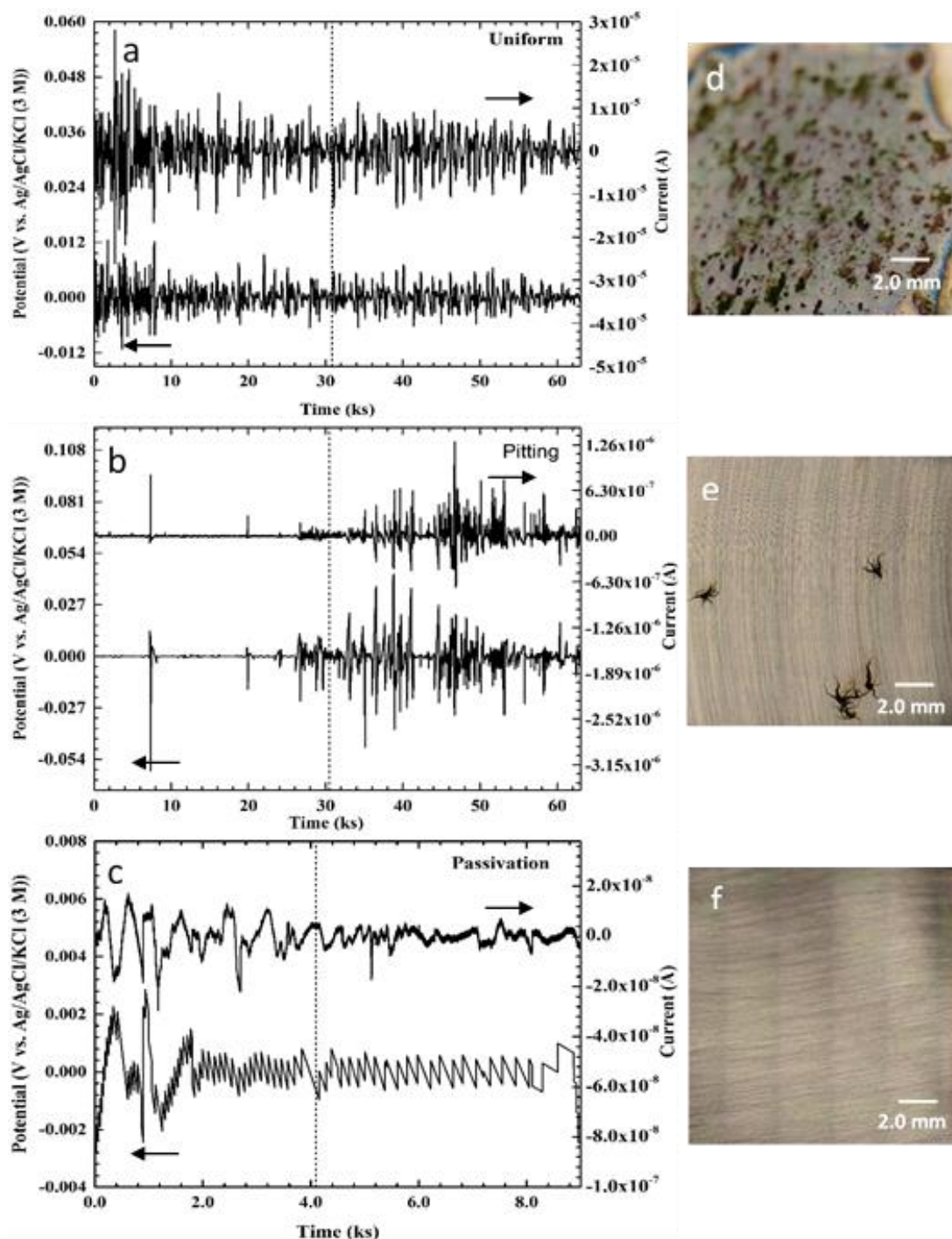


Figure 4-2: Electrochemical potential (bottom line) and current (top line) noise signals and associated appearance of steel surfaces for three types of corrosion (a, d) uniform (b, e) pitting (c, f) passivation.

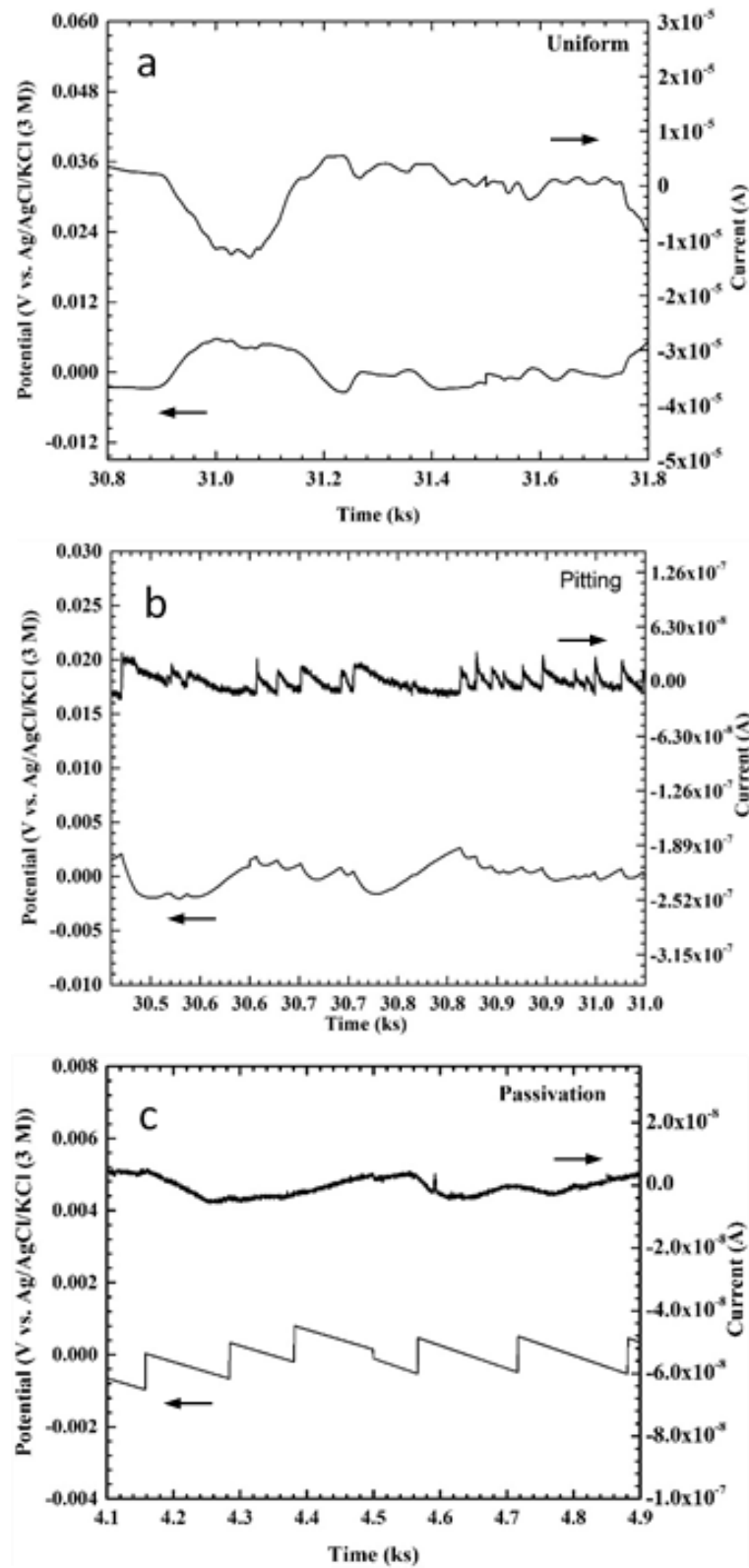


Figure 4-3: Enlarged portions of marked areas in Figure 4-2 (a) Uniform corrosion (b) Pitting (c) Passivation.

The recurrence plots of the signals are shown in Figure 4-4. The ECN data for uniform corrosion, pitting and passivation is chopped into 70, 75 and 10 non-

overlapping time series segments respectively. Each of the segments contains 1800 data points. The threshold used to generate the RPs is 0.2σ , where σ refers to the standard deviation of individual current noise data segments. Four randomly selected RPs from the uniform corrosion process are given in the top row of the figure, to give an indication of the recurrence structures and their variation. Likewise, the images in the second and third rows represent the recurrence plots for pitting corrosion and passivation respectively.

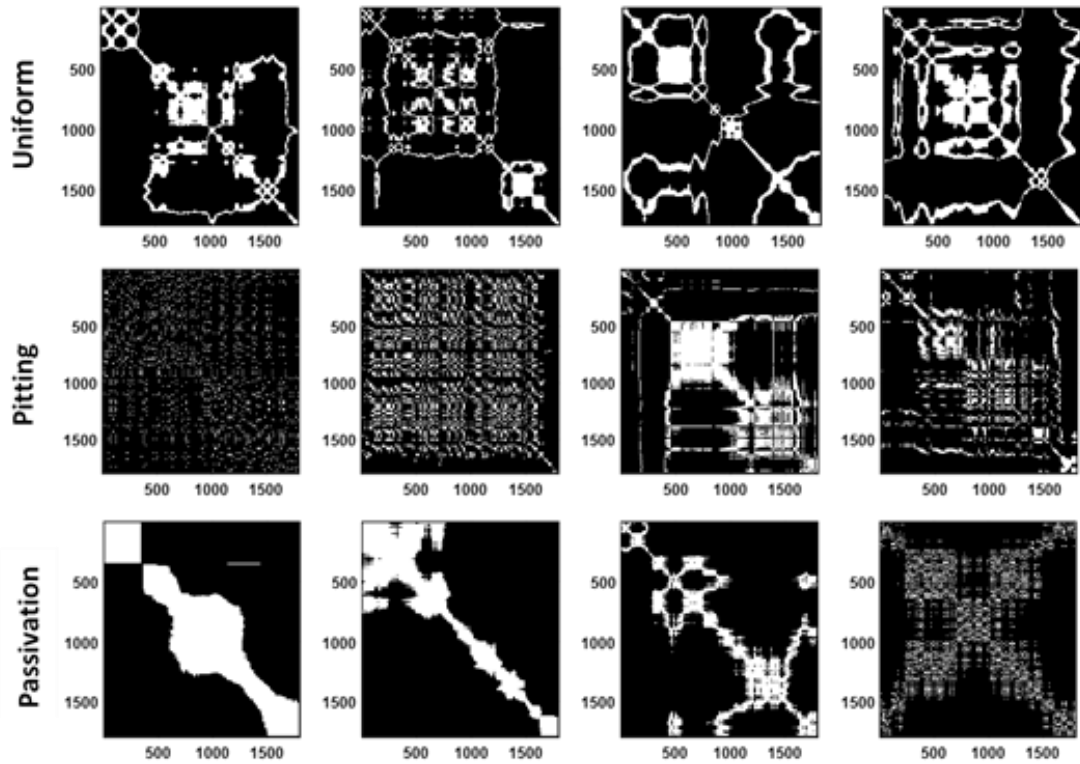


Figure 4-4: Recurrence plots for different current data segments of three corrosion types, i.e., uniform (first row), pitting (second row) and passivation (third row).

The calculated RQA variables (variable numbers 1, 2, 3 and 5 shown in Table 3-1) for the different corrosion systems are shown in Figure 4-5. The vertical lines separate the three different corrosion systems, i.e. uniform corrosion, pitting corrosion and passivation, from left to right. It is indicated that, in the studied systems, *DET* and *ENTR1* were capable of distinguishing different corrosion types to some extent. For example, the *ENTR1* values fluctuate between 0 and 2 for uniform corrosion, while that for pitting corrosion are located in the range of -2 to 0. It is difficult, however, to distinguish passivation from pitting. Apparently, *RR* had no capability to discriminate different corrosion systems since all the values fluctuated at around zero. L_{mean} is

similar to RR , but to some extent, L_{mean} performs better in the separation of uniform and pitting corrosion.

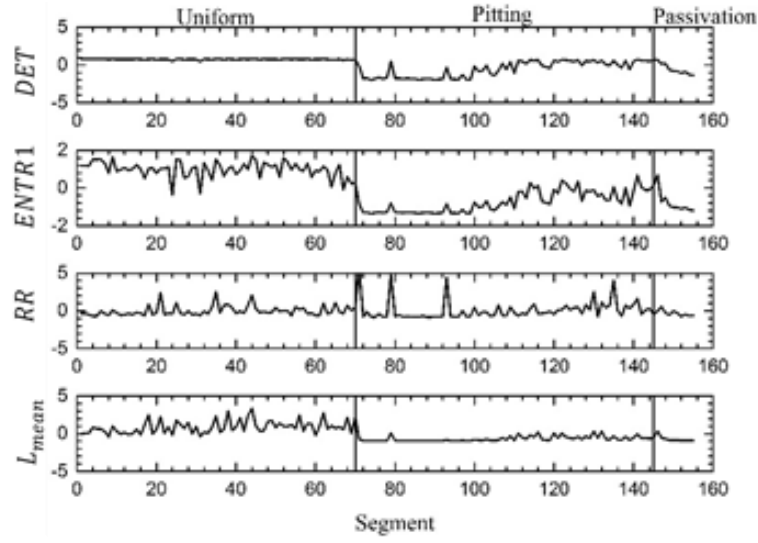


Figure 4-5: Line plots of the zero mean, unit variance scaled values DET , $ENTR1$, RR and L_{mean} (from top to bottom). The vertical lines separate uniform corrosion, pitting corrosion and passivation, from left to right.

The correlational structure of the four variables is shown in Table 4-3. The values in the table represent the linear correlation coefficients between any two variables. This can be calculated from equation

$$r = \frac{cov(X, Y)}{\sigma_X \sigma_Y} \quad (4-1)$$

Where X and Y represent any two RQA variable vectors, $cov(\cdot)$ calculates the covariance between these two vectors, σ_X and σ_Y are the standard deviations of X and Y , and r is the correlation coefficient of these two RQA variables. Since it has been mentioned before that the four RQA variables formed a data matrix \mathbf{Q} , the actual calculation was conducted on \mathbf{Q} using a simple Matlab code.

Table 4-3: Correlation among four RQA variables.

Variables	<i>DET</i>	<i>ENTR1</i>	<i>RR</i>	<i>L_{mean}</i>
<i>DET</i>	1	0.816	0.339	0.550
<i>ENTR1</i>	0.816	1	0.126	0.638
<i>RR</i>	0.339	0.126	1	0.319
<i>L_{mean}</i>	0.550	0.638	0.319	1

It can be seen from Table 4-3, *DET* is strongly correlated with *ENTR1*, indicating that the information contained in **Q** is redundant. In order to reduce the redundancy, principal component analysis (PCA) was conducted on **Q** to extract its principal components (PC). Finally, the first two scores of the corresponding PCs were retained as they collectively explained approximately 89% of the variance of **Q**.

Figure 4-6 shows the scatter plot of the principal component scores for each of the three corrosion systems. Where t_1 and t_2 are the scores of the first two PCs. The percentage of variance explained by each PC is 66.6% and 22.7% respectively. Uniform corrosion appears to be clearly distinguishable from the other two systems, yet it is not possible to discriminate between passivation and pitting corrosion.

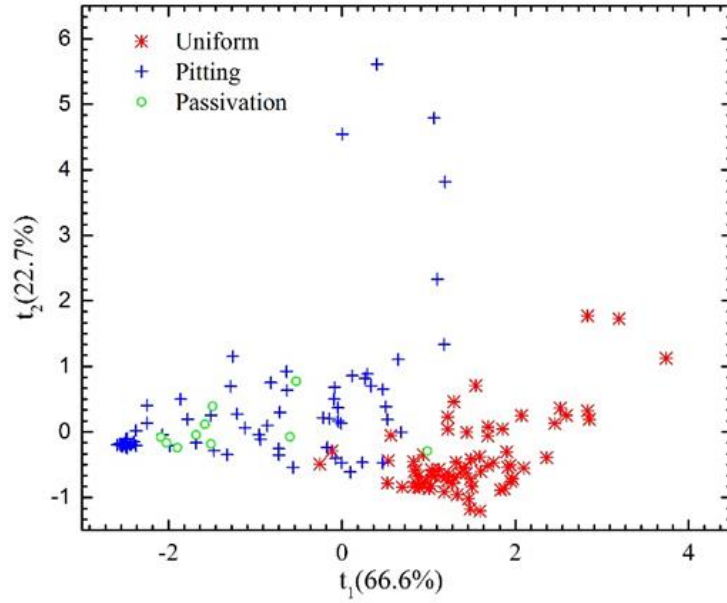


Figure 4-6: Principal component score plot of three corrosion types.

Although Figure 4-5 and Figure 4-6 give some indication of the ability of the variables to discriminate between the different types of corrosion, further quantitative analysis was done by constructing a multilayer neural network model to classify the data, as shown in Figure 4-7. The input layer of the network consisted of four nodes associated with four predictor variables. The hidden layer consisted of 8 nodes, while the output layer had three nodes, since the three different output classes (corrosion types), were coded in a [1 0 0; 0 1 0; 0 0 1] format. Both the hidden and output nodes had bipolar sigmoidal activation functions (*tansig*) and the Levenberg-Marquardt algorithm was used to train the network in Matlab 14b with a cross-entropy error function.

The training data (70 samples from the uniform corrosion system, 75 samples from the pitting corrosion system and 10 samples from the passivation system) were randomly divided between a training data set (60% of the samples), and a validation and test data set, each containing 20% of the samples. The training and validation data sets were used during the construction of the classification models, while the test data served as an independent data set to assess the performance of the trained models.

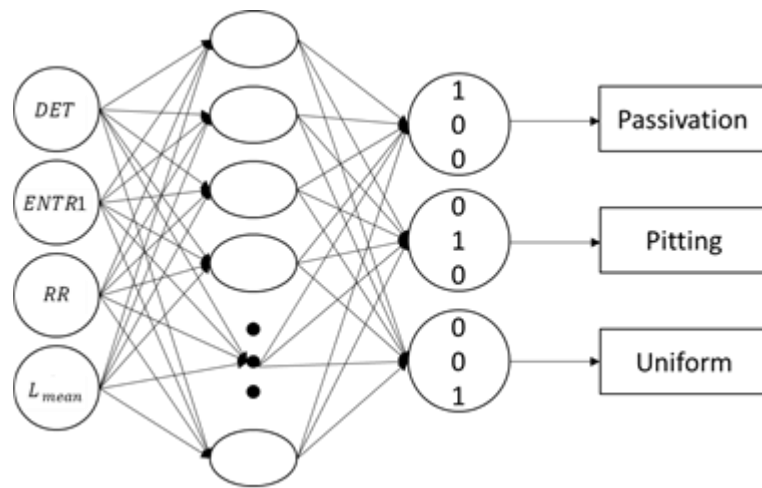


Figure 4-7: Architecture of two-layer feed-forward neural network.

The results are shown in the so-called confusion matrix in Figure 4-8, where classes 1, 2 and 3 correspond with passivation, pitting corrosion and uniform corrosion, respectively. The test data were not used in the development of the model and is used as an indication of the generalized performance of the trained neural network. From Figure 4-8, it can be seen that there were 31 samples in the test set, of which 3 belonged to Class 1, 13 to Class 2 and 15 to Class 3. The neural network was unable to identify Class 1 reliably and misallocated 2 of the 3 samples to Class 2. These results are consistent with the information shown in Figure 4-6, where it is clear that it would be difficult to discriminate between Classes 1 and 2. The overall accuracy of the model was 93.5%. However, since the data sets used in this model were relatively small, especially the data set associated with passivation, these results should be interpreted as indicative only.

Predicted Corrosion Type	1	0	0	100%
	2	13	0	86.7%
	3	0	15	100%
				93.5%
	1	2	3	
	Real Corrosion Type			

Figure 4-8: Confusion matrix for the test data set consisting of 31 samples (Class 1 = passivation, Class 2 = pitting and Class 3 = uniform corrosion).

The significance of the predictor variables in the classification model could also be assessed. This was done by training a multilayer perceptron as before, but with five predictor variables. Four of these were the recurrence variables, DET , $ENTR1$, RR and L_{mean} and the fifth was a random variable with no predictive power. This variable was used to assess the statistical significance of the recurrence variables, as discussed in [24-26].

In the analysis, the classification model was interrogated by repeatedly randomizing each of the predictor variables, one at a time and observing the deterioration of the performance of the model in each case. The results are shown in the variable importance plot in Figure 4-9.

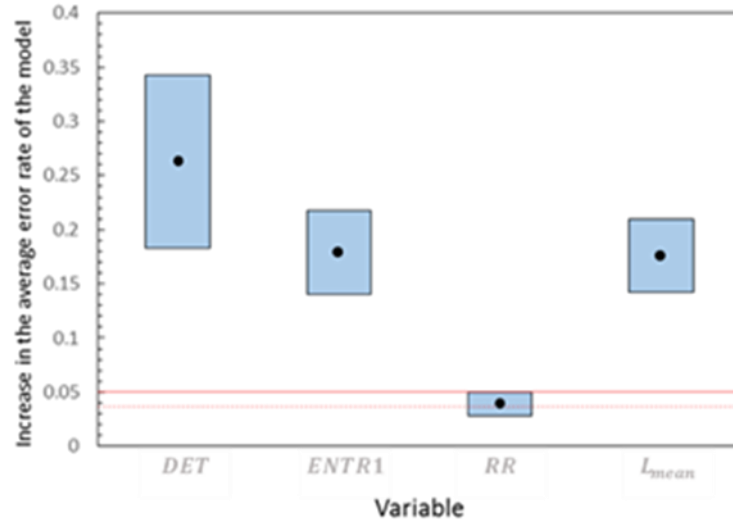


Figure 4-9: Variable importance plot of the recurrence predictor variables in the three corrosion systems.

The black dots in the figure show the average increase in the error rates of the model (in this case based on 30 runs or variable permutations). The top of each box shows the mean value plus three standard deviations, while the bottom of each box indicates the mean value minus three standard deviations. The broken and solid horizontal lines indicate the 95% and 99% significance levels of the increases in the errors, as determined by the dummy (random) variable that was included with the model and discussed in [26]. According to this plot, determinism (*DET*) played the most important role in discriminating between the three corrosion systems, while the recurrence rate (*RR*) did not play a statistically significant role.

4.3.2 Application of corrosion monitoring scheme

The efficacy of the corrosion monitoring scheme is illustrated by the data in Figure 4-10. It is essentially the same as Figure 4-6, except that the data representing uniform corrosion or normal operating conditions have been delineated with a 95% control limit based on the use of a five-Gaussian mixture model.

The first two principal components accounted for 89.3% of the variance of the variables and as indicated, this map can be used in the online monitoring of the corrosion of the system.

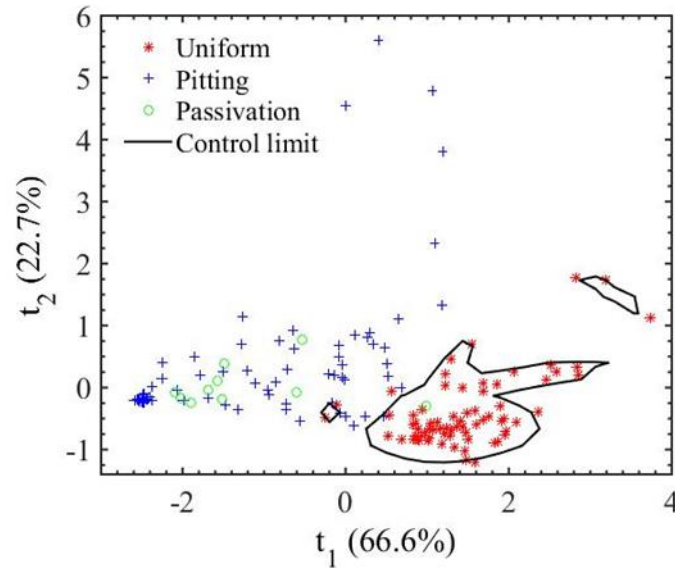


Figure 4-10: Principal component score plot showing uniform corrosion (*) as normal operating conditions and pitting corrosion (+) and passivation (o) as fault conditions.

Some suggestions for other interested researchers towards using the proposed techniques:

- Firstly, the EN data should be recorded continuously under normal operation conditions, i.e. non-localized corrosion conditions, for a sufficient time depending on the actual corrosion system and sampling rate. Ideally, it is better to collect as many data as possible in this condition for computation of a reliable control limit.
- There are no strict rules regarding the choice of sampling rate. Users could customise their own sampling rate as they deem appropriate for the corrosion process under study. However, it is recommended to use a sampling rate of more than 1 Hz.
- After collection of the EN data, users need to decide how many data points there should be contained in each segment. In principle, the length of the time series segment should be sufficient to capture characteristic fluctuations or periodic behaviour in the time series. This can be estimated from the autocorrelation function or the average mutual information of the time series. The point where the autocorrelation function reaches its first minimum value or point of decorrelation, can be used as an indication of

the minimum length of the time series segment (see for example [27, 28], where the same principle is applied to the phase space embedding of time series data).

- After calculating the control limit for normal operation conditions according to the procedures proposed in this paper, users could then record EN data under different test conditions either continuously or intermittently. The sampling rate and the number of points in the new segment should be identical to those used for the normal operating conditions. If the data projected onto the map falls outside the normal operation condition control limit, a potential fault condition is flagged.

4.4 Summary

In this study, the corrosion tests with carbon steel in three different conditions have indicated that the corrosion monitoring map generated based on the use of recurrence quantification analysis and principle component analysis appears to be a promising approach for continuous corrosion process monitoring. New electrochemical noise measurements can be projected onto the map continuously and will be flagged as potential fault conditions if these projections are located outside the boundaries.

It should be pointed out that there are still some issues in need of further investigation. Firstly, the proposed method is not based on any fundamental physical or chemical models at work. The corrosive effects of the different environments to which the steel samples were exposed could not be studied quantitatively and more reliable corrosion data are needed. Secondly, it requires the user to be experienced in deciding when normal conditions prevail, as they are used as a benchmark for the identification of fault or abnormal conditions. Finally, the present monitoring map could not distinguish between passivation and pitting, and this needs to be improved, for example, by considering the use of additional recurrence quantification variables.

However, despite these minor issues, it is possible to promote the automation of corrosion monitoring in industry if the proposed method is carefully used.

References

- [1] P. Bai, H. Zhao, S. Zheng, C. Chen, Initiation and developmental stages of steel corrosion in wet H₂S environments, *Corros Sci*, 93 (2015) 109-119.
- [2] N.A. Hoog, M.J.J. Mayer, H. Miedema, R.M. Wagterveld, M. Saakes, J. Tuinstra, W. Olthuis, A. van den Berg, Stub resonators for online monitoring early stages of corrosion, *Sensors and Actuators B: Chemical*, 202 (2014) 1117-1136.
- [3] Y.J. Tan, Sensing localised corrosion by means of electrochemical noise detection and analysis, *Sensor Actuat B-Chem*, 139 (2009) 688-698.
- [4] A.M. Homborg, T. Tinga, X. Zhang, E.P.M. van Westing, P.J. Oonincx, G.M. Ferrari, J.H.W. de Wit, J.M.C. Mol, Transient analysis through Hilbert spectra of electrochemical noise signals for the identification of localized corrosion of stainless steel, *Electrochimica Acta*, 104 (2013) 84-93.
- [5] E.C. Rios, A.M. Zimer, P.C.D. Mendes, M.B.J. Freitas, E.V.R. de Castro, L.H. Mascaro, E.C. Pereira, Corrosion of AISI 1020 steel in crude oil studied by the electrochemical noise measurements, *Fuel*, 150 (2015) 325-333.
- [6] A.M. Homborg, E.P.M. van Westing, T. Tinga, X. Zhang, P.J. Oonincx, G.M. Ferrari, J.H.W. de Wit, J.M.C. Mol, Novel time-frequency characterization of electrochemical noise data in corrosion studies using Hilbert spectra, *Corros Sci*, 66 (2013) 97-110.
- [7] A. Legat, J. Osredkar, V. Kuhar, M. Leban, Detection of various types of corrosion processes by the chaotic analysis of electrochemical noise, *Mater Sci Forum*, 289-2 (1998) 807-811.
- [8] E. Cazares-Ibanez, G.A. Vazquez-Coutino, E. Garcia-Ochoa, Application of recurrence plots as a new tool in the analysis of electrochemical oscillations of copper, *J Electroanal Chem*, 583 (2005) 17-33.
- [9] Y.F. Cheng, M. Wilmott, J.L. Luo, The role of chloride ions in pitting of carbon steel studied by the statistical analysis of electrochemical noise, *Appl Surf Sci*, 152 (1999) 161-168.

- [10] G. Suresh, U.K. Mudali, Electrochemical noise analysis of pitting corrosion of type 304L stainless Steel, *Corrosion*, 70 (2014).
- [11] N. Upadhyay, M.G. Pujar, C.R. Das, C. Mallika, U.K. Mudali, Pitting corrosion studies on solution-annealed borated type 304L stainless steel using electrochemical noise technique, *Corrosion*, 70 (2014) 781-795.
- [12] C.A. Loto, Electrochemical noise measurement technique in corrosion research, *Int J Electrochem Sc*, 7 (2012) 9248-9270.
- [13] R. Zhao, S.Z. Song, Electrochemical potential noise analysis of 304 stainless steel weld zone exposed to alkaline solutions by different parameters, *Appl Mech Mater*, 331 (2013) 469-473.
- [14] A. Aballe, M. Bethencourt, F.J. Botana, M. Marcos, J.M. Sanchez-Amaya, Use of wavelets to study electrochemical noise transients, *Electrochim Acta*, 46 (2001) 2353-2361.
- [15] D.H. Xia, S.Z. Song, J.H. Wang, J.B. Shi, H.C. Bi, Z.M. Gao, Determination of corrosion types from electrochemical noise by phase space reconstruction theory, *Electrochem Commun*, 15 (2012) 88-92.
- [16] N. Acuna-Gonzalez, E. Garcia-Ochoa, J. Gonzalez-Sanchez, Assessment of the dynamics of corrosion fatigue crack initiation applying recurrence plots to the analysis of electrochemical noise data, *Int J Fatigue*, 30 (2008) 1211-1219.
- [17] C. Lopez-Melendez, E.M. Garcia-Ochoa, M.I. Flores-Zamora, R.G. Bautista-Margulis, C. Carreno-Gallardo, C.P.C. Morquecho, J.G. Chacon-Nava, A. Martinez-Villafane, Dynamic study of current fluctuations of nanostructured films, *Int J Electrochem Sc*, 7 (2012) 1160-1169.
- [18] L.S. Montalban, P. Henttu, R. Piche, Recurrence quantification analysis of electrochemical noise data during pit development, *Int J Bifurcat Chaos*, 17 (2007) 3725-3728.

- [19] E. Garcia-Ochoa, J. Gonzalez-Sanchez, N. Acuna, J. Euan, Analysis of the dynamics of Intergranular corrosion process of sensitised 304 stainless steel using recurrence plots, *J Appl Electrochem*, 39 (2009) 637-645.
- [20] Y.E. Yang, T. Zhang, Y.W. Shao, G.Z. Meng, F.H. Wang, Effect of hydrostatic pressure on the corrosion behaviour of Ni-Cr-Mo-V high strength steel, *Corros Sci*, 52 (2010) 2697-2706.
- [21] T. Sun, Z.Y. Wang, J. Li, T. Zhang, Effect of ultrasonic vibration solidification treatment on the corrosion behavior of AZ80 magnesium alloy, *Int J Electrochem Sc*, 8 (2013) 7298-7319.
- [22] E. Garcia-Ochoa, F. Corvo, Using recurrence plot to study the dynamics of reinforcement steel corrosion, *Prot Met Phys Chem+*, 51 (2015) 716-724.
- [23] J.B. Gao, H.Q. Cai, On the structures and quantification of recurrence plots, *Phys Lett A*, 270 (2000) 75-87.
- [24] C. Aldrich, L. Auret, Fault detection and diagnosis with random forest feature extraction and variable importance methods, in: *IFAC Proceedings Volumes (IFAC-PapersOnline)*, 2010, pp. 79-86.
- [25] L. Auret, C. Aldrich, Empirical comparison of tree ensemble variable importance measures, *Chemometrics and Intelligent Laboratory Systems*, 105 (2011) 157-170.
- [26] L. Auret, C. Aldrich, Interpretation of nonlinear relationships between process variables by use of random forests, *Miner Eng*, 35 (2012) 27-42.
- [27] J.P. Barnard, C. Aldrich, M. Gerber, Identification of dynamic process systems with surrogate data methods. *AIChE J*, 47(9) (2001) 2064-2075.
- [28] C. Aldrich, B.C. Qi, P.J. Botha, Analysis of electrochemical noise with phase space methods. *Miner Eng*, 19(14) (2006) 1402-1409.

CHAPTER 5 CASE STUDY II

Y. Hou, C. Aldrich, K. Lepkova, L.L. Machuca, B. Kinsella, Application of electrochemical noise technique to monitor carbon steel corrosion under sand deposit, paper no. 9103, NACE International Corrosion Conference Series, 2017.

This chapter presents the published paper with modified formats and contents that match the overall style of the thesis.

Application of Electrochemical Noise Technique to Monitor Carbon Steel Corrosion under Sand Deposit

Abstract

The corrosion process of carbon steel in the presence of silica sand deposit in chloride-containing solution at 30 °C was monitored by use of electrochemical noise (EN). Noise resistance calculated from EN was compared with the polarization resistance obtained from conventional corrosion monitoring techniques, such as linear polarization resistance (LPR) and electrochemical impedance spectroscopy (EIS). Recurrence quantification analysis (RQA) was employed to characterize the current noise data associated with different corrosion types and the extracted variables were used for UDC process monitoring. After tests, the corroded steel surfaces were examined using a 3D profilometry to gather information about localized defects. The results demonstrated that electrochemical noise associated with recurrence quantification analysis is a useful tool for monitoring localized corrosion of under deposit corrosion.

Keywords: Carbon steel; Sand deposit; Electrochemical noise; Corrosion monitoring; Recurrence quantification analysis

5.1 Introduction

It is well known that the presence of accumulated sand, debris, biofilm and carbonate species on the bottom of oil and gas pipelines can cause severe localized corrosion, viz. under deposit corrosion (UDC). Monitoring of corrosion processes under deposits could provide valuable information for the development of mitigation programs. However, since UDC often occurs in the form of pitting [1-3], the conventional electrochemical methods such as linear polarization resistance (LPR), electrochemical impedance spectroscopy (EIS) and electrical resistance (ER) may not be particularly useful for early detection and continuous monitoring of localized corrosion, due to the negligible change in resistances associated with pitting. In contrast, methods based on electrochemical noise have been reported as promising indicators of localized corrosion [4-7].

Electrochemical noise (EN) can be ascribed to the formation of micro-cells on the surfaces of metals subject to corrosion. These microcells give rise to oscillating current and potentials that contain important information on the dynamics of the corrosion process [8]. The analysis of EN data relies on two main aspects – determination of electrochemical noise resistance (R_n) and identification of various corrosion types [9]. The electrochemical noise resistance R_n is commonly determined as the standard deviation of potential divided by the standard deviation of current, and it is considered to be equivalent to the polarization resistance. Therefore, it can be used for estimating the general corrosion rate. The derivation of information regarding the corrosion types from EN measurement has attracted even more attention. A number of analytical approaches have been proposed, including fast Fourier transforms, maximum entropy methods based power spectral density analysis [10], wavelet transforms [11], transient analysis [5, 12-13], chaos analysis [14-17] and recurrence quantification analysis [18-22].

Recurrence quantification analysis, in particular, is an emerging approach for studying the dynamics of time series data. It is based on the quantification of a so-called recurrence plot that typically contains the Euclidean distances between measurements in the time series. A number of variables can be extracted from the recurrence plot [23]. Among them, recurrence rate and determinism are frequently used in corrosion studies. It is reported that the dynamics of uniform corrosion tends

to be associated with a higher recurrence rate and a low determinism value, while localized corrosion is characterized with lower recurrence rate and higher determinism [24]. Despite its promise, the recurrence quantification analysis has not yet been used in the study of EN data obtained from UDC processes.

In order to determine if the EN technique associated with recurrence quantification analysis can be used to study and monitor UDC processes, carbon steel covered with a sand deposit, immersed in 0.1 M NaCl solution was chosen as the corrosion system to be studied. The calculated noise resistance R_n was compared with R_p from LPR and R_{ct} from EIS measurements. In addition, recurrence quantification analysis was performed on the electrochemical current noise data. Four variables viz. recurrence rate (RR), determinism (DET), entropy (ENTR) and trapping time (TT) were extracted. These variables were used to characterize and monitor the corrosion process.

5.2 Experimental procedure

5.2.1 Test materials and procedures

The test samples were made of carbon steel 1030 with a dimension of 1.4 x 1.5 x 0.5 cm³. The chemical composition of the steel is as follows (by weight %): C (0.30%), Mn (0.80%), Si (0.25%), S (<0.01%), P (0.01%), Ni (<0.01%), Cr (<0.01%), Mo (<0.01%), Cu (<0.01%), V (<0.01%) and Fe (balance). The samples were electro-coated, leaving 2.1 cm² of the surface exposed. Afterwards, the exposed surface was ground and polished using SiC paper to 1200 grit, rinsed with ultrapure water and AR grade ethanol and finally dried with nitrogen prior to testing.

Silica sand was used as a deposit. It was acid washed and dried in an oven prior to use. The thickness of the sand layer covering the sample surface was maintained at 8 mm. Specifically, The samples were placed in a glass sample holder with working surfaces facing upwards. Then the silica sand was gradually added to the samples holder and carefully flattened using fingers, until the top of the sand layer was about 8 mm above the surface of the steel sample. The sand loaded holder was placed in the test cell (as shown in Figure 5-1) before the test solution was transferred into the cell using a pump.

The test solution composed of 0.1 M sodium chloride (NaCl; Merck, 99.7%), was prepared with ultrapure water and air saturated using an air pump before transferring it into the test cell. An air blanket was created in the cell above the water level and the temperature of the solution was controlled at 30 °C using a hotplate. All tests were carried out under stagnant conditions.

5.2.2 Electrochemical measurements

Electrochemical noise (EN) measurement was carried out in the configuration shown in Figure 5-1. Two of the carbon steel samples, i.e. working electrodes WE1 and WE2, were placed in glass sample holders (facing upwards and parallel to each other) and covered with sand deposit. The inter-electrode spacing was fixed at approximately 3 cm (centre-to-centre). A commercial Ag/AgCl (3 M KCl) electrode was used as reference electrode. The current flowing through the two working electrodes was measured using a Gamry Reference 600 operating in the zero resistance ammeter (ZRA) mode. The potential of the short-circuited WEs was measured with respect to the same reference electrode as used in LPR and EIS measurements. ESA410 data acquisition software was used to collect the EN data. The sampling rate was 2 Hz and the EN data were continuously recorded for 14 days.

Linear polarization resistance (LPR) measurements and potentiostatic electrochemical impedance spectroscopy (EIS) were carried out in a similar configuration, except for the electrodes with only one steel sample covered with sand deposit used as working electrode and a platinum-coated titanium mesh served as the counter electrode. An Ag/AgCl (3 M KCl) electrode was also employed as the reference electrode. The measurements were obtained with a Bio-logic VMP3 multi-channel potentiostat/galvanostat/ZRA. For LPR, the potential range of ± 10 mV against open circuit potential (OCP) was applied with a scan rate of 0.167 mV/s. For EIS, a frequency range of 10 mHz to 10 kHz at 10 points per decade was employed and the AC excitation amplitude was 10 mV vs. OCP. The samples were allowed to rest for 6 h before the first LPR was performed, followed by EIS measurement. During 14 days of testing, LPR and EIS were carried out every 6 h and OCP was recorded during the intervals. There was a 10 min rest between the LPR and EIS measurements. In addition, two samples covered with sand without electrical connections were also

placed in the test cell to conduct microscopy analysis. One of them was taken out after 7 days and the other one was taken out after 14 days, when the test was completed.

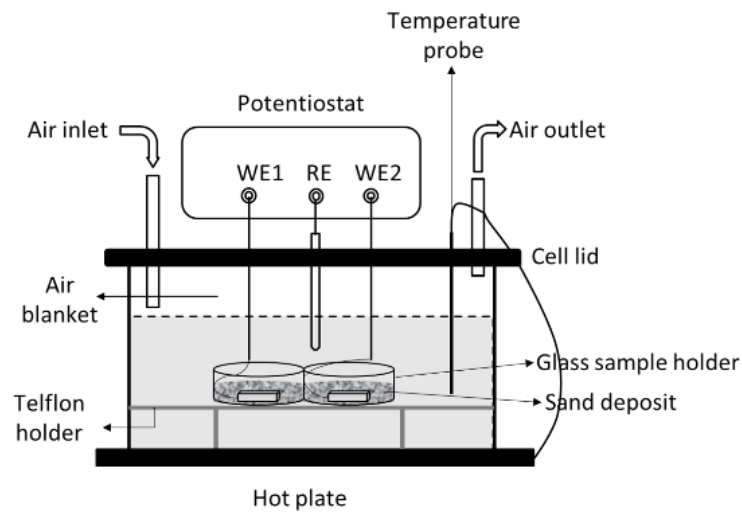


Figure 5-1: Diagrammatic configuration for electrochemical noise measurement.

5.2.3 Surface analysis

After tests, all the samples were flushed with ultrapure water and AR grade ethanol to remove the sand and loose corrosion products. This was followed by immersion in Clarke solution for 30 seconds to remove possible adherent corrosion products on the steel surface. Finally, the samples were dried with nitrogen and stored in a desiccator under vacuum until further analysis.

Visible light microscopy (infinite focus microscope, Alicona instruments) was conducted to characterize the surface morphology of steel samples. Surface profiles of the samples were acquired with the Alicona Infinite Focus software 5.1.

5.3 Results and discussion

5.3.1 Open circuit potential

The open circuit potential was recorded during the interval of the LPR and EIS measurement cycle. The average value recorded during the interval is shown in Figure 5-2. It can be seen that the OCP rapidly decreased during the first day and then gradually increased to the starting level after four days of immersion. Afterwards, the OCP slowly increased at a lower rate from day 5 to day 14.

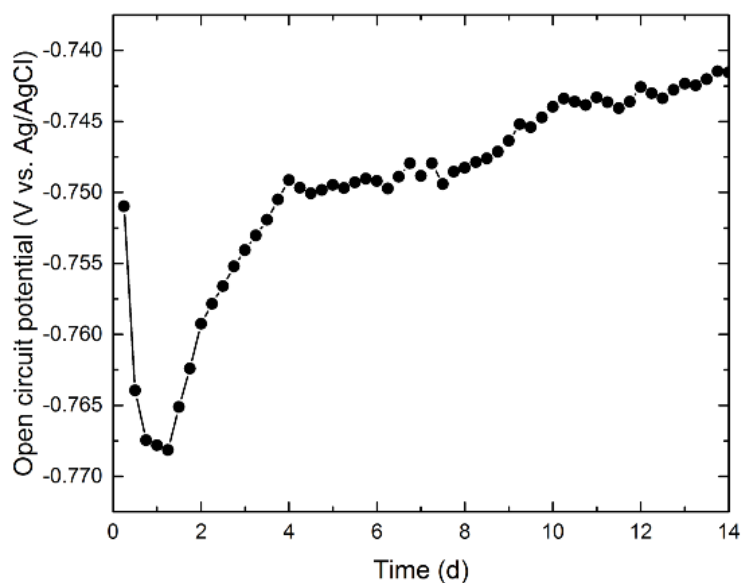


Figure 5-2: Variation of the average open circuit potential with time for carbon steel covered with sand deposit and immersed in 0.1 M NaCl solution.

5.3.2 Electrochemical impedance measurements

Figure 5-3 shows the Nyquist plots and Bode plots obtained from EIS performed on days 1, 4, 7 and 14. The EIS measurements were performed every six hours during 14 days of immersion. Figure 5-3 only shows typical results. The equivalent circuit used for fitting the EIS data is shown as the inset of Figure 5-3 (a). Although after 7 days immersion, corrosion products formed between the sand layer and steel surface, the scale was not sufficient to produce a second constant phase element. Therefore, it was decided to use the simple Randles circuit to fit all the EIS data. The circuit elements are solution resistance (R_s), charge transfer resistance (R_{ct}) and a constant phase element (CPE) that represents the interfacial capacitance [2]. The CPE was used because of the non-ideal frequency response observed in the Nyquist plots (Figure 5-3 (a)), which can be attributed to the non-homogeneity of the steel surface [25]. The fitted parameters, R_s , R_{ct} and n^* are shown in Table 5-1, where n^* is the exponent for the constant phase element.

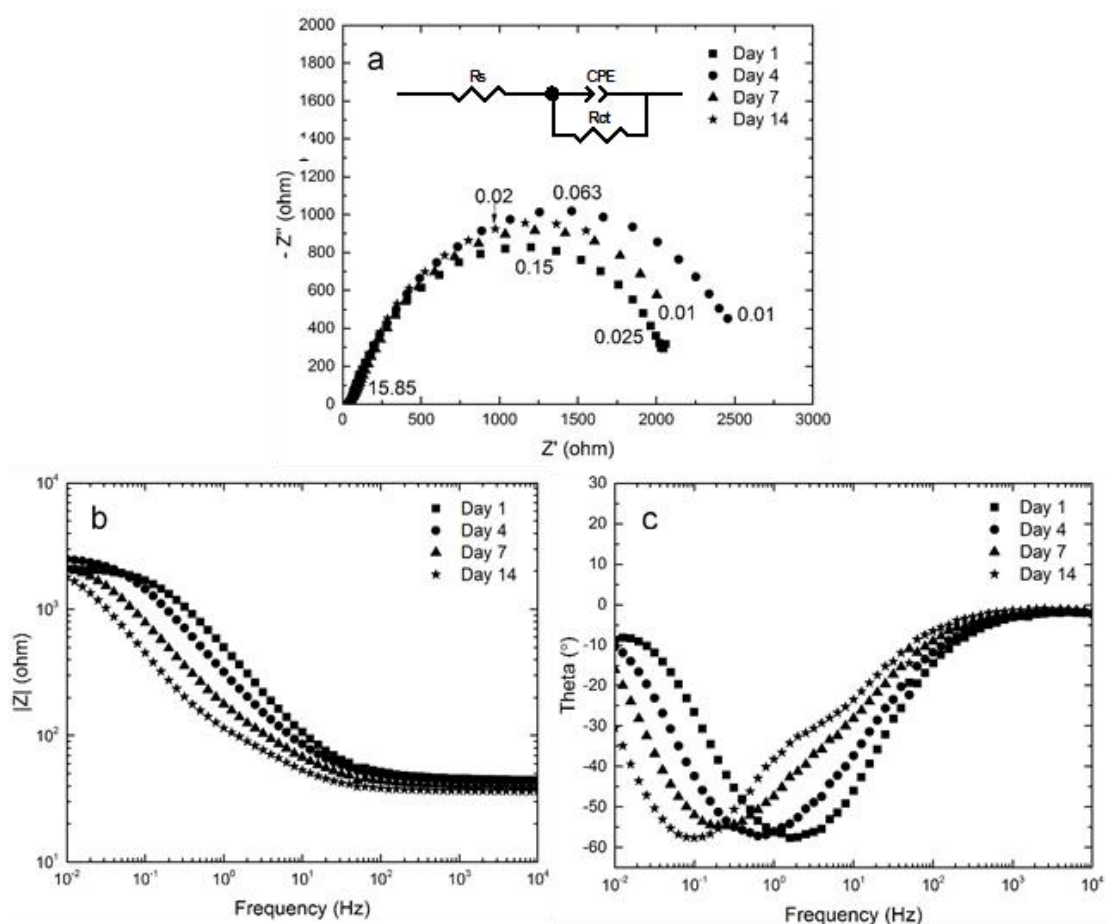


Figure 5-3: Impedance spectra of sand-covered steel surfaces immersed in 0.1 M NaCl solution on days 1, 4, 7 and 14.

Table 5-1: Electrochemical parameters derived from impedance analysis of carbon steel immersed in 0.1 M NaCl solution for 1, 4, 7 and 14 days with sand deposit.

Time	R_s ohm	R_{ct} ohm	Error %	n^*
Day 1	45.30	2208	0.59	0.80
Day 4	42.77	2986	1.92	0.74
Day 7	79.75	2387	1.36	0.82
Day 14	71.94	2656	2.02	0.83

5.3.3 Resistance comparisons

The electrochemical noise resistance is commonly considered as comparable with the polarization resistance obtained from LPR or the total resistance obtained

from EIS, thus it can be used for corrosion rate estimation based on the Stern-Geary relationship. In order to prove this, the potential and current noise data segments, obtained around the same time that LPR and EIS measurements were performed were selected. Each of the noise segments contains 3600 data points, corresponding to 30 minutes of recordings. The DC drift in potential and current noise data segments were removed by fitting the data with a straight line and subtracting it from the original data. Afterwards, R_n was calculated. Figure 5-4 shows R_n values from EN measurements, along with R_p and R_{ct} values derived from LPR and EIS measurements, respectively. It should be pointed out that solution resistances obtained from EIS were subtracted from the R_p values obtained from LPR. The inset of Figure 5-4 shows the fluctuation of R_p and R_{ct} with time.

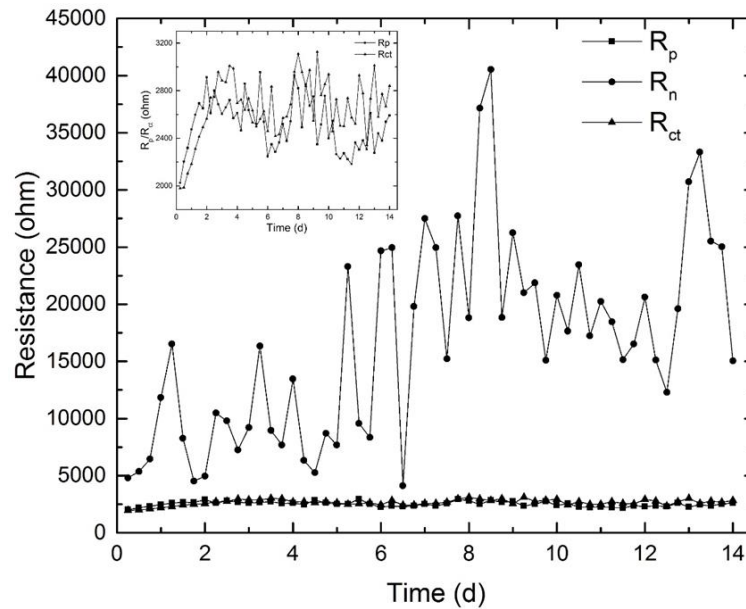


Figure 5-4: Variations of R_n , R_p and R_{ct} with time for carbon steel covered with sand deposit and immersed in 0.1 M NaCl solution.

As can be seen from Figure 5-4, the charge transfer resistance (R_{ct}) calculated from impedance data is close to the polarization resistance (R_p) from LPR. Nevertheless, the noise resistance (R_n) is much higher than R_p and R_{ct} during the entire test period. In this case, the corrosion rate estimated by R_n would be much lower than that estimated by R_{ct}/R_p .

5.3.4 Electrochemical noise

Figure 5-5 shows the typical EN data recorded on days 1, 4, 7 and 14. In Figure 5-5(a) and Figure 5-5(b), corresponding transients in current and potential signals indicate the presence of metastable pitting process [14]. The surface morphology of the steel sample after 14 days of immersion, as shown in Figure 5-6, confirms this assumption. The color bar in Figure 5-6(b) reveals that the maximum pit depth is around 8 μm , which gives a maximum penetration rate of approximately 0.2 mm/y. All the test samples were subjected to 3D profilometry after tests. It was found that the pit depth ranged from 4 μm to 8 μm . It is worth mentioning that from the 3D profilometry of the sample removed from the test cell after 7 days of immersion, the pit depths were in the same range.

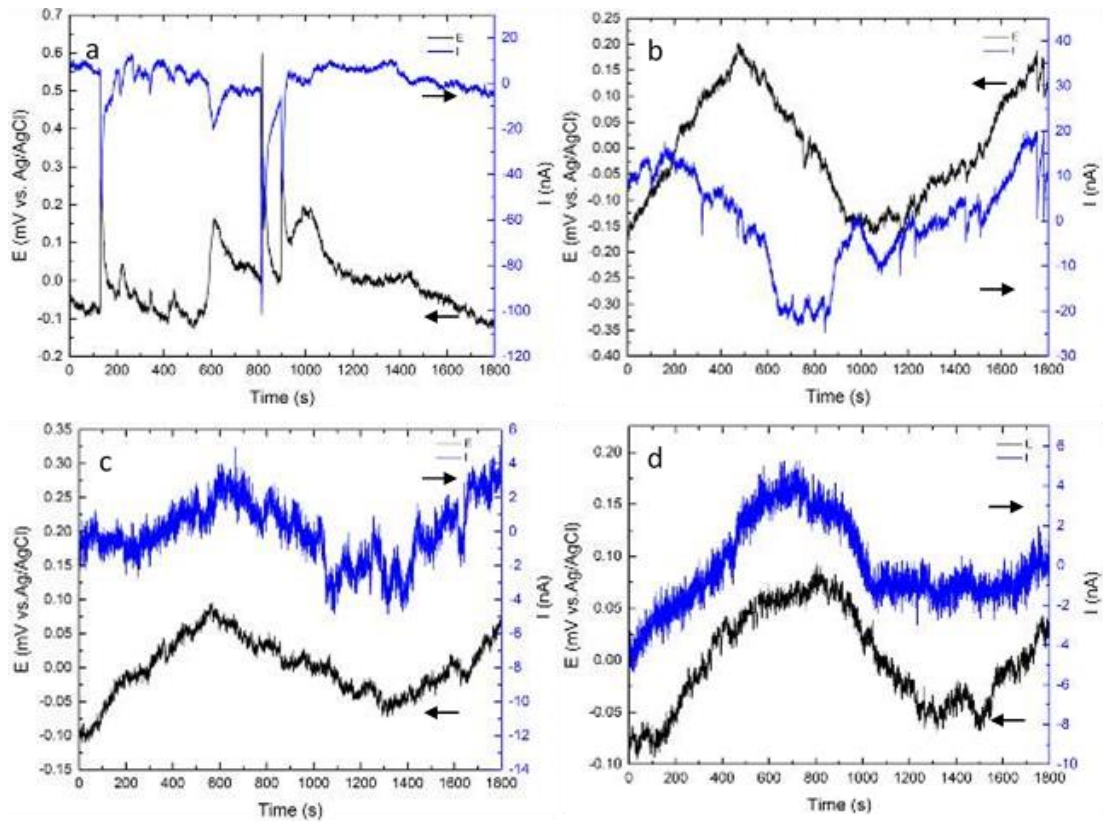


Figure 5-5: Electrochemical current and potential noise signals (after DC trend removal) obtained from (a) day 1, (b) day 4, (c) day 7 and (d) day 14.

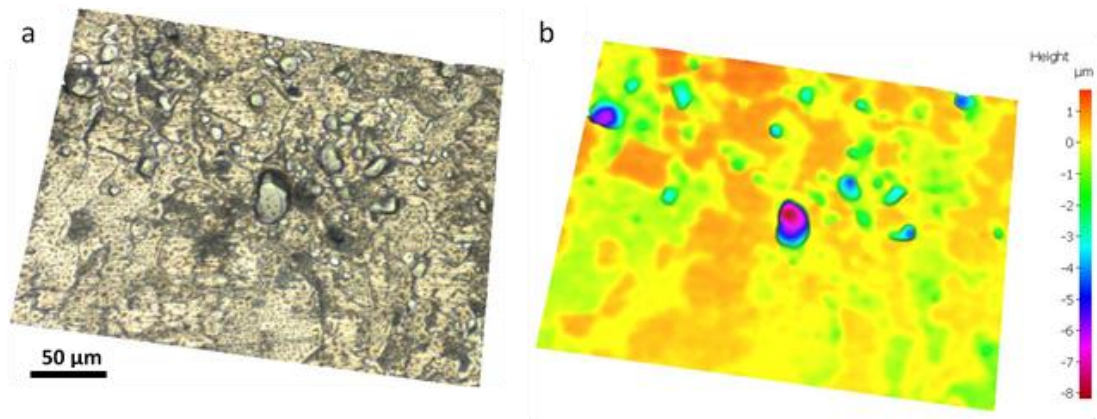


Figure 5-6: 3D image of a steel surface after immersion in 0.1 M NaCl solution at 30 °C for 14 days showing pitting (maximum pit depth 8 μm).

Additionally, it is observed that the maximum amplitude of the current transient decreased from around 100 nA on day 1 to around 20 nA on day 4. Meanwhile, the maximum amplitude of potential transient decreased from approximately 0.6 mV to about 0.15 mV. For simplicity, the EN signals with typical transients recorded on day 1 and day 4 only are present here, in fact, such features appear intermittently in the EN recordings of the first 7 days. In contrast, from day 7 onwards, there were few such transients present in EN signals. Instead, the current and potential fluctuated with amplitudes less than 0.1 mV and 6 nA, respectively, as shown in Figure 5-5(c) and Figure 5-5(d). This indicates that the steel specimens were undergoing uniform corrosion with a low corrosion rate or had achieved a passive state [26]. This fact is also reflected by the changing open circuit potential with time (Figure 5-2).

5.3.5 Recurrence quantification analysis (RQA)

Figure 5-7 shows the RPs of the current data segments shown in Figure 5-5. The threshold value ε was determined as 20% of the standard deviation of the current data segment [22]. Four variables, viz. RR, DET, ENTR and TT were extracted to quantify the recurrence plots. The results are listed in Table 6-2. All the calculations were implemented via a publicly available Matlab toolbox, i.e. the Cross Recurrence Plot Toolbox (version 5.17) developed by Nobeert Marwan [23].

The recurrence rate RR quantifies the percentage of recurrent points in the RP. The more periodic the current signal, the higher RR value. Determinism DET and entropy ENTR are computed based on the diagonal line segments present in an RP. A

diagonal line segment refers to line segments formed by diagonally adjacent recurrent points parallel to the main diagonal line (45° bottom left to top right) in the RP. DET quantifies the ratio of recurrent points that form diagonal line segments to the entire set of recurrent points. It contains information about the duration of a stable interaction. The longer the interactions, the higher the DET value. Similarly, the entropy ENTR comes from Shannon's information theory. It quantifies the distribution of the diagonal lines as an indication of the complexity of the RP [23]. A more complex dynamic will result in an RP with higher ENTR value. In contrast, the trapping time TT is derived from the vertical line segments. Similarly to the definition of diagonal line segments, a vertical line segment is formed by two or more vertically adjacent recurrent points. TT calculates the average length of the vertical lines. It reflects the mean time that the system stays at a specific state or the duration of entrapment of the state.

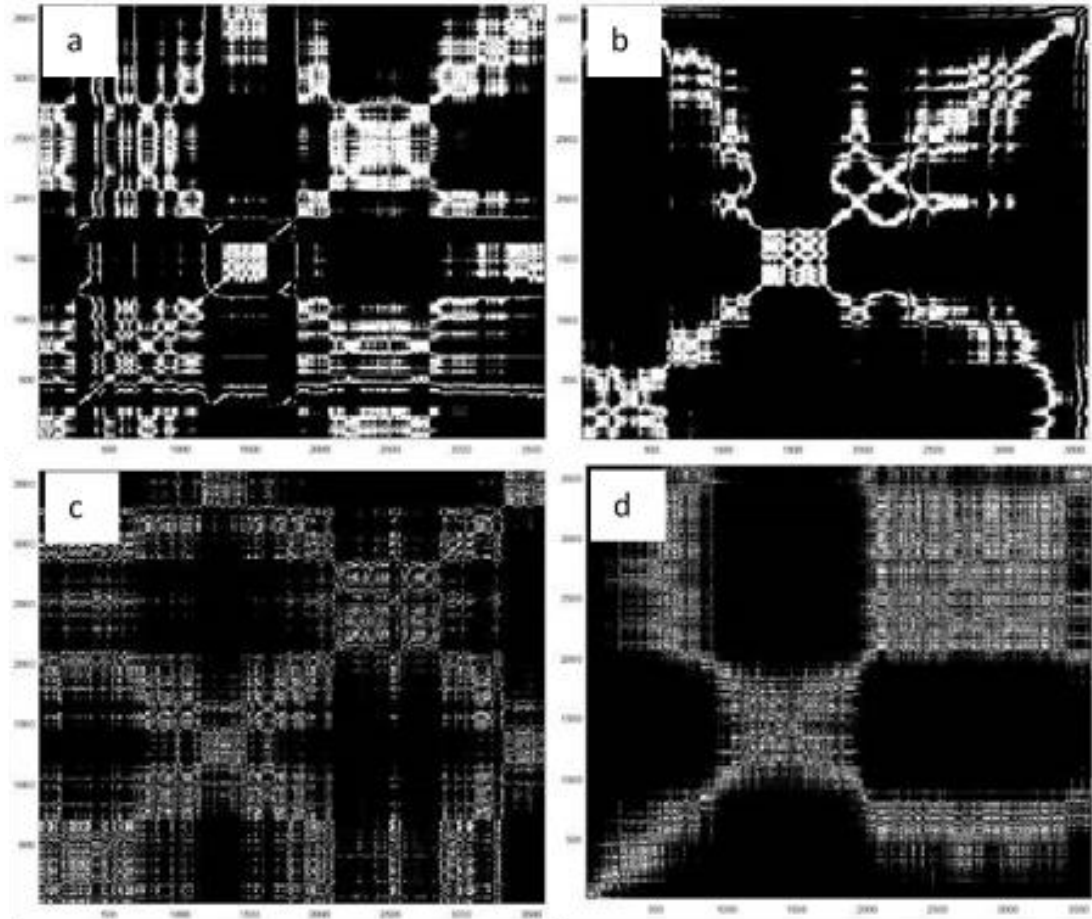


Figure 5-7: Recurrence plots corresponding to the current data shown in Figure 5-5
(a) day 1, (b) day 4, (c) day 7 and (d) day 14.

Table 5-2: Recurrence quantification variables extracted from Figure 5-7.

Time	RR	DET	ENTR	TT
Day 1	0.2109	0.9079	2.5299	9.9227
Day 4	0.1252	0.8944	2.5043	10.1458
Day 7	0.1128	0.4527	0.8584	2.6574
Day 14	0.1443	0.5745	1.0635	2.9395

As indicated in Table 5-2, there is little difference between the RR during the period of metastable pitting (days 1 and 4) and that of uniform corrosion (days 7 and 14). On the contrary, the DET and ENTR values for pitting data are both higher than those for the uniform corrosion data [24]. This means that, compared to uniform corrosion, pitting processes involve longer interaction times among the micro-corrosion cells formed on the steel surface, and the dynamics of this kind of interaction is more complex. In addition, it seems that in pitting processes, the system was trapped at a specific state for a longer time. Indeed, for metastable pitting, an initiated micro-corrosion cell on the steel surface usually takes a longer time to re-passivate compared to the case of uniform corrosion, thus contributing to a higher TT value.

The variations of the RQA variables RR, DET, ENTR and TT during 14 days are plotted as functions of time, shown in Figure 5-8. Each point represents one current data segment mentioned above, i.e. 30 min recordings. Three stages can be assigned. Specifically, in the first 4 days, the corrosion of steel samples under sand deposits has higher DET, ENTR and TT values that are similar to those obtained from metastable pitting process (Table 5-2), indicating that the dominant corrosion type during this period is metastable pitting. From day 7 to day 14, these values fluctuated at lower levels, which are close to those obtained from the uniform corrosion processes (Table 5-2). From day 5 to day 6, the under sand deposit corrosion type seems to be undergoing a transition period from metastable pitting to uniform corrosion. However, the recurrence rate RR was low during the whole test period.

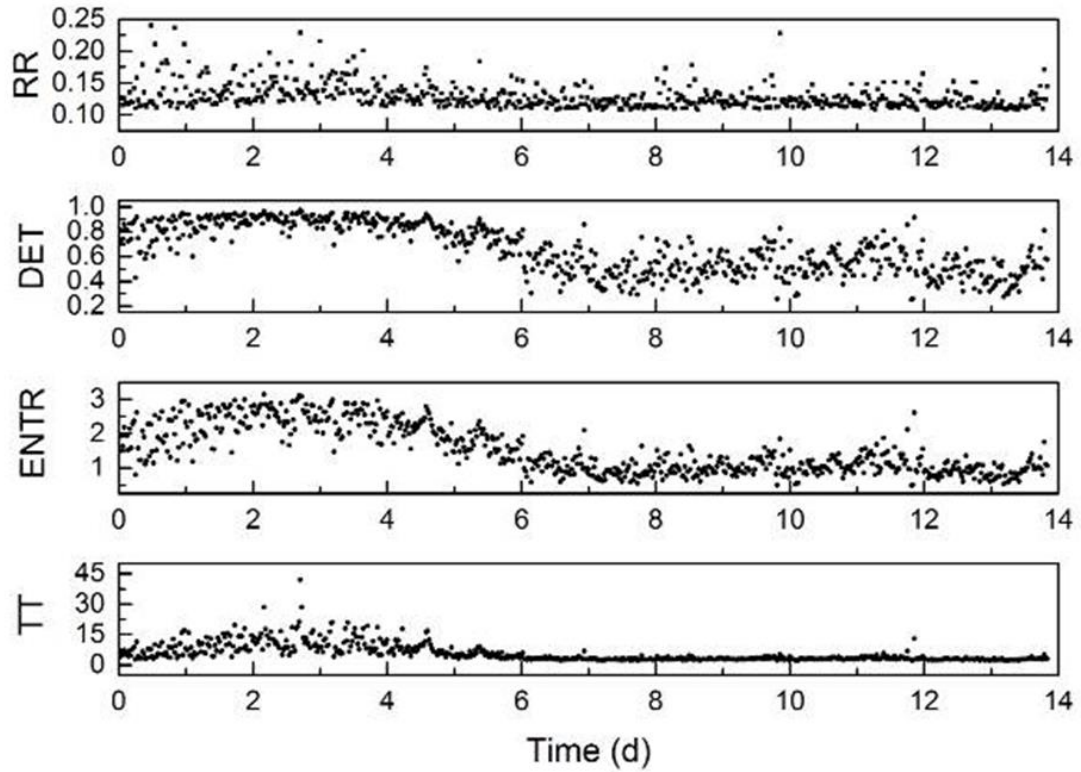


Figure 5-8: Corrosion process monitoring with recurrence quantification variables.

5.4 Summary

The present study explores the potential of electrochemical noise as a useful tool for under deposit corrosion monitoring.

1. It is shown that the noise resistance R_n values were much higher than the R_p and R_{ct} values obtained from conventional electrochemical techniques, namely linear polarization resistance and electrochemical impedance spectroscopy. Therefore, R_n could not be used for the estimation of general corrosion rates in the studied UDC system. It should be used in combination with LPR and EIS techniques in order to provide more reliable data on the general corrosion rate.
2. Recurrence quantification analysis of the electrochemical current noise data shows that RQA variables DET, ENTR and TT could detect metastable pitting from uniform corrosion or passive state of steels under sand deposit. These variables are suitable for long term corrosion type estimation and monitoring, while the recurrence rate RR is not. The results indicate that during the first 4

days of the UDC test, the steel samples mainly underwent metastable pitting, followed by a transition period from day 5 to day 6. From day 7 onwards, the dominant corrosion type became uniform. The surface profiles of steel samples confirmed the presence of metastable pits.

3. Although there are limitations in the proposed monitoring technique and further studies are needed, the preliminary tests have demonstrated that electrochemical noise associated with recurrence quantification analysis is a promising tool for detecting and monitoring localized corrosion of carbon steel under sand deposit.

References

- [1] Y.J. Tan, Y. Fwu, K. Bhardwaj, Electrochemical evaluation of under-deposit corrosion and its inhibition using the wire beam electrode method, *Corros Sci*, 53 (2011) 1254-1261.
- [2] V. Pandarinathan, K. Lepkova, S.I. Bailey, R. Gubner, Evaluation of corrosion inhibition at sand-deposited carbon steel in CO₂-saturated brine, *Corros Sci*, 72 (2013) 108-117.
- [3] V. Pandarinathan, K. Lepková, W. van Bronswijk, Chukanovite (Fe₂(OH)₂CO₃) identified as a corrosion product at sand-deposited carbon steel in CO₂-saturated brine, *Corros Sci*, 85 (2014) 26-32.
- [4] Y. Tan, Sensing localised corrosion by means of electrochemical noise detection and analysis, *Sensors and Actuators B: Chemical*, 139 (2009) 688-698.
- [5] A.M. Homborg, T. Tinga, X. Zhang, E.P.M. van Westing, P.J. Oonincx, G.M. Ferrari, J.H.W. de Wit, J.M.C. Mol, Transient analysis through Hilbert spectra of electrochemical noise signals for the identification of localized corrosion of stainless steel, *Electrochimica Acta*, 104 (2013) 84-93.
- [6] E.C. Rios, A.M. Zimer, P.C.D. Mendes, M.B.J. Freitas, E.V.R. de Castro, L.H. Mascaro, E.C. Pereira, Corrosion of AISI 1020 steel in crude oil studied by the electrochemical noise measurements, *Fuel*, 150 (2015) 325-333.
- [7] M.A. Winters, P.S.N. Stokes, P.O. Zuniga, D.J. Schlottenmier, Real-Time Performance Monitoring of Fouling and under-Deposit Corrosion in Cooling Water-Systems, *Corros Sci*, 35 (1993) 1667-1675.
- [8] A. Legat, J. Osredkar, V. Kuhar, M. Leban, Detection of various types of corrosion processes by the chaotic analysis of electrochemical noise, *Mater Sci Forum*, 289-2 (1998) 807-811.
- [9] R.A. Cottis, An evaluation of electrochemical noise for the estimation of corrosion rate and type, *NACE - International Corrosion Conference Series*, 2006, pp. 064321-0643211.

- [10] C.A. Loto, Electrochemical Noise Measurement Technique in Corrosion Research, *Int J Electrochem Sc*, 7 (2012) 9248-9270.
- [11] S.R. Allahkaram, M. Khodayari, Electrochemical noise analysis of carbon steel in simulated concrete pore solution affected by CO₂ and SO₂ using wavelet transform, *Anti-Corros Method M*, 55 (2008) 250-256.
- [12] A.M. Homborg, E.P.M. van Westing, T. Tinga, X. Zhang, P.J. Oonincx, G.M. Ferrari, J.H.W. de Wit, J.M.C. Mol, Novel time-frequency characterization of electrochemical noise data in corrosion studies using Hilbert spectra, *Corros Sci*, 66 (2013) 97-110.
- [13] A.M. Homborg, E.P.M. van Westing, T. Tinga, G.M. Ferrari, X. Zhang, J.H.W. de Wit, J.M.C. Mol, Application of transient analysis using Hilbert spectra of electrochemical noise to the identification of corrosion inhibition, *Electrochimica Acta*, 116 (2014) 355-365.
- [14] A.N. Chen, F.H. Cao, X.N. Liao, W.J. Liu, L.Y. Zheng, J.Q. Zhang, C.A. Cao, Study of pitting corrosion on mild steel during wet-dry cycles by electrochemical noise analysis based on chaos theory, *Corros Sci*, 66 (2013) 183-195.
- [15] J. Zhan, X.F. Liu, Q. Zhang, Q.J. Liu, F. Long, Chaos Analysis of The Influence of Tensile Stress on Electrochemical Noise, 2009 International Conference on Industrial Mechatronics and Automation, (2009) 418-421.
- [16] D.H. Xia, S.Z. Song, J.H. Wang, J.B. Shi, H.C. Bi, Z.M. Gao, Determination of corrosion types from electrochemical noise by phase space reconstruction theory, *Electrochemistry Communications*, 15 (2012) 88-92.
- [17] C. Aldrich, B.C. Qi, P.J. Botha, Analysis of electrochemical noise data with phase space methods, *Miner Eng*, 19 (2006) 1402-1409.
- [18] E. Cazares-Ibanez, G.A. Vazquez-Coutino, E. Garcia-Ochoa, Application of recurrence plots as a new tool in the analysis of electrochemical oscillations of copper, *J Electroanal Chem*, 583 (2005) 17-33.

- [19] N. Acuna-Gonzalez, E. Garcia-Ochoa, J. Gonzalez-Sanchez, Assessment of the dynamics of corrosion fatigue crack initiation applying recurrence plots to the analysis of electrochemical noise data, *Int J Fatigue*, 30 (2008) 1211-1219.
- [20] L.S. Montalban, P. Henttu, R. Piche, Recurrence quantification analysis of electrochemical noise data during pit development, *Int J Bifurcat Chaos*, 17 (2007) 3725-3728.
- [21] T. Zhang, Y.A. Cong, Y.W. Shao, G.Z. Meng, F.H. Wang, Electrochemical noise analysis on the crevice corrosion behavior of Ni-Cr-Mo-V high strength steel using recurrence plots, *J Appl Electrochem*, 41 (2011) 289-298.
- [22] Y. Hou, C. Aldrich, K. Lepkova, L.L. Machuca, B. Kinsella, Monitoring of carbon steel corrosion by use of electrochemical noise and recurrence quantification analysis, *Corros Sci*.
- [23] N. Marwan, M.C. Romano, M. Thiel, J. Kurths, Recurrence plots for the analysis of complex systems, *Phys Rep*, 438 (2007) 237-329.
- [24] Y.E. Yang, T. Zhang, Y.W. Shao, G.Z. Meng, F.H. Wang, Effect of hydrostatic pressure on the corrosion behaviour of Ni-Cr-Mo-V high strength steel, *Corros Sci*, 52 (2010) 2697-2706.
- [25] J.-B. Jorcin, M.E. Orazem, N. Pébère, B. Tribollet, CPE analysis by local electrochemical impedance spectroscopy, *Electrochim Acta*, 51 (2006) 1473-1479.
- [26] E. García, M.A. Hernández, F.J. Rodríguez, J. Genescá, F.J. Boerio, Oscillation and chaos in pitting corrosion of steel, *Corrosion*, 59 (2003) 50-58.

CHAPTER 6 CASE STUDY III

Y. Hou, C. Aldrich, K. Lepkova, L.L. Machuca, B. Kinsella, Analysis of electrochemical noise data by use of recurrence quantification analysis and machine learning methods, *Electrochimica Acta*, 256, 337-347 (2017).

This chapter presents the published paper with modified formats and contents that match the overall style of the thesis.

Analysis of Electrochemical Noise Data by Use of Recurrence Quantification Analysis and Machine Learning Methods

Abstract

By use of recurrence quantification analysis (RQA), twelve features were extracted from the electrochemical noise signals generated by three types of corrosion: uniform, pitting and passivation. Machine learning methods, i.e. linear discriminant analysis (LDA) and random forests (RF), were used to identify the different corrosion types from those features. Both models gave satisfactory performance, but the RF model showed better prediction accuracy of 93% than the LDA model (88%). Furthermore, an estimation of the importance of the variables by use of the RF model suggested the RQA variables laminarity (LAM) and determinism (DET) played the most significant role with regard to identification of corrosion types. In addition, the comparison of noise resistance with the resistance obtained from EIS measurement showed that the noise resistance can be used for monitoring corrosion rate variations not only for uniform corrosion and passivation, but also for pitting.

Keywords: Electrochemical noise; Recurrence quantification analysis; Linear discriminant analysis; Random forest; Corrosion type identification

6.1 Introduction

The concept of electrochemical noise (EN) was first introduced by Iverson [1] and Tyagai et al. [2] decades ago. Back then, the research focus was merely on potential fluctuations. Subsequently, in 1986, Eden et al. [3] further developed the noise measurement setup, which included two identical working electrodes (WE) connected by a zero resistance ammeter (ZRA), a reference electrode (RE) and a potentiometer, allowing the recording of current and potential noise simultaneously. Since then, EN with ZRA has been widely studied in the corrosion field, owing to its ease of setting up, non-destructiveness, non-intrusiveness and the ability to provide information on both the corrosion rate and type which other electrochemical techniques failed to offer [4-9].

Among various research areas, the identification of different types of corrosion has always attracted considerable interest from corrosion researchers and engineers. Numerous efforts have been made to extract discriminative features from collected EN data to indicate corrosion types. These features can be sourced from three kinds of analytical domains, namely the time domain, frequency domain and time-frequency domain. The primary feature obtained from frequency domain analysis is the roll-off slope of the power spectral density (PSD) plot [10]. A large number of indicators have been extracted from the time domain analysis of the EN data, including:

- Statistics, such as the standard deviation, kurtosis, skewness, and localization index of measurements [11];
- The cumulative probability of corrosion events and Weibull probability plots from transient analysis [12];
- Largest Lyapunov exponent and correlation dimension from chaotic analysis [13, 14];
- Recurrence rate, determinism, maxline, etc. from recurrence quantification analysis [15];
- Hausdorff exponent, Hurst exponent and spectral-power exponents from fractal analysis [16];
- Energy distribution plot from wavelet analysis [17];

- In addition, Homborg et al. [18] have published several papers on the time-frequency joint analysis by Hilbert-Huang transformation which showed good application prospect.

Recently, owing to the rapid development in machine learning techniques, new ideas have been proposed for the interpretation of electrochemical noise. For example, Huang et al. [19-21] made use of cluster analysis of current and potential signals and LDA models to identify different pitting states in low carbon steel exposed to $\text{NaHCO}_3 + \text{NaCl}$ solutions. Li et al. [22] have used features extracted from EN signals generated by uniform corrosion, pitting and passivation in 304 stainless steel as predictors in artificial neural network models designed to distinguish between different types of corrosion.

More recently, the authors [23] have proposed a formal methodology for the identification of localized corrosion in low carbon steel from uniform corrosion based on the use of recurrence quantification analysis (RQA). This statistical process control approach could be used to monitor corrosion in a continuous way with high reliability, although the discrimination between localized corrosion and passivation needs to be further improved. In the previous study, only four RQA variables were used to set up the corrosion monitoring scheme and the number of data in the passivation system was limited.

In this study, to improve the separability of pitting and passivation, the EN signals were collected from the same corrosion systems with different sizes of electrodes, creating a larger database for the following model development. Meanwhile, an extended set of feature variables were extracted by recurrence quantification analysis (RQA) of the EN signals. LDA and RF models were subsequently developed with the extracted RQA variables as predictors to identify different corrosion types. In addition, noise resistance was compared with the corrosion resistance obtained from electrochemical impedance spectroscopy (EIS) to explore its usefulness as a corrosion rate indicator.

6.2 Experimental work

6.2.1 Materials

The material employed in this study was carbon steel 1030. The chemical composition was (wt. %): C (0.37), Mn (0.80), Si (0.282), P (0.012), S (0.001), Cr (0.089), Ni (0.012), Mo (0.004), Sn (0.004), Al (0.01), and Fe (balance). Rectangular steel samples with surface areas of $0.5\text{ cm} \times 0.3\text{ cm}$, $1.4\text{ cm} \times 1.5\text{ cm}$, $2.0\text{ cm} \times 3.1\text{ cm}$ and $3.1\text{ cm} \times 3.3\text{ cm}$ were made from the same material and soldered with a conducting wire to each for electrical connection. Subsequently, the samples were electrocoated (Powercron 6000CX) and embedded in epoxy resin (Epofix), leaving 0.15 cm^2 , 2.1 cm^2 , 6.2 cm^2 and 10.2 cm^2 of the surface exposed respectively. For simplicity, hereafter, these electrodes with different surface areas will be denoted as electrode A0.15, A2, A6 and A10 respectively. Before tests, the exposed surfaces of the steel samples were abraded on silicon carbide paper up to 1200 grit, rinsed with ultrapure water and ethanol and dried with nitrogen. This procedure was conducted prior to each run of the tests. The same set of steel samples with identical grinding procedures prior to each run were used in all the tests. All the tests were conducted at least in duplicate.

Three test solutions were used, viz. 0.1 M sodium chloride (NaCl; Merck, 99.7%), 0.5 M sodium hydrogen carbonate (NaHCO_3 ; Merck, 99.7%), and a solution containing 0.45 M sodium hydrogen carbonate and 0.1 M sodium chloride ($0.45\text{ M NaHCO}_3 + 0.1\text{ M NaCl}$). These solutions were used to set up uniform corrosion, passivation and pitting corrosion, respectively to the carbon steel. All the solutions were prepared with ultrapure water (Milli-Q system, resistivity $18.2\text{ M}\Omega\text{ cm}$) and analytical reagents.

6.2.2 Electrochemical tests

Electrochemical noise measurement

Electrochemical noise (EN) measurement was carried out in a configuration which has been described in detail in our previous work [23]. Only important points and differences are reported here. Two nominally identical (same surface area and same material) aforementioned carbon steel samples were placed parallel to each other as working electrodes (WE 1 and WE 2), facing the operator. The inter-electrode

spacing was fixed at 2.4 cm (centre-to-centre). In addition, a commercial Ag/AgCl electrode was used as reference electrode (single junction electrode placed in a capillary with a porous ceramic tip filled with 3 M KCl solution (0.210 V vs. S.H.E). The current flowing through the two working electrodes was measured using a zero resistance ammeter mode (ZRA) of Gamry Reference 600 and the potential of the short-circuited WEs was measured with regard to the commercial reference electrode. ESA410 data acquisition software was employed to collect the EN data. The sampling rate was 2 Hz.

All the test solutions were air-saturated in a separate cell before pumping into the test cell equipped with the electrodes. During the tests, the temperature of the solution was controlled at 30 ± 1 °C by a hot plate with a temperature probe immersed in the test solution. Air was continuously pumped through the blank space on top of the solution level in the cell, creating an air blanket. This was done to keep the oxygen levels relatively constant in solutions for different experiments. All the tests were carried out under stagnant conditions (without any stirring).

For uniform corrosion, the EN measurements were started immediately after immersion of the test samples and continuously recorded for 20 h. For passivation tests, the duration was different for different electrode sizes. For A2 WEs, the EN data were continuously recorded for 20 h, while for A0.15, A6 and A10 WEs, the EN data were recorded for 4 h after immersion in 0.5 M NaHCO₃ solution. For pitting corrosion tests, the specimens were firstly immersed in 0.5 M NaHCO₃ solution for 4 h. Then NaCl was added to yield a pitting solution – 0.45 M NaHCO₃ + 0.1 M NaCl. The EN measurement started immediately after NaCl addition and the data were recorded continuously for 20 h. However, one should bear in mind that the electrodes could continue to be passivated after chloride addition for some time. Therefore, the 20 h recordings in pitting solutions could contain some passivation-related data at the beginning as well. This may to some extent affect the discrimination of the type of corrosion when RQA is applied.

Potentiostatic electrochemical impedance spectroscopy

Potentiostatic electrochemical impedance spectroscopy (EIS) was carried out to obtain the relevant resistances of the specimens under different corrosion conditions.

A platinum mesh counter electrode and the same Ag/AgCl reference electrode were used in the measurement. Different sizes of steel samples were used as working electrode. A frequency range of 10 mHz to 10 kHz at 10 points per decade was employed and the AC excitation amplitude was 10 mV versus OCP. For general corrosion, the EIS measurement was conducted 2 h after immersion, and the relevant resistance obtained was compared with the noise resistance calculated from the EN data collected in the time period of 2 - 2.5 h. Similarly, for pitting corrosion, EIS test was conducted twice at different times, i.e., 12 h and 19.5 h after NaCl addition and the obtained resistances were compared with noise resistances calculated from EN data collected in the time intervals of 12 – 12.5 h and 19.5 – 20 h. The EIS data were analysed using Gamry Echem Analyst software.

6.2.3 Surface analysis

After each test, the steel samples were rinsed with ultrapure water and ethanol followed by drying with nitrogen. The corrosion products on the steel surfaces were removed using Clarke's solution to facilitate the examination of localized corrosion and the measurement of the maximum pit depth using optical 3D microscope (Infinite focus microscope, Alicona Instruments, Austria).

6.3 Results and discussion

6.3.1 Surface morphologies of specimens

The surface morphologies of the working electrodes were observed under an optical 3D microscope after EN tests. As expected, in the solutions chosen to produce uniform and passive corrosion, the electrode surfaces showed corresponding behaviour. Nevertheless, in the pitting tests, the surface conditions varied according to different electrode sizes. Specifically, none of the A0.15 electrode couple showed any pits after immersion. For A2 and A6 working electrode couples, only one electrode in each couple was pitted. Unlike the others, deep pits were present on both working electrodes A10. Table 6-1 summarises pitting information on electrodes A2, A6 and A10. The maximum pit depth found with working electrode A10 was 89 μm after 20 h immersion, as presented in Figure 6-1 and Table 6-1. All the pits showed similar morphologies and the same trend was observed in repeated measurements.

Table 6-1: Pitting information for working electrodes A0.15, A2, A6 and A10.

Electrode	Total Area, cm ²	Total number of pits		Pit depth range, μm	Number of pits		Depth/Average depth, μm
		Test 1	Test 2		Test 1	Test 2	
A0.15	0.3	0	0	0	0	0	0
A2	4.2	1	1	41-60	1	1	42.5
A6	12.4	4	4	20-40	2	1	31
				41-60	1	2	48.5
				81-89	1	1	82.5
A10	20.4	14	12	20-40	2	3	25
				41-60	10	8	54
				61-80	1	1	65.5
				81-89	1	0	89

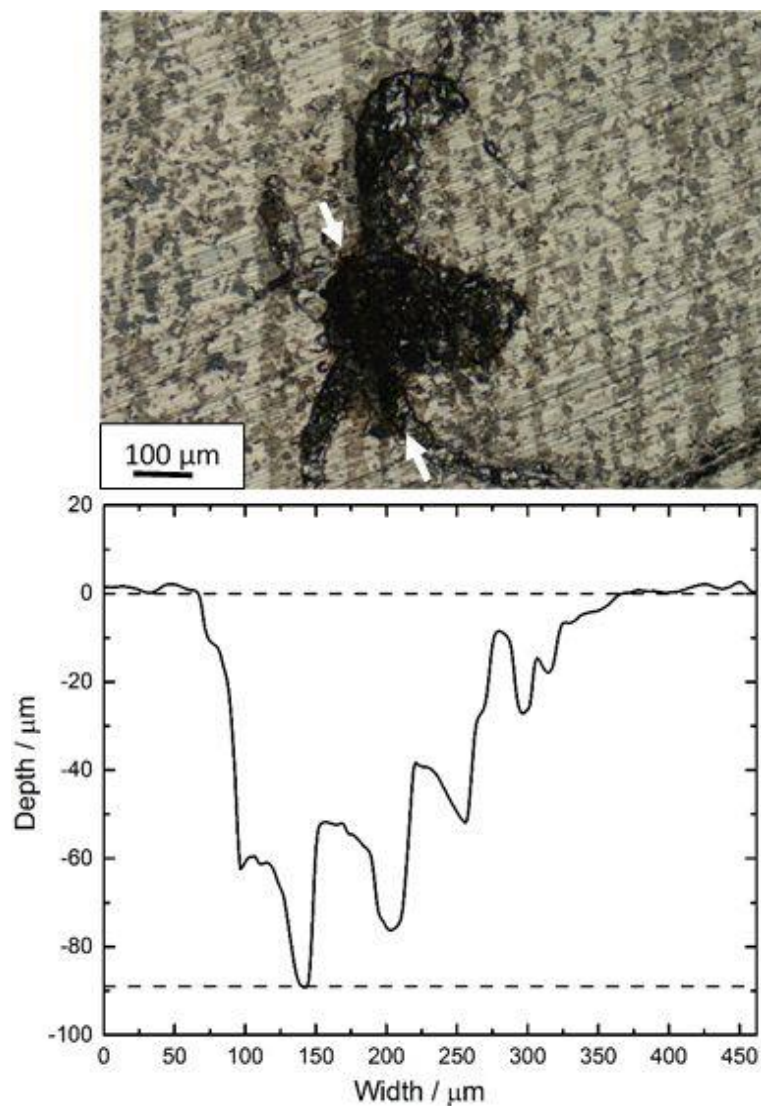


Figure 6-1: A pit found on electrode A10 and its depth measured with a 3D optical microscope. The measurement was made along with the line where the two arrows are placed.

6.3.2 Corrosion type identification

Electrochemical noise signals

The electrochemical noise signals obtained from three different corrosion systems with various electrode sizes are shown in Figure 6-2. The presented EN segments were generated in a different cell but around the same time when EIS tests were conducted. These segments are referred to as uniform, pitting I, pitting II and passivation. Specifically, uniform is related to 30 min recordings after 2 h of immersion in 0.1 M NaCl; pitting I represents 30 min recordings after 12 h of

immersion in 0.45 M $\text{NaHCO}_3 + 0.1 \text{ M NaCl}$; pitting II refers to 30 min recordings after 19.5 h of immersion in 0.45 M $\text{NaHCO}_3 + 0.1 \text{ M NaCl}$; and passivation corresponds to 30 min recordings after 3.5 h of immersion in 0.5 M NaHCO_3 .

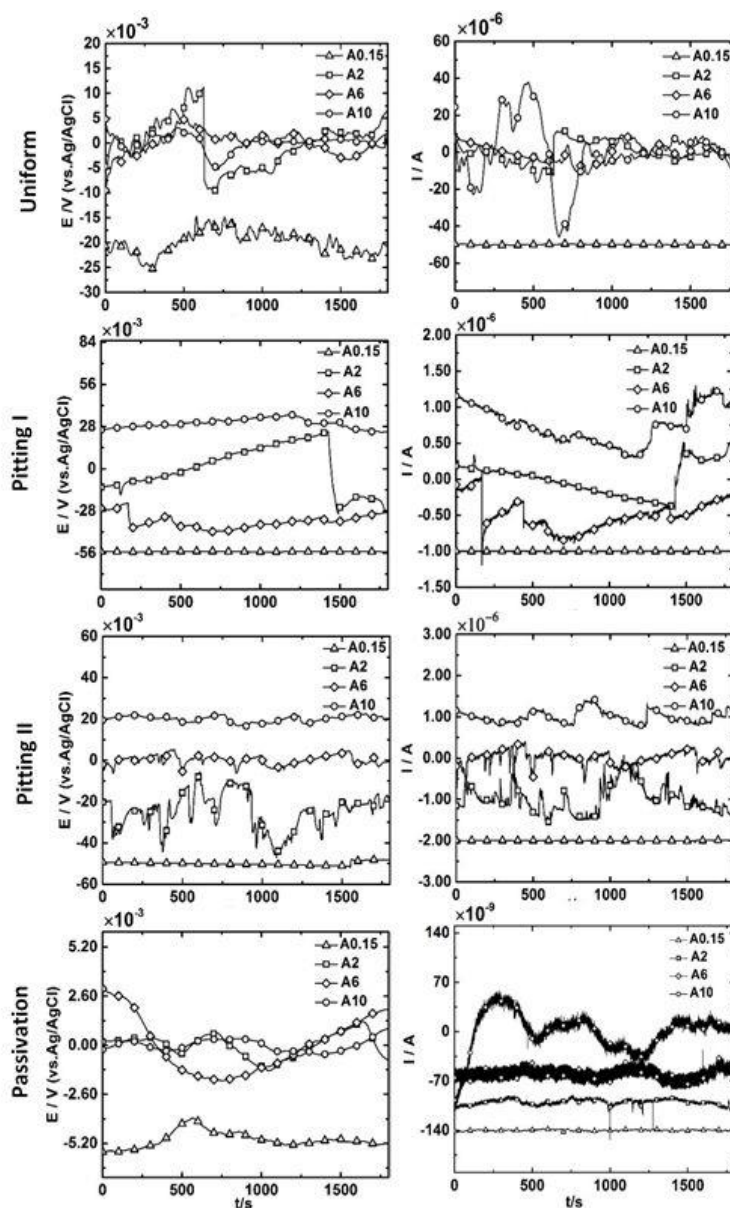


Figure 6-2: Electrochemical potential and current data segments collected with different corrosion systems and electrode sizes.

The DC drift of the EN signal was removed by linear regression. After drift removal, all the EN signals should have average values of zero. However, for ease of visualization and comparison, certain offset values were applied to some of the signals (i.e. signals that are not fluctuating around zero), as shown in Figure 6-2. Note that the

markers represent different electrode sizes and are not related to any filtering of the original data.

As indicated, the EN generated by uniform corrosion was smooth with no sharp potential or current transients. The potential noise signals in passivation systems were similar to those in uniform systems, while the current signals were composed of very frequent oscillations instead of smooth fluctuations. In comparison, EN collected from pitting systems with electrodes A2, A6 and A10 showed typical pitting transients, which mostly occurred simultaneously in potential and current measurements. Moreover, some small and fast transients were found superimposed on larger transients. Additionally, as mentioned before, the electrodes may not start pitting at the beginning. Indeed, profound transients were only observed after 7 h, 2.5 h and 1 h after chloride addition for electrode A2, A6 and A10, respectively. Despite several individual discontinuous transients present during the first few hours, the noise signals resembled those from passivation processes. This situation was observed more clearly for electrode A0.15, i.e., the noise signals for electrodes A0.15 were always similar to those obtained from passivation systems within the entire 20 h recordings. Due to the absence of pits on electrodes A0.15, the generated EN signals could not represent the pitting process of electrodes A0.15. Therefore, the associated EN segments were excluded from further analysis.

Although indicators extracted from both current and potential noise signals could be used to represent underlying corrosion behaviours, the characteristic of current noise signals seems to be more distinctive than that of potential signals, based on Figure 6-2. Moreover, a number of similar studies [15, 24-26] also carried out EN analysis based on current noise data. Therefore, in this study, the electrochemical current noise (ECN) was chosen to demonstrate the proposed corrosion type identification method.

Feature extraction

Electrochemical current noise (ECN) associated with electrodes A2 is used as an example to show the feature extraction process.

- i. *ECN data preparation.* As observed from the raw EN signals obtained from passivation systems, both potential and current data gradually

increased first for 2 h and then reached plateaus. Hence the electrodes in 0.5 M NaHCO₃ solution were considered to have reached stable states after 2 h of immersion. On this basis, the associated ECN data in the first 2 h obtained from passivation systems were excluded from the following corrosion type identification process. For all other ECN time series data, generated by uniform corrosion, pitting corrosion and passivation, were divided into small continuous segments. Each segment consisted of 1800 points (15 min recordings). The DC drift of each segment was removed by linear regression.

- ii. *Recurrence plots (RP) computation.* For ECN segment, in which the DC drift had been removed an RP was generated. 0.02σ (σ is the standard deviation of the linear-detrended data segment) was used as the threshold.
- iii. *Recurrence quantification analysis.* Twelve variables (Table 3-1) were extracted to quantify each RP. These variables are referred to as RQA variables, i.e. 1 – RR , 2 – DET , 3 – L_{mean} , 4 – L_{max} , 5 – $ENTR1$, 6 – LAM , 7 – TT , 8 – V_{max} , 9 – $RT1$, 10 – $RT2$, 11 – $ENTR2$, 12 – $TRANS$.
- iv. *Constructing feature vectors.* The extracted RQA variables for each segment were arranged in a row vector called feature vector. Afterwards, these feature vectors were labelled as 1, 2, or 3 based on the corresponding corrosion types, i.e., uniform corrosion, pitting and passivation, respectively. Finally, all the labelled feature vectors were stacked into a feature matrix or RQA variable matrix.

Figure 6-3 shows the calculated RQA variables extracted from different corrosion systems. The vertical lines at segment 80 and 160 separate the three corrosion types, i.e. uniform, pitting and passivation, from left to right. It can be seen that most of the RQA variables are scattered around the same level except for DET , $ENTR1$ and LAM which seems to be capable of discriminating different corrosion types to some extent, since their values tend to be restrained within certain limits for different systems.

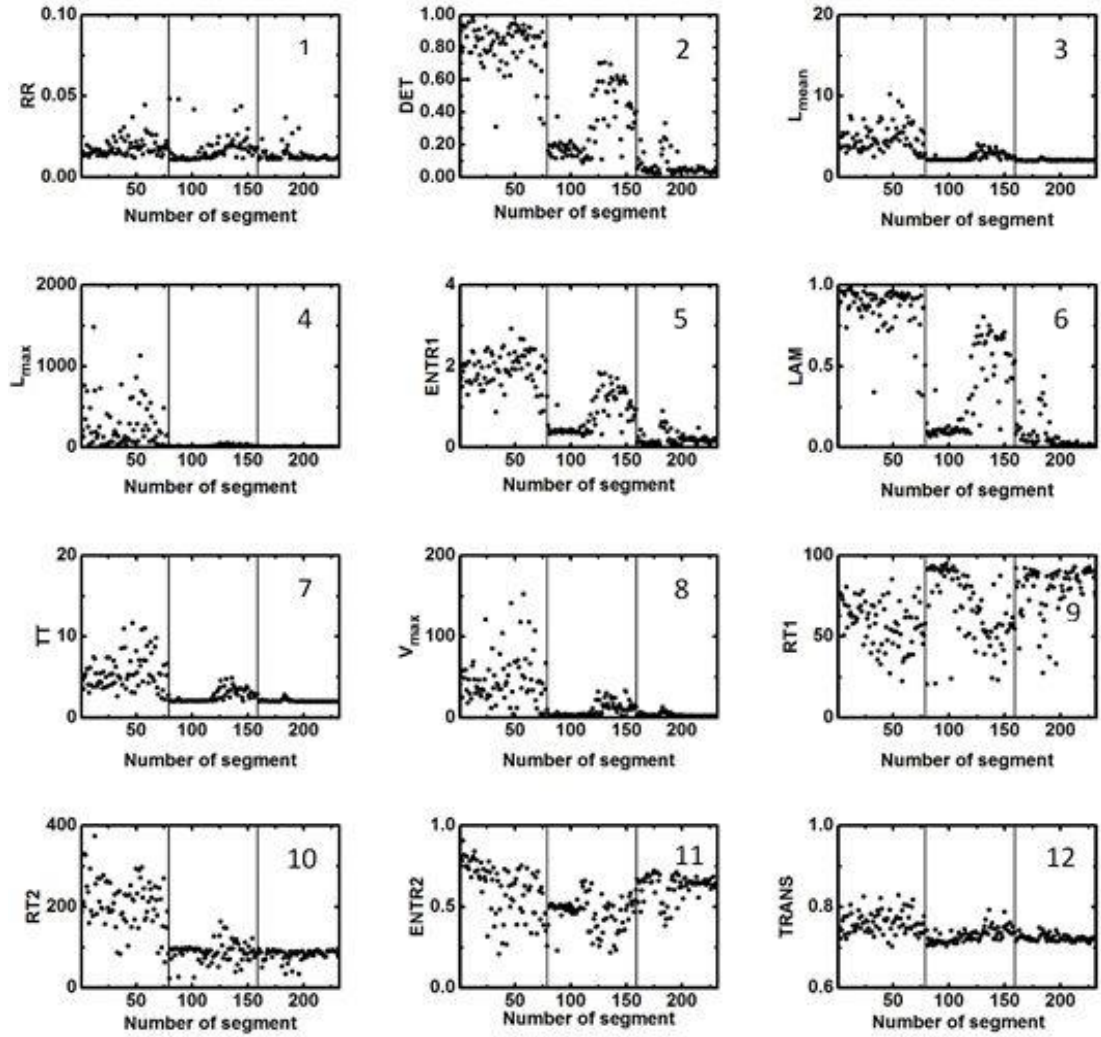


Figure 6-3: Variations of RQA variables (1 – RR , 2 – DET , 3 – L_{mean} , 4 – L_{max} , 5 – $ENTR1$, 6 – LAM , 7 – TT , 8 – V_{max} , 9 – $RT1$, 10 – $RT2$, 11 – $ENTR2$, 12 – $TRANS$) extracted from electrochemical current noise signals collected with electrodes A2.

Results of LDA

Figure 6-4 shows the classification results with the linear discriminant analysis (LDA) model using the labelled recurrence variables. As can be seen, uniform corrosion is well separated from pitting and passivation, despite a few overlapping points. Passivation and pitting are segregated to a lesser extent. However, some overlap between passivation and pitting should be expected because as mentioned before, the electrodes were still passivated for some time after the chloride addition

into the NaHCO_3 solution. This phenomenon was more evident with electrodes A0.15 which were still passivated even after 20 h of immersion in the pitting solution. Despite the overlap, it is clear that the passivation data are located in a small area in the LDA feature space, bordering on the edge of the region occupied by the pitting data. The overall classification accuracy (defined as the number of accurately classified data divided by the total number of data) of the trained LDA model was 88.3%.

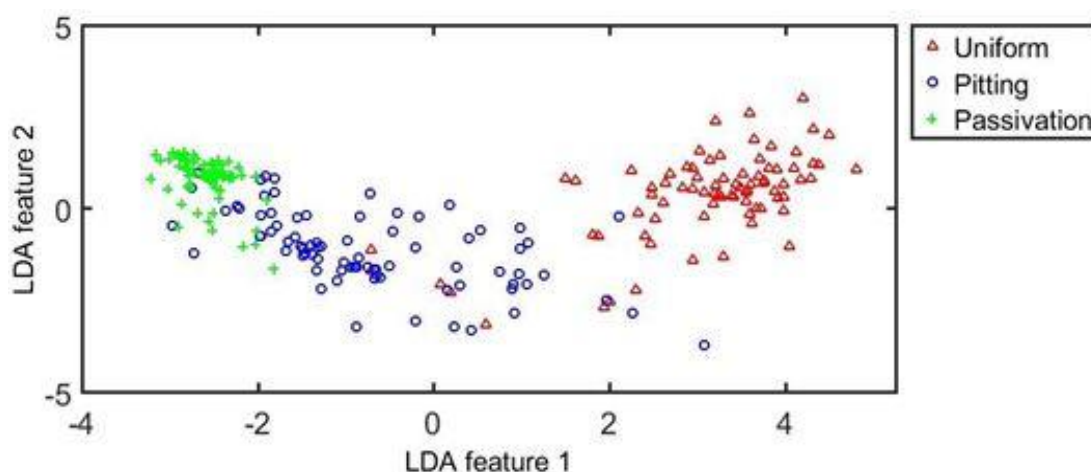


Figure 6-4: LDA feature plot of RQA variables associated with three corrosion systems of electrodes A2.

In order to explore if the electrode size would affect the identification of the corrosion types, a special LDA model was established, as shown in Figure 6-5. In this model, the RQA variables for electrodes A2, A6 and A10, regardless of the corrosion types, were labelled as class A, B and C, respectively. These labelled RQA variables were then presented to the LDA model for training. As indicated in Figure 6-5, all the data are randomly scattered and completely intertwined. Therefore, the electrode sizes cannot be discriminated. In other words, the electrode size is not a major factor for the identification of corrosion types in these systems investigated.

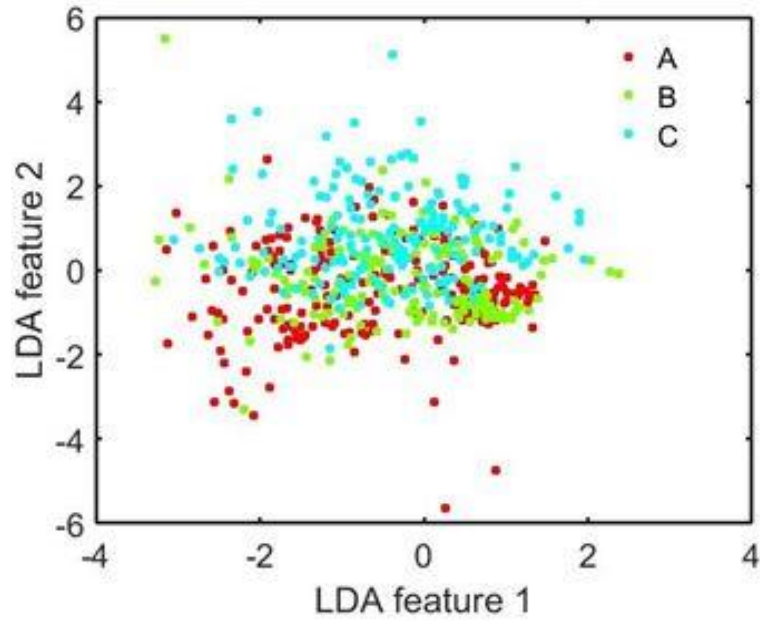


Figure 6-5: LDA feature plot of RQA variables associated with three electrode sizes, i.e. A for A2, B for A6 and C for A10.

Results of RF

As the electrode size does not appear to play a significant role in the identification of corrosion types, the RQA variables corresponding to electrodes A2 were used as a representative dataset to train and test the RF classification model. Among the extracted feature vectors associated with electrodes A2, 75% of which were randomly selected for training and the rest (25%) served as test data to evaluate the generalization of the model in addition to the OOB model error. Test datasets were not involved in the training process.

A random forest composed of 100 decision tree classifiers was constructed. For each tree grown in the forest, four features and 70% of their observations were selected at random for training. The out-of-bag (OOB) classification error decreased as the number of grown trees increased, as shown in Figure 6-6. The OOB error stabilised at a fraction of 0.09 after approximately 30 trees. That is to say, only 9 out of 100 data points were misclassified.

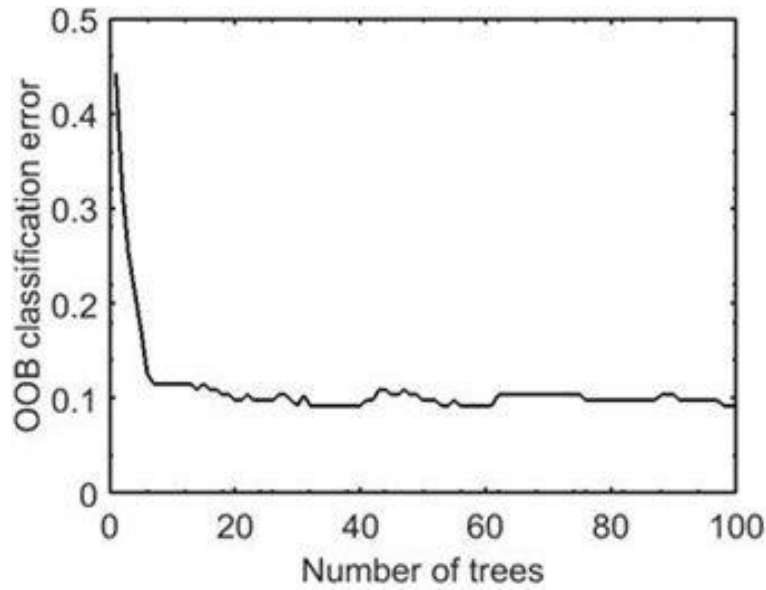


Figure 6-6: Out-of-bag classification errors of the RF model.

The test datasets were presented to the model for corrosion type identification and the result is shown in Figure 6-7. The vertical axis represents corrosion types, i.e. 1 for uniform, 2 for pitting and 3 for passivation. The horizontal axis shows the indices for the test datasets, where the datasets with numbers 1 - 20 were originally from uniform system, 21 - 40 were from pitting system and 41 - 57 were from passivation. It can be seen that three data originally from uniform corrosion were misclassified as pitting and only one data from passivation was misclassified as pitting. In other words, 53 out of 57 data points were correctly classified. Therefore, the classification accuracy of the RF model is 93%. In other words, the classification error is around 0.07, in line with the OOB error. Comparing the 88% accuracy of the LDA model for electrodes A2, the RF model is no doubt better and more promising.

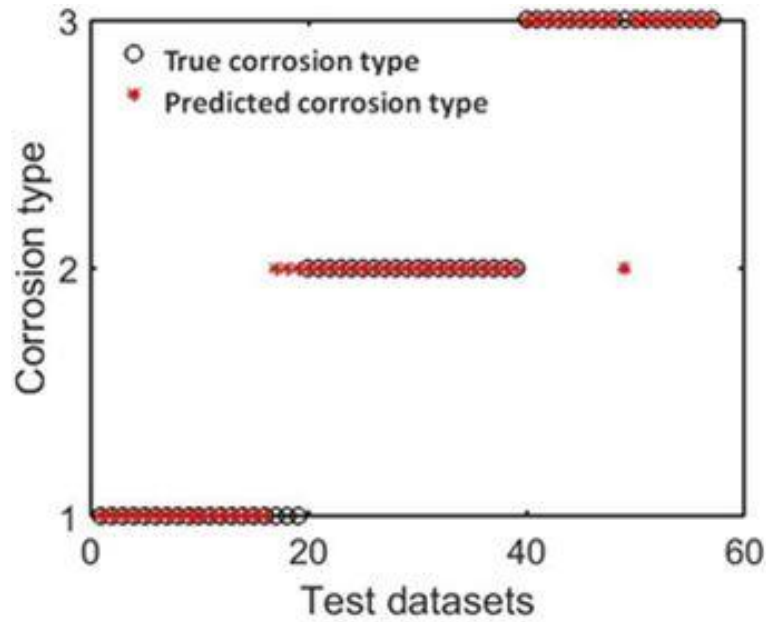


Figure 6-7: Comparison of the predicted corrosion types by RF model with the actual corrosion types for test datasets.

The importance of the RQA variables contributing to the accuracy of the model was estimated by permuting each variable in the OOB samples and evaluating the error in the model. The results are shown in Figure 6-8.

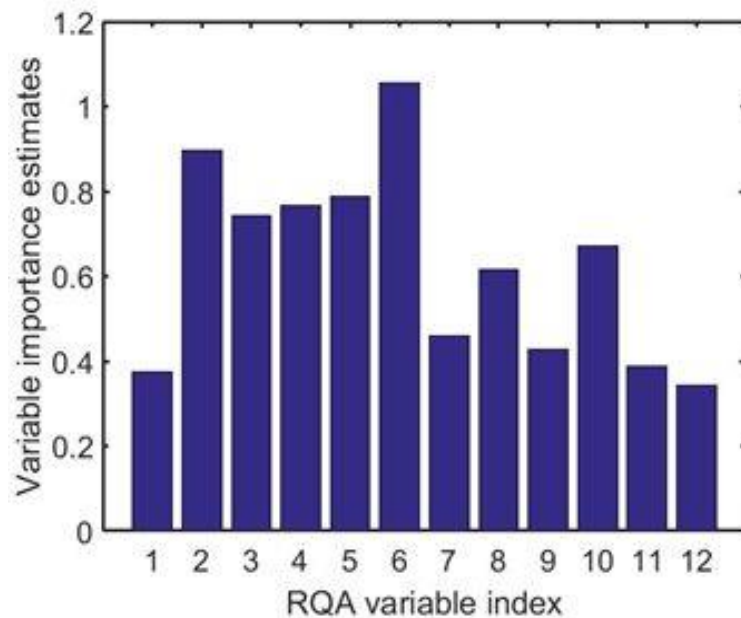


Figure 6-8: RQA variable importance estimates.

It is suggested that all the variables played a role on the improvement of the RF model. Among them, the RQA variable number 6 (*LAM*) was the most significant,

closely followed by variable number 2 (*DET*), 5 (*ENTR1*), 4 (L_{max}) and 3 (L_{mean}). This in part agrees with the observations from Figure 6-3.

6.3.3 Electrochemical impedance spectroscopy (EIS)

The noise resistance, defined as the ratio of potential standard deviation to current standard deviation of the EN segment, is considered to be similar to the corrosion resistance, thus can be potentially used for corrosion rate monitoring. In this study, EIS was carried out as a complementary and comparative method to investigate the corrosion resistances of the steel samples with various corrosion types.

The Nyquist and Bode plots generated by EIS measurements for electrodes A10 in different corrosion systems are shown in Figure 6-9. The inset of Figure 6-9(a₁) represents the equivalent circuit used to fit the impedance data for uniform corrosion. R_s represents the solution resistance, R_{ct} represents charge transfer resistance and CPE represents a constant phase element. The CPE is used instead of a double layer capacitor is because of the non-ideal capacitance behaviour due to surface roughness and nonhomogeneous corrosion products, etc., which is indicated by the depressed semi-circle shown in the Nyquist plot. It should be noted that this one time constant is a probably apparent overall behaviour that appears as the combination of different processes with time constants close enough to be individually resolved. The equivalent circuit applied in analysis of passivation (Figure 6-9 (b₁, b₂)) and pitting (Figure 6-9 (c₁, c₂) and (d₁, d₂)) was chosen according to [26] and is shown as an inset in Figure 6-9 (b₁, c₁ and d₁). Based on [26], CPE₁ represents the constant phase element for the film formed on the steel surface, R_1 represents the film resistance, CPE₂ and R_2 parallel combination represents the contribution of the movement of charged species through the surface film at lower frequency. Table 6-2 shows all the fitting results, where n_1 and n_2 represent the exponents for the constant phase elements CPE₁ and CPE₂.

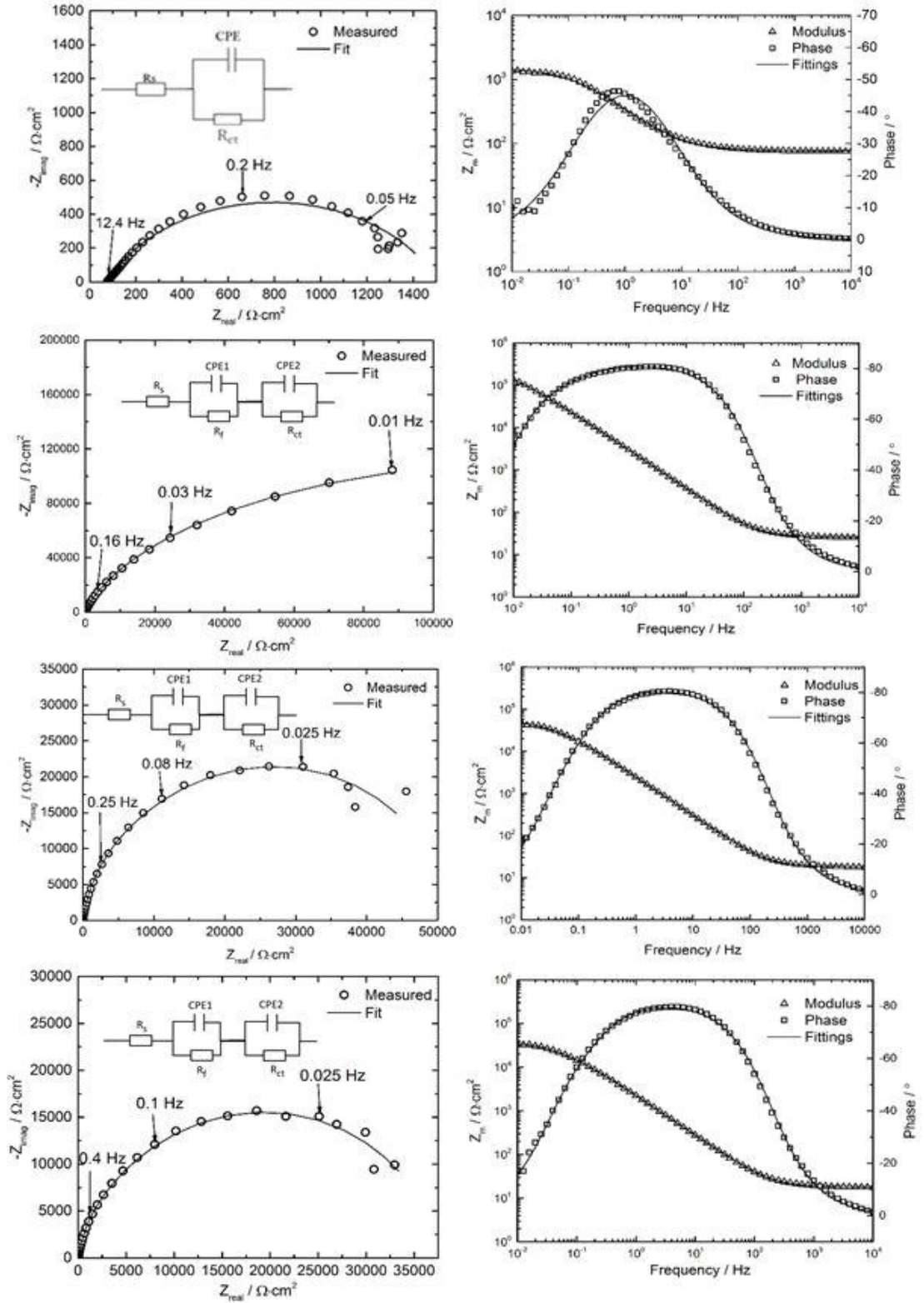


Figure 6-9: Nyquist plots and Bode plots for A10 working electrodes (electrode surface area of 10.2 cm^2) for (a₁, a₂) uniform corrosion, (b₁, b₂) passivation, (c₁, c₂) pitting I, (d₁, d₂) pitting II.

Table 6-2: Calculated parameters used to fit the equivalent circuit.

Parameters	Uniform	Passivation	Pitting I	Pitting II
R_s ($\Omega \text{ cm}^2$)	76.92	26.06	18.35	18.21
CPE ($\mu\text{F}/\text{cm}^2$)	788.60	-	-	-
n^*	0.74	-	-	-
R_f ($\text{k}\Omega \text{ cm}^2$)	-	218.2	47.66	35.50
CPE_1 ($\mu\text{F}/\text{cm}^2$)	-	90.69	98.66	105.6
n_1	-	0.97	0.90	0.90
R_{ct} ($\text{k}\Omega \text{ cm}^2$)	1.43	14.55	4.58	2.28
CPE_2 ($\mu\text{F}/\text{cm}^2$)	-	179.9	312.8	398.9
n_2	-	0.84	0.98	0.99
Chi-square	1.47×10^{-3}	4.61×10^{-4}	5.36×10^{-4}	3.98×10^{-4}

It has been established [27 – 29] that a precipitation film can be formed at the surface of carbon steel immersed in bicarbonate solutions, possibly consisting of $\text{Fe}_3\text{O}_4/\text{Fe}_2\text{O}_3$. However, the film is vulnerable to chloride ions at certain conditions, leading to local breakdown of the film and decrease of its resistance. Indeed, the film resistances R_f for the electrodes undergoing pitting corrosion were significantly lower than that for passivation.

It is known that the noise resistance is comparable with polarisation resistance [30], which is equivalent to the sum of R_s , R_f and R_{ct} , based on the equivalent circuit used in this study. Therefore, the noise resistance was compared with $R_s + R_f + R_{ct}$. The results are shown in Table 6-3, where the noise resistances were computed from the EN segments given in Figure 6-2.

Table 6-3: Electrochemical noise resistance (R_n) for electrode A10 in uniform corrosion, pitting and passivation systems and the corresponding resistance sum obtained from EIS.

	R_n ($k\Omega\text{ cm}^2$)	$R_s + R_f + R_{ct}$ ($k\Omega\text{ cm}^2$)
Uniform	1.03	1.51
Passivation	273.43	232.78
Pitting I	120.90	52.26
Pitting II	103.37	37.80

Apparently, the R_n value coincides with the $R_s + R_{ct}$ value in uniform corrosion and with the summed $R_s + R_f + R_{ct}$ value in passivation. In comparison, the R_n values in pitting process are not comparable with $R_s + R_f + R_{ct}$ values. Nevertheless, it is noticed that both R_n and $R_s + R_f + R_{ct}$ values showed a decreasing trend from pitting I to pitting II. Therefore, in the studied systems, R_n can be used as an indicator for corrosion rate variations (changing trends) not only for uniform corrosion and passivation but also for pitting, although these values may not correspond to the exact corrosion rate. It should be noted that the estimation of corrosion rate from a resistance is only valid for a system that complies with the Butler-Volmer equation. When pitting or passivation occur, only loose indication of corrosion rate can be gained from the resistance value.

6.4 Summary

In this study, carbon steel electrodes with different sizes, i.e., 0.15 cm^2 , 2.1 cm^2 , 6.2 cm^2 and 10.2 cm^2 , were immersed in different solutions, creating three types of corrosion, i.e. uniform, pitting and passivation. Linear discriminant analysis (LDA) and random forests (RF) models were used to identify the corrosion types from twelve features, which were extracted by use of recurrence quantification analysis from the electrochemical noise signals associated with different corrosion systems. In addition, the noise resistance was compared with the resistances obtained from electrochemical impedance spectroscopy. The main conclusions drawn from the experimental study and statistical analysis are as follows:

- Recurrence quantification analysis of the electrochemical current noise data provided valuable features which can be used to differentiate between various corrosion types.
- On the basis of the methodology proposed in our previous work [23], LDA and RF models established in this study with an extended set of RQA features improved the differentiation accuracy between passivation and pitting. The RF model presented better overall prediction accuracy of 93% than the LDA model (88%).
- From the LDA model built with different electrode sizes (A2, A6 and A10) as classes, it was inferred that the electrode size was not a major factor for the corrosion type identification.
- Variable importance estimation by use of the RF model suggested that the RQA features laminarity (*LAM*) and determinism (*DET*) played the most significant role with regard to the identification of corrosion types.
- The noise resistance R_n calculated from EN can be used for monitoring corrosion rate variations during uniform corrosion, passivation and pitting.

It should be pointed out that the above conclusions are based on just one set of corrosion systems under study. It may not be generally applicable. Further investigations are needed to extend the application of the proposed methods.

References

- [1] W.P. Iverson, Transient voltage changes produced in corroding metals and alloys, *J Electrochem Soc*, 115 (1968) 617-618.
- [2] V. Tyagai, Faradaic noise of complex electrochemical reactions, *Electrochimica Acta*, 16 (1971) 1647-1654.
- [3] D. Eden, Electrochemical noise - simultaneous monitoring of potential and current noise signals from corroding electrodes, (1987).
- [4] F. Hass, A.C.T.G. Abrantes, A.N. Diógenes, H.A. Ponte, Evaluation of naphthenic acidity number and temperature on the corrosion behavior of stainless steels by using Electrochemical Noise technique, *Electrochim Acta*, 124 (2014) 206-210.
- [5] R. Moshrefi, M.G. Mahjani, M. Jafarian, Application of wavelet entropy in analysis of electrochemical noise for corrosion type identification, *Electrochem Commun*, 48 (2014) 49-51.
- [6] E.C. Rios, A.M. Zimer, P.C.D. Mendes, M.B.J. Freitas, E.V.R. de Castro, L.H. Mascaro, E.C. Pereira, Corrosion of AISI 1020 steel in crude oil studied by the electrochemical noise measurements, *Fuel*, 150 (2015) 325-333.
- [7] A.N. Chen, F.H. Cao, X.N. Liao, W.J. Liu, L.Y. Zheng, J.Q. Zhang, C.A. Cao, Study of pitting corrosion on mild steel during wet-dry cycles by electrochemical noise analysis based on chaos theory, *Corros Sci*, 66 (2013) 183-195.
- [8] D.H. Xia, S.Z. Song, Y. Behnamian, Detection of corrosion degradation using electrochemical noise (EN): review of signal processing methods for identifying corrosion forms, *Corrosion Engineering, Science and Technology*, 51 (2016) 527-544.
- [9] A. Aballe, A. Bautista, U. Bertocci, F. Huet, Measurement of the noise resistance for corrosion applications, *Corrosion*, 57 (2001) 35-42.
- [10] A. Legat, V. Dolecek, Corrosion monitoring system based on measurement and analysis of electrochemical noise, *Corrosion*, 51 (1995) 295-300.

- [11] C.A. Loto, Electrochemical noise measurement and statistical parameters evaluation of stressed α -brass in Mattsson's solution, Alexandria Eng. J. (2017).
- [12] C. Chandrasatheesh, J. Jayapriya, R.P. George, U.K. Mudali, Detection and analysis of microbiologically influenced corrosion of 316 L stainless steel with electrochemical noise technique, Eng Fail Anal, 42 (2014) 133-142.
- [13] A. Legat, J. Osredkar, V. Kuhar, M. Leban, Detection of various types of corrosion processes by the chaotic analysis of electrochemical noise, Mater Sci Forum, 289-2 (1998) 807-811.
- [14] C. Aldrich, B.C. Qi, P.J. Botha. Analysis of electrochemical noise with phase space methods. Minerals Engineering, 19(14), (2006), 1402-1409.
- [15] E. Cazares-Ibanez, G.A. Vazquez-Coutino, E. Garcia-Ochoa, Application of recurrence plots as a new tool in the analysis of electrochemical oscillations of copper, Electroanal Chem, 583 (2005) 17-33.
- [16] E. Sarmiento, J.G. González-Rodríguez, J. Uruchurtu, A study of the corrosion inhibition of carbon steel in a bromide solution using fractal analysis, Surface and Coatings Technology, 203 (2008) 46-51.
- [17] M. Shahidi, S.M.A. Hosseini, A.H. Jafari, Comparison between ED and SDPS plots as the results of wavelet transform for analyzing electrochemical noise data, Electrochimica Acta, 56 (2011) 9986-9997.
- [18] A.M. Homborg, E.P.M. van Westing, T. Tinga, X. Zhang, P.J. Oonincx, G.M. Ferrari, J.H.W. de Wit, J.M.C. Mol, Novel time-frequency characterization of electrochemical noise data in corrosion studies using Hilbert spectra, Corros Sci, 66 (2013) 97-110.
- [19] J.Y. Huang, X.P. Guo, Y.B. Qiu, Z.Y. Chen, Cluster and discriminant analysis of electrochemical noise data, Electrochimica Acta, 53 (2007) 680-687.
- [20] J.Y. Huang, Y.B. Qiu, X.P. Guo, Cluster and discriminant analysis of electrochemical noise statistical parameters, Electrochimica Acta, 54 (2009) 2218-2223.

- [21] J.Y. Huang, Y.B. Qiu, X.P. Guo, Analysis of electrochemical noise of X70 steel in Ku'erle soil by cluster analysis, *Mater Corros*, 60 (2009) 527-535.
- [22] J. Li, W.K. Kong, J.B. Shi, K. Wang, W.K. Wang, W.P. Zhao, Z.M. Zeng, Determination of corrosion types from electrochemical noise by artificial neural networks, *Int J Electrochem Sc*, 8 (2013) 2365-2377.
- [23] Y. Hou, C. Aldrich, K. Lepkova, L.L. Machuca, B. Kinsella, Monitoring of carbon steel corrosion by use of electrochemical noise and recurrence quantification analysis, *Corros Sci*, 112 (2016) 63-72.
- [24] N. Acuna-Gonzalez, E. Garcia-Ochoa, J. Gonzalez-Sanchez, Assessment of the dynamics of corrosion fatigue crack initiation applying recurrence plots to the analysis of electrochemical noise data, *Int J Fatigue*, 30 (2008) 1211-1219.
- [25] C. Lopez-Melendez, E.M. Garcia-Ochoa, M.I. Flores-Zamora, R.G. Bautista-Margulis, C. Carreno-Gallardo, C.P.C. Morquecho, J.G. Chacon-Nava, A. Martinez-Villafane, Dynamic Study of Current Fluctuations of Nanostructured Films, *Int J Electrochem Sc*, 7 (2012) 1160-1169.
- [26] T. Zhang, Y.A. Cong, Y.W. Shao, G.Z. Meng, F.H. Wang, Electrochemical noise analysis on the crevice corrosion behavior of Ni-Cr-Mo-V high strength steel using recurrence plots, *J Appl Electrochem*, 41 (2011) 289-298.
- [27] V.A. Alves, C.M.A. Brett, Characterisation of passive films formed on mild steels in bicarbonate solution by EIS, *Electrochimica Acta*, 47 (2002) 2081-2091.
- [28] F.F. Eliyan, E.S. Mandi, A. Alfantazi, Electrochemical evaluation of the corrosion behaviour of API-X100 pipeline steel in aerated bicarbonate solutions, *Corros Sci*, 58 (2012) 181-191.
- [29] D.H. Davies, G.T. Burstein, The effects of bicarbonate on the corrosion and passivation of iron, *Corrosion*, 36 (1980) 416-422.
- [30] Y.J. Tan, S. Bailey, and B. Kinsella. Factors affecting the determination of electrochemical noise resistance, *Corrosion*, 55 (1999) 469-475.

CHAPTER 7 CASE STUDY IV

Y. Hou, C. Aldrich, K. Lepkova, B. Kinsella, Detection of under deposit corrosion in a CO₂ environment by using electrochemical noise and recurrence quantification analysis, *Electrochimica Acta*, 274, 160-169 (2018).

This chapter presents the published paper with modified formats and contents that match the overall style of the thesis.

Detection of Under Deposit Corrosion in a CO₂ Environment by using Electrochemical Noise and Recurrence Quantification Analysis

Abstract

In this study, the corrosion of carbon steel immersed in CO₂ saturated aqueous solutions, in the presence and absence of sand deposits, were investigated by electrochemical noise measurement and recurrence quantification analysis. Uniform corrosion occurred at samples without sand deposit while localised corrosion took place at the sand-covered steel samples. These two different corrosion types can be accurately predicted by random forest and principal component models based on recurrence quantification analysis of either electrochemical potential or current noise data regardless of threshold values. The study provides a potential automated online corrosion monitoring scheme to ensure the integrity of pipelines.

Keywords: Carbon steel; Under deposit corrosion; Electrochemical noise; Recurrence quantification analysis; Corrosion monitoring; Random forests

7.1 Introduction

For economic reasons, carbon steel pipelines are widely used for oil and gas transmission and distribution. However, when operating in CO₂ environments, these pipelines are vulnerable to corrosion. The situation is exacerbated in the presence of mineral deposits, such as silica sand, which can be transported along with fluids. Apart from causing erosion-corrosion of the pipelines, these solid particles can also induce severe localized corrosion (e.g. pitting and mesa attack), which is referred to as under deposit corrosion (UDC) when the solids settle at the bottoms of pipelines, owing to low fluid flow velocities or stagnant conditions during shutdowns [1-3].

The control of UDC is currently achieved by pigging and addition of corrosion inhibitors [4, 5]. Effective application of these mitigation techniques should also be carefully considered and is closely related to monitoring pipeline corrosion. Conventionally, some corrosion monitoring techniques, such as linear polarisation resistance (LPR), electrochemical impedance spectroscopy (EIS) and electrical resistance (ER) are employed in laboratory testing or in the field for corrosion rate estimations. The results obtained from these approaches have some instructive value in the development of corrosion control programs. Nevertheless, these techniques may not be particularly useful for monitoring of localized corrosion, which occurs in the case of UDC, since they can only provide information regarding the average corrosion rate [6, 7]. One may find a pipeline with very low corrosion rates, suggested by these approaches, exhibiting severe pitting corrosion beneath a large volume of sediment [5]. Therefore, it is crucial that the occurrence of UDC can be detected and closely monitored.

Electrochemical noise (EN) measurement has been widely used for corrosion studies and field monitoring, owing to its ease of setting up, non-destructiveness, non-intrusiveness and particularly the ability to provide information on the initiation and propagation of localized corrosion events [8-12]. The challenge of this technique lies in the extraction of suitable feature variables from the noise data to distinguish between different types of corrosion. A number of parameters have been proposed for this purpose, including the roll-off slope of power spectral density plot [13], statistical parameters such as standard deviation, skewness and kurtosis [14], energy distribution plot from wavelet analysis of EN data [15] and characteristic charge [16], etc.

Nevertheless, the optimal approach for the analysis of EN data remains uncertain, especially when the automated corrosion monitoring program is considered. Recently, studies have shown the variables extracted by recurrence quantification analysis of EN data, such as recurrence rate and determinism, could be used to characterize the EN signals associated with localized corrosion processes [8, 17-24].

Recurrence plot (RP) is a graphical tool first introduced by Eckmann et al. [25] to visualise the recurrence behaviours in dynamic systems based on phase space reconstruction [26]. It can be mathematically expressed as a matrix according to equation (7-1)

$$R_{i,j} = H(\varepsilon - \|\mathbf{x}_i - \mathbf{x}_j\|), i, j = 1, 2, \dots, N \quad (7-1)$$

where \mathbf{x}_i and \mathbf{x}_j represent the states of the reconstructed phase space trajectory at time i and j , respectively; N is the total number of states in the trajectory; $\|\cdot\|$ calculates the distance between \mathbf{x}_i and \mathbf{x}_j ; ε is a user defined threshold and H is the Heaviside function which gives 0 and 1 depending on the sign of the content within the bracket. $R_{i,j}$ refers to the $(i, j)^{th}$ point in the recurrence matrix. The RPs can be quantified by a number of variables. The quantification of the RPs is called recurrence quantification analysis (RQA). EN signals could be characterised by the variables generated by RQA. Recently, the authors have proposed a corrosion type monitoring scheme [27] and an identification model [28] based on RQA of electrochemical current noise data. In these studies, the recurrence plots were generated without reconstructing the original time recordings to phase space trajectories. Instead, for a given signal, the Euclidean distance between each pair of the measured current values was computed and compared with a pre-defined threshold value. It was demonstrated that the variables extracted from the noise data by RQA were applicable in distinguishing between uniform, pitting and passivation (pseudo-passivation) corrosion processes [27, 28].

In the present study, previously established approaches were applied to analyse the electrochemical noise data obtained from CO₂ corrosion of carbon steel samples with and without sand deposits. Detailed investigations regarding the mechanisms associated with UDC have been carried out previously by other electrochemical methods, including potentiodynamic polarisation, cyclic voltammetry and linear

polarisation resistance [1, 3, 4, 29]. It is expected that localized corrosion would occur at the carbon steel samples covered with sand while uniform corrosion would take place at steel without sand. The aim of the current study was to apply electrochemical noise technique to this corrosion system and examine whether the previously proposed methodology could be used for UDC analysis. It was of particular interest to use EN to detect and monitor localized corrosion (pitting) that has been associated with the UDC. Moreover, comparative studies were conducted on the effect of different model parameters, e.g. the length of a data segment and the threshold value, with respect to the prediction accuracy of the model for identifying different types of corrosion.

7.2 Experimental work

7.2.1 Materials

The samples used in the present work were carbon steel (grade 1030) with chemical compositions of (wt%): C (0.37), Si (0.282), Mn (0.80), P (0.012), S (0.001), Cr (0.089), Ni (0.012), Mo (0.004), Sn (0.004), Al (0.01), and Fe (balance). The steel samples were soldered with conducting wires for electrical connection and then electro-coated using Powercron 6000CX to avoid potential crevice corrosion. Afterwards, the sample was mounted in epoxy resin (Epofix), leaving approximately 2 cm² as working surface. Prior to the test, the working surface was ground using silicon carbide paper up to 1200 grit, followed by rinsing with ultrapure water and ethanol and drying with nitrogen.

The test solution was prepared with analytical grade chemicals and ultrapure water (Milli-Q system, resistivity 18.2 MΩ cm), which consisted of 3 wt% sodium chloride (NaCl; Merck, 99.7%) and 0.01 wt% sodium bicarbonate (NaHCO₃; Merck, 99.7%). Before performing a test, the solution was saturated with CO₂ (oxygen content <10 ppb) at 30 °C. The pH of the test solution was approximately 4.7. The silica sand used as deposit was purchased from Sigma Aldrich. The properties of sand and washing methods employed have been published previously [3].

7.2.2 Electrochemical noise measurement

Two nominally identical steel samples were used as working electrodes (WE1 and WE2). The two samples were positioned as shown in Figure 7-1.

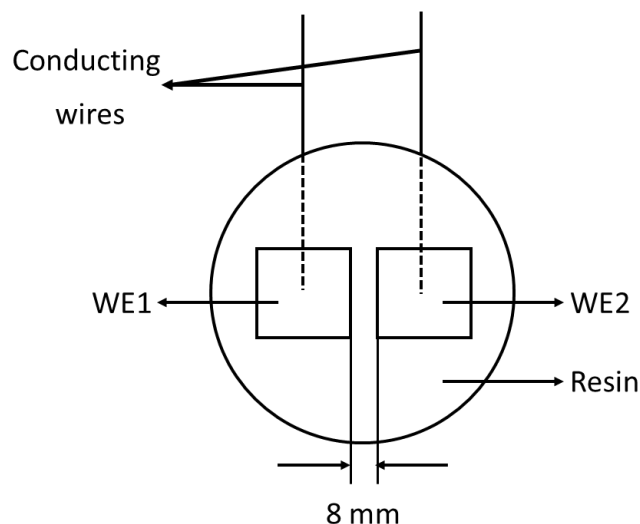


Figure 7-1: Schematic diagram of the working electrodes for EN measurements (total working surface area 4.2 cm²).

Two test cells were set up for the electrochemical noise measurement, one with sand-deposited steel (WE1 and WE2) and one with bare steel samples (no deposit). In both cells, the WEs were placed on a Teflon sample holder with working surfaces facing upwards. For the sand-covered WEs, a mounting cup (Struers) was used to hold the sand. The mass of the silica sand was 15 g, resulting in a thickness of approximately 8 mm above the steel samples. In a separate glass vessel, the test solution was heated up to $30\text{ }^{\circ}\text{C} \pm 1\text{ }^{\circ}\text{C}$ and purged with CO₂ for about 2 h. The two test cells, equipped with steel samples with (cell 1) or without sand (cell 2) deposit, were purged with N₂ for 30 min to create a deaerated environment. Afterwards, the CO₂ saturated test solution was pumped into the test cells. During all the tests, the temperature of the test solution was kept at $30\text{ }^{\circ}\text{C} \pm 1\text{ }^{\circ}\text{C}$ with the use of thermocouple controlled hotplates.

The electrochemical noise signals were measured using Gamry ESA410 software and Gamry Reference 600 potentiostat operating in the zero resistance ammeter (ZRA) mode. In addition to the working electrodes, a Metrohm single-junction Ag/AgCl (3 M) electrode was used as reference electrode and placed in Luggin capillary in close proximity to the working electrodes in order to minimize the iR drop between reference and working electrodes. The current flowing between the two WEs and the potential between the coupled WEs and the reference electrode were recorded simultaneously. In our previous studies with pitting corrosion systems [27, 28], it was found that the sampling rate of 2 Hz was able to pick up most (if not all) of

the pitting events. Therefore, the same sampling frequency was used in this study. During the EN measurements, the test solution was continuously purged with CO₂. Low flow rates in the tests with and without sand deposit were controlled by a gas flowmeter to minimise an impact on the EN measurement.

The EN measurements were carried out for 30 and 17 days respectively for tests with and without sand deposits. Over the test durations, the data were mostly recorded for 4 h per day, unless otherwise stated in this paper.

7.2.3 Post-test surface analysis

After tests, the samples were rinsed with ultrapure water (resistivity – 18.2 MΩ.cm) and ethanol to remove loose corrosion products and/or sand. To further remove the adherent products on the steel surfaces, the samples were treated with Clarke's solution according to ASTM standard G1. Afterwards, the samples were dried with nitrogen and stored in a vacuum desiccator until further analysis. Finally, surface profilometry (Infinite Focus, Alicona Instruments) was used to obtain 3D profile of the corroded samples and the root mean square roughness parameter (R_q).

7.3 Results and discussion

7.3.1 Surface morphology

Figure 7-2 shows surface morphologies of the steel samples after the tests with and without sand deposits. As can be seen that samples without deposit were uniformly corroded during the 17 days of immersion and the surface roughness R_q was 12.9 μm. In fact, previous publication [29] showed that even if the immersion time was extended to 30 days, uniform corrosion was still predominant. In comparison, the samples covered with sand showed less uniform corrosion and the surface roughness was 8.7 μm. However, there were approximately 30 small pits (depths ranging from 40 μm to 77 μm) present on the steel surface, as shown in the circled areas in Figure 7-2(b). Figure 7-3 shows the 3D images of a typical area on the steel surface for each case, which further demonstrates the occurrence of localized corrosion with sand deposit and the uniform corrosion of the steel sample without sand. The depth of the deepest point shown in Figure 7-3(b) was 77 μm.

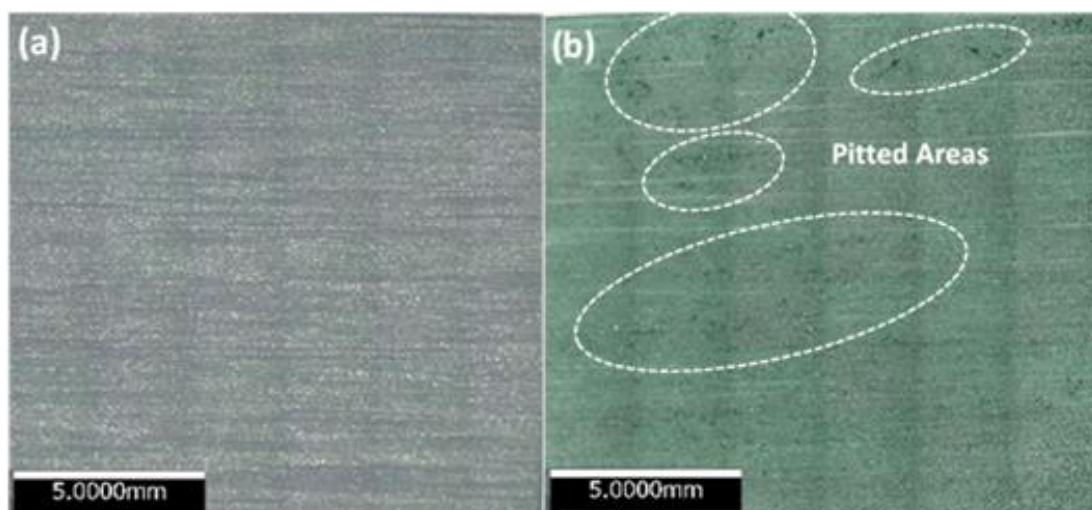


Figure 7-2: The 2D images of the steel surfaces after corrosion products removal (magnification 5x): (a) WE1 without sand after 17 days; (b) WE1 with sand after 30 days. Similar surface conditions were also observed on WE2s.

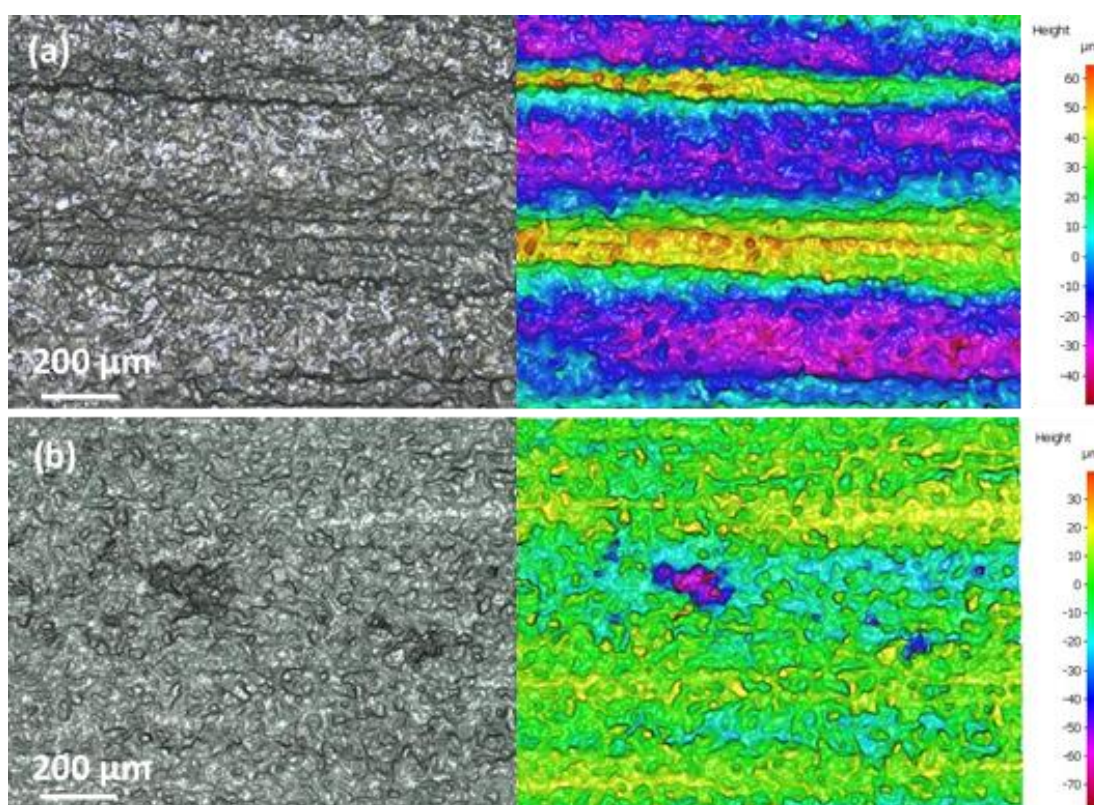


Figure 7-3: The 3D images of the steel surfaces after corrosion products removal (magnification 10x): (a) WE1 without sand after 17 days; (b) WE1 with sand after 30 days. The colour bars indicate the depth values.

7.3.2 Electrochemical noise

Figure 7-4 shows the electrochemical potential and current noise signals obtained on days 1 and 14 from both test cells. All the signals were detrended using linear regression. As can be seen, on day 1, the EN signal for the cell with sand deposit was dominated by a corresponding large transient in both the current and potential noise signals, which was an indication of the occurrence of pitting events on the steel surface [30]. The amplitude of the large transient in potential and current signal was around 2500 μV and 5 μA , respectively. The enlarged views of the EN transients [insets of Figure 7-4(a1, a2)] revealed that, with sand deposit, both potential and current signals had smaller transients occurring simultaneously (at 7.2ks, 7.6ks and 7.8ks) on the descending parts of the large transients. The amplitudes of the smaller transients for potential were about 100 μV – 200 μV and 0.25 μA – 0.5 μA for current. The repetition of the smaller transients reflects the competition of initiation and repassivation of metastable pits on the steel surface [30]. In contrast, without sand coverage, the electrochemical potential and current signals generated by the steel samples showed frequent oscillations with an amplitude of 1000 μV and 20 μA respectively. No pitting transients were found on the EN signal. On day 14, the representative transients were less obvious on the EN signal obtained with the sand-covered steel samples, which implied that the steel surface had reached a relatively stable state [30]. The amplitude of the potential fluctuation was decreased to around 400 μV and that of the current was around 4 μA . The EN collected with the bare steel specimens showed an increased amplitude in the potential noise signals with a significant decrease in frequency of the oscillations, whereas the frequency of the current noise remained rapid and essentially unchanged.

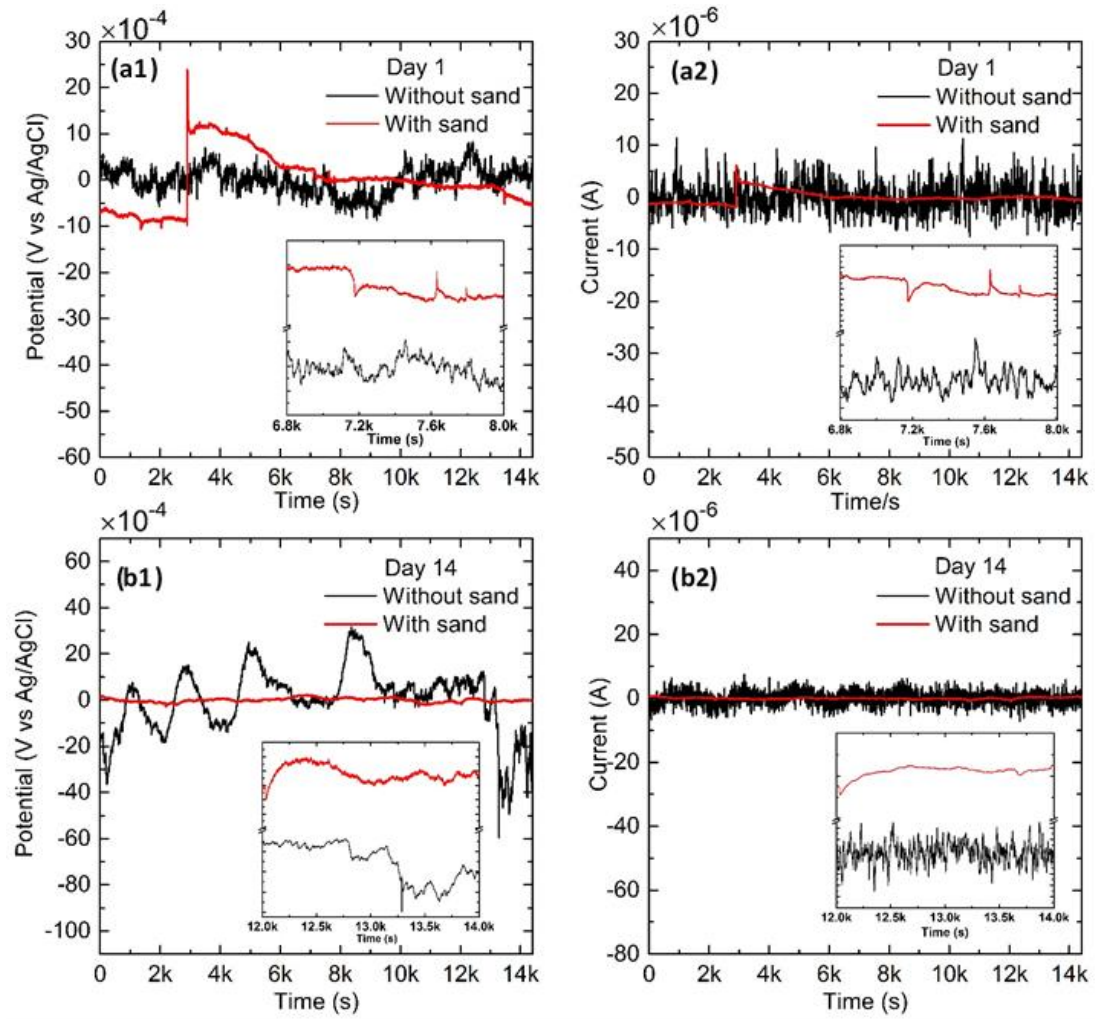


Figure 7-4: EN signals obtained with and without sand deposit on day 1 (a1) and (a2), day 14 (b1) and (b2), for potential and current noise respectively. The insets show the enlarged view of the corresponding EN segments.

Homborg et al. [10] have suggested that the potential data before trend removal reflects the evolution of the open circuit potentials (OCP) of the corrosion system. Therefore, the average potential values calculated from the raw potential noise data obtained each day for both cells are shown in Figure 7-5. As can be seen, without sand deposit, the OCP increased first from day 1 (-0.63 V) to day 6 (-0.57 V) and then stabilized thereafter. In contrast, the OCP of the steel samples covered with sand was relatively lower than that of bare steel samples and it was almost unchanged during the 30-day test. These occurrences could probably be attributed to two aspects: (a) depletion and reduced mass transfer of the corrosive species such as dissolved CO_2 to the sand covered steel surface, resulting in differences in the micro-environment at the deposit-covered steels compared to the deposit-free steels; (b) restriction of the

transportation of iron species between the sand-covered steel surface and the electrolyte, leading to the formation of local anodes and cathodes and hence the occurrence of localized corrosion [31].

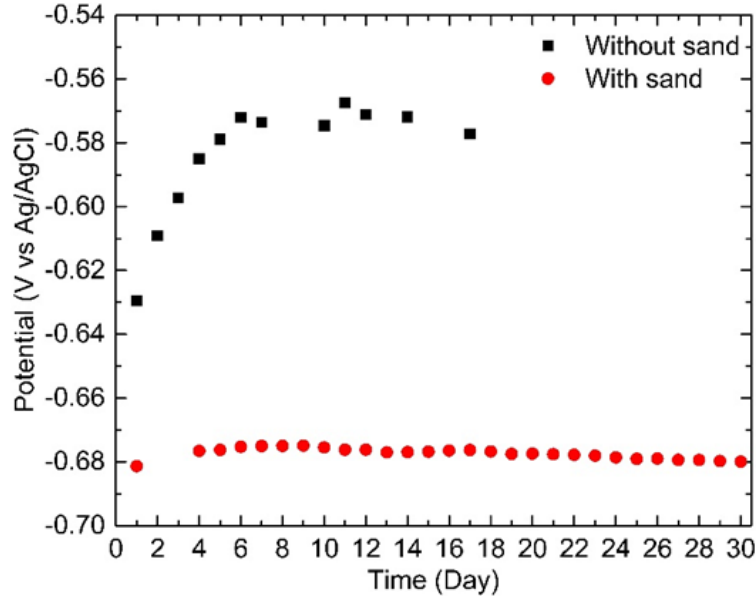


Figure 7-5: Evolution of OCPs for the steel samples with and without sand deposit.

7.3.3 Recurrence quantification analysis (RQA) of EN signals

To extract the recurrence quantification variables from EN signals, the first two parameters that need to be determined is the length of a segment, i.e. the optimal number of data points that should be included in each segment, and the threshold value ϵ for the generation of recurrence plot.

The threshold has a significant influence on the recurrence plots and thereby the quantification variables that are generated subsequently. It is a specified criterion to determine whether the distance between a pair of data points is close enough to be considered as recursive. If ϵ is too small, there may not be enough recurrence points or recurrence structures. On the other hand, if ϵ is too large, almost every point would be recurrence point, which may lead to many artefacts [26]. Several options for the selection of ϵ have been advocated in literature. For example, ϵ can be chosen according to the phase space diameter [32, 33], recurrence rate [34], and standard deviation of the measured time series [35]. Nevertheless, the selection of optimal criterion is strongly dependent on the system under study [26]. In this study, since the measured EN segments are used without embedding in phase space, the diameter of

phase space is not considered. Both a fixed recurrence rate and the standard deviation of the measured EN segment can be used as the criteria. In this work, it was decided to follow the previous work [27, 28] and choose the threshold value according to the standard deviation σ of the detrended EN segments. In order to show the variations of the RQA variables with different threshold values and to determine an optimal threshold that suit the corrosion systems under study, a range of threshold values, i.e. $[0, 0.5 \sigma]$ were investigated.

Twelve RQA variables (Table 3-1) were extracted from each EN segment with various threshold values. These variables were numbered as 1 – 12 for simplicity.

(1) Determination of segment length

Figure 7-6 shows two different current segments obtained with bare steel and sand-deposited steel samples, where NS is the abbreviation for “no sand” and WS is for “with sand”.

To investigate the effect of segment length on the recurrence quantification variables, 512 (i.e. 256 s), 1024 (i.e. 512 s) and 2048 (i.e. 1024 s) data points were used as the lengths of each segment, resulting in NS1, NS2, NS3, WS1, WS2 and WS3.

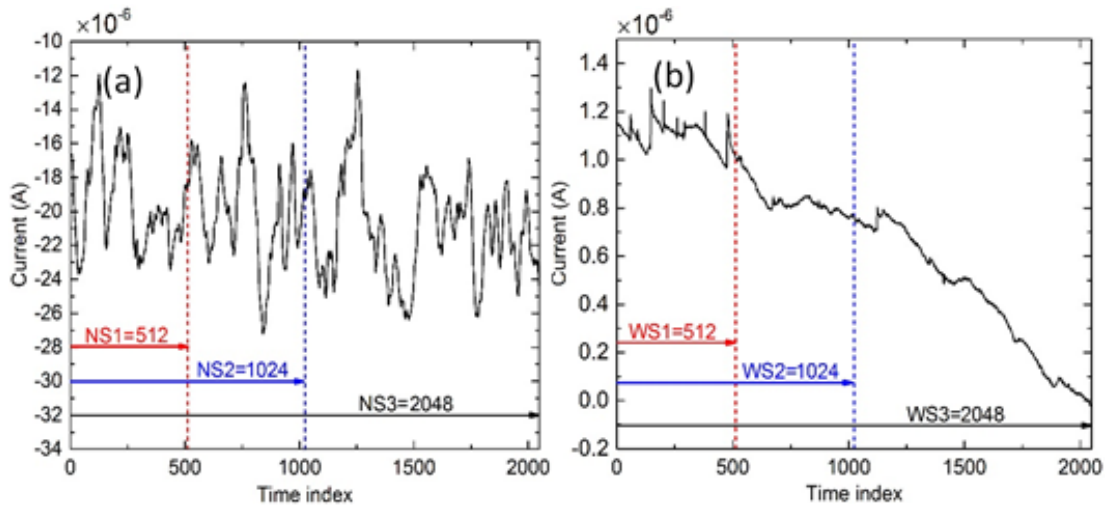


Figure 7-6: Electrochemical current data segments obtained with steel samples (a) without and (b) with sand deposits.

Prior to the calculation of the recurrence plots, the linear trend of each segment was removed and then 12 RQA variables were calculated with a set of threshold values over the range $[0, 0.5]$. The results are presented in Figure 7-7.

The threshold values ranged from 0.01σ (σ is the standard deviation of the trend removed EN segment) to 0.5σ at a step of 0.01σ . It can be seen that, in general, the RQA variables had similar trends with the increasing threshold values. Specifically, for the current signal from the NS system (Figure 7-6(a)), the length of the segment did not have any significant influence on the calculated RQA variables. In comparison with the signal from the WS system (Figure 7-6(b)), which contained some typical pitting peaks, the total number of data points included in a segment did affect some of the RQA variables. Apart from those which showed no apparent change with increasing segment lengths, the RQA variables either increased or decreased with segment lengths, and overall, the difference between WS2 and WS3 was relatively small (Figure 7-7(b)). This could be attributed to the difference in the number and interval of pitting transients that are included in a segment. For example, as shown in Figure 7-6(b), with 512 data points, the segment is dominated by a number of frequent pitting transients. When the length of the segment is extended to contain 1024 data points, a part of signal that contains a different feature (i.e. no obvious pitting transients present for the part from 512 to 1024) is included in the segment. After converting this segment to the recurrence plot, different recurrence structures will appear compared to the shorter segment with only 512 data points, leading to different values of the

quantification variables. When the length of the segment is increased from 1024 to 2048 data points, because the characteristic of the added portion (1024 – 2048) already exists in the previous portion (0 – 1024), the recurrence plots would have similar structures, thus similar RQA variables. Based on these analyses, it was decided that the segment with 1024 data points will be used in this investigation.

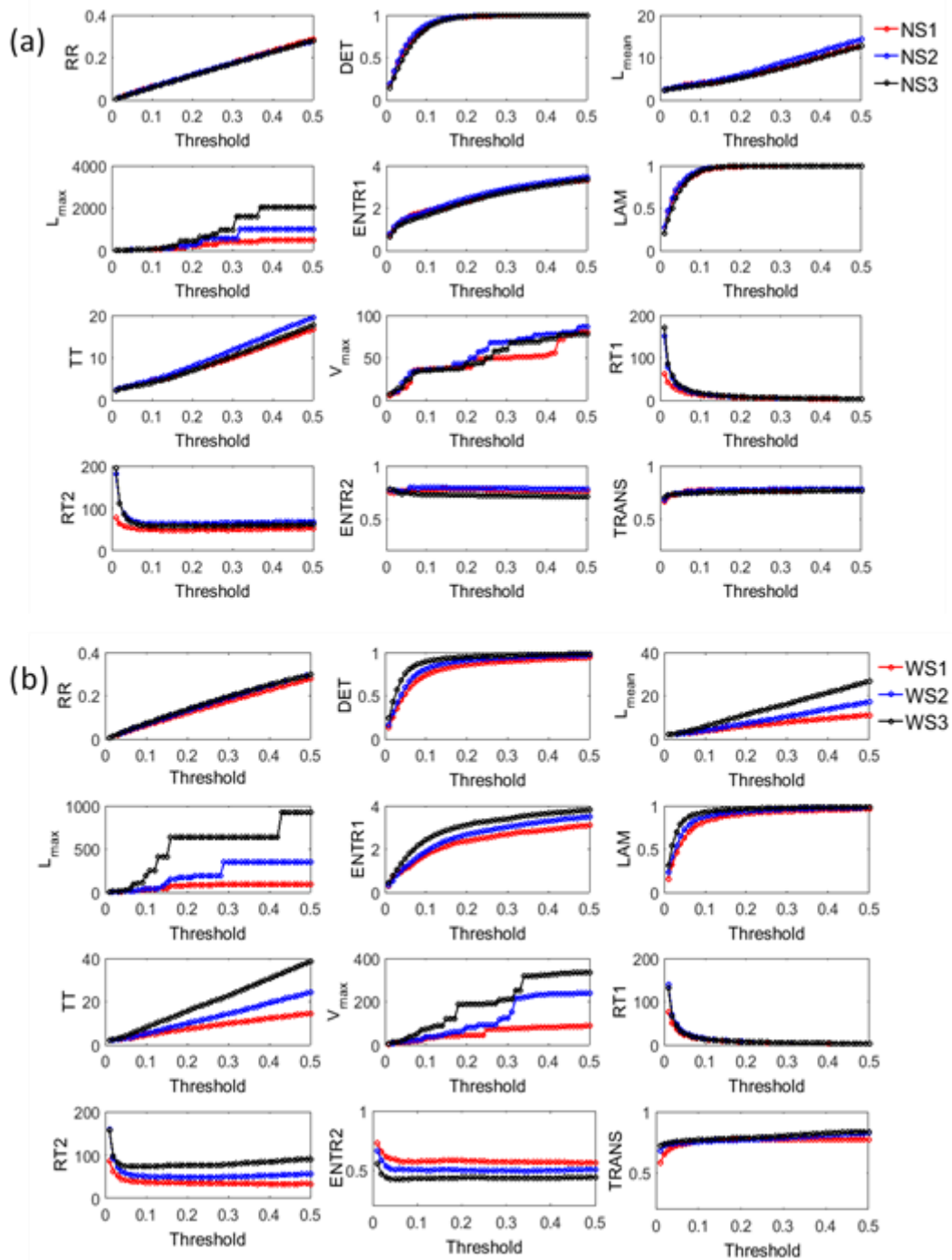


Figure 7-7: Variations of RQA variables with different threshold values and segment lengths: NS1 – NS3 (no sand deposited) and WS1 – WS3 (sand deposited) correspond to the segments shown in Figure 7-6(a) and Figure 7-6(b) respectively.

(2) Selection of threshold value

The threshold value is another important parameter for reliable identification of the EN signals from different corrosion processes using RQA measures. From Figure 7-7, it can be seen that all twelve RQA variables changed and changed

differently with the increase of threshold values, making it difficult to determine the optimal threshold value from inspection of the individual RQA variables.

In order to determine how this parameter influences RQA of the EN signals, the random forest (RF) classification model outlined in our previous work [22] was employed. The idea was to compare the prediction accuracy of the RF model using RQA variables calculated with different threshold values. The data processing procedures are summarized as follows:

- i. All the raw EN data (collected with steel samples with and without sand deposits) were divided into small segments with 1024 points in each.
- ii. The EN segments were detrended by linear regression.
- iii. Twelve RQA variables were extracted from each EN segment using a threshold value of 0.02σ . For each segment, a row vector consisted of the RQA variables was labelled with '1', if the segment was obtained with non-deposited steel samples, or '2' if obtained with sand-deposited steel. Due to the length of testing (17 days without sand and 30 days with sand), a total of 630 vectors labelled '1' and 2,040 vectors labelled '2' were obtained.
- iv. Of the 2,670 vectors, 70% were randomly selected as a training dataset to build the RF model and the remaining 30% were used as a test dataset to validate the prediction accuracy of the RF model.
- v. Step iii was repeated with threshold values equivalent to 0.05σ , 0.2σ , 0.3σ , 0.4σ and 0.5σ and then a repeat of step iv was conducted.

The prediction accuracies with different threshold values were compared, as shown in Figure 7-8. Surprisingly, in all circumstances under study, the prediction accuracy of corresponding RF model was very high – over 99%. Particularly, when the RQA variables were extracted from the current data and the threshold value was equal to or larger than 0.05σ , the test data gave a prediction accuracy of 100%. In addition, when only the potential data were used for extracting RQA variables, the results were slightly worse than those with current data RQA variables.

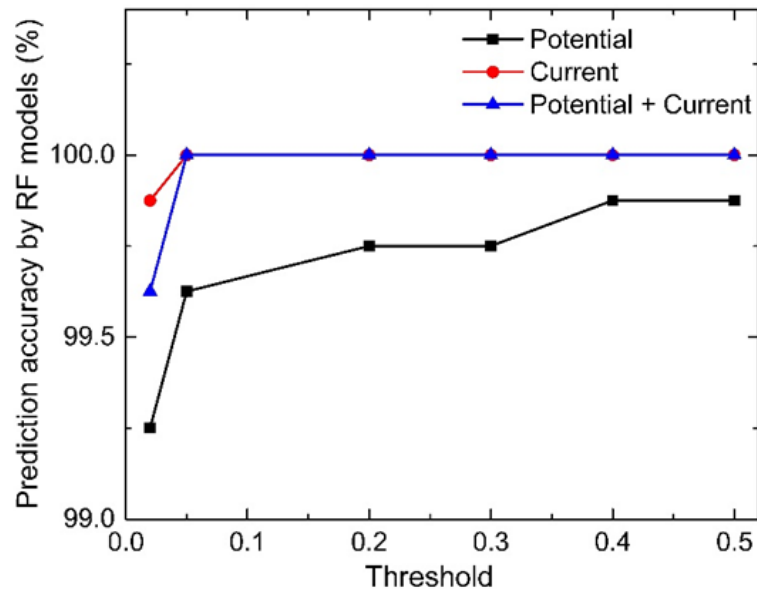


Figure 7-8: Discrimination (between uniform corrosion and UDC) accuracies of the RF models using RQA variables extracted from potential, current and their combination with various threshold values.

For different thresholds, RQA variable 11 (*ENTR2* or the entropy of the recurrence density) consistently appeared to be the most influential variable. This can be seen in Figure 7-9, which shows the importance estimations (*Imp*) of the current RQ variables used for RF model training. Detailed explanation of how the variable importance was estimated can be found in [22], but essentially the importance is linked to the decrease in performance of the model when the variable is omitted from the analysis, so that variables with larger *Imp* values are more important.

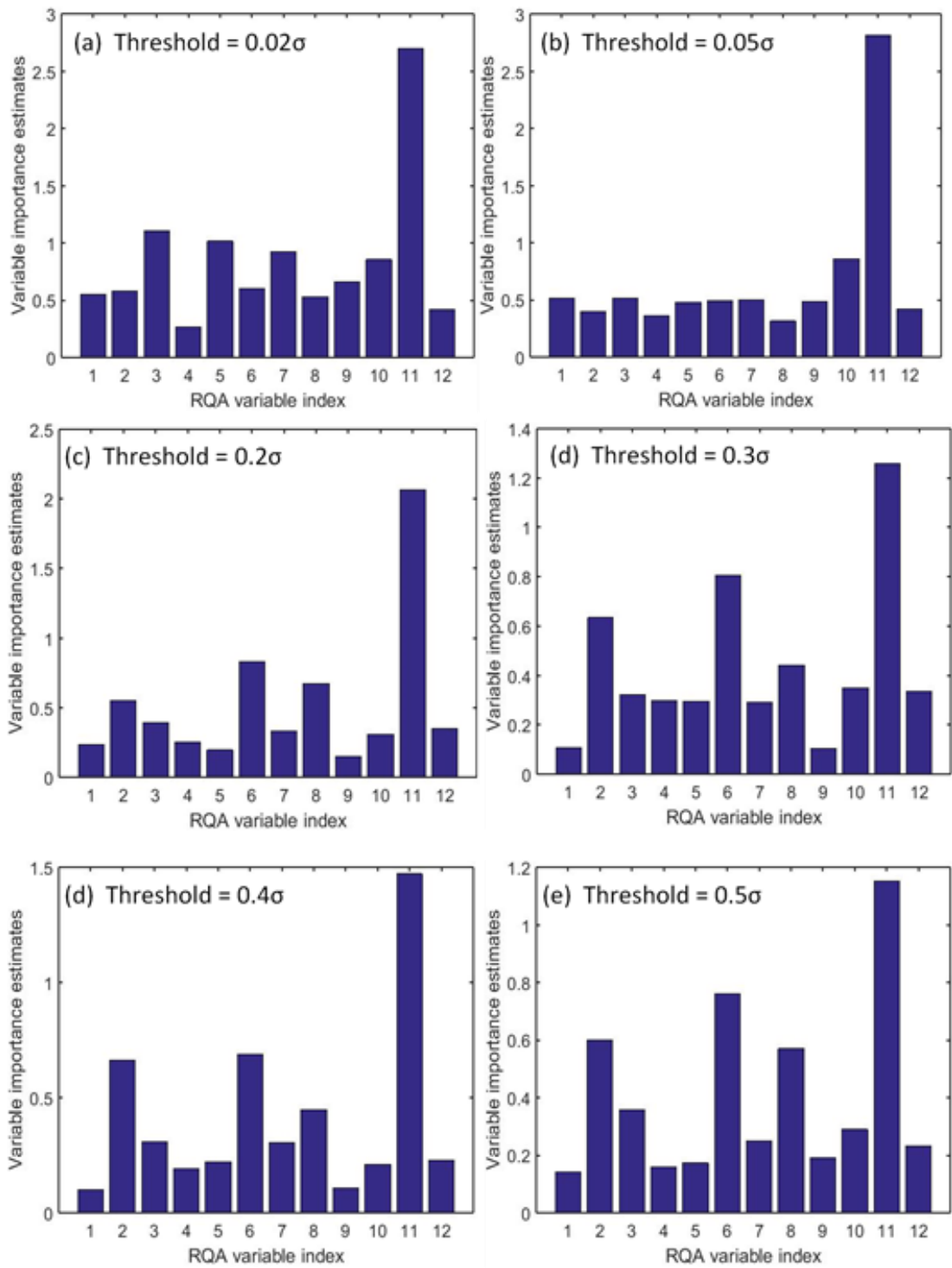


Figure 7-9: RQA variable importance estimations for various threshold values. The variable indices refer to 1 – RR , 2 – DET , 3 – L_{mean} , 4 – L_{max} , 5 – $ENTR1$, 6 – LAM , 7 – TT , 8 – V_{max} , 9 – $RT1$, 10 – $RT2$, 11 – $ENTR2$, 12 – $TRANS$.

With the exception of RQA variable 11, as mentioned above, the importance of the other variables varied with different threshold values. For instance, following

ENTR2, the next three variables that contributed most during the training of the RF model were variable numbers 3, 5 and 7 for a threshold = 0.02σ , while variable numbers 6, 8 and 2 were more influential for threshold values larger than 0.2σ . In the case of threshold = 0.05σ , all the other variables had nearly equal impacts on the prediction accuracy of the RF model. However, without further validation, not too much emphasis should be placed on these results.

Overall, it can be concluded that, for the corrosion systems investigated, the threshold value should not be a significant influencing factor in the identification of different corrosion processes for the specific set of predictor variables.

7.3.4 Application of corrosion monitoring map

To apply the corrosion monitoring map proposed in our previous work [21], in this current study, the RQA variables extracted from electrochemical current data with threshold equivalent to 0.2σ were chosen. In brief, the monitoring scheme was composed of an off-line calibration stage and an on-line monitoring stage. In this study, the uniform corrosion of bare steel samples in a CO_2 environment without sand deposit was regarded as the normal operation condition (NOC).

From the RQA variables associated with NOC, 70% were randomly selected and normalised to zero mean and unit standard deviation. After normalisation, these variables were subjected to principal component analysis (PCA). Subsequently, the PCA model was established and calibrated with a 95% control limit based on the use of a five-component Gaussian mixture model. The remaining 30% of the RQA variables served as a test dataset to verify the effectiveness of the control limit. In the on-line monitoring stage, the RQA variables representing the under deposit corrosion process were continuously projected to the calibrated PCA model. Figure 7-10 illustrates the monitoring process step by step, where the green markers represent the test dataset of NOC and the red markers are used to highlight the newly projected UDC data.

It is clear that the NOC test data were well encapsulated by the 95% control boundary. When the sand was present on the steel surfaces, all the data projected onto the monitoring map were located outside of the control limit, except for a few

individual samples. This demonstrates that when sand is present, the monitoring map is capable of capturing localised corrosion with high reliability.

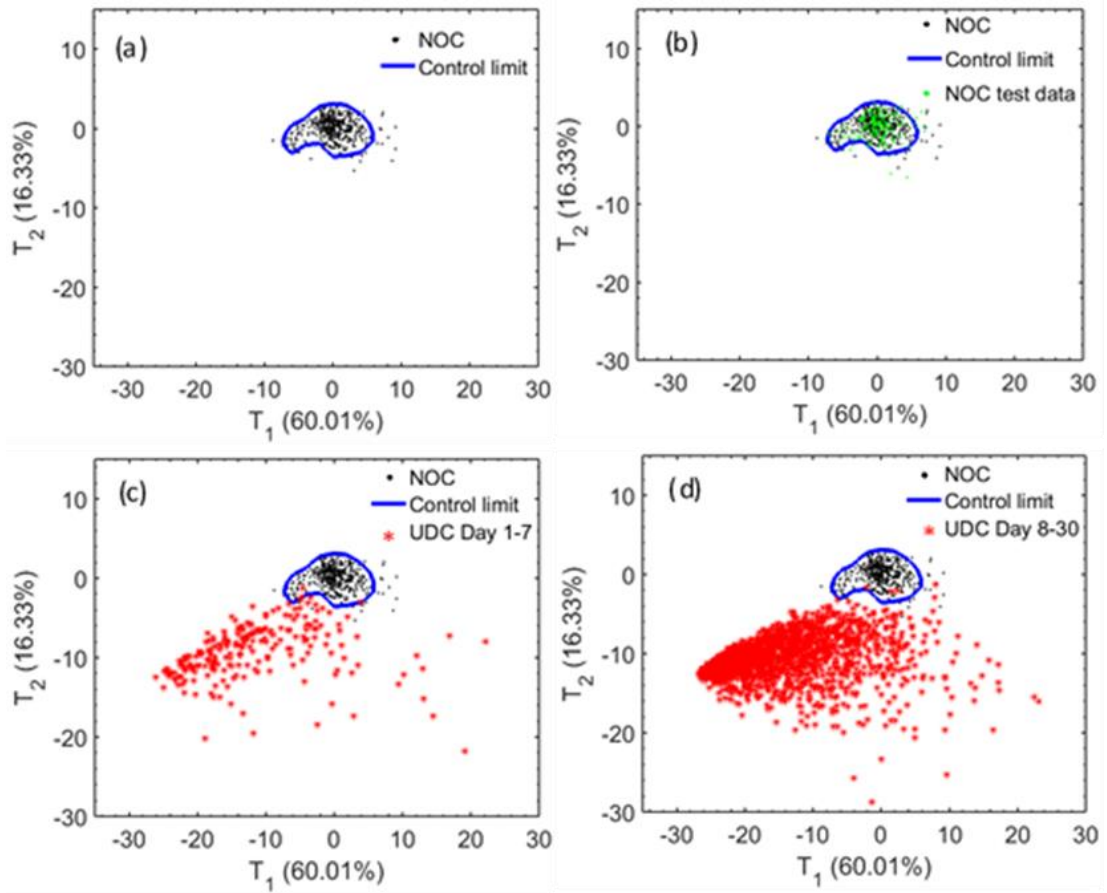


Figure 7-10: Evolution of the corrosion monitoring map (a) Off-line calibrated PCA model, (b) NOC test data projected, (c) UDC RQA data for days 1 – 7 projected, (d) UDC RQA data for days 8 – 30 projected.

7.4 Summary

In this study, electrochemical current and potential noise data were recorded simultaneously at carbon steel samples in the presence and absence of sand deposits in CO_2 environments. The surface morphologies of the steel samples after retrieving from the test cells revealed that the bare steel essentially underwent uniform corrosion, while the sand-covered steel samples were subjected to pitting. These two different types of corrosion can be accurately distinguished from each other by random forest models using variables extracted through recurrence quantification analysis of the EN data.

Moreover, it was found that when current data alone were used for extracting RQA variables, the discrimination result of the RF model was marginally better than that with RQA variables derived from potential measurements, although they both had very high prediction accuracies ($> 99\%$). Additionally, the comparative study on the effect of segment length on the recurrence variable values suggested that for the EN signal corresponding to uniform corrosion, the length of a so-called segment had little impact on its RQ features, while for the EN signal associated with UDC, the segment length affected some of the RQ variables. Hence the determination of the segment length should be carefully considered according to the sampling frequency used and the actual corrosion system under study.

A principal component score plot of the current RQA variables could be used highly effectively for real-time detection of UDC.

References

- [1] V. Pandarinathan, K. Lepková, S.I. Bailey, R. Gubner, Impact of mineral deposits on CO₂ corrosion of carbon steel, paper no. 2579, NACE International Corrosion Conference Series, 2013.
- [2] G.A. Zhang, N. Yu, L.Y. Yang, X.P. Guo, Galvanic corrosion behavior of deposit-covered and uncovered carbon steel, *Corros Sci*, 86 (2014) 202-212.
- [3] V. Pandarinathan, K. Lepková, S.I. Bailey, R. Gubner, Evaluation of corrosion inhibition at sand-deposited carbon steel in CO₂-saturated brine, *Corros Sci*, 72 (2013) 108-117.
- [4] V. Pandarinathan, K. Lepková, R. Gubner, Inhibition Of CO₂ Corrosion Of 1030 Carbon Steel Beneath Sand-Deposits, paper no. 11261, NACE International Corrosion Conference Series, 2011.
- [5] Y. Tan, Y. Fwu, K. Bhardwaj, Electrochemical evaluation of under-deposit corrosion and its inhibition using the wire beam electrode method, *Corros Sci*, 53 (2011) 1254-1261.
- [6] A.M. Homborg, E.P.M. van Westing, T. Tinga, X. Zhang, P.J. Oonincx, G.M. Ferrari, J.H.W. de Wit, J.M.C. Mol, Novel time–frequency characterization of electrochemical noise data in corrosion studies using Hilbert spectra, *Corros Sci*, 66 (2013) 97-110.
- [7] Y. Tan, Sensing localised corrosion by means of electrochemical noise detection and analysis, *Sensors and Actuators B: Chemical*, 139 (2009) 688-698.
- [8] W. Liu, D. Wang, X. Chen, C. Wang, H. Liu, Recurrence plot-based dynamic analysis on electrochemical noise of the evolutive corrosion process, *Corros Sci*, 124 (2017) 93-102.
- [9] S.M. Hoseinie, A.M. Homborg, T. Shahrabi, J.M.C. Mol, B. Ramezanzadeh, A Novel Approach for the Evaluation of Under Deposit Corrosion in Marine Environments Using Combined Analysis by Electrochemical Impedance Spectroscopy and Electrochemical Noise, *Electrochim Acta*, 217 (2016) 226-241.

- [10] A.M. Homborg, C.F. Leon Morales, T. Tinga, J.H.W. de Wit, J.M.C. Mol, Detection of microbiologically influenced corrosion by electrochemical noise transients, *Electrochim Acta*, 136 (2014) 223-232.
- [11] R. Moshrefi, M.G. Mahjani, M. Jafarian, Application of wavelet entropy in analysis of electrochemical noise for corrosion type identification, *Electrochem Commun*, 48 (2014) 49-51.
- [12] A.M. Homborg, R.A. Cottis, J.M.C. Mol, An integrated approach in the time, frequency and time-frequency domain for the identification of corrosion using electrochemical noise, *Electrochim Acta*, 222 (2016) 627-640.
- [13] A. Legat, V. Doleček, Corrosion Monitoring System Based on Measurement and Analysis of Electrochemical Noise, *Corrosion*, 51 (1995) 295-300.
- [14] C.A. Loto, Electrochemical noise measurement and statistical parameters evaluation of stressed α -brass in Mattsson's solution, *Alexandria Engineering Journal*, 57 (2018) 483-490.
- [15] M. Shahidi, S.M.A. Hosseini, A.H. Jafari, Comparison between ED and SDPS plots as the results of wavelet transform for analyzing electrochemical noise data, *Electrochim Acta*, 56 (2011) 9986-9997.
- [16] R.A. Cottis, M.A.A. Al-Awadhi, H. Al-Mazeedi, S. Turgoose, Measures for the detection of localized corrosion with electrochemical noise, *Electrochimica Acta*, 46 (2001) 3665-3674.
- [17] E. Cazares-Ibanez, G.A. Vazquez-Coutino, E. Garcia-Ochoa, Application of recurrence plots as a new tool in the analysis of electrochemical oscillations of copper, *J Electroanal Chem*, 583 (2005) 17-33.
- [18] N. Acuna-Gonzalez, E. Garcia-Ochoa, J. Gonzalez-Sanchez, Assessment of the dynamics of corrosion fatigue crack initiation applying recurrence plots to the analysis of electrochemical noise data, *Int J Fatigue*, 30 (2008) 1211-1219.
- [19] C. Lopez-Melendez, E.M. Garcia-Ochoa, M.I. Flores-Zamora, R.G. Bautista-Margulis, C. Carreno-Gallardo, C.P.C. Morquecho, J.G. Chacon-Nava, A.

Martinez-Villafane, Dynamic study of current fluctuations of nanostructured films, *Int J Electrochem Sc*, 7 (2012) 1160-1169.

- [20] L.S. Montalban, P. Henttu, R. Piche, Recurrence quantification analysis of electrochemical noise data during pit development, *Int J Bifurcat Chaos*, 17 (2007) 3725-3728.
- [21] E. Garcia-Ochoa, J. Gonzalez-Sanchez, N. Acuna, J. Euan, Analysis of the dynamics of Intergranular corrosion process of sensitised 304 stainless steel using recurrence plots, *J Appl Electrochem*, 39 (2009) 637-645.
- [22] Y.E. Yang, T. Zhang, Y.W. Shao, G.Z. Meng, F.H. Wang, Effect of hydrostatic pressure on the corrosion behaviour of Ni-Cr-Mo-V high strength steel, *Corros Sci*, 52 (2010) 2697-2706.
- [23] T. Sun, Z.Y. Wang, J. Li, T. Zhang, Effect of ultrasonic vibration solidification treatment on the corrosion behavior of AZ80 magnesium alloy, *Int J Electrochem Sc*, 8 (2013) 7298-7319.
- [24] E. Garcia-Ochoa, F. Corvo, Using recurrence plot to study the dynamics of reinforcement steel corrosion, *Prot Met Phys Chem*, 51 (2015) 716-724.
- [25] J.P. Eckmann, S.O. Kamphorst, D. Ruelle, Recurrence plots of dynamical systems, *EPL (Europhysics Letters)*, 4 (1987) 973.
- [26] N. Marwan, M. Carmen Romano, M. Thiel, J. Kurths, Recurrence plots for the analysis of complex systems, *Physics Reports*, 438 (2007) 237-329.
- [27] Y. Hou, C. Aldrich, K. Lepkova, L.L. Machuca, B. Kinsella, Monitoring of carbon steel corrosion by use of electrochemical noise and recurrence quantification analysis, *Corros Sci*, 112 (2016) 63-72.
- [28] Y. Hou, C. Aldrich, K. Lepkova, L.L. Machuca, B. Kinsella, Analysis of electrochemical noise data by use of recurrence quantification analysis and machine learning methods, *Electrochim Acta*, 256 (2017) 337-347.

- [29] V. Pandarinathan, K. Lepková, S.I. Bailey, R. Gubner, Inhibition of under-deposit corrosion of carbon steel by thiobenzamide, *J Electrochem Soc*, 160 (2013) C432-C440.
- [30] T. Zhang, Y. Shao, G. Meng, F. Wang, Electrochemical noise analysis of the corrosion of AZ91D magnesium alloy in alkaline chloride solution, *Electrochim Acta*, 53 (2007) 561-568.
- [31] V. Pandarinathan, K. Lepková, W. van Bronswijk, Chukanovite ($\text{Fe}_2(\text{OH})_2\text{CO}_3$) identified as a corrosion product at sand-deposited carbon steel in CO_2 -saturated brine, *Corros Sci*, 85 (2014) 26-32.
- [32] R. Gilmore, Topological analysis of chaotic time series, *Applications of Soft Computing* San Diego, CA, (1997) 243-257.
- [33] J.P. Zbilut, C.L. Webber Jr, Embeddings and delays as derived from quantification of recurrence plots, *Physics Letters A*, 171 (1992) 199-203.
- [34] J.P. Zbilut, J.M. Zaldívar-Comenges, F. Strozzi, Recurrence quantification based Liapunov exponents for monitoring divergence in experimental data, *Physics Letters, Section A: General, Atomic and Solid State Physics*, 297 (2002) 173-181.
- [35] N. Marwan, J.F. Donges, Y. Zou, R.V. Donner, J. Kurths, Complex network approach for recurrence analysis of time series, *Physics Letters, Section A: General, Atomic and Solid State Physics*, 373 (2009) 4246-4254.

CHAPTER 8 CASE STUDY V

Y. Hou, C. Aldrich, K. Lepkova, B. Kinsella, Identifying corrosion of carbon steel buried in iron ore and coal cargoes based on recurrence quantification analysis of electrochemical noise, *Electrochimica Acta*, 283, 212 – 220 (2018).

This chapter presents the published paper with modified formats and contents that match the overall style of the thesis.

Identifying Corrosion of Carbon Steel Buried in Iron Ore and Coal Cargoes Based on Recurrence Quantification Analysis of Electrochemical Noise

Abstract

The effect of bulk cargo materials - iron ore and coal – on the corrosion of cargo hulls in carriers was investigated using electrochemical noise (EN). Two reference corrosion systems were carried out first with the steel samples in contact with moist silica sand and immersed in NaCl solution, which generated localised corrosion and general corrosion, respectively. The electrochemical noise was measured and recurrence quantification analysis was used to extract feature variables. A random forest model developed using these feature variables as predictors was able to discriminate between the two reference corrosion systems. This model was successfully applied to assessment of carbon steel corrosion in iron ore and coal. The results predicted by the model were in agreement with visual and microscopic observations of the relevant corroded steel samples. This work provides a novel analytical approach for future on-line monitoring of carrier structures in contact with bulk cargoes.

Keywords: Bulk Cargo Carriers; Corrosion; Electrochemical Noise; Recurrence Quantification Analysis; Corrosion Type Identification; Random Forests

8.1 Introduction

Steel carriers are commonly used for transportation of cargoes, such as coal and iron ore [1, 2]. Corrosion has been identified as one of the major causes of ship structural failures [3-5]. Fortunately, with adequate maintenance and proper protection of the steel structures, the impact of corrosion could be controlled. However, field observations revealed that the maintenance practices were not always sufficient and some areas, such as the lower parts of the bulk coal and iron ore carriers, might not be suitable for the implementation of protection measures [3]. Therefore, an enhanced corrosion monitoring program is called for to guide efficient inspections and timely maintenance plans.

Corrosion can occur in different forms at different positions of the cargo hold of the bulk carrier. The overall thickness of the steel structure could be considerably reduced due to continuous general corrosion. In comparison, localized corrosion may result in little mass loss, but could lead to decrease of the strength of the steel structure and cause crack or penetration of the steel structure without pre-warning [6, 7]. Real-time monitoring of the corrosion processes could increase the chance of capturing the fault conditions of the steel structures and reduce unnecessary inspections, thereby decreasing the maintenance cost.

Previous experimental studies on corrosion of steels by bulk cargoes, like coal and iron ore, mainly focused on the factors that influenced general corrosion rates, including particle size, quantity of moisture, pH level as well as chloride and sulphate concentrations in the water phase of the ores [8-10]. To date, little attention has been paid to the real-time monitoring of the corrosion process at steels in contact with bulk cargoes and no studies have been carried out on the identification of different corrosion types.

There are a number of corrosion monitoring techniques that are frequently used in industries to assist the development and implementation of inspection and maintenance programs, such as electrical resistance (ER), linear polarisation resistance (LPR) and electrochemical impedance spectroscopy (EIS). Although these techniques could provide near real-time corrosion rate related to general corrosion process, they are not particularly useful in detecting localised corrosion events [11, 12].

It is widely recognized that electrochemical noise (EN) generated from corrosion processes bears valuable information regarding the underlying forms of corrosion [13-16]. Localised corrosion events can be revealed by indicators derived from the collected EN signals with appropriate analytical approaches. Over the past few decades, a variety of parameters derived from the EN data have been proposed for corrosion monitoring and corrosion type identification, e.g. localisation index or pitting factor [17], characteristic charge and frequency [18], roll-off slope of the power spectral density plot [19], correlation dimension [20], energy distribution plot (EDP) [21]. Nevertheless, contradictory results have been observed and no agreement has been reached as to the optimal measures.

More recently, recurrence quantification analysis (RQA) has been employed to interpret EN data [22-24]. It was demonstrated that feature variables extracted from EN data by use of RQA were capable of capturing the characteristics of different types of corrosion processes. Furthermore, in our recent studies [25-27], the combination of RQA and advanced machine learning methods was shown to be capable of distinguishing localised corrosion from general corrosion *in-situ*.

Specifically, the EN data segment was first converted to a so-called recurrence plot, from which twelve variables were then extracted. A recurrence plot is in essence a graphical representation of a square matrix, which is commonly expressed as $R_{i,j} = H(\varepsilon - \|\mathbf{x}_i - \mathbf{x}_j\|)$. In our studies, $R_{i,j}$ represents the $(i,j)^{\text{th}}$ point in the recurrence plot, ε is a predefined threshold value, $\mathbf{x}_i, \mathbf{x}_j$ are the measured EN values at times i and j , and $\|\cdot\|$ refers to the Euclidean distance between this pair of data points. $H(\cdot)$ represents the Heaviside function, which gives the value of one, if the distance between \mathbf{x}_i and \mathbf{x}_j falls within the threshold. Otherwise, it is zero. The quantification of the recurrence plots is termed as recurrence quantification analysis (RQA), by which various feature variables can be derived.

In previous investigations [25, 26], twelve variables extracted by RQA method, as shown in Table 3-1, were used as predictors of a random forest (RF) model to distinguish between uniform, pitting and passivation processes of carbon steel in NaCl solution, $\text{NaHCO}_3 + \text{NaCl}$ solution, and NaHCO_3 solution respectively. Furthermore,

the RF model was capable of identifying pitting corrosion of carbon steel beneath sand deposit and general corrosion in CO₂-saturated brine [27].

The present study is an extended application of the existing methodologies [25-27]. The objective is to identify the types of corrosion process that take place at carbon steel exposed to the two bulk cargoes investigated. Two other corrosive systems, which are expected to result in general and localized corrosion, are used to obtain electrochemical noise data for development of the random forest model. Specifically, carbon steel immersed in NaCl solution will be used for general corrosion assessment, and silica sand moist with NaCl solution is used for localized corrosion assessment. Deposits of silica sand at carbon steel have been previously shown to cause pitting [28]. A random forest model will be developed based on recurrence quantification analysis of the EN data generated from these two reference corrosion systems to discriminate between the two types of corrosion. Once established, this model will be applied to identify the corrosion types of specimens buried in iron ore and coal cargoes on the basis of associated EN recordings. This could be accomplished in real time, without having to take the specimens out. It is expected that this work could offer an additional analytical method for corrosion monitoring of bulk cargo carriers.

8.2 Experimental work

8.2.1 Materials

Carbon steel specimens (grade 1030) with chemical compositions of (wt.%): C (0.37), Si (0.282), Mn (0.80), P (0.012), S (0.001), Cr (0.089), Ni (0.012), Mo (0.004), Sn (0.004), Al (0.01), and Fe (balance) were used in this study. Two rectangular specimens with the same dimensions of 1.5 cm × 1.4 cm × 0.5 cm were soldered with a conducting wire for electrical connection and then electrocoated using Powercron 6000CX. Afterwards, the two specimens were mounted together in epoxy resin (Epofix), leaving approximately 2 cm² for each specimen as a working surface. This assembly, named as EN electrode, was used as working electrode in the electrochemical noise tests. Prior to EN tests, the electrode was ground on silicon carbide paper up to 240 grit, followed by rinsing with ultrapure water and ethanol and finally drying with nitrogen.

Corrosiveness of two different bulk cargo materials, iron ore and coal, was assessed in separate tests. The moisture contents of the as-received iron ore and coal materials were 8.6 wt.% and 5.8 wt.%, respectively. In addition, test with 0.04 wt.% NaCl solution (no solid material tested), and one with silica sand moistened with NaCl (0.04 wt.%) were carried out as reference systems. The concentration of NaCl of 0.04 wt.% in the test solution was used to match the conductivity of the leached solutions from iron ore and coal materials. The conductivity was determined using 500 g of iron ore that was immersed in 500 mL ultrapure water at room temperature. The conductivity of the supernatant after 24 h of immersion was 372 $\mu\text{S}/\text{cm}$. Similarly, the conductivity of the supernatant from coal was 654 $\mu\text{S}/\text{cm}$. Therefore, 0.04 wt.% NaCl solution equivalent to a conductivity value of 625 $\mu\text{S}/\text{cm}$ was chosen. The moist silica sand used in the electrochemical test was prepared using silica sand (Sigma Aldrich) with average particle size of 303 μm mixed with NaCl solution. The sand amount of 1 kg was mixed thoroughly with 10 ml of the NaCl solution (0.04 wt.%) for the test..

8.2.2 Electrochemical noise measurement

The EN test with NaCl solution was conducted in at ambient temperature (22 ± 1 °C). The EN electrodes was placed horizontally in the cell with the working surface facing upwards and then 50 ml of the test solution was added. A double junction Ag/AgCl electrode (Orion) used as reference electrode was placed in a Luggin capillary filled with agar (1.5 wt.%) and KCl (3.5 wt.%) mixture. The Luggin capillary was inserted in the test cell with the tip in close proximity to the EN electrode. The test cell was aerated throughout the test. For sand and iron ore, the test was conducted in a 1 L glass vessel with glass lid at ambient temperature. The cell was filled with the test materials to the vessel neck. The solids were added to the cell by layering the tested material. The thickness of the first layer was about 40 mm. The bottom layer was compacted using a 'D' type Proctor/Fagerberg hammer specific for these material compaction. Then the carbon steel electrode was placed on top of this layer with the working surface facing upwards. In addition, the Luggin capillary was inserted into the cell and its tip was kept as close as possible to the working surface of the electrode by using an iron stand to maintain its position. Afterwards, the second layer of the solids with a thickness of 15 mm was added and gently compacted with fingers. Similarly, another 5 layers with a thickness about 15 mm for each was added in

sequence. The total height of the solids in the cell was 130 mm. Finally, the cell was covered with the glass lid fitted with Luggin capillary and the conducting wires of the EN electrode. All the unused openings were closed with fittings. For the test with coal cargo, the cell setup was similar except that the cell lid was additionally equipped with a condenser and the test cell was placed in a water bath to maintain constant temperature of 55 ± 1 °C. This temperature is generally considered the maximum temperature simulating real cargo shipping conditions and is also prescribed in classification procedures of corrosive substances (in liquids) [29]. The cell was carefully sealed with Parafilm to ensure no loss of moisture during the test.

A Gamry potentiostat Reference 600 operating in the zero resistance ammeter (ZRA) mode using ESA410 data acquisition software was used in this study. The current flowing between the two steel specimens and the potential between the coupled WEs and the reference electrode were recorded simultaneously. The data sampling rate was 2 Hz since the preliminary work showed that the sampling rate of 2 Hz allowed for detection of pitting events. All the tests were conducted for 7 days, following the test methods recommended by the United Nations on the classification of corrosive substances for transportation [29].

An open source Matlab toolbox, *Cross Recurrence Plot Toolbox*, developed by Marwan et al. [30] was used for the recurrence quantification analysis of EN data.

8.2.3 Surface profile analysis

After completing a test, the electrodes retrieved from the test cells, were flushed with ultrapure water and ethanol to remove any residual ore cargo material, as well as loose corrosion products. To further remove adherent products, the EN electrode was treated repeatedly with Clarke's solution according to ASTM standard G1 [31] in an ultrasonic water bath. Afterwards, the EN electrode was dried with nitrogen gas and stored in a vacuum desiccator for further analysis. The 3D profiles of the specimens were examined using a 3D profilometer (Alicona Instruments, IFM G4).

8.3 Results and discussion

8.3.1 Corrosion of carbon steel in NaCl solution and in moist silica sand

Post-immersion surface profilometry analysis

For the specimens immersed in NaCl solution (0.04 wt.%), it was expected that the specimens would undergo minor general corrosion. Indeed, as indicated in Figure 8-1(a₁), the specimen exhibited general corrosion and no localised corrosion was observed at the surface. The image (Figure 8-1 (a₂)) with a larger magnification further confirmed the corrosion morphology of the specimen. By contrast, the specimens buried in silica sand were subjected to localised corrosion, as shown in Figure 8-1 (b₁). The pit depths were in the range of 20-120 μm . Figure 8-1 (b₂) shows a magnified area with a large pit. The deepest point marked by an arrow has a depth of 113 μm .

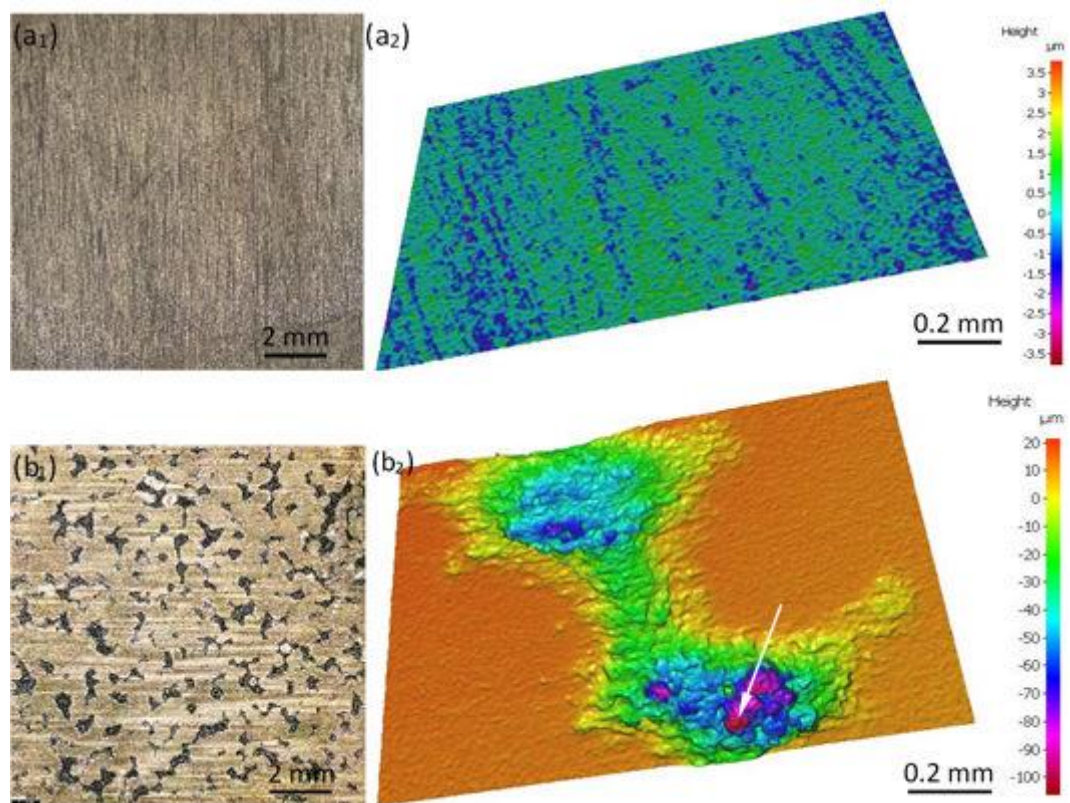


Figure 8-1: Surface morphologies of specimens retrieved from tests cell with (a₁, a₂) NaCl solution (0.04 wt.%), (b₁, b₂) silica sand + NaCl solution (0.04 wt.%). The arrow indicates the deepest point of the pit.

Development of the classification model for corrosion type identification

To distinguish between the general corrosion and localised corrosion generated by the reference tests, the raw electrochemical current data were first divided into short contiguous segments. Each of the segments contained 1024 data points, equivalent to a time frame of 512 s. After removing the linear trend of each current segment, recurrence plots were generated by applying a threshold to the distance matrices derived from each segment. The threshold (ϵ) has a significant influence on the appearance of the recurrence plots and by extension the quantification variables subsequently generated from these plots. If ϵ is too small, there may not be enough recurrence points or recurrence structures. On the other hand, if ϵ is too large, almost every point would be recurrence point, which may lead to many spurious artefacts [30]. Several options for the selection of ϵ have been proposed in literature.

For example, ϵ can be chosen according to the phase space diameter [32, 33], recurrence rate [34], standard deviation of the observational noise [35], and standard deviation of the measured time series [36]. Nevertheless, selection of the optimal criterion is strongly dependent on the system under study [30]. In this investigation, the threshold value was selected following previous studies [25-27], i.e. based on the standard deviation (σ) of the measured electrochemical current time series.

In the preliminary work, several threshold values (0.02σ , 0.2σ and 0.5σ) were examined and 0.5σ was selected since the developed RF model could best differentiate between the two types of corrosion. Figure 8-2 shows two examples of detrended current segments and associated recurrence plots using 0.5σ as the threshold. As can be seen, the pattern of the RP obtained from uniform corrosion process differs from that associated with localised corrosion. It can be expected that the quantification variables extracted from these RPs would have different values, by which localised corrosion and uniform corrosion processes can be discriminated.

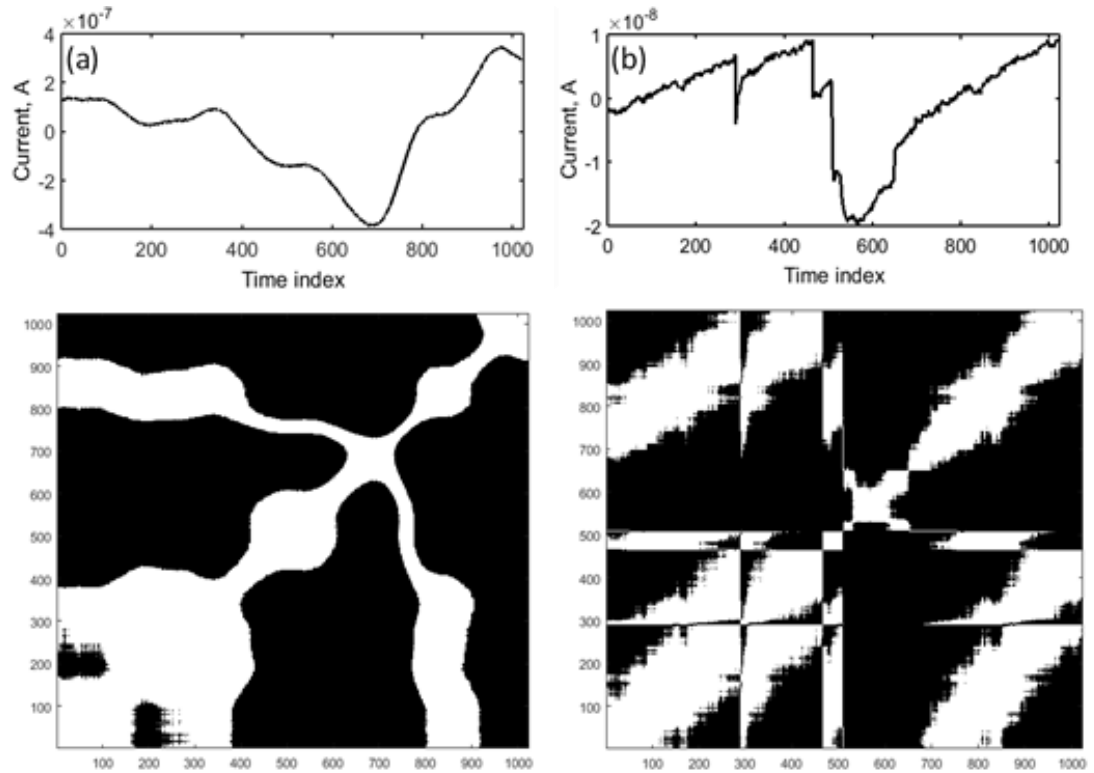


Figure 8-2: Detrended current segments and associated recurrence plots selected from corrosion processes (a) general corrosion and (b) localised corrosion.

The discrimination of corrosion general corrosion and localised corrosion was realised by random forest (RF) model trained with recurrence quantification variables (denoted as RQA variables) extracted from the recurrence plots. The procedures are briefly outlined below. Details about the calculations and concepts related to the RF model can be obtained from previous studies by Hou et al. [25-27].

- a. Twelve RQA variables were extracted from each one of the current noise segments.
- b. Row vectors comprising the RQA variables were labelled with 'A' and 'B' depending on the type of corrosion from which the current signals were recorded. As a result, 2349 row vectors with labels were obtained in total.
- c. From the 2349 labelled vectors, 70% were randomly selected as training data to build the RF model and the remaining 30% constituted a test dataset for validation purpose.

- d. The trained RF model was evaluated by the so-called ‘out-of-bag’ (OOB) errors approach.
- e. The test datasets were submitted to the RF model for classification. Finally, the misclassification error, defined as the ratio of incorrectly classified data to the total number of test data, was calculated.

Figure 8-3 shows the OOB errors of the developed RF model. The results from five independent runs suggest that when the number of trees contained in the ensemble was more than 40, the RF model based on the current data exhibited low classification errors for the discrimination between general corrosion and localised corrosion. The misclassification error of the test dataset was 0.12, meaning only 12 out of 100 data were misclassified by the RF model. This is in line with the result presented in Figure 8-3. In other words, the classification accuracy of the RF model was 88%. Subsequently, the current RF model was employed to identify the corrosion types for the specimens buried in coal and iron ore.

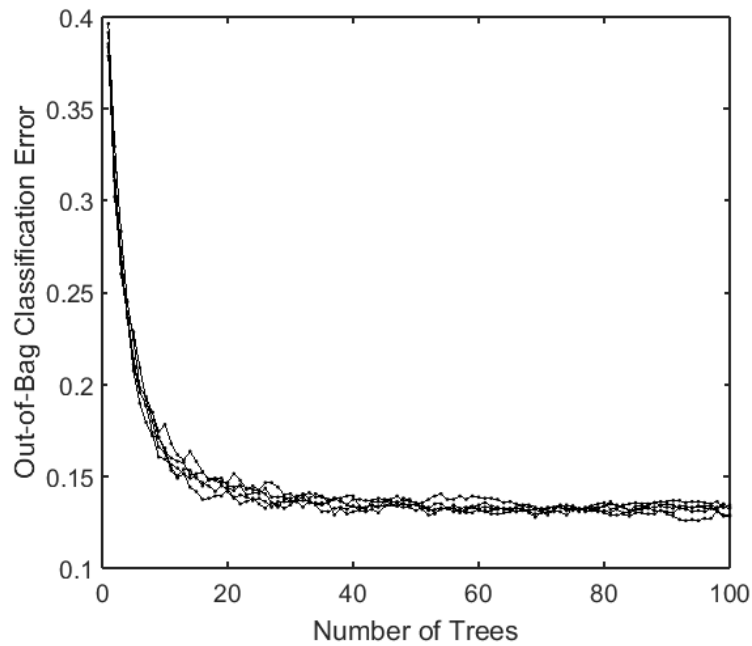


Figure 8-3: Out-of-bag classification errors of random forest models.

In addition, the importance (*Imp*) of individual RQA variables was estimated during training of the RF model. Detailed explanation of how the *Imp* was computed can be found in [26], but essentially the importance is linked to the decrease in performance of the model when the variable is omitted from the analysis. Variables

with larger Imp values are more important. As shown clearly in Figure 8-4, the variables L_{max} and $ENTR2$ have the highest values, and were thus the most predictive variables in the RF model.

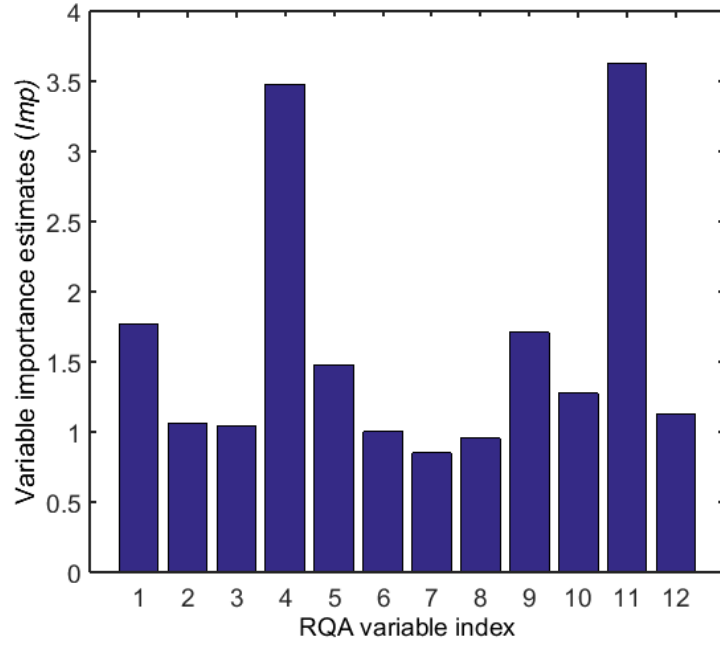


Figure 8-4: Current RQA variable importance estimations. The variable indices refer to 1 – RR , 2 – DET , 3 – L_{mean} , 4 – L_{max} , 5 – $ENTR1$, 6 – LAM , 7 – TT , 8 – V_{max} , 9 – $RT1$, 10 – $RT2$, 11 – $ENTR2$, 12 – $TRANS$.

8.3.2 Corrosion of carbon steel exposed to coal and iron ore

Identification of corrosion types for coal and iron ore

Figure 8-5 shows an EN segment (after linear trend removal) obtained on the first day of the tests with coal and iron ore. It can be seen that the patterns of the segments appear to be close to those generated with sand (Figure 8-2(b)).

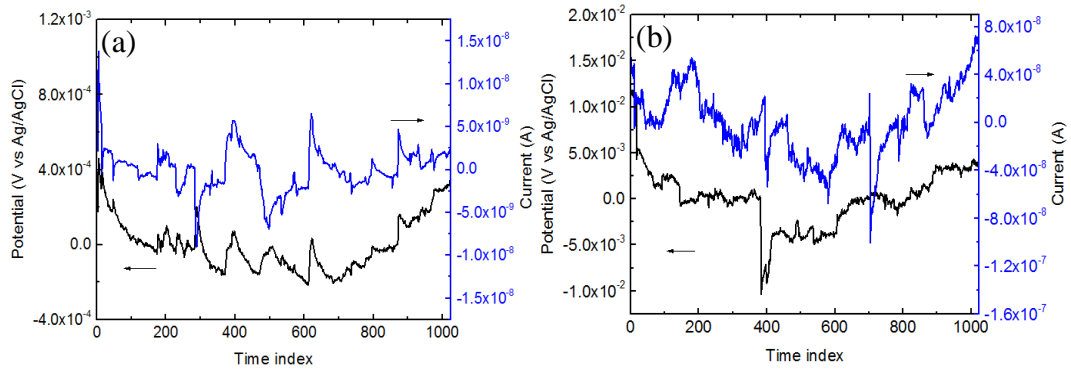


Figure 8-5: EN signals obtained from tests with (a) iron ore and (b) coal.

Similar to the EN data treatment associated with NaCl solution and sand, after segmentation and trend removal, RQA variables were extracted from the abovementioned current noise signals and submitted to the previously developed RF model for corrosion type identification. The prediction results are displayed in Figure 8-6, where each star corresponds to a current segment measured during the test. As it can be seen, the RF model predicted that during the 7-day tests the steel samples buried in iron ore and coal underwent different types of corrosion. Specifically, the iron ore mainly produced localised corrosion (98%) while the coal cargo generated both general corrosion (41%) and local corrosion (59%) corrosion on the specimens.

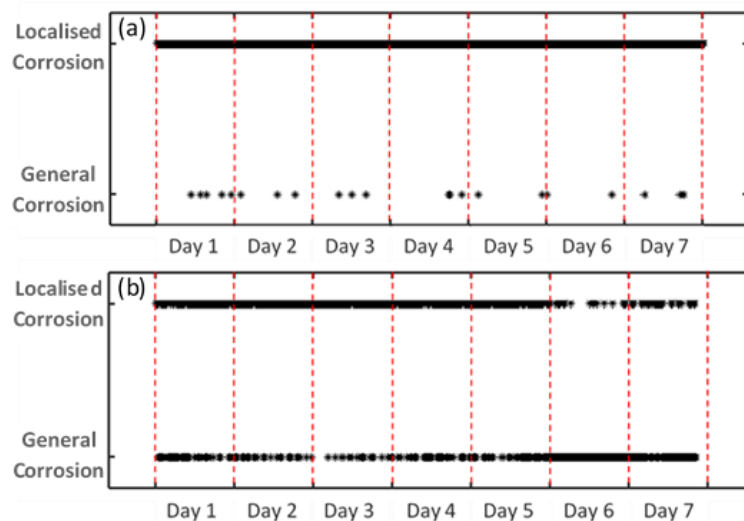


Figure 8-6: Predicted types of corrosion during the 7-day tests with (a) iron ore and (b) coal by the random forest model.

Table 8-1 shows the percentages of the current segments predicted as general corrosion and localised corrosion on a daily basis. For instance, for each day, the EN data obtained for 24 h were divided into 168 segments. The RF model would predict the corrosion type for each data segment. Therefore, on day 1, 3.6% for general corrosion means only 6 out of the 168 segments were identified as general corrosion. It can be seen that localised corrosion occurred predominantly on the specimens buried in iron ore during the entire test period. In comparison, the specimens buried in coal mainly underwent localised attack from day 1 to day 5. Afterwards, from day 6 onwards, the majority of localised corrosion events appeared to cease and the specimens managed to reach a relatively stable state with general corrosion taking place until the end of the test.

Table 8-1: Percentages of current segments identified as general and localised corrosion for the tests with coal and iron ore.

Day	Iron ore		Coal	
	General (%)	Localised (%)	General (%)	Localised (%)
1	3.6	96.4	33.3	66.7
2	1.8	98.2	17.8	82.2
3	1.8	98.2	11.3	88.7
4	1.8	98.2	24.8	75.2
5	1.2	98.8	32.1	67.9
6	1.2	98.8	85.1	14.9
7	1.8	98.2	77.4	22.6

Post-immersion surface profilometry analysis

The prediction results presented in Figure 8-6 are confirmed by the surface morphologies of the retrieved specimens, which are shown in Figure 8-7(a₁, a₂). The specimens retrieved from the test cell with iron ore exhibited localised corrosion morphologies similar to that observed in Figure 8-1(b₁, b₂). Figure 8-7(a₂) is an enlarged image of the red circled area shown in Figure 8-7(a₁), the deepest point of

which reached 120 μm . By contrast, from Figure 8-7(b₁), it is clear that the entire surface area was corroded to some extent. The average surface roughness R_q (excluding pitted areas) was 4.8 μm , which was close to that observed with the specimens immersed in 0.04 wt.% NaCl solution (3.6 μm). In addition, there were some local areas that showed more severe corrosion, such as the one marked by the dashed red line. An enlarged image of this area is presented in Figure 8-7 (b₂). The 3D surface profile measurement suggested a maximum depth of 170 μm . Other locally corroded areas ranged from 100 μm to 120 μm in depth.

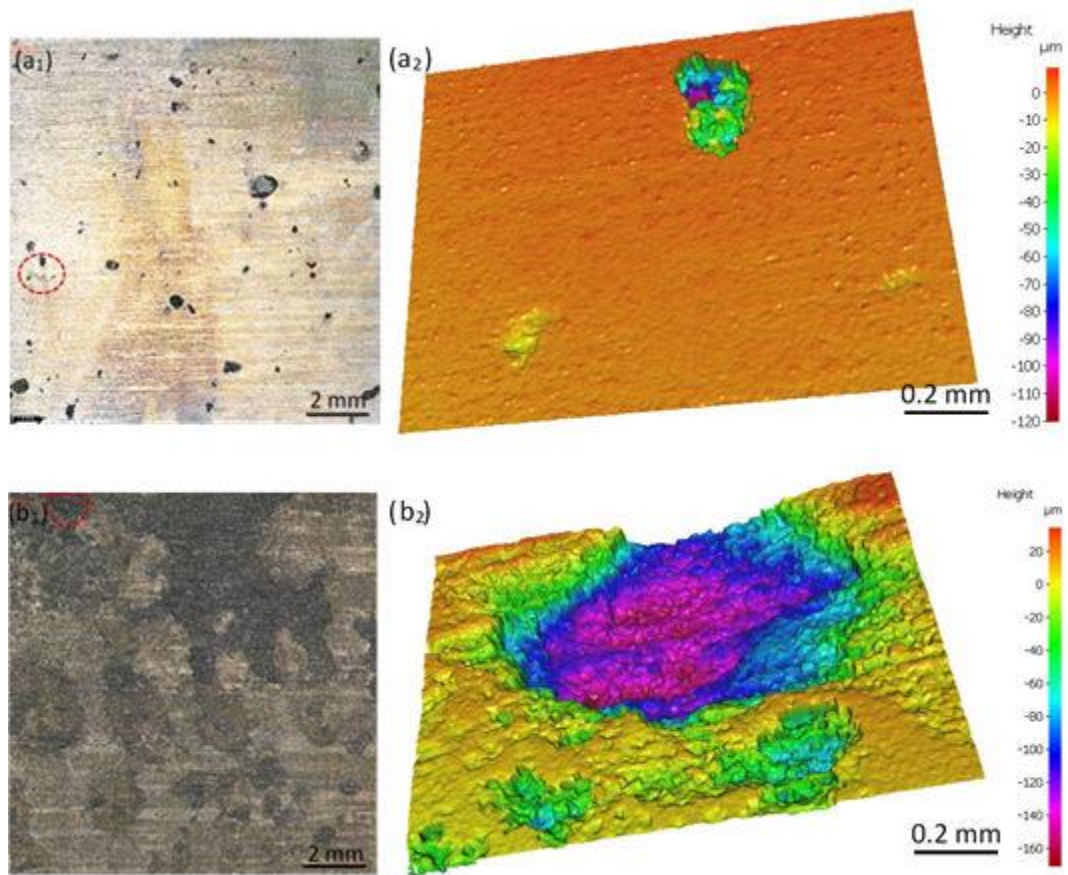


Figure 8-7 Surface morphologies of the specimens retrieved from test cells with (a₁, a₂) iron ore and (b₁, b₂) coal.

8.3.3 Discrimination of corrosion types using localisation index and shot noise parameter

Localisation index

Localisation index (LI) or pitting index is one of the most widely used parameters to indicate localised corrosion. It is defined as the standard deviation of current divided by the root mean square current [37, 38]. In general, a value approaching 1 is considered as indicative of localised corrosion.

The LI values for all the corrosion systems under investigation were calculated and plotted against the segment number of the current noise signals, as shown in Figure 8-8. Please be reminded that the current noise data were firstly divided into continuous segments. Each segment contained 1024 data points, which is equivalent to a time frame of 512 s.

As can be seen from Figure 8-8(a), from segment 300 to 400, the corrosion system with NaCl solution produced high LI values (close to 1), which is an indication of localised corrosion. However, it has been shown in Figure 8-1 that only uniform corrosion occurred to the steel samples. Moreover, the moist sand produced localised corrosion to the steel samples (as presented in Figure 8-1), thus high LI values were expected. Nevertheless, as can be seen from Figure 8-8(b), all the LI values were below 0.01. In addition, for the localised corrosion system generated with carbon steel buried in iron ore (Figure 8-8(c)), most of the LI values were below 0.4.

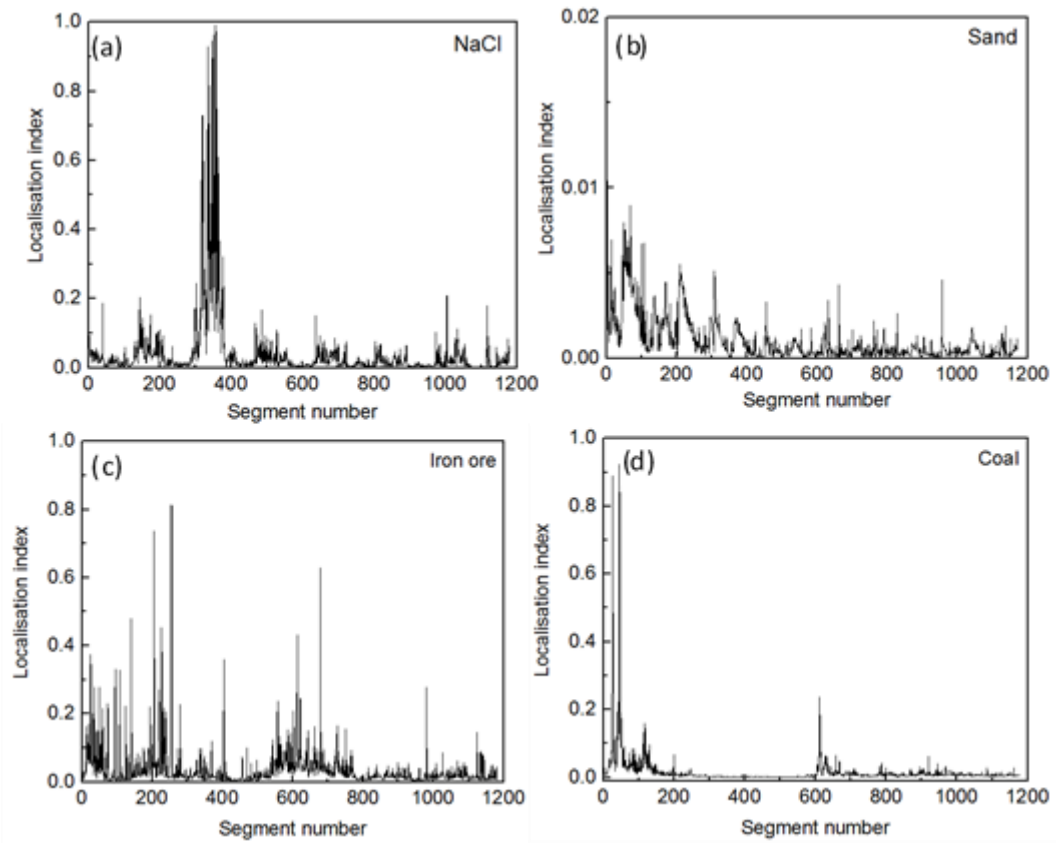


Figure 8-8 Localisation index for all the corrosion systems tested: (a) 0.04 wt.% NaCl (b) sand mixed with 0.04 wt.% NaCl (c) iron ore (d) coal.

According to these observations, it can be concluded that the localisation/pitting index is not a reliable indicator of localised corrosion for the investigated systems.

Shot noise parameter

The characteristic frequency f_n is a parameter derived from shot noise theory. It can be expressed as $f_n = \frac{B^2}{\psi_E A}$, where B is the Stern-Geary coefficient, ψ_E is the low-frequency power spectral density (PSD) of the potential noise, and A is the surface area of the sample [37-39]. In this study, a value of 0.026 V per decade was used for the coefficient B and ψ_E was determined as the potential PSD at 10^{-3} Hz. It is reported that uniform corrosion would have a large f_n , while pitting corrosion is expected to have a lower f_n [39].

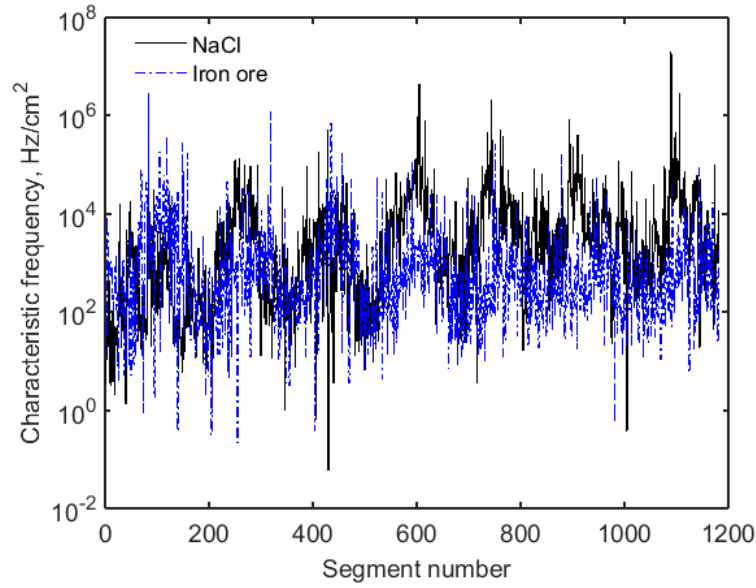


Figure 8-9 Characteristic frequency for all the data segments collected from uniform corrosion system (NaCl) and pitting system (Iron ore).

However, as can be seen from Figure 8-9, which shows the calculated f_n for the uniform corrosion system (0.04 wt.% NaCl) and pitting system (iron ore), the characteristic frequency values overlap within the same frequency range. In other words, for the present study, f_n is not an effective measure for the discrimination of localised corrosion and uniform corrosion processes.

8.4 Summary

In this study, carbon steel electrode immersed in NaCl solution (0.04 wt.%) and buried in silica sand that was moistened with NaCl solution were used as references to create different types of corrosion. Surface analyses of the retrieved steel specimens from the NaCl solution and silica sand revealed two distinct corrosion types, viz. general corrosion and localised corrosion. Electrochemical current noise data collected from the reference tests were subjected to recurrence quantification analysis and the extracted RQA variables were used as predictors to develop a random forest classification model.

The RF model could discriminate between these two types of corrosion with an accuracy of 88%. Subsequently, the established model was used to identify and monitor the corrosion processes of the carbon steel specimens buried in iron ore and

coal cargoes. Prediction results showed that during the 7-day tests, dominant form of corrosion to the steel specimens buried in coal at 55 °C was localised corrosion during the first 5 days, whereas general corrosion predominantly took place from day 6 onwards. By contrast, the iron ore resulted in localised corrosion (pitting) for the duration of the test. The morphologies of the retrieved steel specimens at the end of the tests agreed well with the predictions by the RF model.

Localisation index and the shot noise parameter f_n were also investigated for identification of localised corrosion. However, it was demonstrated that neither of them were effective measures for the discrimination of different corrosion processes under investigation.

The present work is an extended application and demonstration of the concepts and methodologies proposed in our previous studies [25-27]. The results yielded by this investigation further underscore the applicability of the proposed techniques. It can be expected that the combined recurrence quantification analysis of EN data and machine learning are valuable for future automated monitoring and identification of specific corrosion phenomena. Moreover, it provides a possible analytical method for investigation of the corrosive effects of cargoes on the carrier structures and can possibly be extended to corrosion under deposits with low moisture content.

References

- [1] C.P. Gardiner, R.E. Melchers, Corrosion analysis of bulk carriers, Part I: operational parameters influencing corrosion rates, *Mar Struct*, 16 (2003) 547-566.
- [2] J. Hua, C.W. Cheng, Corrosion of high tensile steel onboard bulk carrier loaded with coal of different origins, *Ocean Engineering*, 69 (2013) 24-33.
- [3] S. Qin, W. Cui, Effect of corrosion models on the time-dependent reliability of steel plated elements, *Mar Struct*, 16 (2003) 15-34.
- [4] S.E. Roberts, P.B. Marlow, Casualties in dry bulk shipping (1963–1996), *Marine Policy*, 26 (2002) 437-450.
- [5] Lloyd's Register of Shipping, Marine Division. Bulk Carriers—an update, 1998.
- [6] J.K. Paik, A.K. Thayamballi, Y.I. Park, J.S. Hwang, A time-dependent corrosion wastage model for seawater ballast tank structures of ships, *Corros Sci*, 46 (2004) 471-486.
- [7] J.K. Paik, J.M. Lee, Y. Park II, J.S. Hwang, C.W. Kim, Time-variant ultimate longitudinal strength of corroded bulk carriers, *Mar Struct*, 16 (2003) 567-600.
- [8] C.P. Gardiner, R.E. Melchers, Corrosion of mild steel by coal and iron ore, *Corros Sci*, 44 (2002) 2665-2673.
- [9] C.P. Gardiner, R.E. Melchers, Corrosion of mild steel in porous media, *Corros Sci*, 44 (2002) 2459-2478.
- [10] A. Garrett, N. Ahmed, Proceedings of Corrosion & Prevention, Perth, Australia, 1995, Paper 26.
- [11] A.M. Homborg, E.P.M. van Westing, T. Tinga, X. Zhang, P.J. Oonincx, G.M. Ferrari, J.H.W. de Wit, J.M.C. Mol, Novel time–frequency characterization of electrochemical noise data in corrosion studies using Hilbert spectra, *Corros Sci*, 66 (2013) 97-110.

- [12] Y. Tan, Sensing localised corrosion by means of electrochemical noise detection and analysis, *Sensors and Actuators B: Chemical*, 139 (2009) 688-698.
- [13] J. Li, W.K. Kong, J.B. Shi, K. Wang, W.K. Wang, W.P. Zhao, Z.M. Zeng, Determination of Corrosion Types from Electrochemical Noise by Artificial Neural Networks, *Int J Electrochem Sc*, 8 (2013) 2365-2377.
- [14] A.M. Homborg, E.P.M. van Westing, T. Tinga, G.M. Ferrari, X. Zhang, J.H.W. de Wit, J.M.C. Mol, Application of transient analysis using Hilbert spectra of electrochemical noise to the identification of corrosion inhibition, *Electrochim Acta*, 116 (2014) 355-365.
- [15] H.A.A. Al-Mazeedi, R.A. Cottis, A practical evaluation of electrochemical noise parameters as indicators of corrosion type, *Electrochim Acta*, 49 (2004) 2787-2793.
- [16] R. Moshrefi, M.G. Mahjani, M. Jafarian, Application of wavelet entropy in analysis of electrochemical noise for corrosion type identification, *Electrochem Commun*, 48 (2014) 49-51.
- [17] D.H. Xia, S.Z. Song, Y. Behnamian, Detection of corrosion degradation using electrochemical noise (EN): review of signal processing methods for identifying corrosion forms, *Corrosion Engineering, Science and Technology*, 51 (2016) 527-544.
- [18] H.A. Al-Mazeedi, R.A. Cottis, Parameter maps for the assessment of corrosion type from electrochemical noise data, *Corrosion conference, NACE International*, 2004, paper No. 460.
- [19] A. Legat, V. Doleček, Corrosion Monitoring System Based on Measurement and Analysis of Electrochemical Noise, *Corrosion*, 51 (1995) 295-300.
- [20] D. Xia, S. Song, J. Wang, J. Shi, H. Bi, Z. Gao, Determination of corrosion types from electrochemical noise by phase space reconstruction theory, *Electrochem Commun*, 15 (2012) 88-92.

- [21] R. Moshrefi, M.G. Mahjani, M. Jafarian, Application of wavelet entropy in analysis of electrochemical noise for corrosion type identification, *Electrochem Commun*, 48 (2014) 49-51.
- [22] T. Zhang, Y.A. Cong, Y.W. Shao, G.Z. Meng, F.H. Wang, Electrochemical noise analysis on the crevice corrosion behavior of Ni-Cr-Mo-V high strength steel using recurrence plots, *J Appl Electrochem*, 41 (2011) 289-298.
- [23] E. Cazares-Ibanez, G.A. Vazquez-Coutino, E. Garcia-Ochoa, Application of recurrence plots as a new tool in the analysis of electrochemical oscillations of copper, *J Electroanal Chem*, 583 (2005) 17-33.
- [24] E. Garcia-Ochoa, F. Corvo, Using recurrence plot to study the dynamics of reinforcement steel corrosion, *Prot Met Phys Chem+*, 51 (2015) 716-724.
- [25] Y. Hou, C. Aldrich, K. Lepkova, L.L. Machuca, B. Kinsella, Monitoring of carbon steel corrosion by use of electrochemical noise and recurrence quantification analysis, *Corros Sci*, 112 (2016) 63-72.
- [26] Y. Hou, C. Aldrich, K. Lepkova, L.L. Machuca, B. Kinsella, Analysis of electrochemical noise data by use of recurrence quantification analysis and machine learning methods, *Electrochim Acta*, 256 (2017) 337-347.
- [27] Y. Hou, C. Aldrich, K. Lepková, B. Kinsella, Detection of under deposit corrosion in CO₂ environment by electrochemical noise and recurrence quantification analysis, *Electrochim Acta*, 274 (2018) 160-169.
- [28] V. Pandarinathan, K. Lepková, S.I. Bailey, R. Gubner, Evaluation of corrosion inhibition at sand-deposited carbon steel in CO₂-saturated brine, *Corros Sci*, 72 (2013) 108-117.
- [29] UN (2011), "Classification procedures, test methods and criteria relating to class 2, class 3, class 4, division 5.1, class 8 and class 9", in *Recommendations on the transport of dangerous goods: manual of tests and criteria - 5th revised edition*, United Nations, New York, <http://dx.doi.org/10.18356/bbaae943-en>.

- [30] N. Marwan, M. Carmen Romano, M. Thiel, J. Kurths, Recurrence plots for the analysis of complex systems, *Physics Reports*, 438 (2007) 237-329.
- [31] ASTM G1-03(2017)e1, Standard Practice for Preparing, Cleaning, and Evaluating Corrosion Test Specimens, ASTM International, West Conshohocken, PA, 2017, www.astm.org.
- [32] R. Gilmore, Topological analysis of chaotic time series, *Applications of Soft Computing* San Diego, CA, (1997) 243-257.
- [33] J.P. Zbilut, C.L. Webber Jr, Embeddings and delays as derived from quantification of recurrence plots, *Physics Letters A*, 171 (1992) 199-203.
- [34] J.P. Zbilut, J.M. Zaldivar-Comenges, F. Strozzi, Recurrence quantification based Liapunov exponents for monitoring divergence in experimental data, *Physics Letters, Section A: General, Atomic and Solid State Physics*, 297 (2002) 173-181.
- [35] M. Thiel, M.C. Romano, J. Kurths, R. Meucci, E. Allaria, F.T. Arecchi, Influence of observational noise on the recurrence quantification analysis, *Physica D: Nonlinear Phenomena*, 171 (2002) 138-152.
- [36] N. Marwan, J.F. Donges, Y. Zou, R.V. Donner, J. Kurths, Complex network approach for recurrence analysis of time series, *Physics Letters, Section A: General, Atomic and Solid State Physics*, 373 (2009) 4246-4254.
- [37] H.A.A. Al-Mazeedi, R.A. Cottis, A practical evaluation of electrochemical noise parameters as indicators of corrosion type, *Electrochim Acta*, 49 (2004) 2787-2793.
- [38] R.A. Cottis, M.A.A. Al-Awadhi, H. Al-Mazeedi, S. Turgoose, Measures for the detection of localized corrosion with electrochemical noise, *Electrochim Acta*, 46 (2001) 3665-3674.
- [39] J.M. Sanchez-Amaya, R.A. Cottis, F.J. Botana, Shot noise and statistical parameters for the estimation of corrosion mechanisms, *Corros Sci*, 47 (2005) 3280-3299.

CHAPTER 9 CONCLUSIONS AND FUTURE WORK

The objectives of this thesis were to:

1. Design corrosion monitoring and diagnostic frameworks based on the use of RQA variables extracted from EN data and machine learning methods.

The frameworks will be able to:

- a. Discriminate different corrosion types, especially to distinguish localised corrosion from uniform corrosion and passivation.
 - b. Monitor corrosion processes continuously and flag unexpected corrosion processes automatically.
2. Examine the feasibility of the designed frameworks using preliminary EN data generated from uniform corrosion, pitting and passivation of carbon steel samples exposed to NaCl, NaHCO₃+NaCl and NaHCO₃ solutions.
 3. Carry out different case studies to evaluate the feasibility of the developed methodologies for corrosion monitoring and localised corrosion detection.

In light of these objectives, a PCA-based corrosion monitoring model and a RF-based corrosion type diagnostic model have been developed and demonstrated with several case studies. Recurrence quantification analysis (RQA) of EN data laid the foundation for the development of both models. It provided multiple discriminative variables (referred to as RQA variables) so that various corrosion types could be successfully identified by these models. Overall, twelve RQA variables were used, including recurrence rate (RR), determinism (DET), average diagonal line length (L_{mean}), maximum diagonal line length (L_{max}), entropy of diagonal line length ($ENTR1$), laminarity (LAM), trapping time (TT), maximum vertical line length (V_{max}), recurrence time of 1st type ($RT1$), recurrence time of 2nd type ($RT2$), entropy of the recurrence period density ($ENTR2$) and transitivity ($TRANS$).

9.1 Development and application of a PCA model for corrosion process monitoring

9.1.1 Development of the framework

Consider the following scenario: uniform corrosion prevails at normal operation conditions (NOC) and it is unknown whether non-uniform corrosion will take place if the operating condition changed. The condition could be changed intentionally by operators or unintentionally because of some unknown reasons. A corrosion monitoring scheme based on a PCA model was developed to deal with this kind of situation.

In summary, this framework contains two stages, i.e. off-line calibration stage and on-line monitoring stage.

(1) Off-line calibration stage

a. Electrochemical noise data should be recorded continuously under normal operation conditions (NOC) for a sufficient time depending on the actual corrosion system and sampling rate.

b. The collected EN data need to be properly segmented according to desired inspection interval. In principle, the length of the time series segment should be sufficient to capture characteristic fluctuations or periodic behaviour in the time series.

c. The EN segments are then converted to recurrence plots, from which twelve variables can be extracted.

d. Principal component analysis is implemented to transform the RQA variables into principal component scores.

e. A control limit based on a Gaussian mixture model is calculated to enclose the principal component scores for NOC. With this, the calibration of the PCA model is completed. Ideally, it is better to collect as many data as possible in this stage for computation of a reliable control limit.

(2) On-line monitoring stage

a. For the on-line corrosion process monitoring, EN could be measured continuously or intermittently. The newly measured EN data should be processed exactly the same way as for NOC data to generate new RQA variables.

b. The RQA variables are then projected to the calibrated PCA model and compared with the control limit. If the projected data fall outside the NOC control limit, a potential change of the corrosion form is signalled.

For this corrosion monitoring scheme to work successfully, the quality of the collected data in the off-line stage is of vital importance. The user should ensure that the associated corrosion process is representative of the normal operation conditions and is well understood as well as under control. This may require some experience and knowledge from corrosion experts.

9.1.2 Case studies

The efficacy of this corrosion monitoring framework was demonstrated by two case studies.

Preliminary tests involving three corrosion systems (i.e. uniform corrosion, pitting and passivation) were carried out with carbon steel samples immersed in aqueous media. Electrochemical current noise data collected from uniform corrosion process were used as NOC data, while that collected from pitting and passivating processes were regarded as being obtained during the on-line monitoring process. Four RQA variables were used in this case study. Results showed that the calibrated PCA monitoring scheme could differentiate between uniform and non-uniform corrosion.

The second case study using the PCA based corrosion monitoring framework was associated with under deposit corrosion of carbon steel in CO₂ saturated brine solution. EN data were measured with carbon steel samples with and without sand deposit. Uniform corrosion occurred at samples not covered by sand while localised corrosion took place at samples covered with sand. The former was considered as NOC and the latter was the change that needs to be captured. In this case study, twelve RQA variables were used. The obtained PCA monitoring model could effectively detect the UDC process.

9.2 Development and application of a RF model for corrosion type diagnosis

9.2.1 Development of the framework

The random forest model is designed to deal with the task of identifying different forms of corrosion. The idea of this diagnostic framework is as follows:

- a. EN data should be collected from several corroding systems of interest that generate different types of corrosion.
- b. The collected EN data need to be divided into short segments. The length of each segment should be determined by taking into consideration the inspection time interval later at the on-line monitoring stage.
- c. Each data segment need to be labelled with a symbol to represent the corresponding corrosion type. Then the data segments are converted into the recurrence plots to extract RQA variables.
- d. A proportion (e.g. 70%) of the RQA variables with labels are given to the RF model for “learning”, so that different types of corrosion can be identified.
- e. The remaining labelled RQA variables are used as a test dataset to examine the classification accuracy of the trained RF model.
- f. Once the RF model is established, it can be applied for on-line corrosion type diagnoses. Newly measured EN data is processed the same way as in step c to obtain RQA variables. Then the label, i.e. corrosion type, of the new data can be identified by the RF model.

9.2.2 Case studies

The efficacy of the RF model was demonstrated in three case studies.

Firstly, the RF model was applied to the preliminary tests which generated uniform corrosion, pitting and passivating systems. Since the passivating data were found not sufficient when the PCA model was applied, it was decided to extend the

length for passivating. Moreover, an extended set of RQA variables (twelve in total) were extracted from each current noise data segment. 75% of the labelled RQA variables were used for training the RF model and the remaining 25% served as a test dataset to examine the accuracy of the developed model. Results showed that the RF model could correctly identify the three types of corrosion with an overall accuracy of 93%. In addition, a linear discriminant analysis (LDA) model was also tried to distinguish uniform corrosion, pitting and passivating. Nevertheless, the classification accuracy was lower (88%) compared to that of the RF model.

The second application was also carried out with the UDC experiments. In this case study, three different RF models, i.e. potential RF model, current RF model and the combination model, were developed and compared. The potential RF model is simply the model based on the use of electrochemical potential noise data and current RF model is related to current noise data. The combination model refers to the model based on the collective use of both potential and current data. All three RF models showed very high discrimination accuracy (over 99%) between the corrosion of bare steel and that of sand-deposited steel.

Furthermore, the developed methodology was applied to investigate corrosion processes occurring in solids. Firstly, two reference tests using carbon steel immersed in NaCl solution (0.04 wt.%) and buried in moistened silica sand were carried out. Two distinct corrosion types were observed: general corrosion and localised corrosion. RQA variables were extracted from the obtained electrochemical current noise data and then used to set up the RF model to distinguish the two corrosion types. The developed RF model could reliably differentiate general and localised corrosion with a classification accuracy of 88%. Then this model was employed to identify the corrosion types of carbon steel samples associated with iron ore and coal cargoes over 7 days. Prediction results showed that, the dominant form of corrosion to the steel specimens buried in coal at 55 °C was localised corrosion during first 5 days, whereas general corrosion predominantly took place from day 6 onwards. By contrast, the iron ore only generated localised corrosion over 7 days on the buried EN electrode at room temperature. Microscopic analysis of the retrieved steel samples after tests agreed well with the classification results of the RF model.

9.2.3 Estimation of variable importance

The RF method provided a means to evaluate the importance of different RQA variables for the discrimination of different corrosion types. It was done by permuting each predictor variable during the training of the RF model and observing the variation in the prediction error of the model in each case. The more errors generated by this procedure, the more important the associated variable is.

In the case study where the RF model was used to distinguish between uniform corrosion, pitting and passivating, the RQA variables DET , L_{mean} , L_{max} , $ENTR1$ and LAM presented similar high importance for the classification accuracy of the RF model. In the case study associated with under deposit corrosion (UDC), $ENTR2$ played the most significant role for the discrimination between uniform corrosion and UDC. Similarly, $ENTR2$ and L_{max} were the most important variables in the study correlated with cargo corrosion.

9.3 Recommendations for future work

This research innovatively used recurrence quantification analysis to extract feature variables from electrochemical noise data for corrosion monitoring and corrosion type identification. Two frameworks based on the use of multiple predictor variables and machine learning methods have been proposed and their capabilities being demonstrated with different case studies. Some recommendations for further research in this area are presented below.

- Apply the proposed methodologies to study the efficacy of corrosion inhibitors and corrosion resistant coatings.
- Current case studies mainly focus on the differentiation between uniform corrosion and pitting corrosion. It is worthwhile to apply the random forest based framework to distinguish between various types of localised corrosion.
- The discrimination between metastable pitting and stable pitting is as important as the separation of uniform and localised corrosion. It is worthwhile to explore the feasibility of the proposed methodology in this regard.

- Apply the proposed methods to field corrosion monitoring programmes.
- Further improve the accuracy of the proposed models by optimising the selection of threshold values while converting EN data to recurrence plots and developing more discriminative variables with recurrence quantification analysis.

CHAPTER 10 APPENDICES

Appendix 1. Validation of EN measurements

The validation of EN measurements were conducted according to [1]. The procedures are shown as follows:

(1) Estimation of instrumental noise

- i. Connect dummy cell which consists of three 1 M Ω resistors with a star arrangement.
- ii. Warm up the system ($t > 15$ min).
- iii. EN measurement with a sampling rate of 1 Hz for 1 h 10 min to obtain 16384 data points.
- iv. EN measurement with a sampling rate of 10 Hz for 30 min.
- v. Calculate the PSDs of the EN data sets using the programme described in [1].
- vi. Plot the raw EN data to check for quantisation. Quantisation appeared as a set of clear steps in the time record, which is a reflection of the resolution of the data acquisition system.
- vii. Analyse the PSDs to see whether a proper anti-aliasing filter is used and to check the overlap of the PSDs obtained with different sampling rates.

(2) Validation of the EN measurement in real corrosion systems

- i. Collect EN data with a sampling rate of 2 Hz for 2 h 17 min.
- ii. Collect EN data with a sampling rate of 10 Hz for 30 min.
- iii. Calculate the PSDs of the EN data.
- iv. Plot the raw EN data.
- v. Check the overlap of the PSDs.
- vi. Compare the PSDs with those obtained in step (1).

Figure 10-1 shows the raw EN data measured using dummy cell with sampling rates of 1 Hz and 10 Hz. As can be seen, there is no sign of quantisation in the time

domain data. The amplitudes for potential and current are approximately 30 μV and 8 pA, respectively.

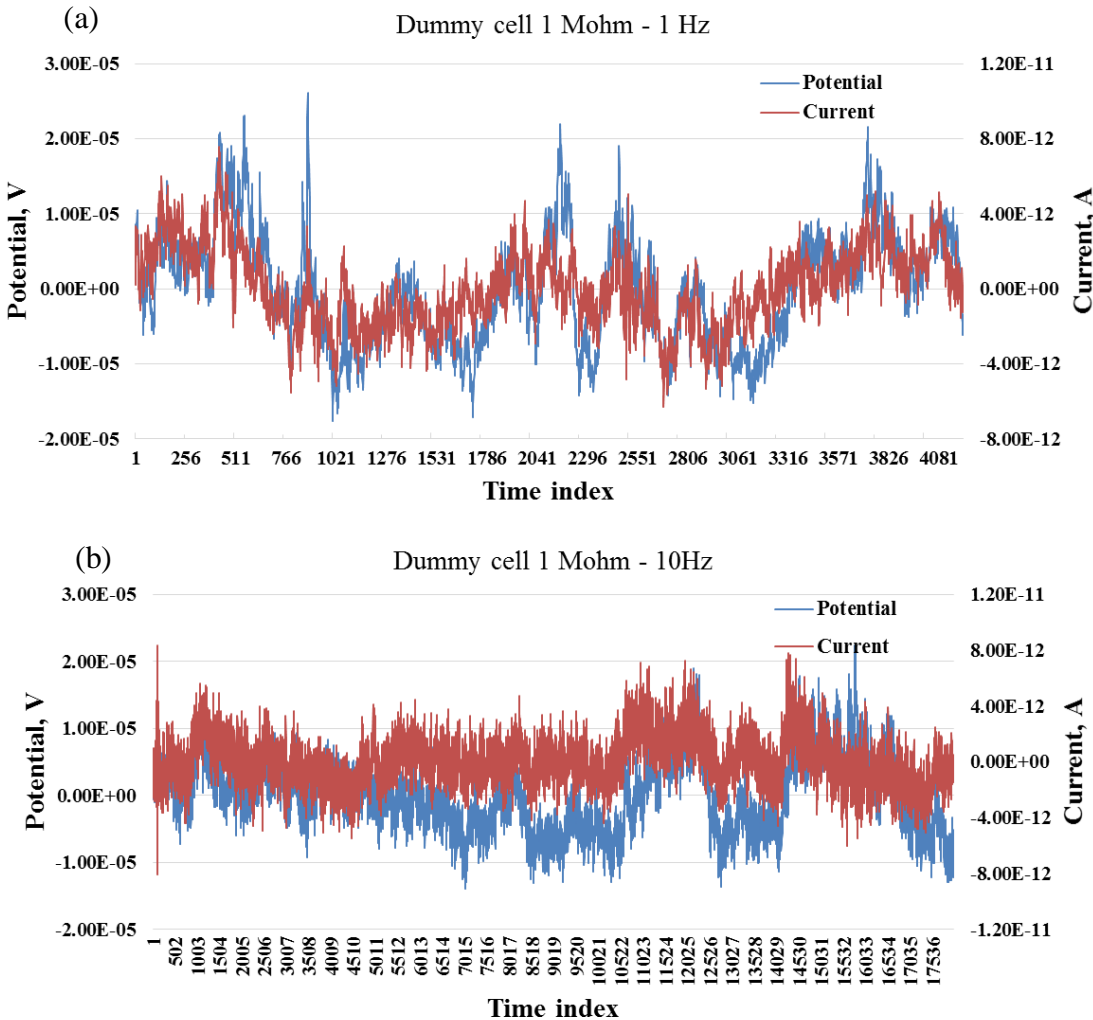


Figure 10-1: Raw EN data obtained with 1 M Ω dummy cell (a) sampling rate 1 Hz
(b) sampling rate 10 Hz.

Figure 10-2 presents the calculated potential and current PSDs by dividing the raw EN data into 1024 data points segments and averaging the PSDs of all segments.

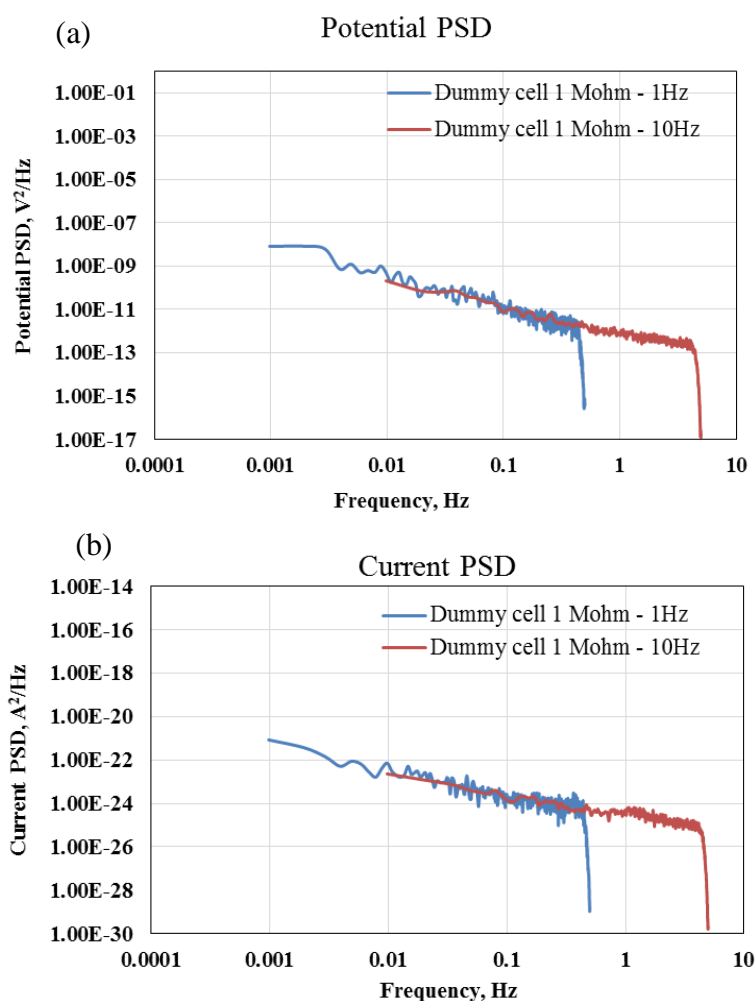


Figure 10-2: Potential (a) and current (b) PSDs of EN data measured with dummy cell.

As can be seen, there is a decrease towards the highest frequency in each PSD, indicating that the data acquisition device is equipped with efficient anti-aliasing filters. Moreover, both the potential and current PSDs associated with 1 Hz and 10 Hz sampling rates show good overlaps. In addition, at 0.1 Hz, the potential PSD is in the order of 10^{-11} V²/Hz, while the current PSD is in the order of 10^{-24} A²/Hz. In this study, these two values are used as the baseline instrumental noise level for easy comparison.

Figure 10-3 shows the raw EN data measured in a pitting system with sampling rates of 2 Hz and 10 Hz. No quantisation phenomena are observed.

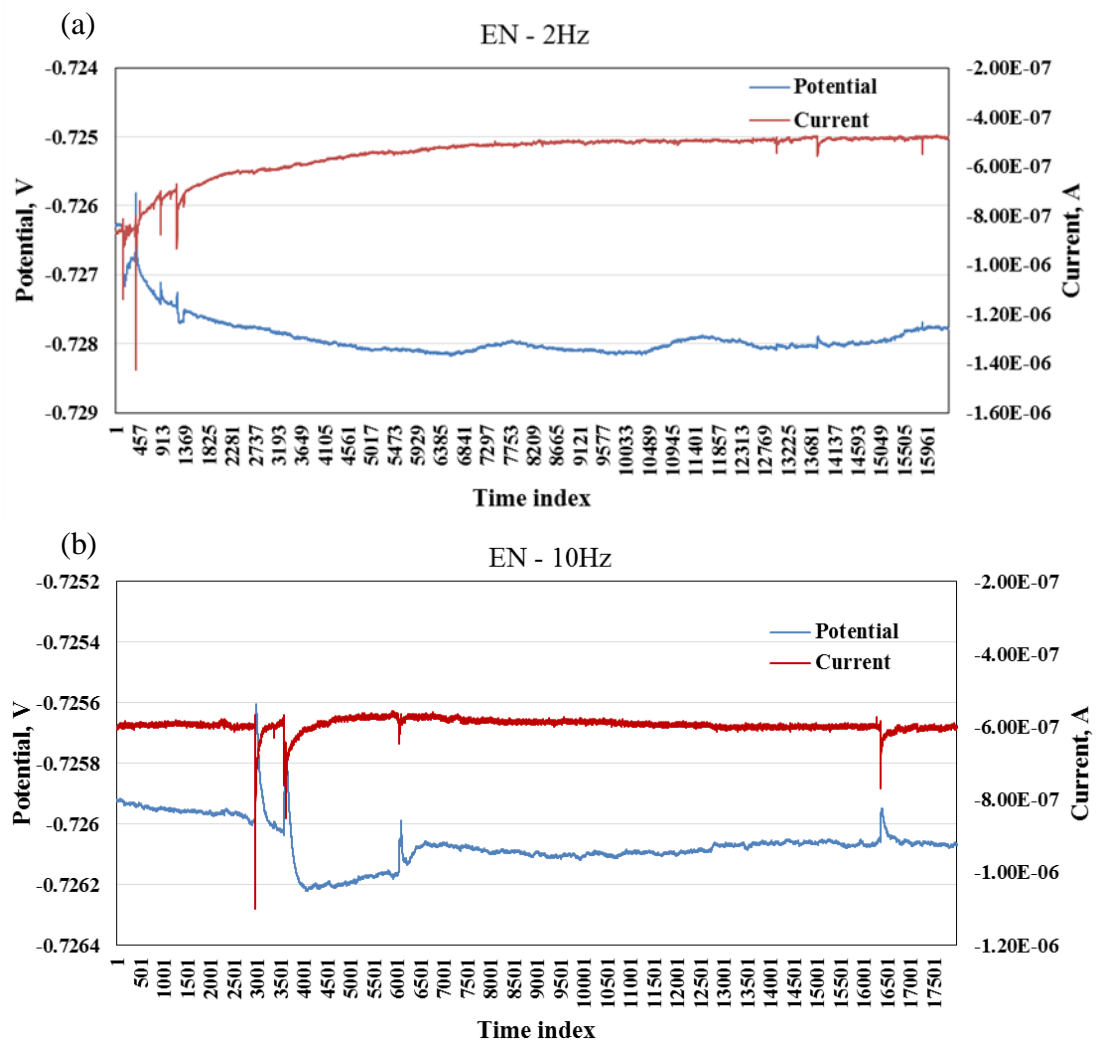


Figure 10-3: Raw EN data measured in a pitting system with sampling rate (a) 2 Hz
(b) 10 Hz.

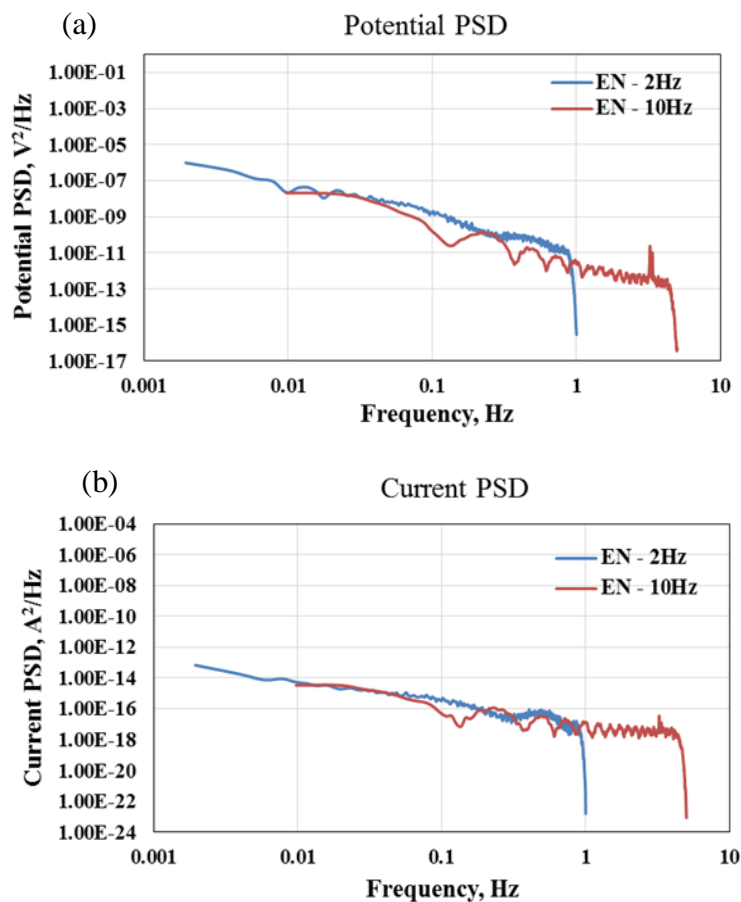


Figure 10-4: Potential (a) and current (b) PSDs of EN data measured in pitting system.

It can be seen from Figure 10-4, both the potential and current PSDs associated with sampling rates of 2 Hz and 10 Hz overlap well. In addition, at 0.1 Hz, the potential PSD is approximately in the order of 10^{-9} V²/Hz, while the current PSD is in around the order of 10^{-16} A²/Hz. Both values are higher than the instrumental noise level, which means the EN measurements are reliable and valid.

Reference

- [1] S. Ritter, F. Huet, R.A. Cottis, Guideline for an assessment of electrochemical noise measurement devices, *Mater Corros*, 63 (2012) 297-302.

Appendix 2. Application of Electrochemical Noise Technique to Study Corrosion Induced by Sulphate Reducing Bacteria

This is an experimental report on the corrosion of carbon steel induced by sulphate reducing bacteria.

It was expected that the sulphate reducing bacteria (SRB) could induce localised corrosion in carbon steel, which could be detected by electrochemical noise. Therefore, the objective was to apply the proposed methodologies to study this microbial corrosion process. However, it was observed that the differences between the corrosion morphologies of carbon steel samples in the presence and absence of SRBs were not as obvious as expected.

This appendix mainly presents the test procedures and observations during and after tests.

Experimental

Materials

The specimens used in this study was carbon steel 1030, which was the same as those used in aforementioned case studies. Rectangular samples with dimensions approximately $2.4\text{ cm} \times 2.5\text{ cm}$ were firstly soldered with conductive wires and then electrocoated with Powercron 6000CX. The average working surface area of the samples was 6 cm^2 . All samples were abraded with silicon carbide paper up to 600 grit, rinsed with ultrapure water and ethanol, dried with nitrogen and stored in a vacuum desiccator until used.

The test media used in this study was natural seawater obtained from Indian Ocean at Hillarys, Perth, Western Australia. Three test cells, A, B and C, were set up in this study. Cell A was filled with 800 mL of the natural seawater and supplemented with 1 mL sodium DL-lactate (60% syrup in water, Sigma Aldrich). Pure culture sulphate reducing bacteria (SRB), *Desulfovibrio alaskensis* DSM 17464, was inoculated in cell A at the beginning of the test. However, because the SRBs did not grow as expected, a second inoculation was performed on day 4 in combination with supplements addition – 1 mL of vitamin solution, 1 mL of modified Wolfe's mineral elixir and 0.2 g/L $\text{FeSO}_4 \cdot 7\text{H}_2\text{O}$. The compositions and concentrations of the vitamin solution and modified Wolfe's mineral elixir are presented in Table 10-1 and Table 10-2 respectively. These solutions were prepared with DI water (Milli-Q system, resistivity $18.2\text{ M}\Omega \cdot \text{cm}$) and analytical grade reagents. Before adding to cell A, these solutions were sterilized with syringe filters ($0.2\text{ }\mu\text{m}$). The added chemicals were to facilitate bacteria growth. Test cells B and C were used as controls. In cell B, the test solution was filtered seawater without SRB addition and supplemented with nutrients same as in cell A. In cell C, only filtered seawater was used with no supplements or SRB.

Table 10-1: Composition and concentration of vitamin solution.

Chemical	Ascorbic acid	Nicotinic acid	Vitamin B ₁	Vitamin B ₁₂	Vitamin B ₂	Vitamin B ₅	Vitamin B ₆	Vitamin H
Concentration (mg/L)	100	0.5	0.6	0.05	0.2	0.6	0.6	0.01

Table 10-2: Composition and concentration of modified Wolfe's mineral elixir.

Chemical	Concentration (g/L)
C ₆ H ₉ NO ₆	1.5
MgSO ₄ ·7H ₂ O	3.0
MnSO ₄ ·H ₂ O	0.5
NaCl	1.0
FeSO ₄ ·7H ₂ O	0.1
CoSO ₄ ·7H ₂ O	0.1
NiCl ₂ ·6H ₂ O	0.1
CaCl ₂ ·2H ₂ O	0.1
ZnSO ₄ ·7H ₂ O	0.1
CuSO ₄ ·5H ₂ O	0.01
AlKSO ₄	0.01
H ₃ BO ₃	0.01
Na ₂ MoO ₄ ·2H ₂ O	0.01
Na ₂ SeO ₃	0.001

Before tests, all glassware, fittings and tubes were wrapped with aluminium foil and sterilized in an autoclave (134 °C and 3.1 bar) for about 43 min. The solutions were deaerated by purging with 80 N₂/20 (volume %) CO₂ gas mixture for over 2 h before pumping into the test cells equipped with steel samples. In addition, the test cells were also deaerated with pure N₂ (99.99%) for 30 min before test media transferring. The initial pH values of the test solutions in all the cells were adjusted to around 7 with syringe filtered (0.2 µm) NaHCO₃ (Merck, 99.7%) solution (saturated).

During the test, half volume of the solution in cell A was pumped out of the cell and replaced with fresh natural seawater every 7 days. Specifically, 400 mL of natural seawater with 1 mL sodium DL-lactate was purged with N₂/CO₂ mixture for one hour. Before transferring, the pH of the fresh media was adjusted to 7 with syringe filtered saturated NaHCO₃ solution. This was done in order to make sure the SRB had enough nutrition for growing. No replacements were conducted for cell B and cell C.

Bacteria cultures

The bacteria *D. alaskensis* served as inoculums was cultivated in Postgate B solution in a 10 mL vial modified with 2 wt. % NaCl. The compositions of the culture media are presented in Table 10-3.

The addition of the *D. alaskensis* was conducted according to the following procedures.

- 1) The cell density in the culture vial was counted using Thoma counting chamber.
- 2) 1 mL SRB containing media was taken out of the 10 mL culture vial and injected into a 15 mL sterile falcon tube which was previously filled with 9 mL natural seawater.
- 3) The falcon tube was centrifuged at 1000 xg and 4 °C for 3 min to remove the iron sulphide precipitates.
- 4) The supernatant was collected and transferred into a new falcon tube.

- 5) The new falcon tube was centrifuged at 3800 xg and 4 °C for 20 min. Then, the supernatant was discarded and the pellet was resuspended in 10 mL natural seawater.
- 6) Procedure 5) was repeated.
- 7) 1 mL of the SRB suspended natural seawater was taken out and diluted in 9 mL natural seawater.
- 8) 1 mL solution was taken out from the solution obtained in 7) and injected into test cell A. By calculation, the final cell density of the *D. alaskensis* in cell A was around 10^3 cell/mL.

However, as the SRBs did not grow as expected, a second inoculation was performed on day 4 following the same procedures.

Table 10-3: Compositions of Postgate B culture media (pH = 7.3).

Composition	Concentration (g/L DI water)
KH ₂ PO ₄	0.5
NH ₄ Cl	1.0
CaSO ₄	1.0
MgSO ₄ ·7H ₂ O	2.0
Sodium DL-Lactate (Syrup, 60% (w/w))	10 mL
Yeast extract	1.0
Thioglycollate broth	0.1
Ascorbic acid	0.1
FeSO ₄ ·7H ₂ O	0.5

Analytical methods

Bacteria cell density and activity

The SRB cell density in test cell A was estimated via serial dilution method. The sample solution was extracted from the test cell under sterile conditions. Then 1 mL of the extracted sample was injected into a 10 mL vial which contained 9 mL Postgate B culture media (sterile and deaerated). Afterwards, the vial was vigorously shaken to make the solution even. Then 1 mL of the mixed solution was extracted using a sterile syringe with needle and injected into a second culture vial. Again, 1 mL of the mixture was extracted from the second vial and injected into a third vial and so on until the 9th culture vial. At last, these vials were incubated in a hot room at 30 °C. The viable SRB cell density was indicated by the number of vials that turned black after three days. For instance, if the vial numbers 1 – 5 turned black after incubating for three days, it means the original cell density of the test solution in cell A was approximately 10^5 cell/mL.

Test media chemistry

Sulphate (SO_4^{2-}) and sulphide (S^{2-}) concentrations of test solutions were measured by spectrophotometer (Hatch, DR3900). The method for determination of SO_4^{2-} was USEPA SulfaVer 4 and that for S^{2-} was Methylene Blue.

Electrochemical noise measurement

The electrochemical noise was measured using Gamry Reference 600 potentiostat/galvanostat/ZRA and ESA410 software. Two nominally identical steel samples aforementioned were used as working electrode and counter electrodes. A commercial Ag/AgCl reference electrode was placed in a long Luggin capillary filled with Agar (1.5 wt.%) and KCl (3.5 wt.%) mixture. The current flowing between the two steel samples was recorded via the zero resistance ammeter (ZRA) and the potential between the coupled working electrodes and the reference electrode was recorded simultaneously by the potentiometer of the Gamry instrument. In each day, the electrochemical noise data were recorded for 4 h at a sampling frequency of 2 Hz.

Post-test analysis

Apart from the two samples for EN measurement in the three cells, another three samples with no electric connection were also placed in cell A and two samples each in cell B and C. At the end of the test period, cell A was moved to a glovebox with pure N₂ atmosphere. All the samples were taken out from the cell within the glovebox and rinsed with sterile phosphate buffer saline (PBS) buffer (pH=7.3). Two of the samples were used for weight loss measurements, one for ATP analysis and the two electrode samples were used for SEM/EDS analysis.

ATP analysis

ATP analysis of the total sessile bacteria on the sample surface was carried out using LuminUltra **2nd Generation ATP®** test kit, specifically, the Deposit and Surface Analysis (DSA) test kit. It is designed to test attached/sessile microorganisms.

SEM/EDS

The morphology and chemical composition of the corrosion products/biofilm was investigated by Zeiss Neon 40EsB dual beam focussed ion beam scanning electron microscope (FIBSEM), equipped with energy dispersive X-ray spectroscopy (EDS). The surfaces were prepared following the steps below.

- 1) Rinse the steel sample with sterile PBS buffer to remove loose deposits/bacteria cells.
- 2) Immerse the steel sample in 0.025M PBS solution containing 2.5 (w/v) % glutaraldehyde (Sigma-Aldrich, USA) and 0.15 (w/v)% Alcian blue (Sigma-Aldrich, USA) for 24 h at room temperature.
- 3) Take out the sample and rinse it with sterile PBS.
- 4) Dehydrate the sample by sequentially immersing it in 30 %, 50 %, 70 %, 80 %, 90 %, 95 % and 100 % ethanol for 10 min in each.
- 5) Dry the dehydrated sample with nitrogen.
- 6) Sputter coat the sample with 5 nm of platinum.

Weight loss measurement

Corrosion products were removed according to the standard chemical cleaning procedure and the weight loss corrosion rates were determined based on ASTM G1 standard from duplicate steel samples.

Corrosion depth measurement

All the sample surfaces after corrosion products removal were observed under an infinite focus optical microscope (Alicona Instruments) to determine the depth of corrosion.

Results and discussion

Visual observations

Figure 10-5 shows the test cell A and control cells B and C after 15 days. It can be seen that test cell A was characterised with black precipitates on the surfaces of samples and solution was black as well. In cell B, there were also black corrosion products present on the surfaces of the samples whereas the solution was clear. Moreover, the thick brown precipitates formed not only on the sample surfaces but also at the bottom and the surface on the sample holder. The black corrosion products in cell A can be attributed to the SRB metabolic activities while the black precipitates in cell B without bacteria were probably due to the addition of the supplementary chemicals, i.e. lactate, vitamin solution, modified Wolfe's mineral elixir and 0.2 g/L $\text{FeSO}_4 \cdot 7\text{H}_2\text{O}$. In addition, these products were relatively loose and easier to be rinsed away compared to the biogenic black corrosion products observed in cell A. By contrast, without these supplements, in cell C, no black corrosion products were formed on the sample surfaces.

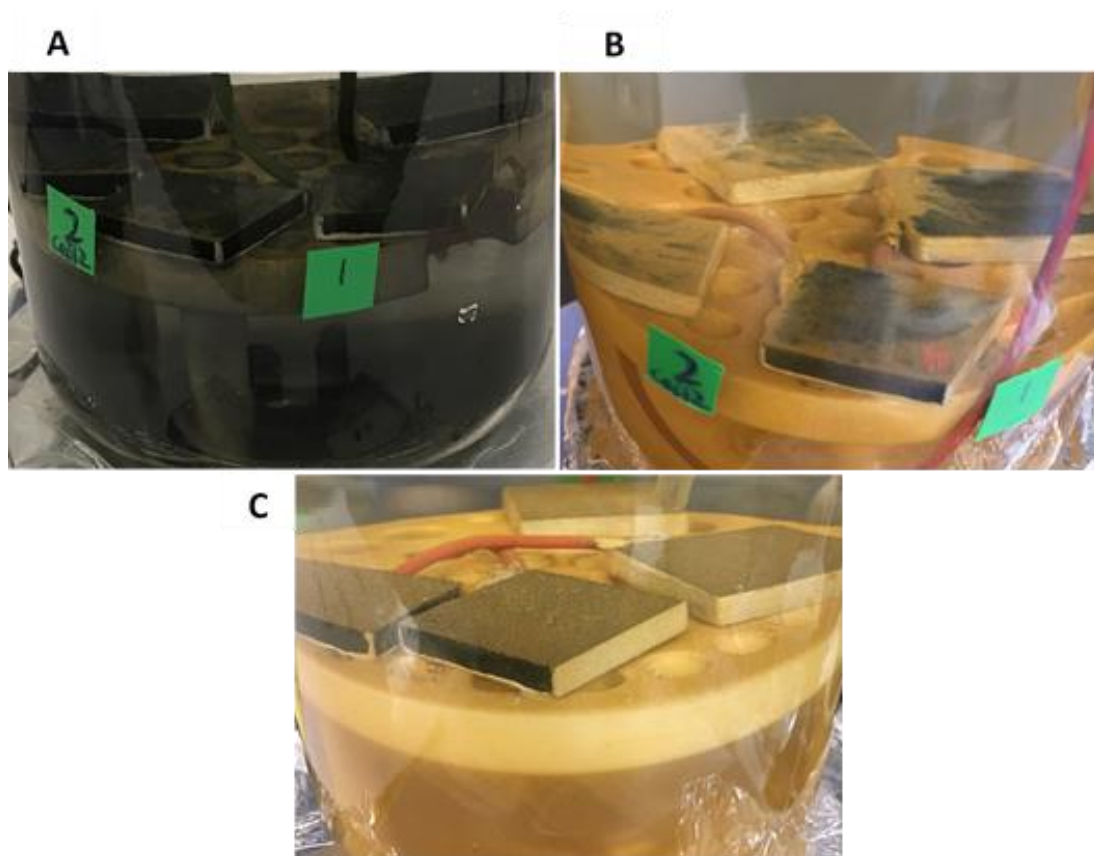


Figure 10-5: Photos of test cells A (with SRB), B (without SRB but with supplements) and C (without SRB and supplements) after 15 days.

Monitoring of bacteria activities and solution chemistry

Since the bacteria started growing after three days of the second inoculation, which was indicated by the colour of the test solution in cell A turning to black, measurements of the bacteria cell densities and the solution chemistry were performed from day 7. Table 10-4 shows the variations of the *D. alaskensis* cell densities as well as the solution chemistry.

As can be seen, the cell densities of SRB increased in general and the sulphate concentration decreased during the test period between two solution replacements. Theoretically, the decrease in sulphate concentration should be associated with an increase in sulphide concentration due to the metabolic activities of the SRB. Surprisingly, during the whole test period, the concentration of dissolved sulphide in the solution was undetectable even though the test solution was blackening with time. This might be because of the free S^{2-} being oxidised by the dissolved oxygen or by chemical interference from other solution components with the kit reagents. In addition,

it was noticed that between the solution replacements, the pH values of the test solution were almost unchanged.

By contrast, the sulphate concentrations of cell B and C remained constant at around 3000 mg/L and 2700 mg/L, respectively.

Table 10-4: Cell density and chemical monitoring for cell A.

Time (day)	SRB cell density (cell/mL)	SO ₄ ²⁻ (mg/L)	pH	Notes
7	10 ⁴	3,200	7.03	First solution replacing
10	10 ⁵	-	7.04	
15	-	3,600	7.04	Second solution replacing
17	10 ⁶	3,300	7.01	
20	-	3,200	7.02	
22	10 ⁵	3,900	7.05	Third solution replacing
24	10 ⁷	3,800	7.07	
27	-	3,200	7.07	
30	-	4,000	7.08	Fourth solution replacing
34	-	3,000	7.04	
36	10 ⁶	2,700	7.06	
37	-	3,000	7.09	ATP analysis: 2107.88 pg/cm ²

Microscopic analysis

Figure 10-6 shows the SEM images of the corrosion products formed at the steel surfaces. The associated EDS spectra are shown in Figure 10-7.

As can be seen from Figure 10-6(a), on the sample retrieved from cell A after 37 days, the curved rod-like bacteria (enclosed by a dashed circle) were incorporated inside of the corrosion products instead of forming a biofilm and the volume fraction

of the bacteria was rather small. At a lower magnification (Figure 10-6 (b)), aggregated granular products were found to be intertwined with other products featured with straight rod and needle shapes.

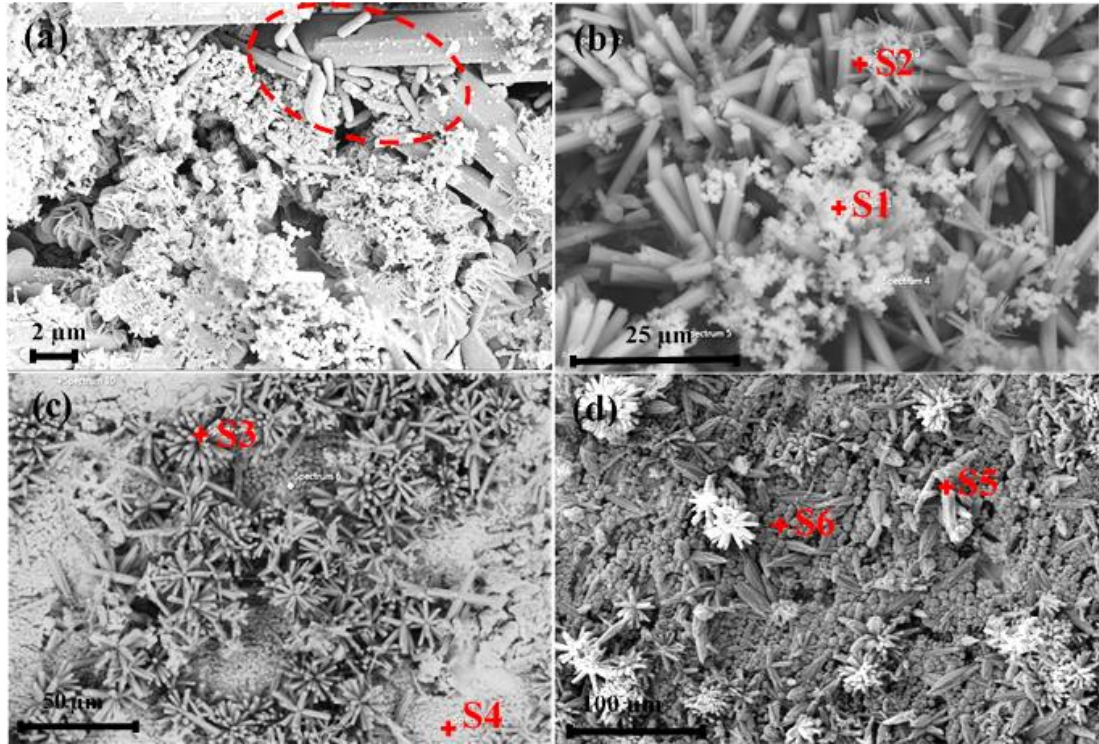


Figure 10-6: SEM images of corrosion products formed on the steel surface after (a, b) 37 days in cell A with SRB (c) 21 days in cell B without SRB but with supplements (d) 21 days in cell C without SRB and supplements.

Based on the EDS spectra shown in Figure 10-7, the granular products were mainly composed of S, Fe, Ca and O, whereas the straight rod shaped products were consisted of C, O and Ca. Because of the seawater environment and the presence of sulphate reducing bacteria, it can be inferred that the primary corrosion products formed on the steels in cell A were iron sulphide, iron oxides/hydroxides and calcium carbonate [1, 2]. However, it should be noted that the corrosion product layer was heterogeneous. The element S shown in spectrum S1 may also come from sulphated green rust ($\text{GR}(\text{SO}_4^{2-}) = \text{Fe}_4^{\text{II}}\text{Fe}_2^{\text{III}}(\text{OH})_{12}\text{SO}_4 \cdot 8\text{H}_2\text{O}$), which is commonly found for carbon steels immersed in seawater [1, 3, 4].

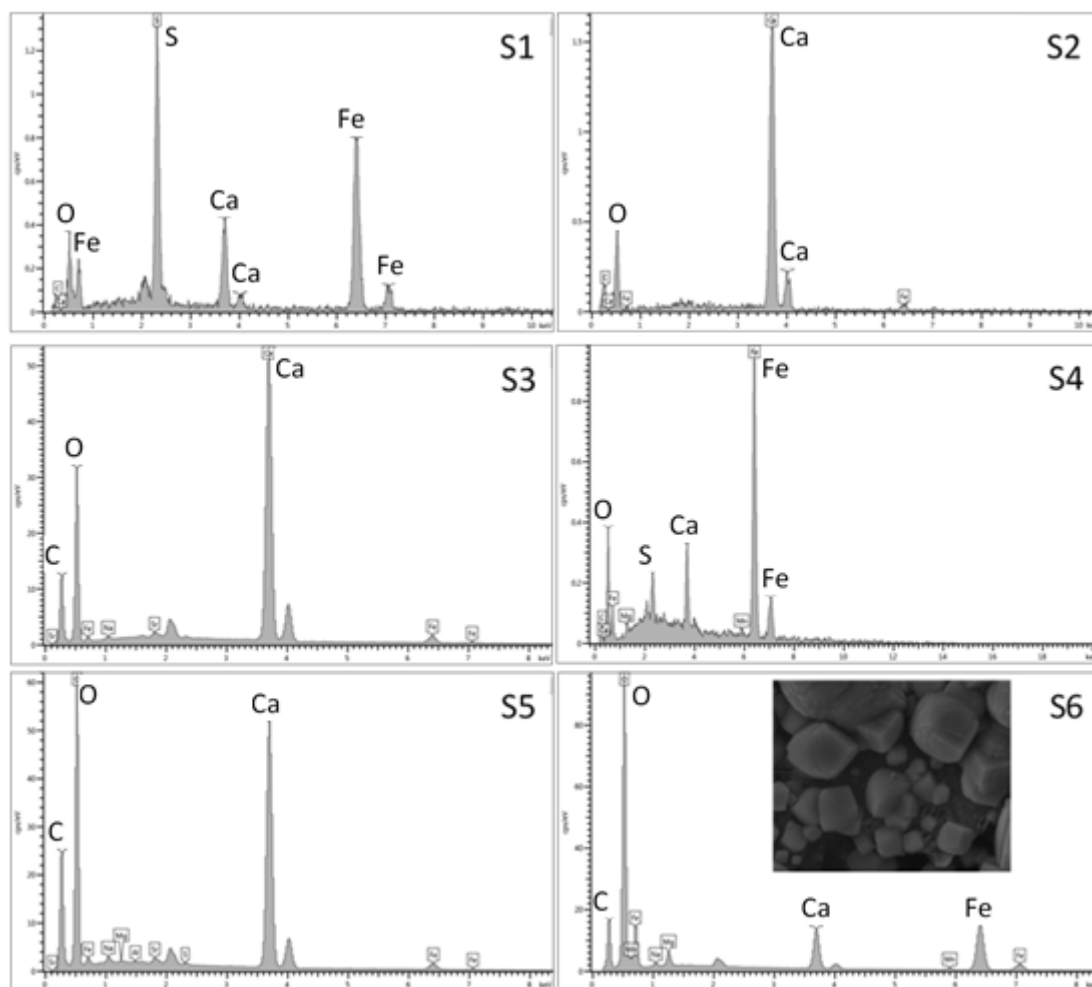


Figure 10-7: EDS spectra of the marked positions in Figure 10-6.

Figure 10-6(c) shows the SEM image of an area with black deposits on the surface of the steel sample in cell B. Similarly, the straight rod-like products constituted of flower-shaped structures (Figure 10-6(c)), which were determined to be calcium carbonate by the EDS spectrum S3. The chemical elements detected at site S4 (Figure 10-7(S4)) were also similar to those at site S1 (Figure 10-7(S1)), i.e. S, Fe, Ca and O. In combination with the black deposits observed in Figure 10-5(B), site S4 could be composed of calcareous products intermingled with FeS or Fe₃O₄. In addition, Figure 10-8 shows an EDS spectrum of a site in the area without black deposits on the same steel sample retrieved from cell B. As can be seen, apart from the calcareous products, it was mainly composed of elements Fe and O, suggesting that the brown/yellowish products were iron oxides/hydroxides.

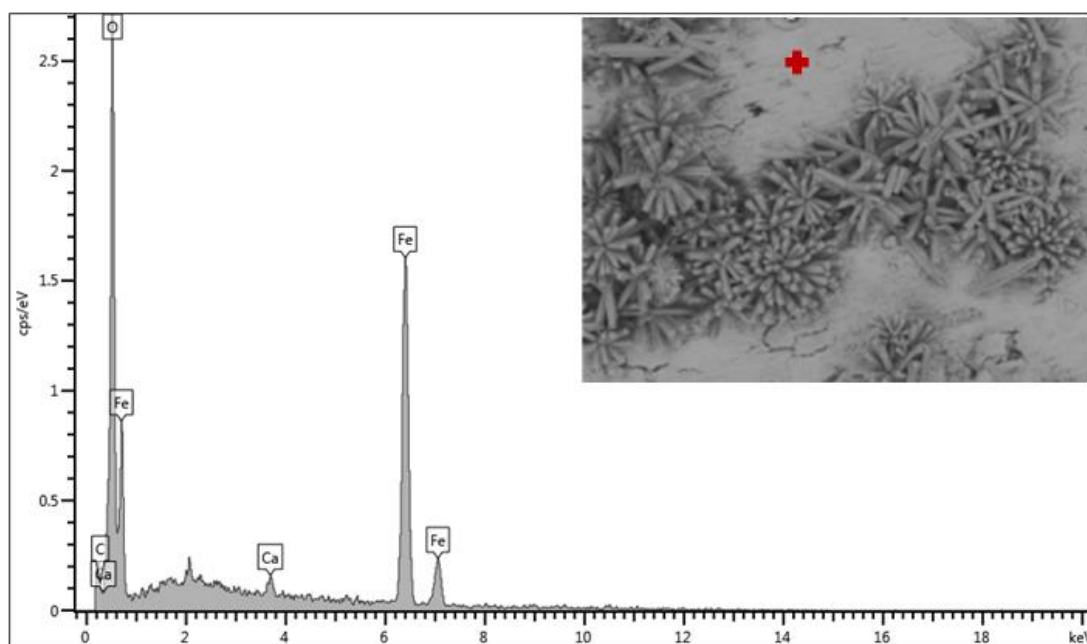


Figure 10-8: EDS spectrum of a site (indicated by the cross mark) within the area without black deposits on the steel sample retrieved from cell B after 21 days of immersion. The inset image shows the micromorphology of the examined area.

In comparison, for the steel samples immersed in the filtered seawater, the morphologies of the corrosion products were different. As can be seen from Figure 10-6(d) and Figure 10-7(S5), calcium carbonate products were also formed. In addition, the particulate products (enlarged image shown in Figure 10-7(S6)) were composed of elements Fe, O, Ca, C and Mg, which could be the constituents of mixed carbonate minerals.

Electrochemical noise

Figure 10-9 shows the typical EN segments obtained on days 2, 8 and 18 for cells A, B and C. The signals were linearly detrended and certain offset was applied for better visualisation. As can be seen, the potential fluctuations for different cells were all similar on various days. The average potential values (V vs. Ag/AgCl) of each potential segment (before drift removal) are presented in Table 10-5. It can be seen that the potential values of the steel samples in test cell A were lower than those in the control cells B and C at all times. Without the addition of chemical supplements in the test solution (cell C), the average potential values of the steel samples were slightly

lower than those in cell B on days 2 and 8, but on day 18, the potential value was increased and reached a similar level as cell B.

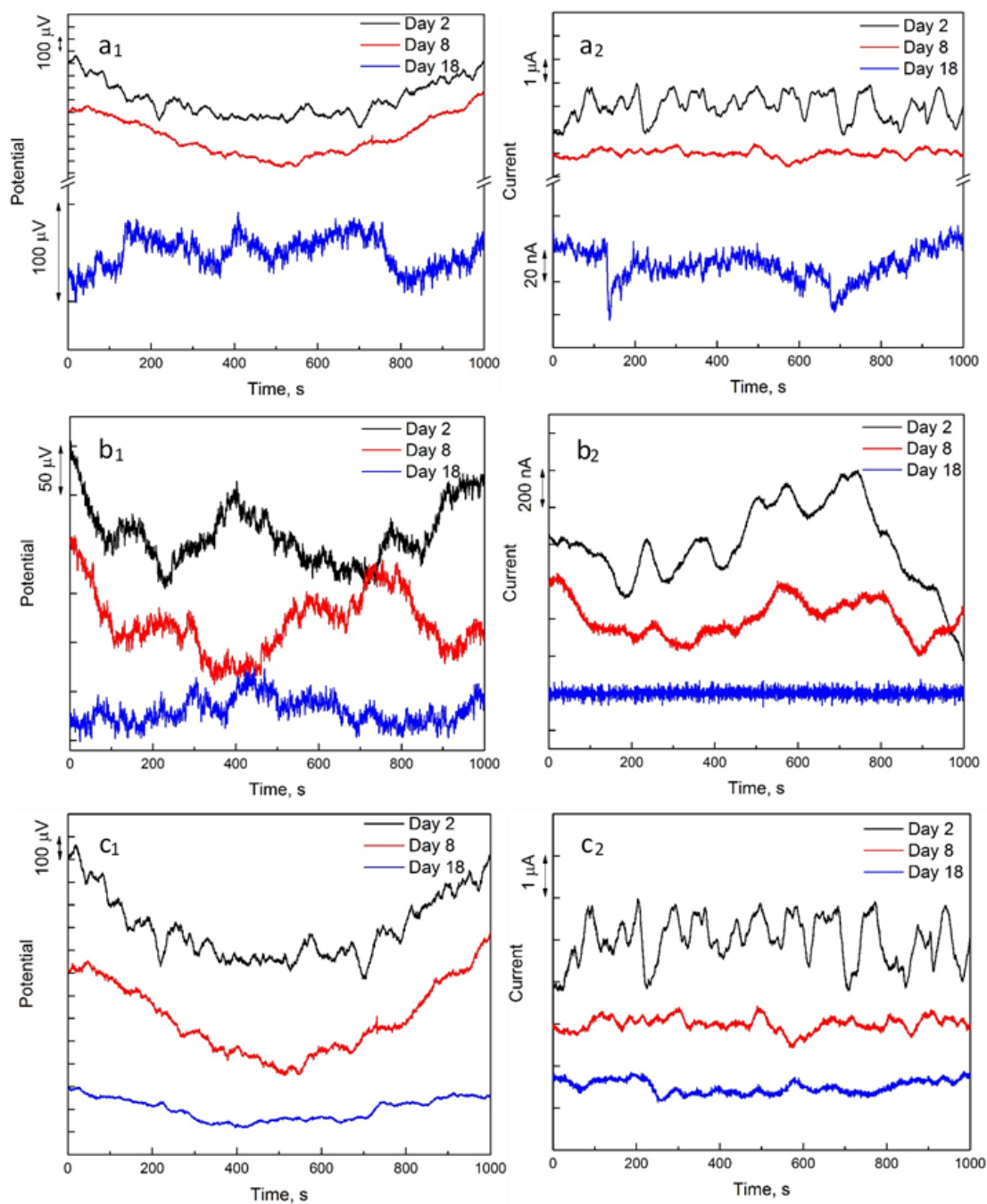


Figure 10-9: Electrochemical noise segments obtained on days 2, 8 and 18 for (a₁, a₂) Cell A with SRB, (b₁, b₂) Cell B without SRB but with supplements, (c₁, c₂) Cell C without SRB and supplements.

Table 10-5: Average potential values (V vs. Ag/AgCl) of cells A, B and C obtained on days 2, 8 and 18.

	Cell A	Cell B	Cell C
Day 2	-0.7387	-0.6799	-0.7058
Day 8	-0.7247	-0.6948	-0.7145
Day 18	-0.7539	-0.6846	-0.6740

From the current signals, it is noticed that at the beginning (day 2) of all the tests, the current fluctuations were all similar with relatively large amplitudes which decreased later with time. On day 18, the characteristic pitting transients were shown in the current signal obtained with the steel samples in test cell A, while no such transients were observed for the two control cells. It was expected that similar transients should be present in the corresponding potential signal. Nevertheless, it seems that such peaks were not very obvious in the potential noise data. This could be traced back to the actual corrosion morphologies of the steel samples underneath the corrosion products.

Figure 10-10 shows the microscopic images of steel electrodes after corrosion product removal. As can be seen, the steel samples in the control cells B and C basically underwent uniform corrosion during 21 days of immersion in the seawater environment without bacteria. In contrast, the samples retrieved from cell A with SRB addition exhibited specific areas where more severe corrosion were concentrated, while only mild general corrosion attack was observed outside of the area. Clearly, it can be seen from Figure 10-10(a₁) and (a₂), the areas with lighter colour were more corroded with a depth in the range of 5 – 10 µm and width about 200 µm, compared to the darker area. Therefore, it could be inferred that, in the presence of indigenous bacteria and the added *D. alaskensis* in seawater, the steel samples underwent mixed type of corrosion processes with general corrosion as the dominant form. This could be correlated with the electrochemical noise signals shown in Figure 10-9(a₁, a₂), where only a few characteristic current transients were observed and the potential transients were not clearly visible.

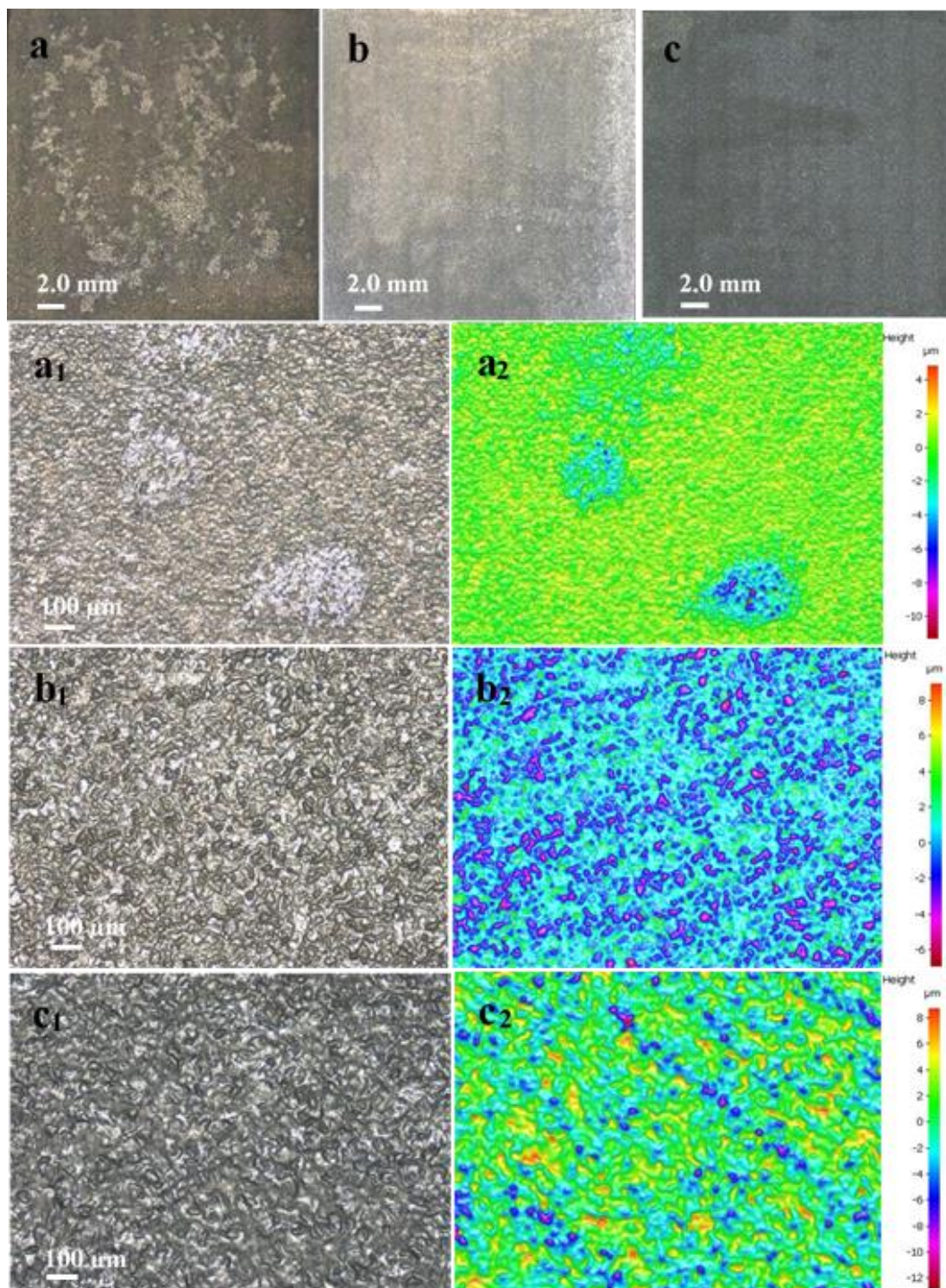


Figure 10-10: Microscopic images of steel electrodes after corrosion product removal.

Specifically, Figure 10-10(a) is a 2D image (5x) of the general surface of a working electrode retrieved from cell A after 37 days; (a₁, a₂) 3D images (10x) of an area showing concentrated corrosion on the steel sample (a); (b) 2D image (5x) of the

general surface of a working electrode retrieved from cell B after 21 days; (b₁, b₂) 3D images (10x) of a typical area showing general corrosion of the steel sample (b); (c) 2D image (5x) of the general surface of a working electrode retrieved from cell C after 21 days; (c₁, c₂) 3D images (10x) of a typical area showing general corrosion of the steel sample (c).

It is commonly acknowledged that the electrochemical noise resistance, defined as the ratio of potential standard deviation to current standard deviation, is equivalent to the polarisation resistance obtained from LPR technique, thus can be used as an indicator of the variation of general corrosion rate. In this study, the EN signals obtained from each day were divided into small segments, followed by linear trend removal. Each segment contained 1024 data points for the current and potential, respectively. The noise resistances were calculated with the EN segments for each day and the average values are shown in Figure 10-11.

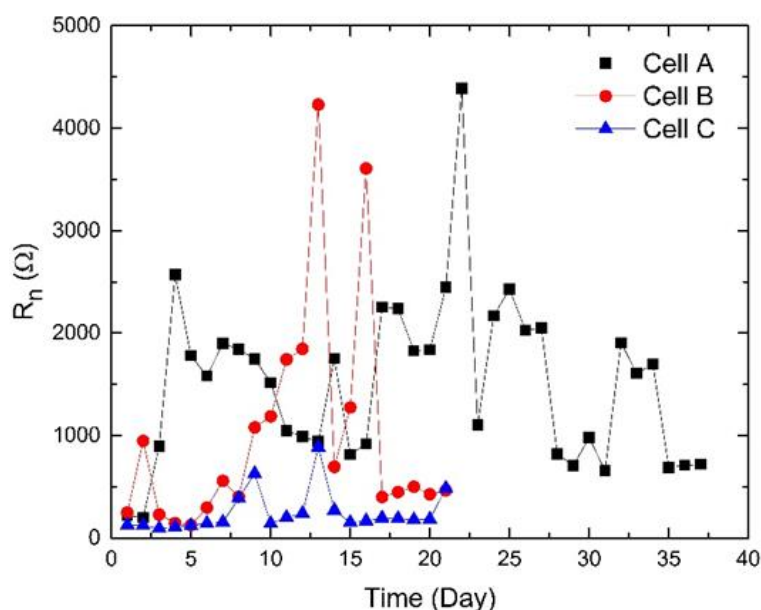


Figure 10-11: Variation of electrochemical noise resistances with time for different test cells.

Evidently, the noise resistances of the steel samples in cell A were relatively higher than those obtained with the samples from two control cells, indicating a lower general corrosion rate. This is in line with the corrosion rates computed from weight loss, as shown in Table 10-6, where the R_n values were the average values of the those shown in Figure 10-11, the corrosion rates by R_n were determined based on ASTM

standard G102 using the parameter $B = 0.026 \text{ V/decade}$, and the corrosion rates from weight loss were determined with duplicate coupons according to ASTM standard G1.

Table 10-6: Corrosion rates of the steel samples in different cells.

	Average R_n (Ω)	Corrosion rate (mm/y, by R_n)	Corrosion rate (mm/y, by weight loss)
Cell A	1,513	0.65*	0.65*
Cell B	994	0.05	0.08
Cell C	247	0.18	0.11

* The unit of corrosion rates for cell A is $\text{g} \cdot \text{m}^{-2} \cdot \text{day}^{-1}$.

Interestingly, the corrosion rates calculated with the average R_n were very close to those from weight loss. It should be noted that since the specimens in cell A underwent some extent of localised corrosion, the mass loss in g per unit area per day was reported as the corrosion rate.

Recurrence quantification analysis of EN

The current segments shown in Figure 10-9 were converted to recurrence plots with a threshold value of 0.1σ , as presented in Figure 10-12. Twelve variables described in previous chapters were extracted from each current data segment and the results are displayed in Figure 10-13. Please note that the recurrence quantification analysis of each current segment was conducted on an epoch by epoch basis. Each epoch contained 1024 data points (corresponding to 512 s), which was shifted by 100 data points to the later progressively. For example, in the case of the current segment associated with cell A – day 2, the first epoch was associated with data points 1 – 1024, which was shifted by 100 data points in the next step, resulting in the second epoch containing data points 101 – 1124, and so on. Twelve variables were obtained from each epoch and there were 10 epochs in total for each current segment.

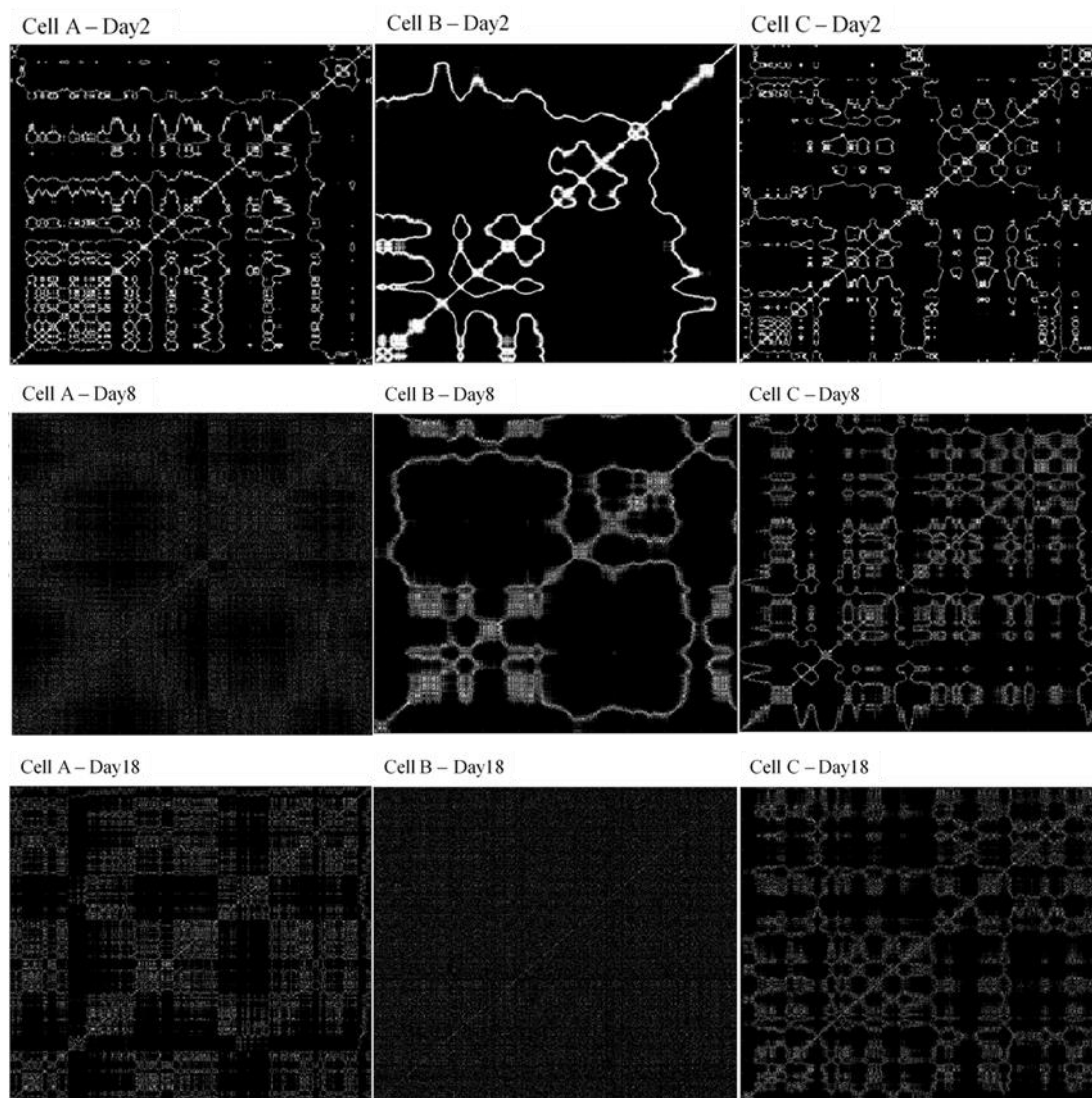


Figure 10-12: Recurrence plots of the current segments shown in Figure 10-9.

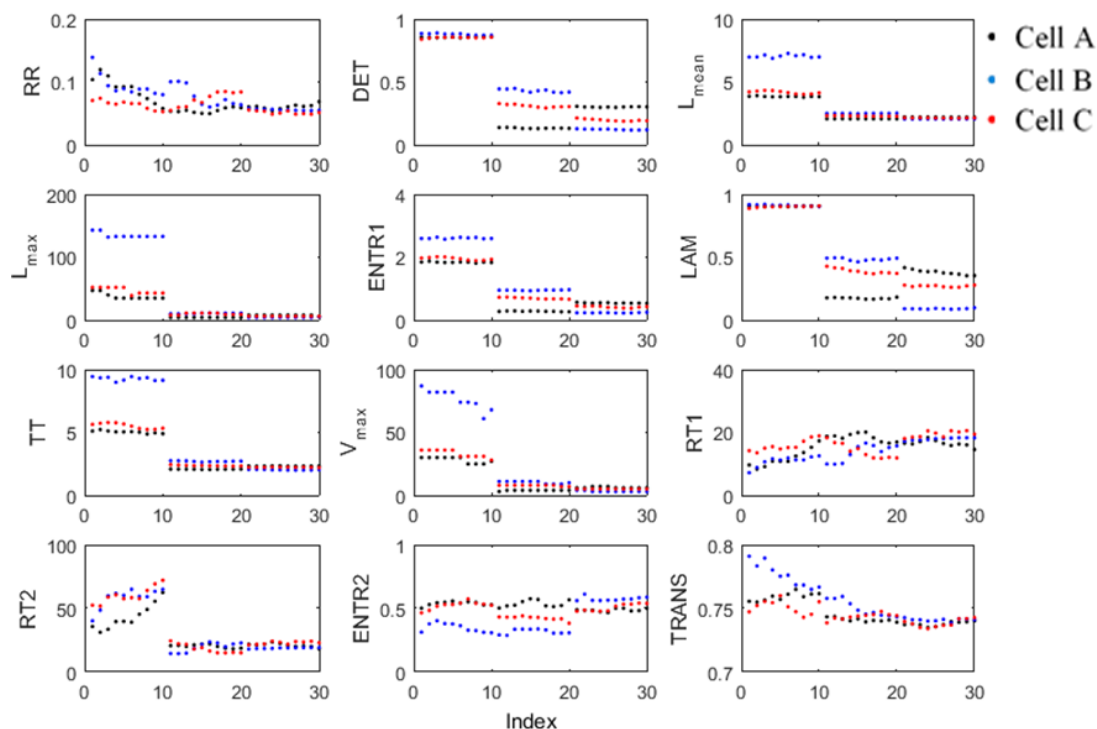


Figure 10-13: RQA variables calculated from the current segments presented in Figure 10-9. Indices (1-10) correspond to day 2, (11 - 20) day 8 and (21-30) day 18.

It can be seen from Figure 10-13, for all the cells, almost all the RQA variables decreased from day 2 to day 8 and day 18. Moreover, as mentioned before, on day 18, the characteristic pitting transients were shown in the current signal obtained with the steel samples in test cell A, which is distinct from those obtained in cell B and cell C. From Figure 10-13, it appears that on day 18 (index 20 – 30), only variables *DET* and *LAM* showed relatively large difference between cell A, B and C. Similar trend is observed, i.e. the values associated with cell A are higher than those related to cell B and cell C.

Summary

In this study, the effect of SRB on corrosion of carbon steel was investigated by using electrochemical noise and microscopic analysis.

Scanning electron microscopy (SEM) images of the corrosion products formed at the steel surfaces indicated that curved rod-like bacteria were incorporated inside of the corrosion products instead of forming a biofilm. The composition of corrosion products formed on the steel samples of biotic and abiotic tests was determined with

energy dispersive spectroscopy (EDS). Results showed that, in the presence of SRB, the main corrosion products were iron sulphide, iron oxides/hydroxides and calcium carbonate. In the control cells, the corrosion products were mainly composed of calcium carbonate and other carbonate minerals.

The surface profile analysis of the steel samples after removal of corrosion products revealed that, in the presence of SRB, the corrosion of steel exhibited some extent of localisation, while only low general corrosion occurred to the steel in the control tests. Overall, the differences between the surface morphologies of biotic and abiotic samples were not as distinctive as expected.

The electrochemical current noise data obtained from the test with SRB showed a few pitting transients after 18 days, yet no such transients were observed for the control tests. This in part agreed with the observed surface morphologies.

The average corrosion rates of the samples in all the tests were evaluated by weight loss measurements and the results were compared with those obtained with electrochemical noise resistance (R_n) calculated from EN data. It was found that the corrosion rates calculated with the average R_n were very close to those from weight loss. Moreover, the average corrosion rates for all the tests were low, but the steels in the control cells were corroded with a relatively higher rate than those in the test cell with SRB.

In addition, from recurrence quantification analysis of the selected EN data, RQA variables *DET* and *LAM* appeared to be able to capture the difference between the EN signals associated with different test cells.

Overall, the added SRB did not induce significant localised corrosion to steel as expected. It also happens often in the industry that there is active bacteria present but there is no MIC issues in the system. This is due to the fact that microorganisms and biofilms are very complex and can influence the surface reactions in different ways and at different times.

References

- [1] M. Stipaničev, F. Turcu, L. Esnault, E.W. Schweitzer, R. Kilian, R. Basseguy, Corrosion behavior of carbon steel in presence of sulfate-reducing bacteria in seawater environment, *Electrochim Acta*, 113 (2013) 390-406.
- [2] P. Refait, M. Jeannin, R. Sabot, H. Antony, S. Pineau, Electrochemical formation and transformation of corrosion products on carbon steel under cathodic protection in seawater, *Corros Sci*, 71 (2013) 32-36.
- [3] S. Pineau, R. Sabot, L. Quillet, M. Jeannin, C. Caplat, I. Dupont-Morral, P. Refait, Formation of the Fe(II–III) hydroxysulphate green rust during marine corrosion of steel associated to molecular detection of dissimilatory sulphite-reductase, *Corros Sci*, 50 (2008) 1099-1111.
- [4] P. Refait, M. Abdelmoula, J.-M.R. Génin, R. Sabot, Green rusts in electrochemical and microbially influenced corrosion of steel, *Comptes Rendus Geoscience*, 338 (2006) 476-487.

Appendix 3. Written Statements from Co-authors of the Publications

1. Written statements from co-authors of the publication entitled “Monitoring of carbon steel corrosion by use of electrochemical noise and recurrence quantification analysis”.

2. Written statements from co-authors of the publication entitled “Application of electrochemical noise technique to monitor carbon steel corrosion under sand deposit”.

3. Written statements from co-authors of the publication entitled “Analysis of electrochemical noise data by use of recurrence quantification analysis and machine learning methods”.

4. Written statements from co-authors of the publication entitled “Detection of under deposit corrosion in CO₂ environment by using electrochemical noise and recurrence quantification analysis”.

5. Written statements from co-authors of the submitted manuscript entitled “Identifying corrosion of carbon steel buried in iron ore and coal cargoes based on recurrence quantification analysis of electrochemical noise”.

Appendix 3. Written Statements from Co-authors of the Publications

To Whom It May Concern,

I, Yang Hou, contributed by conducting the research, interpreting the obtained data and writing up contents reported in the publication entitled “**Monitoring of carbon steel corrosion by use of electrochemical noise and recurrence quantification analysis**”.


Signature of Candidate 16/04/2018

I, as a Co-Author, endorse that this level of contribution by the candidate indicated above is appropriate.

Chris Aldrich

Full Name of Co-Author 1

Kateřina Lepková

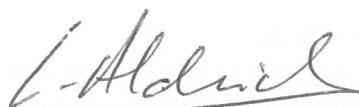
Full Name of Co-Author 2

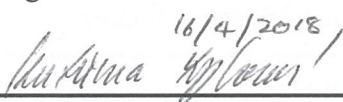
Laura Machuca Suarez

Full Name of Co-Author 3

Brian Kinsella

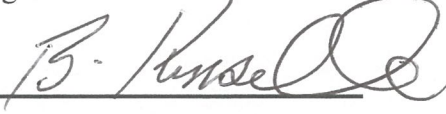
Full Name of Co-Author 4


Signature of Co-Author 1


Signature of Co-Author 2 16/4/2018


Signature of Co-Author 3 16/4/2018

Signature of Co-Author 3


Signature of Co-Author 4 17/4/2018

To Whom It May Concern,

I, Yang Hou, contributed by conducting the research, interpreting the obtained data and writing up contents reported in the publication entitled “**Application of electrochemical noise technique to monitor carbon steel corrosion under sand deposit**”.

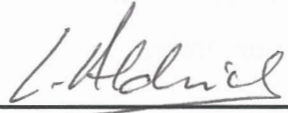


Signature of Candidate 16/04/2018

I, as a Co-Author, endorse that this level of contribution by the candidate indicated above is appropriate.

Chris Aldrich

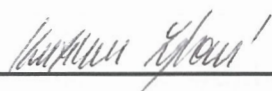
Full Name of Co-Author 1



Signature of Co-Author 1 16/4/2018

Kateřina Lepková


Full Name of Co-Author 2



Signature of Co-Author 2 16/4/2018

Laura Machuca Suarez

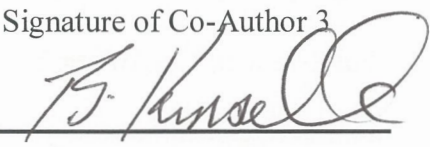
Full Name of Co-Author 3



Signature of Co-Author 3 16/4/2018

Brian Kinsella

Full Name of Co-Author 4



Signature of Co-Author 4 17/4/2018

To Whom It May Concern,

I, Yang Hou, contributed by conducting the research, interpreting the obtained data and writing up contents reported in the publication entitled “**Analysis of electrochemical noise data by use of recurrence quantification analysis and machine learning methods**”.

Yang Hou 16/04/2018
Signature of Candidate

I, as a Co-Author, endorse that this level of contribution by the candidate indicated above is appropriate.

Chris Aldrich

Full Name of Co-Author 1

C. Aldrich

Signature of Co-Author 1 16/4/2018

Kateřina Lepková

Full Name of Co-Author 2

Kateřina Lepková

Signature of Co-Author 2 16/4/2018

Laura Machuca Suarez

Full Name of Co-Author 3

Laura Machuca Suarez

Signature of Co-Author 3

Brian Kinsella

Full Name of Co-Author 4

B. Kinsella

Signature of Co-Author 4 17/4/2018

To Whom It May Concern,

I, Yang Hou, contributed by conducting the research, interpreting the obtained data and writing up contents reported in the publication entitled “**Detection of under deposit corrosion in CO₂ environment by electrochemical noise and recurrence quantification analysis**”.

Yang Hou 16/04/2018
Signature of Candidate

I, as a Co-Author, endorse that this level of contribution by the candidate indicated above is appropriate.

Chris Aldrich
Full Name of Co-Author 1

Chris Aldrich
Signature of Co-Author 1 16/4/2018

Kateřina Lepková
Full Name of Co-Author 2

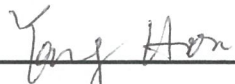
Kateřina Lepková
Signature of Co-Author 2 16/4/2018

Brian Kinsella
Full Name of Co-Author 3

B. Kinsella 17/4/2018
Signature of Co-Author 3

To Whom It May Concern,

I, Yang Hou, contributed by conducting the research, interpreting the obtained data and writing up contents reported in the submitted manuscript entitled “**Identifying corrosion of carbon steel buried in iron ore and coal cargoes based on recurrence quantification analysis of electrochemical noise**”.



Signature of Candidate 16/04/2018

I, as a Co-Author, endorse that this level of contribution by the candidate indicated above is appropriate.

Chris Aldrich

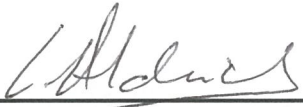
Full Name of Co-Author 1

Kateřina Lepková


Full Name of Co-Author 2

Brian Kinsella

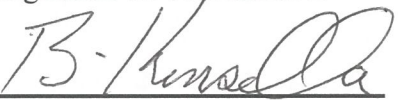
Full Name of Co-Author 3



Signature of Co-Author 1 16/4/2018.



Signature of Co-Author 2 16/4/2018



Signature of Co-Author 3 17/4/2018

Appendix 4. Copyright Statements

The rights granted by Elsevier to reproduce the published materials that form chapters 4, 6, 7 and 8 of this thesis.

The rights granted by NACE International to reproduce the published material that forms chapter 5 of this thesis.



RightsLink®

Home

Create
Account

Help



Title: Monitoring of carbon steel corrosion by use of electrochemical noise and recurrence quantification analysis

Author: Y. Hou, C. Aldrich, K. Lepkova, L.L. Machuca, B. Kinsella

Publication: Corrosion Science

Publisher: Elsevier

Date: November 2016

© 2016 Elsevier Ltd. All rights reserved.

LOGIN

If you're a **copyright.com user**, you can login to RightsLink using your copyright.com credentials.

Already a **RightsLink user** or want to [learn more?](#)

Please note that, as the author of this Elsevier article, you retain the right to include it in a thesis or dissertation, provided it is not published commercially. Permission is not required, but please ensure that you reference the journal as the original source. For more information on this and on your other retained rights, please visit: <https://www.elsevier.com/about/our-business/policies/copyright#Author-rights>

BACK

CLOSE WINDOW

Copyright © 2018 [Copyright Clearance Center, Inc.](#) All Rights Reserved. [Privacy statement](#). [Terms and Conditions](#).
Comments? We would like to hear from you. E-mail us at customercare@copyright.com



RightsLink®

Home

Create
Account

Help



Title: Analysis of electrochemical noise data by use of recurrence quantification analysis and machine learning methods

Author: Y. Hou, C. Aldrich, K. Lepkova, L.L. Machuca, B. Kinsella

Publication: Electrochimica Acta

Publisher: Elsevier

Date: 1 December 2017

© 2017 Published by Elsevier Ltd.

LOGIN

If you're a **copyright.com user**, you can login to RightsLink using your copyright.com credentials.

Already a **RightsLink user** or want to [learn more?](#)

Please note that, as the author of this Elsevier article, you retain the right to include it in a thesis or dissertation, provided it is not published commercially. Permission is not required, but please ensure that you reference the journal as the original source. For more information on this and on your other retained rights, please visit: <https://www.elsevier.com/about/our-business/policies/copyright#Author-rights>

BACK

CLOSE WINDOW

Copyright © 2018 [Copyright Clearance Center, Inc.](#) All Rights Reserved. [Privacy statement](#). [Terms and Conditions](#).
Comments? We would like to hear from you. E-mail us at customercare@copyright.com



RightsLink®

Home

Create
Account

Help



Title: Detection of under deposit corrosion in CO₂ environment by electrochemical noise and recurrence quantification analysis

Author: Y. Hou, C. Aldrich, K. Lepkova, B. Kinsella

Publication: Electrochimica Acta

Publisher: Elsevier

Date: 1 June 2018

© 2018 Elsevier Ltd. All rights reserved.

LOGIN

If you're a **copyright.com user**, you can login to RightsLink using your copyright.com credentials. Already a **RightsLink user** or want to [learn more?](#)

Please note that, as the author of this Elsevier article, you retain the right to include it in a thesis or dissertation, provided it is not published commercially. Permission is not required, but please ensure that you reference the journal as the original source. For more information on this and on your other retained rights, please visit: <https://www.elsevier.com/about/our-business/policies/copyright#Author-rights>

BACK

CLOSE WINDOW

Copyright © 2018 [Copyright Clearance Center, Inc.](#) All Rights Reserved. [Privacy statement](#). [Terms and Conditions](#). Comments? We would like to hear from you. E-mail us at customercare@copyright.com



RightsLink®

[Home](#)
[Create Account](#)
[Help](#)


Title: Identifying corrosion of carbon steel buried in iron ore and coal cargoes based on recurrence quantification analysis of electrochemical noise

Author: Y. Hou, C. Aldrich, K. Lepkova, B. Kinsella

Publication: Electrochimica Acta

Publisher: Elsevier

Date: 1 September 2018

© 2018 Elsevier Ltd. All rights reserved.

[LOGIN](#)

If you're a **copyright.com user**, you can login to RightsLink using your copyright.com credentials.

Already a **RightsLink user** or want to [learn more?](#)

Please note that, as the author of this Elsevier article, you retain the right to include it in a thesis or dissertation, provided it is not published commercially. Permission is not required, but please ensure that you reference the journal as the original source. For more information on this and on your other retained rights, please visit: <https://www.elsevier.com/about/our-business/policies/copyright#Author-rights>

[BACK](#)
[CLOSE WINDOW](#)

Copyright © 2018 [Copyright Clearance Center, Inc.](#) All Rights Reserved. [Privacy statement](#). [Terms and Conditions](#). Comments? We would like to hear from you. E-mail us at customercare@copyright.com

Permission to Republish NACE International
Copyrighted Paper/Article

Date: 19/04/2018

Name: Yang Hou Title: Ms

Company ("Publisher"): Curtin University

Address: Kent Street, Bentley, Perth, Western Australia - 6845

Tel: +61451170506 Fax: _____

Email: yang.hou1@postgrad.curtin.edu.au

Publication Media: Check the applicable Box:

☐ Magazine/Journal ("Periodical"): _____ Issue: _____

☒ Web Site URL ("Web Site"): https://espace.curtin.edu.au

Circle the source: Materials Performance CORROSION Conference Paper Standards

Paper/Article Title: Application of electrochemical noise technique to monitor carbon steel corrosion under sand deposit ("Work") Conference Paper No./Year: 9103/2017

Authors: Yang Hou, Chris Aldrich, Katerina Lepkova, Laura Machuca Suarez, Brian Kinsella

NACE International ("NACE") hereby grants to "Publisher" the right to publish the Work utilizing the Publication Media elected above. To the extent the Publication Media is a Periodical, the publication right is limited to publication in the specific Issue identified above of the Periodical identified above and this right shall automatically terminate upon the date of issue of the particular Issue of the Periodical, whether or not such Work is actually published. To the extent the Publication Media is a Web Site, the publication right is limited to publication at the specific Web Site identified above. Any right granted herein is a limited, non-transferable, non-exclusive right. No other rights in the Work are granted herein. The Publisher agrees to hold NACE harmless and indemnify NACE against any and all legal action and expenses arising out of the Publisher's use and editing of NACE material.

Notwithstanding the foregoing, Publisher may edit or otherwise modify the Work as reasonably necessary to accommodate the style and size requirements of the specific publication so long as the published Work that will appear in the Publication remains substantially similar to the original Work. Any such permitted edit or modification shall maintain the integrity of the overall original Work.

Publisher shall obtain a copy of the original Work directly from NACE International and shall not utilize copies of the Work from other sources, including the author(s). Publisher shall include on the published version of the Work the names of all authors listed on the original Work.

The Publisher shall include the following applicable Copyright notation with any publication of the Work:*

A. Conference Paper

Reproduced with permission from NACE International, Houston, TX. All rights reserved. Author(s), Paper NUMBER presented at CORROSION/YEAR, City, State. © NACE International FIRST YEAR OF PUBLICATION.

B. Journal Article

Reproduced with permission from NACE International, Houston, TX. All rights reserved. Author(s) name, Article title, Journal title, Vol. no., Issue no., and publication year. © NACE International FIRST YEAR OF PUBLICATION.

C. Magazine Article

Reproduced with permission from NACE International, Houston, TX. All rights reserved. Author(s) name, Article title, Magazine title, Vol. no., Issue no., and publication year. © NACE International FIRST YEAR OF PUBLICATION.

D. Standards

STANDARDS/TECHNICAL COMMITTEE REPORT NAME. © NACE International YEAR. All rights reserved by NACE. Reprinted with permission. NACE standards are revised periodically. Users are cautioned to obtain the latest edition; information in an outdated version of the standard may not be accurate.

* Modifications to Notations: Other reference wording can be used, but must be approved by NACE in writing *in advance*.

As between NACE and Publisher, Publisher acknowledges that NACE owns all rights in the Works. Publisher shall not be entitled to any compensation for its efforts in promoting the Work.

THE WORK IS PROVIDED "AS IS." ALL EXPRESS OR IMPLIED COVENANTS, CONDITIONS, REPRESENTATIONS OR WARRANTIES, INCLUDING ANY IMPLIED WARRANTY OF MERCHANTABILITY OR FITNESS FOR A PARTICULAR PURPOSE OR CONDITIONS OF ACCURACY, COMPLETENESS OR QUALITY AND THOSE ARISING BY STATUTE OR OTHERWISE IN LAW, ARE HEREBY DISCLAIMED.

IN NO EVENT WILL NACE BE LIABLE FOR ANY DIRECT, INDIRECT, PUNITIVE, SPECIAL, INCIDENTAL OR CONSEQUENTIAL DAMAGES IN CONNECTION WITH OR RELATED TO THIS AGREEMENT (INCLUDING LOSS OF PROFITS, USE, DATA, OR OTHER ECONOMIC ADVANTAGE), HOWSOEVER ARISING.

This Agreement and the rights granted herein may be terminated immediately by NACE upon breach of this Agreement by Publisher. Unless earlier terminated, this Agreement and the rights granted herein will automatically terminate 6 months from the Date set forth above. If the Work has not been published within that time period, a new Agreement must be obtained.

Publisher may not, directly or indirectly, sell, assign, sublicense, lease, rent, distribute, or otherwise transfer this Agreement or any rights granted herein, without the prior written consent of NACE.

If any provision of this Agreement is found to be unenforceable, then this Agreement shall be deemed to be amended by modifying such provision to the extent necessary to make it legal and enforceable while preserving its intent. The remainder of this Agreement shall not be affected by such modification.

This Agreement does not create, and shall not be construed to create, any employer-employee, joint venture or partnership relationship between the parties. No officer, employee, agent, servant or independent contractor of either party shall at any time be deemed to be an employee, servant, agent or contractor of any other party for any purpose whatsoever.

This Agreement shall be governed by, and construed and enforced in accordance with, the laws of the State of Texas, without regard to the choice of law provisions of that State.

This Agreement shall only be effective if signed by authorized representatives of both parties. This Agreement constitutes the entire Agreement between the parties with respect to the subject matter of this Agreement. Any change, modification or waiver hereto must be in writing and signed by authorized representatives of both parties.

Other Terms & Conditions: _____

Publisher hereby requests permission to publish the paper/article described above and agrees to comply with all Terms and Conditions listed above.

Request submitted by:

Yang Hou

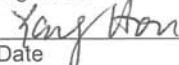
Printed Name

Yang Hou

Title

Ms

Signature



Date

19/04/2018

Request agreed to by:

Yang Hou

Lead Author Printed Name

Yang Hou

Lead Author Title

Ms

Lead Author Signature



Date

19/04/2018

Request approved by NACE:

Daniela Freeman

Printed Name

Daniela Freeman

Title

Copyright Permissions

 Digitally signed by

daniela.freeman@nace.org

e.org

Date

4/23/2018

daniela.freeman@nace.org
DN: cn=daniela.freeman@nace.org
Date: 2018.04.23 08:54:03 -05'00'

Third parties requesting permission to use NACE articles
FM_PUB_05
Revised 07/20/2015